A Semi-Annual Peer-Reviewed Scientific Journal
Concerned with publishing research and studies.
in the humanities

الأربعين

A Semi-Annual Peer-Reviewed Scientific Journal

Concerned With Publishing Research And Studies

In The Humanities

* * *

The Holy Husseiniya Shrine

Karbala Studies and Research Center

* * *

Vol.4, 4th year , March 2026 A.M - Ramadan 1447 A.H

Supplement (9) A special issue of the ninth International

Conference for the Ziyarte Al Arba'een

A Semi-Annual Peer-Reviewed
Scientific Journal
Concerned With Publishing Research And
Studies
In The Humanities

Vol.4, 4th year , Supplement (9)
March 2026 - Ramadan 1447 Ah /3rd year

Republic Of Iraq - Karbala Governorate
The Holy Husseiniya Shrine
Karbala Studies And Research Center

Deposit Number In The Iraqi Books And
Documents House
Baghdad (2610) For The Year 2023

Correspondence
All Correspondence Related To The Journal
Should Be Addressed To:
Al-Arbaeen Journal - Karbala Center For Studies
And Research

E-Mail: Arbnj.k.center@Gmail.com

P.o. Box 428 Karbala

Phone Number: +964775332066

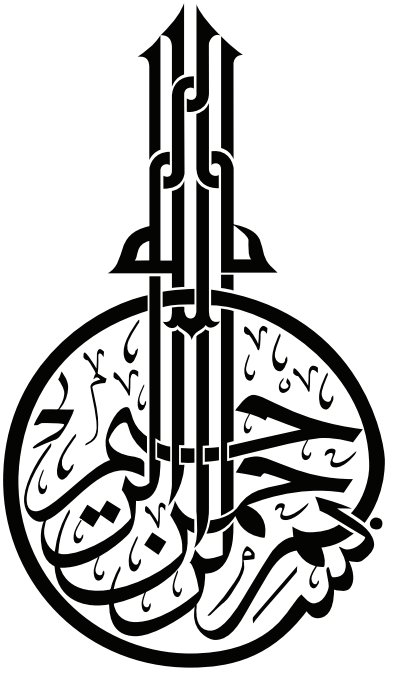
بسم الله الرحمن الرحيم

Editor-in-Chief: Prof. Dr. Nathir Jabbar Hussein al-Hindawi

Scientific Associate at Karbala Center for Studies and Research

Managing Editor: Prof. Dr. Thamer Makki Ali Al-Shammari

College of Arts / Al-Mustansiriyah University

Dr. Hussein Sayyid Noor Al-Arajy **(College of Education/ Wasit University/ Iraq)**

Dr. Burzan Maysar Hameed **(College of Education for Humanities/ University of Mosul/ Iraq)**

Dr. Iyad Mohammed Ali Al-Arnaouti **(College of Arts/ University of Baghdad/ Iraq)**

Dr. Talal Khalifa Salman **(College of Education for Girls/ University of Baghdad/ Iraq)**

Dr. Abdul Ali Kazim Al-Fatlawi **(College of Tourism Sciences/ University of Karbala/ Iraq)**

Dr. Wijdan Saleh Abbas Mohammed **(College of Arts/ University of Kufa/ Iraq)**

Dr. Fadel Madb Al-Masoudi **(College of Islamic Sciences/ University of Kufa/ Iraq)**

Dr. Salah al-Din Al-Ameri **(Higher Institute for Islamic Civilization/ Zitouna University/ Tunisia)**

Dr. Nour al-Din Abu Lahia **(College of Islamic Sciences/ University of Algiers/ Algeria)**

Dr. Adel Mohamed Ziada **(Faculty of Archaeology/ Cairo University/ Egypt)**

Dr. Hanna Jameel Eskandar **(Faculty of Middle Eastern Studies/ Suleiman International University/ Lebanon)**

Dr. Rasoul Ja'farian **(Library of Islamic and Iranian History/ Iran)**

Dr. Wang You Yong **(Research Institute for International Studies/ Shanghai University/ China)**

Dr. Rana Saad Al-Soufi **(Institute for the Study of Islamic Culture and Religion/ Goethe University/ Germany)**

Assistant Prof. Ghusun Mazhar Hussein **(College of Arts/ Mustansiriya University/ Iraq)**

Assistant Prof. Kamil Jasim Dahsh **(College of Basic Education/ University of Misan/ Iraq)**

Assistant Prof. Jaafar Ali Ashour **(College of Arts/ Ahlulbait University/ Iraq)**

Assistant Prof. Muayyad Najee Ahmed **(Open Educational College/ Ministry of Education/ Iraq)**

Dr. Alaa Abdul Hadi Al-Maliki **(Karbala Center for Studies and Research/ Iraq)**

Dr. Mohammed Jamal Al-Taif **(College of Tourism Sciences/ Ahlulbait University/ Iraq)**

Dr. Mohammed Reda Al-Nawwab **(College of Social Sciences for Media and Communication/ Iran)**

Language Review

Arabic Language:

Dr. Iyad Mohammed Ali Al-Arnaouti (University of Baghdad)

Assistant Prof. Jaafar Ali Ashour (Ahlulbait University)

English Language:

Assistant Prof. Muayyad Najee Ahmed (Open Educational College - Baghdad)

Persian Language:

Dr. Abdul Ali Kazim Al-Fatlawi (University of Karbala)

Mohammed Jamal Al-Taif, M.Sc. (University of the Prophets' Heritage)

Artistic Direction:

Emad Mohammed Al-Birmani

Nabaa Haider Al-shamari

Baidaa Ghalib Al-musawi

Journal Objectives:

1. Preserving And Documenting The Ziyarte Al Arba'een As A Religious-Social Ritual Using The Most Modern Methods Of Documentation And Presentation And Monitoring Its Effects On The Individual And Society.
2. Determine The Basic Requirements For The Ziyarte Al Arba'een And Secure Its Needs In Various Fields And Dimensions.
3. Drawing Inspiration From The Lessons Of Imam Hussein's Revolution In Promoting The Concepts Of Unity And Peace And Confronting The War Of Soft Ideas.
4. Linking Qur'anic, Religious, And Doctrinal Concepts To The Husseini Heritage And The Arba'een Visit To Increase Culture And Awareness Among The Family And Youth.
5. Monitoring The Challenges Facing Visitors In All Service Sectors And Provid-Ing Ways To Address Them And Develop Solutions To Them Scientifically And Practically.
6. Providing Researchers, Readers, And Those Interested In Research And Special-Ized Studies In The Ziyarte Al Arba'een.
7. Seeking To Inform The International Community Of The Importance Of The Visit And Its Community Of Millions; Because It Represents A Cultural And Human Heritage For Iraqi Society In Particular, And Lovers Of Ahl Albayt In General, It Can Also Be A Scientific Resource For Those Interested In Visiting Arba'in And An Important Factor In Preserving The File Of Providing Service And Hospitality At Ziyarte Al Arba'een After It Was Officially Registered In The Unesco Educational, Scientific And Cultural Organization (Unesco). In 2019 Ad, By The Center In Cooperation With The Ministry Of Culture, Tour-Ism And Antiquities.

Journal Vision:

The Arbaeen Peer-Reviewed Scientific Journal Seeks To Be A Scientific Platform For Publishing Research And Studies Related To The Ziyarte Al Arba'een. To Achieve A Scientific Addition For Those Interested In This

Blessed Ritual.

Privacy Policy:

The Arbaeen Peer-Reviewed Scientific Journal Is Characterized By Accuracy, Sobriety, And Confidentiality In Its Work, As It Maintains The Integrity Of The Research It Receives And Is Committed To The Privacy Of The Data And Information That The User Sends, Without Disclosing It To Any Party.

Publishing Policy In The Journal:

The Peer-Reviewed Scientific Journal Al-Arbaeen Welcomes The Productions Of Researchers From Inside And Outside Iraq, And Publishes Their Research Across Various Humanitarian, Scientific And Applied Specializations In Arabic And English, Most Notably: (Social Studies And Anthropology, Cultural, Intellectual And Ideological Studies, Historical And Heritage Studies, Geographical And Spatial Studies, Economic And Tourism Studies, Legal And Regulatory Studies, In Accordance With The Following Rules:

1. The Research To Be Published Must Be Distinct And New In Its Subject Matter And Fulfill The Conditions Of The Approved Scientific Research Method.
2. The Research Must Not Be Published In A Journal Inside Or Outside Iraq, Or Taken From A Book, Or Copied From The International Information Network (The Internet), Provided That The Researcher Submits A Written Pledge To That Effect To Be Attached To The Research. The Research Must Be Returned To The Researcher If The Degree Of Detection Of Plagiarism Is More Than 20%.
3. The Research Must Be Free Of Linguistic And Grammatical Errors, Considering Accuracy In Style.
4. The Researcher Adheres To The Technical Conditions Followed In Writing Scien-Tific Research In Terms Of Arrangement And Organization.
5. Be Sure To Place Maps, Pictures, And Tables In Their Place Wherever They Appear In The Research Text.
6. The Research Is Submitted To The Editorial Board Printed On The Word System, A4 Paper, With A Cd Containing The Research Material, The Font

Style (Times New Roman), And The Font Size (14) For Arabic Research And (12) For The Eng-Lish Language, Provided That The Research Pages Do Not Exceed 1. (25) Pages And More Than That, The Researcher Is Responsible For Paying His Financial Dues, And They Must Not Be Less Than (10) Pages.

7. The Sources Must Be Placed At The End Of The Research In Alphabetical Order, And Their Arrangement Must Be Followed In The Usual Ways In Writing Scien-Tific Sources, As Follows: Title, Name Of The Author, Name Of The Book, Name Of The Investigator (If The Book Is Verified), Edition Number, Name Of The Printing Press, Place Of Publication, Year Of Publication.

8. Formatting The Footnotes According To The Implicit System (Apa) In Accord-Ance With The Standards Approved By The Ministry Of Higher Education And Scientific Research.

9. The Researcher Must Attach With His Research A Summary Of His Scientific Biography, If He Is Dealing With The Journal For The First Time.

10. The First Page Of The Research Should Contain The Following Information: The Researcher's Address, Name, Place Of Work, Phone Number, And E-Mail, Considering Not Mentioning The Name Of The Researcher Or Researchers In The Body Of The Research Or Any Reference To That In Arabic Or English, As In The Journal's Template.

11. All Research Is Subject To Confidential Scientific Evaluation By The Editorial Board And A Large Group Of Professors In Various Scientific Specializations, To Indicate The Validity Of Its Publication. Research Is Not Returned To Its Own-Ers, Whether It Is Accepted For Publication Or Not, According To The Following Mechanism:

- The Researcher Will Be Informed Of The Receipt Of The Material Sent For Pub-Lication Within A Maximum Period Of Two Weeks From The Date Of Receipt.

- Authors Of Research Accepted For Publication Shall Be Notified Of The Edito-Rial Board's Approval For Publication.

- Research That The Evaluators Deem Necessary To Make Amendments Or Addi-Tions To Before Publication, Will Be Returned To Their Owners With Specific Comments To Make Final Amendments To Them.

- Rejected Research Will Be Notified To Its Authors Without The Need To Pro-Vide Reasons For Rejection.

- Each Researcher Is Given One Copy Of The Issue In Which His Research Was Published Electronically Or In Paper.

12. The Order Of Published Research Is Subject To Technical Requirements, And The Priority Of Publication Considers The Following:

- The Date The Editor-In-Chief Received The Research.

- The Date Of Submission Of The Research That Is Being Modified.

- Scientific Title Of The Researcher.

13. The Researcher May Not Request That His Research Not Be Published After Sub-Mitting It To The Editorial Board, Except For Reasons Of Which The Editorial Board Is Convinced, If It Is Within A Period Of Two Weeks From The Date Of Submission Of His Research.

14. The Arbaeen Peer-Reviewed Scientific Journal Is Committed To Preserving The Intellectual Property Rights Of Authors.

15. The Author Grants Exclusive Rights To The Journal, Including Publication, Paper And Electronic Distribution, Storage, And Reuse For Research.

16. Research Papers Should Be Sent To The E-Mail Address Of The International Peer-Reviewed Scientific Journal:

Arbnj.k.center@Gmail.com

For Inquiries, Call:

00964775332066

Journal Adress

Iraq - Holy Karbala - Bab Baghdad - Sayyida Zainab Al-Kubra Street

Karbala Center For Studies And Research - Arbaeen Visitation Division.

All opinions expressed in this journal express the opinions of its authors and do not necessarily reflect the vision of the journal.

بسم الله الرحمن الرحيم

جمهورية العراق
وزارة التعليم العالي والبحث العلمي
دائرة البحث والتطوير
قسم الشؤون العلمية

Republic of Iraq
Ministry of Higher Education & Scientific Research
Research & Development Department

الرقم: ب ت ع/ ٥٦٢٥
التاريخ: ٢٠٢٣/٧/٤

No.:
Date:

الامانة العامة للعتبة الحسينية المقدسة / مركز كربلاء للدراسات والبحوث

م/ مجلة الاربعين

السلام عليكم ورحمة الله وبركاته

اشارة الى كتابكم المرقم م/٤٨١ بتاريخ ٢٠٢٣/٣/٨ ، والمتضمن استحداث واعتماد مجلتكم لاغراض النشر والترقيات العلمية وتسجيلها ضمن موقع المجلات الاكاديمية العلمية العراقية ، حصلت الموافقة بتاريخ ٢٠٢٣/٦/٢١ على أعتماد المجلة المذكورة في الترقيات العلمية والنشاطات العلمية المختلفة الاخرى ، واعتباراً من المجلد الاول – العدد الصفري - آذار- لسنة ٢٠٢٣ لتسجيل المجلة في موقع المجلات الاكاديمية العلمية العراقية.

للتفضل بالاطلاع وابلاغ مخول المجلة لمراجعة دائرتنا لتزويده بأسم المستخدم وكلمة المرور ليتسنى له تسجيل المجلة ضمن موقع المجلات الاكاديمية العلمية العراقية وفهرسة اعدادها ، ويعتبر ذلك شرطاً أساسياً في أعتمادها بموجب الفقرة (٣١) من ضوابط استحداث واصدار المجلات العلمية في وزارتنا.

...مع وافر التقدير

أ.د. لبنى خميس مهدي
المدير العام لدائرة البحث والتطوير
٢٠٢٣/ ٧ /٤

نسخة منه الى:
- مكتب السيد وكيل الوزارة لشؤون البحث العلمي/ أشارة الى موافقة سيادته المذكورة أعلاه والمثبتة على أصل مذكرتنا المرقمة ب ت م/٥٠٩١/٤ في ٢٠٢٣/٦/٢١
- قسم الشؤون العلمية/ شعبة التأليف والترجمة و النشر.... مع الاوليات
- الصادره

مهند ابراهيم
٦/٢٦ – ٧/٣

International accreditation certificate for the Karbala Center for Studies and Research from UNESCO (Global Memory Program)

Approval date: 102014/28/ AD

United Nations Educational, Scientific and Cultural Organization

Intangible Cultural Heritage

Convention for the Safeguarding of the Intangible Cultural Heritage

The Intergovernmental Committee for the Safeguarding of the Intangible Cultural Heritage has inscribed

Provision of services and hospitality during the Arba'in visitation

on the Representative List of the Intangible Cultural Heritage of Humanity upon the proposal of Iraq

Inscription on this List contributes to ensuring better visibility of intangible cultural heritage and awareness of its significance, and to encouraging dialogue that respects cultural diversity

Date of inscription

12 December 2019

Director-General of UNESCO

Certificate of registration for the file (providing service and hospitality during the Arba'een Ziyarte) registered by the Karbala Center for Studies and Research in cooperation with the Ministry of Culture, Tourism and Antiquities of the Educational, Scientific and Cultural Organization (UNESCO) On 1416- December 2019

Contents

Study of Hiding Text Messages 21
Prof. Dr. Hiba Khudair Abbas Jasem Al-Jubouri , Prof.Sameera Naji Kadhem
Asst. Prof. Dr. Haidar Jawad Mohammed

Dynamics of Crowds on The Road Between The Two Holy Mosques. 57
Asst.Prof.Dr. Maan A. Rasheed, Asst.Lect .Hiba Ali Kareem

Developing of an Integrated Framework Leveraging Statistical Analysis and Deep Learning Techniquesto Optimize Transportation Servicesfor Arbaeen Visitors.....77
Prof.Samira Naji Kadhim , Asst.Prof.Asraa Muayed Abdalah

Arbaeen Pilgrimage: surveillance and control of Microbial infections: A review.....99
Prof.Dr.Qais Gheema, Prof.Dr.Abdul Ameer Gharib

The Best routes to placement the Piezoeleric in holy Karbala using remote sensing and GIS techniques 131
Prof . Ebtesam F. khanjer , Asst.Lect.Mustafa S. Srayyih
Prof .Ban A. Al-Razaq , Khudhur Ahmed Hussein

Spatial-Temporal Distribution of Particulate Matter in holy Karbala Governorate by using Remote Sensing Dataset and GIS.....143
Prof.Sabah Hussien Ali , Asst.Prof.Alaa Nabeel Hamdon
Asst.Prof Abdulrahman Ramzi Qubaa

Semi-Annual Scientific Journal
www.arbnj.com
Ramadan 1447 A.H, March 2026 A.D

Design of New Cryptosystem to Protect the Transmitted Data for Imam Hussein's Visitors or Protection Units.....163
Prof.Faez Hassan, Prof. Samira Naji Kadhim , Asst.Dr.Adnan Mohammed Ali

Utilising Piezoelectric Technology of Energy Harvesting from Human Footsteps: Arbaeen-Karbala as an Application Model Case Study.....183
Asst. Prof. Dr. Israa Badr Al-Mashhadani , Asst. Lecturer Lara Muwafaq
Assoc. Prof. Dr. Najah Abd , Prof. Qusay Yaseen , Ahmed Aliwi Abdul Ridha

Using Machine Learning for Detecting and Mitigating Cyber Threats in IOT Dvices Deployed During the Arbaeen Pilgrimage.....217
Asst. Prof.rD.Yusra Abdul Sahib Saifuddin , Asst. Lecturer Abeer Issa Abd
Asst. Lecturer Fadhel Jabbar Kazem , Asst. Lecturer Ghufran Ali Imran

The Path And Landing Places On The Road Of Imam Hussein From Mecca To Karbala: A Modern And Satellite-Bas Study A proach.....251
Asst.Prof.Dr.Abdulkareem Abd Ali , Dr.Parviz Tarikhib

The influence of environmental conditions and human congregation on the immune system response: systematic review article 299
Asst. Prof. Dr. Wasan adai Al-Marsoumi.

Design of A Freshwater Production System Based on Solar Energy.....321
Asst. Prof.Dr. Firas Abdulrazzaq Hadi , Rounaq Adel Abdulwahab
Mustafa Sinan Fadhil

Recycling the PET plastic bottle waste accumulated during the Arabian Pilgrimage into 3D printing filament to print durable material models and use them in designs that support the eternal memory.....337
Asst prof .Dr.Samara Jasim Mohammad , Yaqeen Ammar Mahdi

Sustainable Plastic Waste Management During the Arbaeen Pilgrimage: Cost-Effective Strategies for Recycling PET Water Bottles.....357
Asst.Lect.Ali Saadi Abd , Asst. Prof.Dr. Israa Badr Al-Mashhadani
Asst.Lect. Lara Muwafaq Falah , Asst.Lect.Faten alkubaisy

Leveraging Doppler Satellite Remote Sensing to Assess Spatiotemporal Air Qualit Dynamics inthe Baghdad-Karbala-Najaf Urban Corridor.....375
Asst.Dr. Hasan Jaber Atta , Asst.Prof.Dr.Najah Abd , Tabarak Al-Kanani

Intelligent crowd monitoring and prediction system during the Arbain Pilgrimage using digital twin simulation 397
Asst.Dr. Zainab Hussam Al-Araji , Prof. Dr. Samira Naji Kadhim
Prof. Dr. Alexey Viktorovich Bashkirov2

Designing an intelligent electronic system for Disaster Management and visitor protection in the Arbain Pilgrimage using artificial intelligence and the Internet of Things (AIoT)technologies (AIoT).....427
Asst.Dr.Zainab Hussam Al-Araji , Asst. Prof. Dr. Nisreen kh. Abdalameer

Using Drones to Fix GPS Coordinates of Holy Shrines: Imam Hussein and Imam Abbas 459
Asst. Dr .Hussein Tbena Kadhim , Asst.Lect.Bassad Mohamed ,
Saud Syed Niyasudin

Semi-Annual Scientific Journal
www.arbnj.com
Ramadan 1447 A.H, March 2026 A.D

Monitoring and Analyzing Crowd Dynamics during the Arbaeen Ziyarat in the Karbala Using Satellite Imagery Techniques.....477
Dr. Malik Rasheed Abbas , Assoc. Prof.Dr. Aleh Akbari , Zaid Ali Mo'nis

Utilizing Image Processing Algorithms and Remote Sensing Technique for Proposing Solar Cell Sites Along the Pilgrimage Route from Baghdad to Karbala 501
Asst.Lect.Noor Ali Hameed , Prof.Dr. Jafar Fadel Ouda
Asst.Lect. Mohammed Ahmed Mohammed , Asst.Lect.Abdulrahman Bilal Ali

Editorial of the issue

In the Name of God, the Most Gracious, the Most Merciful Praise be to God, Lord of the Worlds, and may blessings and peace be upon the guiding and faithful Prophet, Abu Al-Qasim Muhammad, and upon his pure and virtuous family and companions.

The Arbaeen pilgrimage is a prominent religious and social occasion observed on the twentieth day of Safar each Hijri year. Given the profound religious, social, educational, and ethical significance of this event, which attracts millions of participants, and its role as a marker of cultural and civilizational identity for the followers of Ahl al-Bayt (peace be upon them), the Karbala Center for Studies and Research at the Holy Shrine of Imam Hussein has devoted considerable attention to this blessed ritual.

With the objective of preserving the heritage of the Arbaeen pilgrimage, the initiative to establish this academic journal emerged. This journal represents a foundational step toward addressing Arbaeen-related matters through scientific and academic research.

From this perspective, the idea of establishing this scholarly journal emerged, representing the nucleus of academic and scientific engagement with issues related to Arbaeen. This commitment was clearly demonstrated through the organization of the International Scientific Conference on Arbaeen by the Center, in its nine editions, which witnessed wide participation from specialists across various fields through precise scientific research and studies covering multiple aspects of this blessed pilgrimage.

Accordingly, the "Vol.4, Supplement (9) / 4th year " of the Arbaeen Journal aims to comprehensively reinforce multidisciplinary scientific approaches in the study of Arbaeen as a major human phenomenon that intersects religious, social, media, security, and developmental dimensions. This issue addresses topics such as discourse, communication, and influence,

Semi-Annual Scientific Journal
www.arbnj.com
Ramadan 1447 A.H, March 2026 A.D

in addition to crowd organization and human flow management based on scientific principles, while highlighting the importance of comprehensive and digital security in supporting stability, and emphasizing the utilization of modern technologies and innovation to serve people, the city, and the event.

The goal of this work is to deepen understanding of the Arbaeen pilgrimage and provide a scientific perspective that supports planning and decision-making. We hope that this journal will provide meaningful insights for readers and serve as a significant contribution to the Arabic and Islamic scholarly tradition.

Praise be to Allah, the Lord of the Worlds.

Scientific Committee of the Conference

managing editor

1447 AH – 2026 AD

Study of Hiding Text Messages Technique in Digital Images

Prof. Dr. Hiba Khudair Abbas Jasem Al-Jubouri

Al-Mustansiriyah University / College of Science / Department of Physics

Hebaka_phys@csw.uobaghda.edu.iq

Prof.Sameera Naji Kadhem

University of Baghdad / College of Science for Women / Department of Mathematics

Samirank_math@csw.uobaghdad.edu.iq

Asst. Prof. Dr. Haidar Jawad Mohammed
Al-Mustansiriyah University / Department of Physics

haidar.mohamad@uomustansiriyah.edu.iq

Abstract:

Steganography is a data security method that conceals information within a medium, ensuring no suspicion about a link between two parties. During the Arbaeen pilgrimage, a study used the least significant bit (LSB) concealment method, extracting letters from text within a coloured digital image, converting them into binary numbers, and embedding them within the image. This process resulted in an image containing textual information, allowing comparison with the original image to observe additive noise differences. The most significant noise effects were observed in homogenous areas and edge regions, with a pronounced impact of masking across all color packets. The study used statistical metrics like mean square error (MSE) and peak-to-noise ratio (PSNR) to analyze the quality and effectiveness of the outputs. The best stenographic effect occurs when the message size is small, the image size is large, and there are fewer bits to be hidden. The best reduction effect is achieved when the message size is small and the image size is large, with fewer bits to hide. The blue, red, and green bars exhibit the best steganography effects, ensuring the security of pilgrims in Karbala Governorate and elsewhere, and facilitating easy and secure data transmission.

Keywords: Cryptography, Steganography, Least Significant Bit Strategy, Statistical Detection

Introduction

Interpersonal communication is one of the most crucial aspects of human growth (Suresh & Parthasarathy, 2016). The secrecy of the data being communicated is necessary for this operation (Al-Saedi, 2016). Humans have looked for different strategies to guarantee the quick transfer of information (Resham et al., 2021). Information security and secrecy are maintained using various methods, including steganography and encryption (Iacovitti, 2022). The encryptor can now access and change data thanks to the development of hacking techniques (Clemen & Teleron, 2023). Information preservation required a more secret method (Abbas et al., 2021). Thus, steganography was employed, which hides the transferred data inside the transmitted media—text, music, pictures, and videos —so that no one can see it (Muhammad et al., 2015). The science of encrypting and decrypting data using mathematics is known as cryptography. Only the intended recipient may access sensitive data stored or sent over unprotected networks (like the internet) thanks to cryptography (Habeeb, 2020). Both cryptography and cryptanalysis are included in cryptography (Mustafa, 2020). Strong and poor encryption are both possible. The amount of time and resources needed to retrieve the plaintext is a measure of an encryption's strength(Derea et al., 2019). Strong encryption produces ciphertext that is challenging to decode without the right decryption software (Hassan & Gutub, 2021). The strength of the encryption algorithm and the key's secrecy are the only factors that affect the security of encrypted data (Khaldi, 2019). The technique of hiding a secret communication behind another harmless medium (text, image, sound, video, etc.) is called steganography (Greek: מראורה, meaning cover, and graphein, meaning writing). Security in steganography depends on the likelihood that a secret message won't be detected or found, whereas, in cryptography(Al-Obaidi et al., 2023),

security depends on the encrypted information being unintelligible to unauthorized individuals (Kim et al., 2021). Modifying portions of a chosen file's code is required to embed a message. Making these modifications undetectable or inaudible is the fundamental goal of steganography. The risk of modification will go unnoticed and increases with the message and file size (Jawad et al., 2022). Three factors form the basis of steganography properties: Robustness guarantees that confidential data cannot be erased without seriously harming the reputation (Mohamad et al., 2019).

This field has been investigated by several academics. In (2022), Nada Abdul Aziz Mustafa generates a practical steganography procedure to hide the text in the image. This operation allows the user to provide the system with both text and cover image, and to find a resulting image that comprises the hidden text inside. The suggested technique is to hide text inside the header formats of a digital image. The Least Significant Bit (LSB) method to hide the message or text, to keep the features and characteristics of the original image are used. A new method is applied using the whole image (header formats) to hide the image. From the experimental results, the suggested technique gives a higher embedding of several stages of complexity. Also, the LSB method uses the whole image to increase the security and robustness of the proposed method as compared to state-of-the-art methods (Abdul & Mustafa, 2022). In (2024), Ali Salem Ali and Suray Alsamaraee proposed a scheme consisting of four phases with different contributions. The first phase was used to preprocess the secret messages and cover images. In this phase, the confidential message is compressed using the Huffman method. The second phase involved the embedding procedure. This phase consists of HMPSO and DDV contributions. The HMPSO is responsible for the optimal pixels' selection. The DDV contribution is responsible for the embedding process. The third

phase involves the extraction method. In extraction, the reverse processes are implemented in the previous steps. SSIM, PSNR, HVS, Histogram analysis, and chi-square test were used to validate and test different evaluation parameters. Based on the findings, the proposed scheme has solved the privacy, and integrity challenges and provides a robust steganography system (Ali et al., 2024).

This research aims to employ varying levels of text concealment in digital photographs, thereby enhancing the secrecy of the concealed data and making it more challenging to recover, especially in Arbaeen pilgrimage. The program was created to solve the data masking and retrieval operation. To include information in a particular medium without raising suspicions about correspondence between two parties, one method used to protect information is the act of hiding. In this case, it is easy to send sensitive information without discovering during Arbaeen pilgrimage.

Theoretical Background

Least Significant Bit (LSB):

LSB gathers everything related to data concealment by modifying the low-order bit of an element. Modification of the value of a pixel or the modification of the value of a DCT coefficient in the case of the JPEG standard (Abbas & Mohamad, 2021). All are based on the insensitivity of the human visual system to a small change in colors. There are two LSB methods: LSB replacement consists of substituting the least significant bits of the pixels for the message bits to be inserted. LSB matching steganography, Least Significant Bit (LSB) matching steganography, also named ±1 embedding, is a slightly more sophisticated version of LSB embedding. The LSB correspondence steganography method does not alter

the first order statistical distribution of the host support. So All first-order statistical attacks are ineffective, Least Significant Bit Strategy Spatial (Image) domain strategy: in image domain, the LSB technique is the most important and the easiest one to embed information in a cover image. Popular stenographic tools that are based on LSB embedding vary in their approach for hiding information. Methods like Steganos and Stools use LSB embedding in the spatial domain, while others like Jsteg and Out-Guess embed the message in the frequency domain(Awad et al., 2018). With a well-chosen image, one can even hide the message in the least as well as second to least significant bit and still not see the difference and Transform domain strategy: these strategies based on hiding information in more significant areas of the cover image making it more robust.

Algorithms of the hiding text:

ALGORITHM (I): Hiding the Text Message in One Row in the Color Digital Image

- Step1: Read color digital image I1
- Step2: Choose color band of digital image (R,G,B)
- Step3: Enter the number of bits to be hidden in the text [1 or 2]
- Step4: Determining the hiding location in which bits we want to hide [1 2] In other words, it is the place to hide the first bit and the second bit
- Step5: Select the row in which to hide the text row=50;
- Step6: Steganography Process
  - generate color image at the same color image entering resulting image in which hide the text I2
  - choose a color band (R,G,B) from the generated image in which the text will be hidden
  - Select the text message to be hidden in the image and the color band

- convert haracter in the text message to a binary number with 8 bits using code bins= dec2bin(str,8)
- transform each row into a column and each column is a row bin2
- Making reshap bins=bin2(:)' so that the message is in one line, its kind char, take these bits and hide them in the image
- transform each character into one location that contains each character binv=bins-48; where msg=binv
- determine the length of the text by the number of characters L=numel(str), and the length of the text by binary LL=8*L
- Determine the number of Step that moves through it: step= no. of bits entered* fix (no. of column / LL), where fix () is a function in MATLAB approximates in the positive infinity direction, LL<no. of column
- Specifies the pixel in which to hide the text: A=I2(no. of row, pixel position, band type)
- The pixel value has changed because of masking: A2=bitset(A, location hide bit, no. of bit)
- Repeat the step

– Step7: De- steganography process: To return the text message to characters

- Read steganography image I3
- Read the color band (R,G,B) from I3
- make a counter from 1 to LL step no. of bits
- Image element (pixel) in which text is hidden A1=I1(The number of the row in which it was hidden, position of pixel in the row)
- determine the value of the first bit and the second bit in which the hiding occurred for each element in which the operation was hidden so that generate a vector EE(j)of length LL using code EE(j)=A1; L=length (EE)
- divide it into 8 bits, each 8 bits representing a character NT=round (L/8)
- generate a function to convert each 8 bits into a character using the codeVT=bin2char (TT) where TT=EE(j:j+7)

- Step8: end algorithm

ALGORITHM (II): Hide the Text Message in All Rows of the Color Digital Image

- Step1: Read color digital image I1.
- Step2: Choose color band of digital image (R,G,B).
- Step3: Enter the number of bits to be hidden in the text [1 or 2].
- Step4: Determining the hiding location in which bits we want to hide [1 2] In other words, it is the place to hide the first bit and the second bit.
- Step5: Steganography Process.
  - generate color image at the same color image entered get an image in which hide the text I2
  - choose a color band(R,G,B) from the generated image in which the text will be hidden
  - Select the text message to be hidden in the image and the color band
  - convert each character in the text message to a binary number with 8 bits using code bins= dec2bin(str,8)
  - transform each row into a column and each column is a row bin2=
  - Making reshap bins=bin2(:)' so that the message is in one line, its kind char, take these bits and hide them in the image
  - transform character into one location binv=bins-48; where msg=binv
  - determine the length of the text by the number of characters L=numel(str), and the length of the text by binary LL=8*L
  - Determine the number of Step that moves through it: step= no. of bits entered* fix (no. of column / LL), where fix () is a function in MATLAB approximates in the positive infinity direction, LL<no. of column
  - Make a counter from row; for i=1: r where i counter for row and r no. of row in image
  - Specifies the pixel in which to hide the text: A=I2(i, pixel position,

band type)

- The pixel value has changed because of masking: A2=bitset (A, location hide bit, no. of bit)
- Repeat the step

- Step6: De- steganography process: To return the text message to characters
  - Read steganography image I3
  - Read the color band (R,G,B) from I3
  - make a counter from 1 to LL step no. of bits
  - Image element (pixel) in which text is hidden A1=I1(The number of the row in which it was hidden, position of pixel in the row)
  - determine the value of the first bit and the second bit in which the hiding occurred for each element in which the operation was hidden so that generate a vector EE(j)of length LL using code EE(j)=A1 ; L=length (EE)
  - divide it into 8 bits, each 8 bits representing a character NT=round (L/8)
  - generate a function to convert each 8 bit into a character using the code VT=bin2char(TT) where TT=EE(j:j+7)
- Step7: end algorithm

ALGORITHM (III): Calculation of statistical criteria to evaluate the quality and efficiency of the results

- Step1: read color digital image I1
- Step2: read steganography color digital image I2
- Step3: Calculate Mean Square Error between I1,I2 using MSE = immse(I1,I2)where immse function to calculate mean square error
- Step4: Calculate Peak Signal to Noise Ratio between I1,I2 using PPsnr= psnr(I1,I2)

Experimental steps

Hiding text messages in digital color images. Where it relied on colored digital images of different sizes, and text messages of different lengths were hidden. The process of hiding included two parts:

First was to hide text messages in one row of the colored digital image, and the second part included hiding text messages in all rows of the colored digital image. The quality and efficiency of the images resulting from the steganography process were evaluated based on two statistical criteria (Mean Square Error (MSE) and Peak Signal to Noise Ratio (PSNR))(Abbas et al., 2019). The type of noise that will be caused by the process of adding information was also studied. As well as note the effect of the largest noise on the image and color bands (RGB). The programs were built and developed using MATLAB (2020). The work plan consists of four parts; Part one: It includes the process of hiding text messages of different lengths in one row from the color digital images approved in the study. The second part: includes the process of hiding text messages of different lengths in all the rows of the color digital image approved in the study. The third part includes calculating the statistical characteristics to estimate and know the efficiency of the resulting images. The fourth part includes calculating the difference between the original image and the steganography image, which represents the observation of the effect of noise in the image and color bands (RGB).

Flag Image is downloaded online and used widely during Arbaeen pilgrimage. Image size is (225×225) elements and a gray intensity for each band ranging from (0-255). Bit depth is 24 bits/pixel, and its type is JPG, as shown in figure (1).

Figure (1): Flag color digital image

Text Messages to be hidden in the Image:

Three text messages of different lengths were used to hide them in the digital images adopted in the study

1.The text message is represented by 14 characters that are hidden in the images represented by the text phrase as in Figure (2).

Hello everyone

(a)

(b)

Figure (2): text message with 14 characters (a) decimal and (b) binary data.

Where each decimal character corresponds to 8-bit binary as shown in the table (1).

Table (1): The decimal character and its 8-bit binary equivalent for the message (A)

decimal	Binary	decimal	binary
H	01001000	E	01100101
e	01100101	V	01110110
l	01101100	E	01100101
l	01101100	R	01110010
o	01101111	Y	01111001
	00100000	O	01101111
		N	01101110
		E	01100101

2.The text message is represented by 31 characters that are hidden in the images represented by the text phrase as in Figure (3).

Hello everyone; have good time.

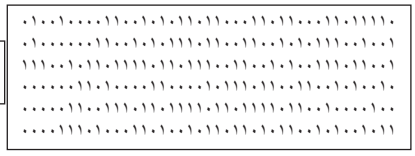

Figure (3): The text massage with 31 characters in (a) decimal and (b) binary data.

Where each decimal character corresponds to 8-bit binary as shown in the table (2).

Table (2): The decimal character and its 8-bit binary equivalent for the message in Figure (3)

decimal	Binary	decimal	binary
H	01001000	h	01101000
e	01100101	a	01100001
l	01101100	v	01110110
l	01101100	e	01100101
o	01101111		00100000
	00100000	g	01100111
e	01100101	o	01101111
v	01110110	o	01101111
e	01100101	d	01100100
r	01110010		00100000
y	01111001	t	01110100
o	01101111	i	01101001
n	01101110	m	01101101
e	01100101	e	01100101
;	00111011	.	00101110
	00100000		

Results and discussion

The most significant findings obtained from the implementation of the hiding operations suggested in the study are discussed to be send in the Arbaeen pilgrimage. Three text messages with a total length of 14, 31 characters were used, and several bits (1 and 2) were concealed in the first and second-bit positions of the pixel. This process includes two methods for hiding information: the first involves hiding text message in a single row of the color digital image, and the second includes hiding the text message in every row of the color digital image. The difference between the original and stenographical images was calculated to note the impact of noise on the image and the color band (RGB). The results were discussed for both methods, which involved applying the steganography process to each band of the color digital image. The effectiveness of the stenographical process's output was assessed using effective statistical criteria (MSE and PSNR)(Derea et al., 2019).

The Results of Hiding Information in One Row of the Color Digital Image:

The information was hidden in one row of the color digital image, as the process included reliance on two text messages and the process of hiding based on one bit and two bits, and this was applied to the approved digital images and their color bands (RGB).

1.The Results of the Hiding Process Based on the Text Message with a Length of 14 Characters and several bits

The hiding process, in (algorithm I), was applied to the digital images approved in the study. The information was hidden in one row, where the length of the text message was 14 characters, and the number of bits was 1.

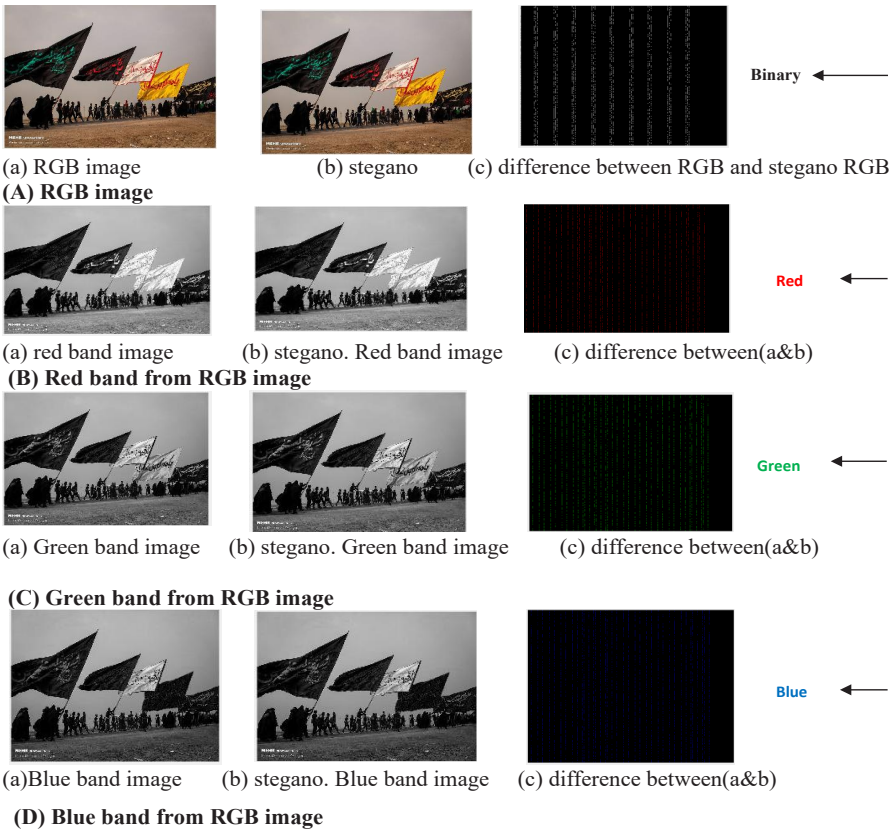

Figure (4): hiding process and difference for a color digital image (A) RGB image, (B) Red band image, (C) Green band image, and (D) Blue band image, From the figures (4), the difference was very clear because of the small size of the image.

Results of Estimation of the Efficiency and Quality of Images:

The results of the resulting images before and after the steganography process, represented by one line of a 14-character message length, were estimated to hide 1 bit in the first and second positions of the pixel, depending on the statistical quality criteria represented by (MSE) and (PSNR) according (algorithm III) as in the table (3).

Table (3): Statistical quality criteria for color images and color bands (massage 14 characters, 1bit)

Color images	MSE	PSNR
Red -band	0.0187	65.4144
Green –band	0.0186	65.4308
Blue-band	0.0189	65.3570

2.The Results of the Hiding Process Based on the Text Message with a Length of 14 Characters and several bits 2

The steganography process (algorithm I) was applied to digital color images when the text message length was 14 characters, and the number of bits was 2.

Results of the steganography process on digital color images:

The algorithm (I) was applied to the certified color digital images, applied to the color bands (RGB) of the image, and calculated the difference between the digital image and the stegano. image, then calculated the difference (noise effect) between the color bands (RGB) and the bands of the image steganography (RGB).

(a) color image (b) stegano (c) difference between RGB and stegano RGB

(A): RGB image

(a) red band (b) stegano (c) difference between (a & b)

(B): Red band from RGB image

(a) Green band (b) stegano (c) difference between (a & b)

(C): Green band from RGB image

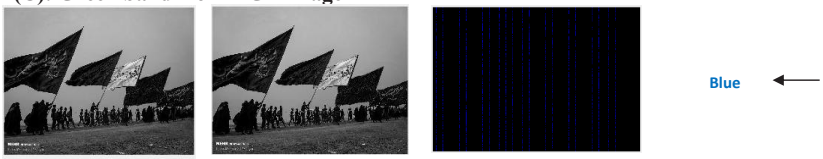

(a)Blue band (b) stegano (c) difference between (a & b)

(D): Blue band from RGB image

Figure (5): hiding process and difference for a color digital image; (A) RGB mage, (B) Red band image, (C) Green band image, and (D) Blue band image, From the results of the images in the figures (4 and 5), the image is clearer in the difference between the original image and the stegano.

Results of Statistical Quality Criteria's

Statistical criteria were calculated for the images before and after the steganography process, represented by hiding information in one row of the image with a 14-character text message to hide 2 bits in the first and second positions of the color digital image element (pixel).

Table (4): Statistical quality criteria (massage 14 characters, 2bits)

Color images	MSE	PSNR
Red –band	0.0396	62.1497
Green –band	0.0399	62.1223
Blue-band	0.0401	62.0945

Where notice that the value of (MSE) is very small and the value of (PSNR) in it is very large and note that the effect of adding information to the image is not equal between color bands (RGB).

The Results of the Hiding Process Based on the Text Message with a Length of (31) Characters and several bits 1.

The hiding process in (algorithm I) was applied to the digital images approved in the study, and the information was hidden in one row, where the length of the text message was 31 characters.

(a) RGB image (b) stegano (c) difference between RGB and stegano RGB

(A) RGB image

(a) red band (b) stegano Red band (c) difference between (a & b)

(B): Red band from RGB image

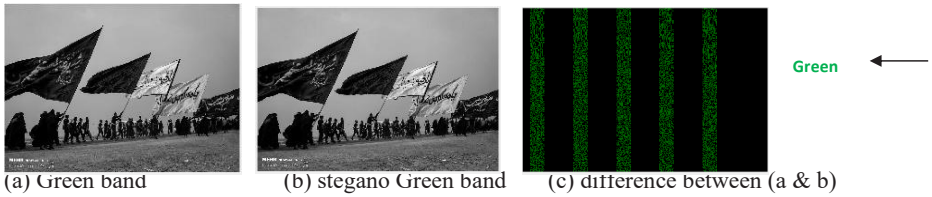

(a) Green band (b) stegano Green band (c) difference between (a & b)

(C) Green band from RGB image

(a)Blue band (b) stegano Blue band (c) difference between (a & b)

(D) Blue band from RGB image

Figure (6): stegano process and difference for a color digital image (A) RGB image, (B)Red band image, (C) Green band image and (D) Blue band image, From the figures (6), the process of hiding between the bands was different, as we notice that the blue band has more concealment, than the red band, then the green band.

Results of Statistical Quality Criteria's

Statistical criteria were calculated for the images before and after the steganography process, represented by hiding information in one row of the image with 31 characters text message to hide 1 bit in the first and second positions of the color digital image element (pixel), as in Table (5).

Table (5): Statistical quality criteria for color images and color bands.

Color images	MSE	PSNR	
Red -band	0.0494	61.1936	31 characters text massage length 1bit
Green –band	0.0492	61.2150	
Blue-band	0.0489	61.2337	

From the results of the table (5), the koala image recorded the lowest value for MSE and the highest value for the criterion PSNR, which confirms that the process of information disappearance in the image with a large size is better than the image of a small size, also note that the process of hiding information in color bands is not equal, as note that the blue band is better at hiding information than red and green, and the green band is not good at hiding information because its MSE value is greater than the rest of the color band values RB.

The Results of the Hiding Process Based on the Text Message with a Length of (31) Characters and several bits 2:

The hiding process in (algorithm I) was applied to the digital images approved in the study, and the information was hidden in one row, where the length of the text message was 31 characters, and the number of bits was 1 for Arbaeen pilgrimage image.

Results of the method applied to approved images:

The steganography method was applied to color digital images by hiding a text message of (31) characters in length in one row of the image, and the number of bits 2 that were hidden in the first and second positions of the image element(pixel), as well as applied to the images of the three-color bands of the image (RGB).

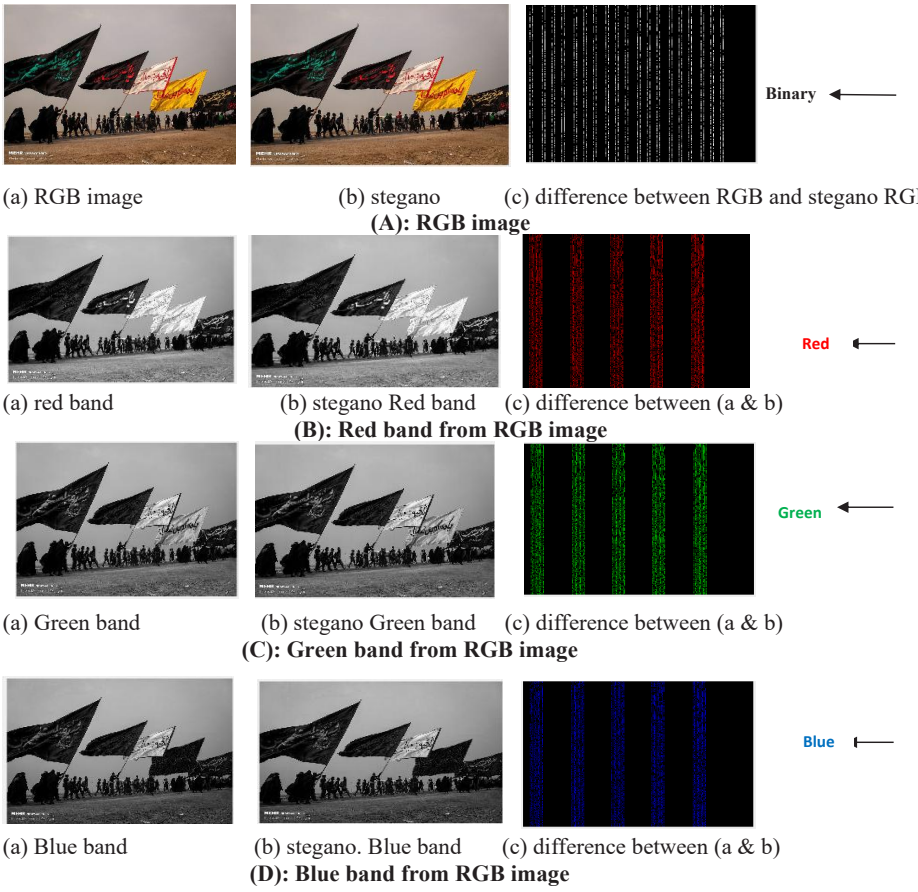

(a) RGB image (b) stegano (c) difference between RGB and stegano RGB

(A): RGB image

(a) red band (b) stegano Red band (c) difference between (a & b)

(B): Red band from RGB image

(a) Green band (b) stegano Green band (c) difference between (a & b)

(C): Green band from RGB image

(a) Blue band (b) stegano. Blue band (c) difference between (a & b)

(D): Blue band from RGB image

Figure (7): stegano process and difference for a olor digital image; (A) RGB image, (B) Red band image, (C) Green band image (D) Blue band image, From Figures (7), the stegano process has become weak, because the image of the difference appeared more clearly than the previous methods, but despite that it also notes that the stegano.

Results of Statistical Quality Criteria's:

Statistical criteria were calculated for the images before and after the steganography process, represented by hiding information in one row of the image with 31 characters text message to hide 2 bits in the first and second positions of the color digital image element(pixel), as in Table (6)

Table (6): Statistical quality criteria for color images and color bands.

Color images	MSE	PSNR	
Red -band	0.01154	57.5088	31 characters text massage length 2 bit
Green –band	0.01146	57.5399	
Blue-band	0.01149	57.5275	

From the results of the table (6), the process of hiding information in color bands is not equal, as note that the green band is better at hiding information than red and blue, and the red band is not good at hiding information because its MSE value is greater than the rest of the color band values.

The Results of Hiding Information in All Rows of the Color Digital Image

The information was hidden in all rows of the color digital image, as the process included reliance on two text messages in Arbaeen pilgrimage image, as well as the process of hiding based on one bit and two bits, and this was applied to the approved digital images and their color bands (RGB).

The Results of the Hiding Process Based on the Text Message with a Length of 14 Characters and several bits 1:

The hiding process in (algorithm II) was applied to the digital images approved in the study, and the information was hidden in all rows, where the length of the text message was 14 characters, and the number of bits was 1.

Results of the method applied to approved images

The second method was applied to the approved color digital images, as well as to the color bands (RGB) dependent on the Arbaeen pilgrimage image, and the difference (noise effect) image was calculated between the digital image and the steganography image, then calculated the difference (noise effect) between the color bands (RGB) and steganography image bands (RGB) as shown in figure (8).

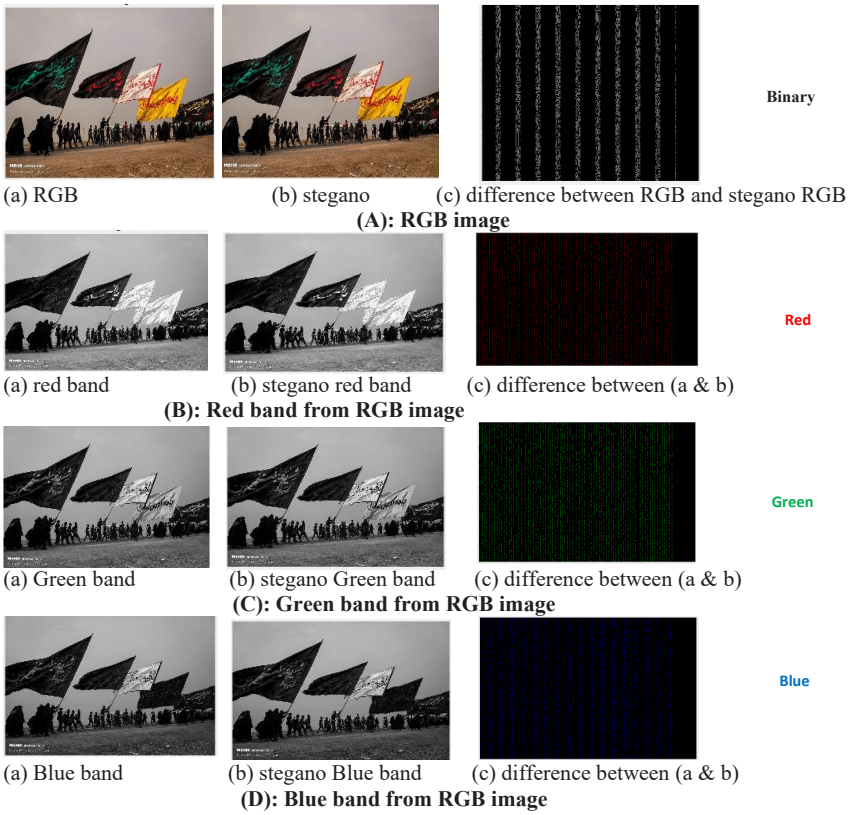

Figure (8): stegano process and difference for a color digital image; (A) RGB image, (B)Red band image, (C) Green band image and (D) Blue band image ,From Figures (8), the difference in the image and color bands was very clear.

Results of Estimation of the Efficiency and Quality of Images:

The results of the resulting images before and after the steganography process, represented by all rows of 14-character message length, were estimated to hide 1 bit in the first and second positions of the pixel, depending on the statistical quality criteria represented by (MSE) and (PSNR) according (algorithm III) as in table (7).

Table (7): Statistical quality criteria for color images and color bands (massage 14 characters, 1bit)

Color images	MSE	PSNR
Red -band	0.03745	62.3957
Green –band	0.03737	62.4051
Blue-band	0.03745	62.3953

From the results of table (7), the noise effect of the color bands (RGB) is not equal. From this can be concluded that the larger the image size, the more efficient and good hiding results.

The Results of the stegano Process Based on the Text Message with a Length of 14 Characters and several bits 2.

The steganography process (algorithm II) was applied to digital color images when the text message length was 14 characters, and the number of bits was 2.

Results of the steganography process on digital color images:

Algorithm (II) was applied to the certified Arbaeen pilgrimage digital image, applied to the color bands (RGB) of the image, and calculated the difference between the digital image and the stegano. Then calculated the difference (noise effect) between the color bands (RGB) and the bands of the image steganography (RGB), as shown in Figure (9).

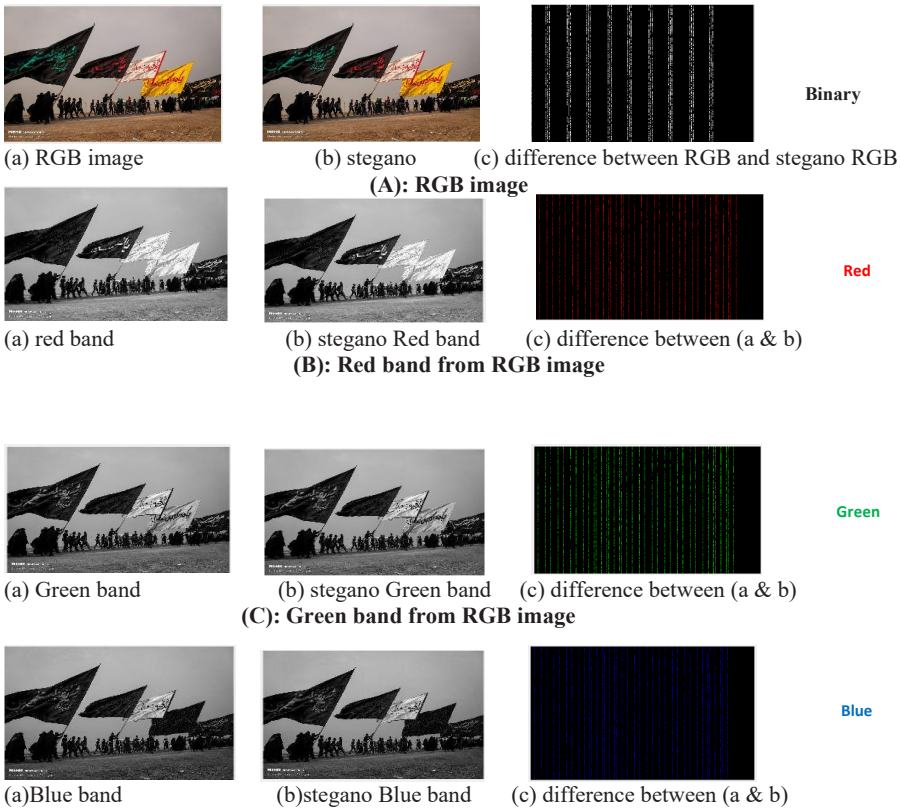

(a) RGB image (b) stegano (c) difference between RGB and stegano RGB

(A): RGB image

(a) red band (b) stegano Red band (c) difference between (a & b)

(B): Red band from RGB image

(a) Green band (b) stegano Green band (c) difference between (a & b)

(C): Green band from RGB image

(a)Blue band (b)stegano Blue band (c) difference between (a & b)

(D): Blue band from RGB image

Figure (9): stegano process and difference for a color digital image (A) RGB image, (B) Red band image, (C) Green band image and (D) Blue band image

Figure (9): stegano process and difference for a color digital image (A)RGB image, (B) Red band image, (C) Green band image and (D) Blue band image, From the results of the images in the figures (9), the sharpness of the difference increased between the original image and the steganography image, as the difference in image was very large and clear and in all rows of the image.

Results of Statistical Quality Criteria's

Statistical criteria were calculated for the images before and after the steganography process, represented by hiding information in all rows of the image with 14-character text message to hide 2 bits in the first and second positions of the color digital image element (pixel), as in Table (8).

Table (8): Statistical quality criteria for color images and color bands (massage 14 characters, 2bits)

Color images	MSE	PSNR
Red -band	0.0806	59.0664
Green –band	0.0797	59.1136
Blue-band	0.0805	59.0727

From the results of the table (8), the process of hiding the message in the image, where notice that the value of (MSE) very small and the value of (PSNR) in it is very large and note that the effect of adding information to the image is not equal between color bands (RGB).

The Results of the Steganography Process Based on the Text Message with a Length of (31) Characters and several bits 1

The process of masking in (Algorithm II) was applied to the digital images adopted in the study, and information was hidden in all rows, where the length of the text message was 31 characters, and the number of bits was 1 for Arbaeen pilgrimage image.

Results of the method applied to approved images:

The steganography method was applied to color digital images by hiding a text message of (٣١) characters in length in all rows of the Arbaeen pilgrimage image, and the number of bits that were hidden in the first and second positions of the image element (pixel), as well as applied to the images of the three color bands of the image (RGB), as shown in Figures (10).

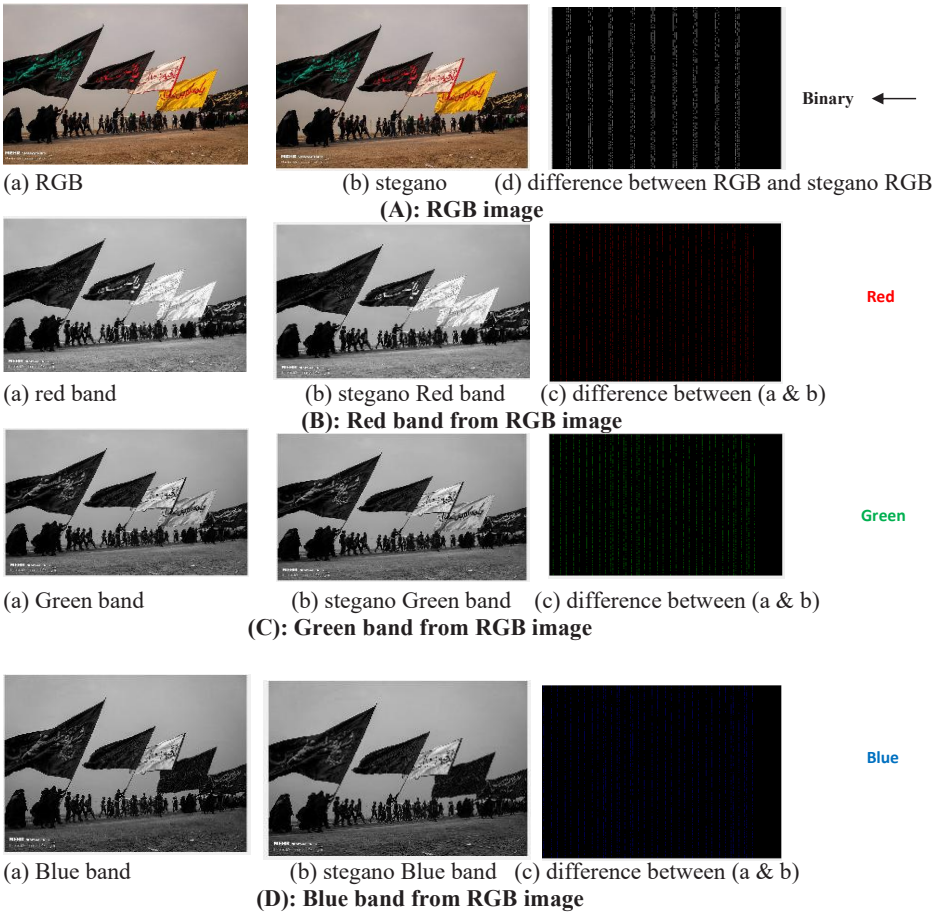

(a) RGB (b) stegano (d) difference between RGB and stegano RGB

(A): RGB image

(a) red band (b) stegano Red band (c) difference between (a & b)

(B): Red band from RGB image

(a) Green band (b) stegano Green band (c) difference between (a & b)

(C): Green band from RGB image

(a) Blue band (b) stegano Blue band (c) difference between (a & b)

(D): Blue band from RGB image

Figure (10): stegano process and difference for a olor digital image (A) RGB image, (B) Red band image, (C) Green band image and (D) Blue band image

Results of Statistical Quality Criteria's

Statistical criteria were calculated for the images before and after the steganography process, represented by hiding information in one row of the image with a 31-character text message to hide 1 bit in the first and second positions of the color digital image element(pixel), as in Table (9).

Table (9): Statistical quality criteria for color images and color bands.

Color images	MSE	PSNR	
Red -band	0.018691	65.4144	31 characters text massage length 1bit
Green –band	0.018620	65.4308	
Blue-band	0.018940	65.3569	

From the results of the table (9), which note that the process of hiding information in color bands is not equal, as note that the green band is better at hiding information than red and blue, because its MSE value is greater than the rest of the color band values RB.

The Results of the Hiding Process Based on the Text Message with a Length of (31) Characters and several bits 2:

The hiding process in (algorithm II) was applied to the digital images approved in the study, and the information was hidden in one row, where the length of the text message was 31 characters, and the number of bits was 2 for Arbaeen pilgrimage image.

Results of the method applied to approved images

The steganography method was applied to color digital images by hiding a text message of (31) characters in length in one row of the image, and three-color bands of the image (RGB), as shown in Figures 11.

(a) RGB image (b) stegano (c) difference between RGB and stegano RGB

(A): RGB image

(a) red band (b) stegano Red band (c) difference between (a & b)

(B): Red band from RGB image

(a) Green band (b) stegano Green band (c) difference between (a & b)

(C): Green band from RGB image

(a) Blue band (b) stegano Blue band (c) difference between (a & b)

(D): Blue band from RGB image

Figure (11): stegano process and difference for a color digital image (A) RGB image, (B) Red band image, (C) Green band image and (D) Blue band image, From Figures (11), can be seen that the stegano process has become weak, because the image of the difference appeared more clearly than the previous methods, but despite that also note that the stegano.

Results of Statistical Quality Criteria's

Statistical criteria were calculated for the images before and after the steganography process, represented by hiding information in one row of the image with a (31)-character text message to hide 2 bits in the first and second positions of the color digital image element(pixel), as in Table (10).

Table (10): Statistical quality criteria for color images and color bands

Color images	MSE	PSNR	
Red -band	0.03963	62.14966	31 characters text massage length 2 bit
Green –band	0.03988	62.12226	
Blue-band	0.04014	62.09449	

From the results of the table (10), notice that the koala image recorded the lowest value for (MSE) and the highest value for the criterion(PSNR), which confirms that the process of information disappearance in the image with a large size is better than the image of a small size, also note that the process of hiding information in color bands is not equal, as note that the blue band is better at hiding information than red and green, and the green band is not good at hiding information because its(MSE) value is greater than the rest of the color band values(RB).

Conclusions

The Iraqi government prioritizes hiding information within images during the Arbaeen pilgrimage. The best method is to use color digital images, with larger images requiring less bit hiding and smaller message sizes. Steganography in color bands is uneven, with the best hiding in blue, red, and green bands. Hiding information in one row is better than hiding all rows. The length of the text message should match the image size. The Arbaeen pilgrimage image had minimal information hiding due to its small size and few features and colors. Steganography results with 1 bit masking are better than masking with 2 bits. The MSE for 1 bit in 14 characters is 0.0186 and PSNR is 65.4308, while if the 14 characters are inserted in all rows, the MSE is 0.03745 and PSNR is 62.4051. It means the change in the image details are changed and the is a small noise appearing in the resulting image because of the added information. The new ideas located in testing audio, video, and high text information. Then trying to adopt different methods to hide security data in Arbaeen pilgrimage. Moreover, trying different locations in the image to hide the text information.

References

1. Abbas, H. K., Al-Saleh, A. H., Mohamad, H. J., & Al-Zuky, A. A. (2021). New algorithms to Enhanced Fused Images from Auto-Focus Images [Article]. Baghdad Science Journal, 18(1), 124-131. https://doi.org/10.21123/bsj.2021.18.1.0124
2. Abbas, H. K., & Mohamad, H. J. (2021). Feature extraction in six blocks to detect and recognize english numbers [Article]. Iraqi Journal of Science, 62(10), 3790-3803. https://doi.org/10.24996/ijs.2021.62.10.37
3. Abbas, H. K., Mohamad, H. J., Al-Saleh, A. H., & Al-Zuky, A. A. (2019). Modelling vision angles of optical camera zoom using image processing algorithm. IOP Conference Series: Materials Science and Engineering,
4. Abdul, N., & Mustafa, N. (2022). An Improved Method for Hiding Text in Image Using Header Image. Wasit Journal of Computer and Mathematics Science, 1. https://doi.org/10.31185/wjcm.79
5. Al-Obaidi, F. E. M., Salman, S. S., Al-Saleh, A. H., Al-Zuky, A. A. D., & Abbas, W. A. (2023). Real-Night-time Road Sign Detection by the Use of Cascade Object Detector. Iraqi Journal of Science, 64(6), 3164-3175. https://doi.org/10.24996/ijs.2023.64.6.43
6. Al-Saedi, A. K. H. (2016). A method to hide text in image. Journal of Missan Researches, 12(24).
7. Ali, A. S., Alsamaraee, S., & Hussein, A. A. (2024). Optimize Image Steganography Based on Distinction Disparity Value and HMPSO to Ensure Confidentiality and Integrity. Journal of Computer Networks and Communications, 2024(1), 2516567. https://doi.org/https://doi.org/10.1155/2024/2516567
8. Awad, R., Al-Zuky, A. A., Al-Saleh, A. H., & Mohamad, H. J. (2018). Enhance Video Film using Retnix method. Journal of Physics: Conference Series,

9. Clemen, J. M., & Teleron, J. (2023). Advancements in Encryption Techniques for Secure Data Communication. International Journal of Advanced Research in Science, Communication and Technology, 444-451. https://doi.org/10.48175/IJARSCT-13875

10. Derea, A. S., Abbas, H. K., Mohamad, H. J., & Al-Zuky, A. A. (2019). Adopting Run Length Features to Detect and Recognize Brain Tumor in Magnetic Resonance Images. 1st International Scientific Conference of Computer and Applied Sciences, CAS 2019,

11. Habeeb, A. (2020). A New Method for Hiding Text in a Digital Image. Journal of Southwest Jiaotong University, 55. https://doi.org/10.35741/issn.0258-2724.55.2.4

12. Hassan, F. S., & Gutub, A. A.-A. (2021). Improving data hiding within colour images using hue component of HSV colour space. CAAI Trans. Intell. Technol., 7, 56-68.

13. Iacovitti, G. (2022). How technology influences information gathering and information spreading. Church, Communication and Culture, 7(1), 76-90. https://doi.org/10.1080/23753234.2022.2032781

14. Jawad, E. M., Daway, H. G., & Mohamad, H. J. (2022). Retinal Image Enhancement by using Adapted Histogram Equalization based on Segmentation and Lab Color Space [Article]. International Journal of Intelligent Engineering and Systems, 15(3), 614-622. https://doi.org/10.22266/ijies2022.0630.52

15. Khaldi, A. (2019). Steganographic Techniques Classification According to Image Format. International Annals of Science, 8, 143-149. https://doi.org/10.21467/ias.8.1.143-149

16. Kim, C., Yang, C.-N., Baek, J., & Leng, L. (2021). Survey on Data Hiding Based on Block Truncation Coding. Applied Sciences.

17. Mohamad, H. J., Hashim, S. A., & Al-Saleh, A. H. (2019). Recognize printed Arabic letter using new geometrical features [Article]. Indonesian Journal of Electrical Engineering and Computer Science, 14(3), 1518-1524. https://doi.org/10.11591/ijeecs.v14.i3.pp1518-1524

18. Muhammad, K., Ahmad, J., Farman, H., & Zubair, M. (2015). A Novel Image Steganographic Approach for Hiding Text in Color Images using HSI Color Model. ArXiv, abs/1503.00388.

19. Mustafa, N. (2020). Text hiding in text using invisible character. International Journal of Electrical and Computer Engineering (IJECE), 10, 3550. https://doi.org/10.11591/ijece.v10i4.pp3550-3557.

20. Resham, N. H., Abbas, H. K., Mohamad, H. J., & Al-Saleh, A. H. (2021). Noise Reduction, Enhancement and Classification for Sonar Images [Article]. Iraqi Journal of Science, 62(11), 4439-4452. https://doi.org/10.24996/ijs.2021.62.11(SI).25

21. Suresh, D., & Parthasarathy, K. A. (2016). Secret data hiding with images using data compression and embedding algorithm. IIOAB, 7, 144-151.

Dynamics of Crowds on The Road Between The Two Holy Mosques

Asst.Prof.Dr. Maan A. Rasheed

maan.a@csw.uobaghdad.edu.iq

Asst.Lect .Hiba Ali Kareem

hiba.ali.k@csw.uobaghdad.edu.iq

Department of Mathematics ,College of Science
for Women,University of Baghdad

Abstract

In this paper ,we use one of mathematical crowd models to represent the movement of crowds arriving for the Arbaeen pilgrimage Specifically, we aim to understand the dynamics of crowds on the road between the two holy mosques. Firstly, we introduce the proposed Mathematical crowd motion. In this model, we define a spontaneous speed corresponding to the speed each individual would like to reach in the absence of others. The actual speed is then calculated as a projection of the spontaneous speed onto a set of feasible speeds (i.e., speeds that do not violate the non-interference constraint). Secondly, the numerical computations are conducted using finite difference method and projection techniques. We also perform numerical simulations using an (Open AI, 2025).The obtained results can assist in designing emergency exits, reducing congestion, and improving crowd distribution.

Keywords: Mathematical modeling, Arbaeen pilgrimage, Differential inclusion, Finite difference, The road between the two holy mosques.

Introduction

The human-crowd phenomenon has been a constant concern for experts from various fields. Since the last decade, dynamics of crowds (crowd's behaviors) under normal and emergent situations have been investigated based on modeling simulation technologies (Maury, B., & Venel, J. 2009).Human crowds show complex behaviors, driven by the decisions of individuals, which depend on their environment, goals, obstacles, and interactions with other nearby individuals. The problem of simulating virtual crowds has attracted many researchers recently, see for instance (Yang et al., 2020; Maury & Venel, 2008; Zhou et al., 2010; Narain et al., 2009; Maury & Venel, 2007; Venel, 2009; Løvås, 1994; Degond & Delitala, 2008; Bellomo, Piccoli, & Tosin, 2012), because of its applications in emergency training, architectural design, education and entertainment, urban planning, traffic engineering, policy making,.. etc.

Existing models separate global planning from local collision avoidance and that can simplify modeling.

The local collision avoidance models require that each person take into account the motion of their nearby neighbors. However, for very dense crowds, this step can quickly lead to complicated computational processes

Traditional models (microscopic and macroscopic models) can simulate general crowd dynamics with the advantages of the two types)Maury & Venel, 2007(. To simulate realistic crowds, recent studies of crowds have taken into account the social psychology of crowds. Many other studies on the human crowd and traffic flow can be seen in (Elaiw et al., 2019; Cheng & Li, 2022; Bellomo et al., 2022; Abdulameer & Sarsam, 2014; Sarsam, 2025a, 2025b; Al-Ahbabi & Al-Alwan, 2023; Ghafel & Al-Jawari, 2024).

In (Maury, B., & Venel, J. 2009), the authors proposed a crowd motion model, with a numerical technique. The proposed model depends on two principles: The spontaneous velocity that corresponds to the velocity that each person want to achieve if he is alone. Then, the actual velocity is computed as the projection of the spontaneous velocity onto the set of feasible velocities (velocities that do not allow the non-overlapping). Moreover, they described the new realistic mathematical framework and studied the well-posedness of the model. In addition, they investigated the convergence of the proposed numerical scheme.

The purpose of this paper is to simulate and represent the movement of crowds arriving for the Arbaeen pilgrimage. Specifically, we aim to simulate the dynamics of human crowds on the two-way road between the two holy mosques, which is the place located between the shrine of Imam Hussein and the shrine of Abu al-Fadl al-Abbas in Karbala-Iraq.

During many occasions of the year, particularly during the Arbaeen pilgrimage time, we can see a heavy crowd covering the whole this road. Therefore, it is difficult to assist in designing emergency exits and reducing congestion. The present work can help in understanding the dynamics of crowds on the road between the two holy mosques. This will help us in estimating the required time for people walking in both directions of the road to transition from randomness to structured lanes, while avoiding overlapping and collisions.

For this goal, we consider the simplest model (assuming the same behavior for all people, and they do not use complex ways to escape). Moreover, we apply the Mathematical crowd model proposed in)Maury, B., & Venel, J. 2009(. We solve this model numerically using a numerical scheme, based on finite difference and projection techniques, and we perform the numerical simulations using AI-driven simulations.

The outline of this work is as follows: in the second section, we introduce the proposed crowd motion. In the third section we suggested a numerical technique to solve the model. In section four, we simulate the dynamics of crowds in the a road between the two holy mosques. Based on the obtained results, some observations are pointed out in section five. In the last section, some conclusions and future works are suggested.

Mathematical Crowd Model

In this section, we recall the so called Mathematical crowd model (Maury, B., & Venel, J. 2009).

Consider that we have N people in a domain $\Omega \subset R_2$. Each person (i-th) is identified with a disc of radius r, and center c_i.

The set of configurations is defined as follows:

$$Q = \{q \in R^{2N},\ \ q = (c_1, c_2, \cdots, c_N)\}$$

Also, we assume that denotes the velocity that person (No i) can achieve, if we ignore the existence of others, So we can introduce a spontaneous velocity field as follows:

$$U = (U_1, U_2 ..., U_N)$$

With assuming that all people have the same behavior, and they have no complex escaping strategies, a global spontaneous velocity field can be introduced as follows: $U: Q \rightarrow R^n$

$$U (q) = (U_0 (q_1), U_0 (q_2), ..., U_0(q_n))$$

Moreover, In this domain, overlapping is not allowed, so,the following set of feasible configurations can be defined as:

$$Q_0 = \{q \in Q, \quad D_{i,j}(q) = |q_j - q_i| > 2r, \quad \forall i \neq j\}$$

As overlapping is not allowed, if two people are in contact with each other, then we can increase distance between them. So, the set of feasible velocities takes the form:

$$V_q = \{v \in R^{2N}, G_{i,j}(q).v \geq 0, when\ , D_{i,j}(q) = 0\}$$

where : $G_{i,j} = (0, \cdots 0, -e_{i,j}, 0, \cdots, 0, e_{i,j}, 0, \cdots, 0) \in R^{2N}$

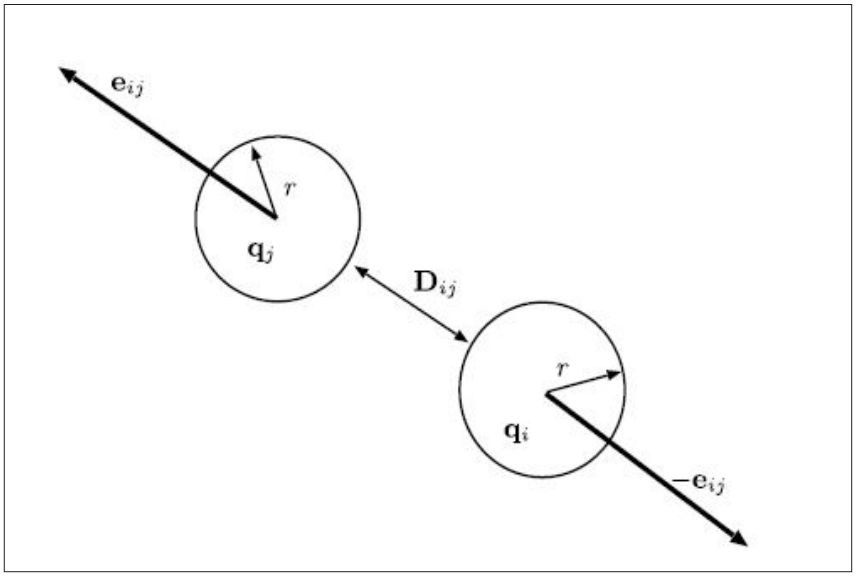

Figure 1 :The distance between two persons

The basic form of the model can be stated as: the actual feasible velocity field is the closest to the spontaneous velocity field, for the Euclidean distance. So the model takes the form:

$$\frac{dq}{dt} = P_{V_q} U(q) \qquad (1)$$

where Pv_q refers to Euclidean-projection onto the closed convex cone , and in general the global velocity field can be written as follows:

$$U(q) = (U_1(q), U_2(q), \cdots, U_N(q))$$

where : $U_i(q) = U_0(q_i)$ for i=1,2,…,N.

Thus equation (1) can be written as a system of ODEs as follows:

$$\left.\begin{aligned} \frac{dq_1}{dt} &= P_{V_q} U_0(q_1) \\ \frac{dq_2}{dt} &= P_{V_q} U_0(q_2) \\ &\vdots \\ \frac{dq_N}{dt} &= P_{V_q} U_0(q_N) \end{aligned}\right] \qquad (2)$$

1. Remark

In this work, we limit our scope to the simplest behavioral model. However, we can integrated sophisticated strategies to this approach. For example, the spontaneous velocity of a person may depend upon their abilities such as physical force or personality. In addition, the velocity may be affected by the positions of his neighbors based on social rules or self- optimization strategy.

Although this model is simple, However, it cannot use directly into a standard framework. Therefore, the problem can be reformulated.We introduce N_q , as the outward normal cone to the set of feasible configurations: Q_0 .

Based on the classical orthogonal-decomposition of Hilbert space, and according to Farkas' lemma, equation (1) becomes:

$$\frac{dq}{dt} + N_q \ni U(q) , \qquad (3)$$

which is a differential inclusion, and it is a generalization of ODEs (1).

For free motion, we get the ODE:

Numerical Technique

This section is devoted to derive a numerical scheme 1, based on finite difference and projection techniques, that is used to solve equation (3),

We divide the time interval (0,T) into m points. That is

$$t_0 = 0,\ t_{n+1} = t_n + h \text{ , for } n = 0,1,\dots m-1,\ t_m = T ,\ h = T/m$$

Let q^n, U^n denote the approximation values of $q(t_n)$, $U(t_n)$ respectively.

$$(q_1^n, q_2^n, \dots, q_N^n) , \qquad U^n = (U_0(q_1^n), U_0(q_2^n), \cdots, U_0(q_N^n))$$

By replacing the time derivative at in equation (4) by the Backward finite difference formula, we get:

$$\frac{q^{n+1} - q^n}{h} = U^{n+1}$$

So, we get $q^{n+1} = q^n + hU^{n+1}$,

where U^{n+1} minimizes $\frac{1}{2}|v - U(q^n)|^2$ over

$$V_{q^n}^h = \{v, D_{i,j}(q^n) + hG_{i,j}(q^n).v \geq 0\}$$

overIt follows that $U^{n+1} = Proj_{V_{q^n}^h}(U(q^n))$

The convergence results of this scheme can be found in (Maury, B., & Venel, J. 2009).

Algorithm steps

- Define $t_0 = 0, t_{n+1} = t_n + h$, for n =0,1...m-1,$t_m + t$, h = T/m
- Evaluate the desired velocity: $U^n = \left(U_0(q_1^n), U_0(q_2^n), \cdots, U_0(q_N^n)\right)$
- Put n = 0
- Predict the free motion: $q^{n+1} = q^n + hU^{n+1}$
- Project back onto the constraint set$U^{n+1} = Proj_{V_{q^n}^h}(U(q^n))$, where

U^{n+1} minimizes $\frac{1}{2}|v - U(q^n)|^2$ over

$$V_{q^n}^h = \left\{v, D_{i,j}(q^n) + hG_{i,j}(q^n).v \geq 0\right\}$$

- Repeat the steps above for all time levels (n =1,2,...m) until final time T.

Remark 2.

The main computational effort is in computing the projection in the fifth step. That involves solving a convex quadratic program. This can be efficiently done using:

- Gradient projection methods
- Proximal point algorithms
- Newton-type or interior-point methods

For small N, it can be done directly. For large crowds, more scalable methods (e.g. splitting methods or alternating projections) are needed.

Numerical Simulations of Dynamics of Crowds on the Road Between the Two Holy Mosques

In this section, we apply the simplest model, we proposed in this paper, to simulate the dynamics of crowds on the road between the two holy mosques, which is the place located between the shrine of Imam Hussein and the shrine of Abu al-Fadl al-Abbas, and it is a path 378 m long) WikiShia, 2025(, and 40m width. The total area of the road is . If we assume 5 persons for each 1, then the Road capacity is persons.

We assume that it is allowed to walk two-way on the road which is bi-dimensional domain. We assume that two populations of people are walking in the road. They are denoted in Blue (B) and Red (R) in the figures. B-individuals want to go to the left, and R-individuals are going to the opposite direction. We assuming the same desired velocity:). The number of individuals in each population is 200 (N=400).

In order to present the numerical simulations of this problem, we apply the numerical algorithm, presented in the last section, and due to the complexity of the problem, we use an (Open AI, 2025) in the computations and simulations processes.

Figure 2. shows the two populations (R and B), at times (in seconds) 0 (random distribution), 25, 75, 50, 75, 100, 125, 150, 175, and 200 (T=200), based on the proposed numerical algorithm.

Road between the two holy mosques

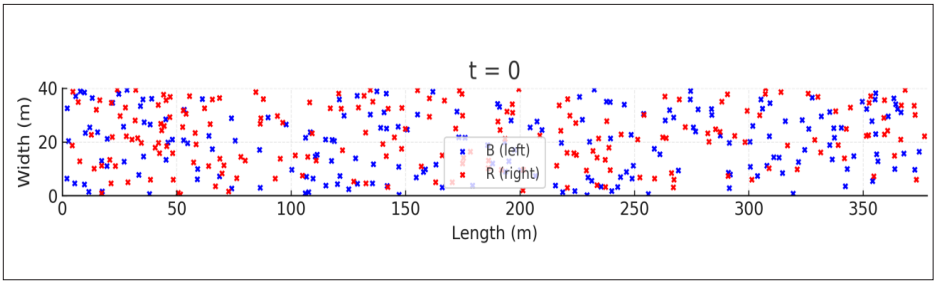

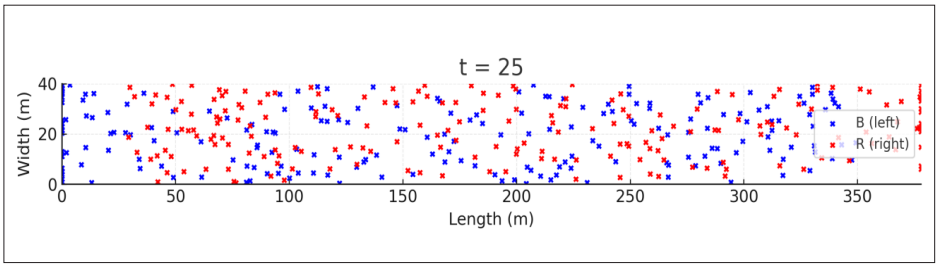

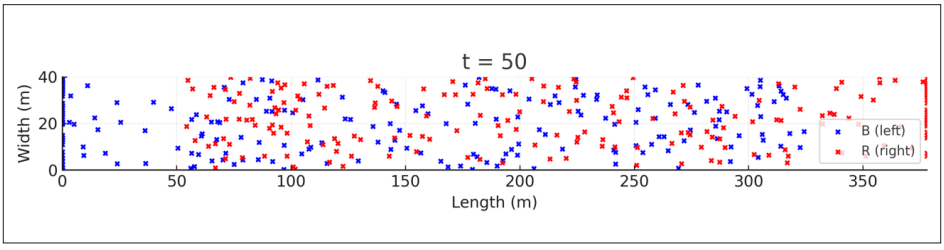

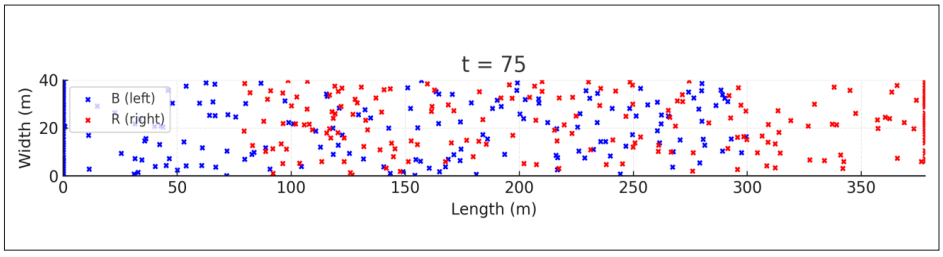

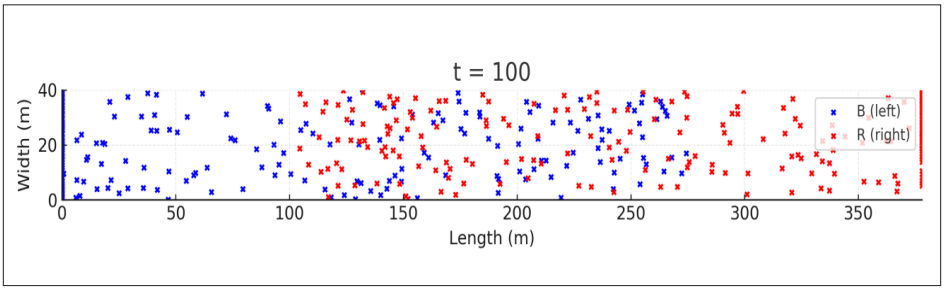

Semi-Annual Scientific Journal
w w w . a r b n j . c o m
Ramadan 1447 A.H, March 2026 A.D

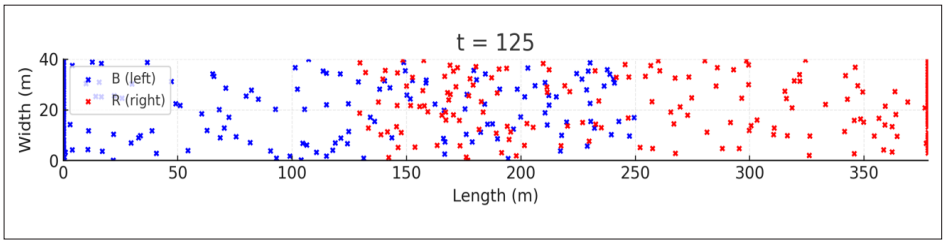
t = 125
B (left)
R (right)
Width (m)
Length (m)
0
20
40
0
50
100
150
200
250
300
350

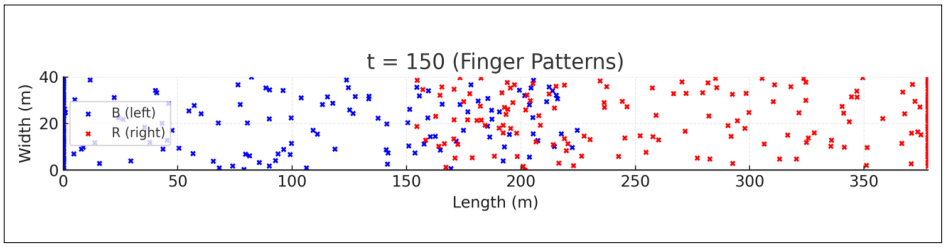
t = 150 (Finger Patterns)
B (left)
R (right)
Width (m)
Length (m)
0
20
40
0
50
100
150
200
250
300
350

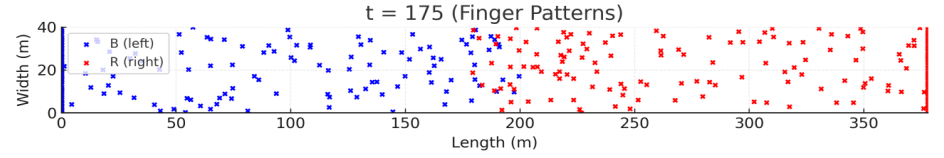
t = 175 (Finger Patterns)
B (left)
R (right)
Width (m)
Length (m)
0
20
40
0
50
100
150
200
250
300
350

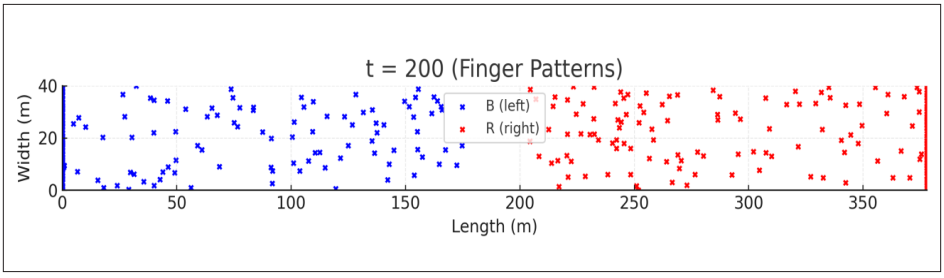
t = 200 (Finger Patterns)
B (left)
R (right)
Width (m)
Length (m)
0
20
40
0
50
100
150
200
250
300
350

Figure 2.

Numerical Simulation showing the movement of the two populations over time

Observations

Based on Figures 2, we can point out the observations:

1. Individuals repel each other when they get too close, so clustering and overlapping are avoided.
2. To avoid collisions, people spread more across the road width (y-axis), especially in the central region where the two flows interact.
3. Over time, the system transitions from randomness to structured lanes, illustrating the emergence of order from simple rules.
4. Despite repulsion and spatial constraints, desired directionality (left for B, right for R) is maintained throughout the simulation. This illustrates the model's stability in preserving macroscopic flow goals while resolving microscopic constraints.
5. At later times (t=150,175 and 200), there are clearer alternating spatial streams forming where Blue and Red populations interact. These narrow, elongated paths are characteristic of the so-called finger patterns)Helbing & Molnar, 1995(. The populations start to self-organize into structured, side-by-side "fingers", reducing direct frontal collisions.

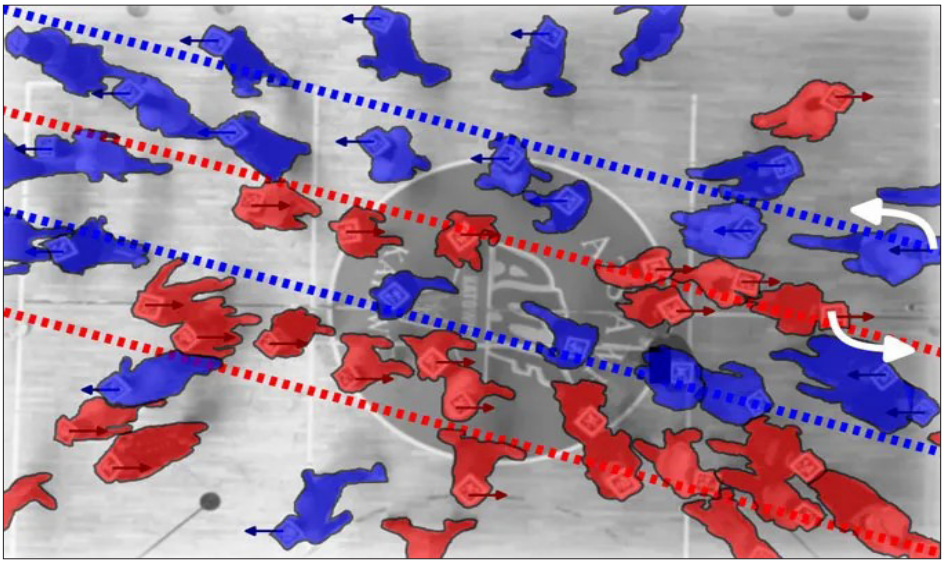

Finger Patterns

Conclusions and Future Studies

Based on the numerical simulation results obtained in the last section, we can understand the dynamics of crowds during the Arbaeen Pilgrimage time, specifically on the road between the two holy mosques. The numerical simulation successfully captures the emergence of finger patterns, ensures feasibility under rigid disc constraints, and exhibits collective behavior consistent with bidirectional pedestrian flows.

The novelty of this work is that it uses AI to simulate the governed problem based on the proposed mathematical crowd model and the numerical technique. The obtained results can assist in designing emergency exits, reducing congestion, and improving crowd distribution, and estimating the required time for people walking in both directions of the road to transition from randomness to structured lanes, while avoiding overlapping and collisions.

As possible future works, we can integrated sophisticated strategies to this approach. For example, the spontaneous velocity of a person may depend upon their abilities such as physical force or personality. In addition, the velocity may be affected by the positions of his neighbors based on social rules or self-optimization strategy.

Acknowledgements

The authors are grateful to the organizers of the 9th Karbala Conference for the Arbaeen Pilgrimage for providing the opportunity to participate in the conference. Also, they would like to thank the University of Baghdad for supporting this work.

References

1. Abdulameer, M. W., & Sarsam, S. I. (2014). Evaluation of pedestrians walking speeds in Baghdad city. Journal of Engineering, 20(9), 1–9.
2. Al-Ahbabi, S., & Al-Alwan, H. (2023). Enhancing pedestrian safety from traffic accidents at the Jadiriya Complex within the University of Baghdad, Iraq. ISVS e-journal, 10(7).
3. Bellomo, N., Gibelli, L., Quaini, A., & Reali, A. (2022). Towards a mathematical theory of behavioral human crowds. Mathematical Models and Methods in Applied Sciences, 32(2), 321–358.
4. Bellomo, N., Piccoli, B., & Tosin, A. (2012). Modeling crowd dynamics from a complex system viewpoint. Mathematical Models and Methods in Applied Sciences, 22(Suppl. 2), 1230004.
5. Cheng, C., & Li, J. (2022). ODEs learn to walk: ODE-Net based data-driven modeling for crowd dynamics. arXiv preprint arXiv:2210.09602.

6. Degond, P., & Delitala, M. (2008). Modelling and simulation of vehicular traffic jam formation. Kinet. Relat. Models, 1(2), 279–293.

7. Elaiw, A., Al-Turki, Y., & Alghamdi, M. (2019). A critical analysis of behavioural crowd dynamics – From a modelling strategy to kinetic theory methods. Symmetry, 11(7), 851.

8. Ghafel, A. H., & Al-Jawari, S. M. (2024). The role of road elements in providing a safe environment for pedestrians. In AIP Conference Proceedings (Vol. 3092, No. 1). AIP Publishing.

9. Helbing, D., & Molnár, P. (1995). Social force model for pedestrian dynamics. Physical Review E, 51(5), 4282–4286.

10. Løvås, G. G. (1994). Modeling and simulation of pedestrian traffic flow. Transportation Research Part B: Methodological, 28(6), 429–443.

11. Maury, B., & Venel, J. (2007). Un modèle de mouvements de foule. In ESAIM: Proceedings (Vol. 18, pp. 143–152). EDP Sciences.

12. Maury, B., & Venel, J. (2008). A mathematical framework for a crowd motion model. Comptes Rendus Mathematique, 346(23–24), 1245–1250.

13. Maury, B., & Venel, J. (2009). Handling of contacts in crowd motion simulations. In Traffic and Granular Flow'07 (pp. 171–180). Springer Berlin Heidelberg.

14. Narain, R., Golas, A., Curtis, S., & Lin, M. C. (2009). Aggregate dynamics for dense crowd simulation. In ACM SIGGRAPH Asia 2009 Papers (pp. 1–8).

15. Sarsam, S. I. (2025a). Comparative modeling of pedestrian traffic stream in the CBD area. Journal of Environmental Engineering and Its Scope, 8(2), 35–45.

16. Sarsam, S. I. (2025b). Influence of dressing style of pedestrians on their traffic stream in the CBD area. Journal of Transportation Engineering and Traffic Management, 6(3), 17–27.

17. Venel, J. (2009). Integrating strategies in numerical modelling of crowd motion. In Pedestrian and Evacuation Dynamics 2008 (pp. 641–646). Springer Berlin Heidelberg.

18. WikiShia. (2025). Bayn al-Haramayn. https://en.wikishia.net/view/Main_Page

19. Yang, S., Li, T., Gong, X., Peng, B., & Hu, J. (2020). A review on crowd simulation and modeling. Graphical Models, 111, 101081.

20. Zhou, S., Chen, D., Cai, W., Luo, L., Low, M. Y. H., Tian, F., ... & Hamilton, B. D. (2010). Crowd modeling and simulation technologies. ACM Transactions on Modeling and Computer Simulation (TOMACS), 20(4), 1–35.

Developing of an Integrated Framework Leveraging Statistical Analysis and Deep Learning Techniquesto Optimize Transportation Servicesfor Arbaeen Visitors

Prof.Samira Naji Kadhim
University of Baghdad - College of Science for Women - Department of Mathematics
Samirank_math@csw.uobaghdad.edu.iq

Asst.Prof.Asraa Muayed Abdalah
University of Baghdad - College of Science for Women - Department of Computer Science
Asraa.m@csw.uobaghdad.edu.iq

Abstract

The Arbaeen pilgrimage continuous to show increase in the size of the crowed, emphasizing the essential demand for precise analytical system to optimize crowed organization, service managing, and decision support. The present work develops two frameworks that employ predictive statistical modeling combined with contemporary artificial intelligence based solutions for managing this extensive religious occasion. In this regrad, the first framework involves a thorough analysis on established and other types of forecasting methods such as Box–Jenkins time series models, nonparametric regressions (Nadaraya–Watson and Epanechnikov kernels), and so on. One-way ANOVA—combined with multilayer perceptron models applied to forecast health indicators such as pilgrim birth rates. Inspired by best practices in the classification of Arbaeen films; the second framework proposes Comparison Replicating best practices from the Arbaeen film scene classification, the second strand, a video scene recognition method is proposed based on transfer learning from Inception V3 and VGG-16. These neural networks trained to recognize and distinguish between images from the Arbaeen procession and other mass gatherings, this system improves deeper machine-based understanding of context and support the implementation of AI-driven surveillance systems.Using transfer learning results in ingesting and interpreting largescale pilgrimage data. Engineered to suit Arbaeen's distinct characteristics,this plan also provides a flexible foundation for managing similar large-scale events such as other eligious or public gatherings. To support real time monitoring we explore visual scene recognition after presenting forecasting.

Keywords: Arbaeen Pilgrimage, Inception V3, Nonparametric Regression, Pilgrim Services, Scene Classification, Time Series Analysis, Transfer Learning, VGG-16.

Introduction

One of the largest religiuos gatherings globally is the annual Arbaeen pilgrimage in Karbala, Iraq, where millions of Shia Muslims are drawing each year. With the growing number of attendees at this significant religious event, the relevant authorities are facing numerous and escalating challenges in crowd control, visitor transportation planning, and emergency response.

This study proposes a two-layered framework model that integrates two distinct models. The first model employs statistical methods to forecast the number of future visitors. The second model leverages transfer learning through neural Inception V3 and VGG-16 networks for recognizing and classifying images. The purpose of this model is developed to classify images of the Arbaeen pilgrimage and separating them from other types of crowed gatherings, for example the ones taking place during other religious events or large athletic competitions. This study facilitates both strategic foresight coupled with real time visual observations during the event.

Related Work

Multiple earlier studies have employed statistical approaches to predict visitor counts of the Arbaeen pilgrimage. Al-Razzaq, Mohammed, and Rasheed (2024), they employed geometric and exponential models on 2017-2022 data, predictiong over 35 million visitors by 2030 via the geometric model. Nevertheless, such approaches do not match the precision and flexibility of advanced AI-based forecasting techniques.

Khayyat and Mustafa (2025) in their statistical investigation analyzed the tourists nationalities, showing that Karbala during the Arbaeen

attracted 53.3% of all tourist visits in Iraq during the event.

In their study (Mostafa et al., 2024) investigates the use of solar energy to power service points along the pilgrimage route from Baghdad to Karbala. By applying remote sensing techniques and GIS, the researchers identified optimal locations for photovoltaic installations using satellite imagery and multi-criteria analysis. The simulation of energy production was performed using MATLAB. The study highlights the feasibility of sustainable energy for Arbaeen processions and provides a framework for future renewable energy planning in similar contexts.

Recent developments in deep learning researches have demonstrated encouraging results in classifying visual contents related to high density events. Convolutional Neural Networks (CNNs), especially those applying pre-trained models via transfer learning, achieved notable accuracy levels in recognizing and classifying between different types of mass events based on visual cues.

Wang et al. (2019) proposed a model in which Inception V3 with transfer learning is used for pulmonary image classification. Features are automatically extracted by the model from chest X-ray images and applied various classifiers including Softmax, Logistic Regression, and SVM. Their results showed improved diagnostic accuracy and sensitivity compared to traditional DCNN models. To enhance overall system performance; data augmentation was used. The approach demonstrated the advantages of using transfer learning in medical image analysis.

Tammina, S. (2019) showed that transfer learning can be used for clustering, classification and regression. He used transfer learning based on VGG-16 to enhance the classification of binary image, and showed learning process in a comparative diagram between CNN and transfer learning

using VGG-16 as shown in figure 1. The computational cost was reduced by removing VGG16's fully connected layers and customizing the network while enhancing classification performance. Table 1 shows the results obtained by both networks.

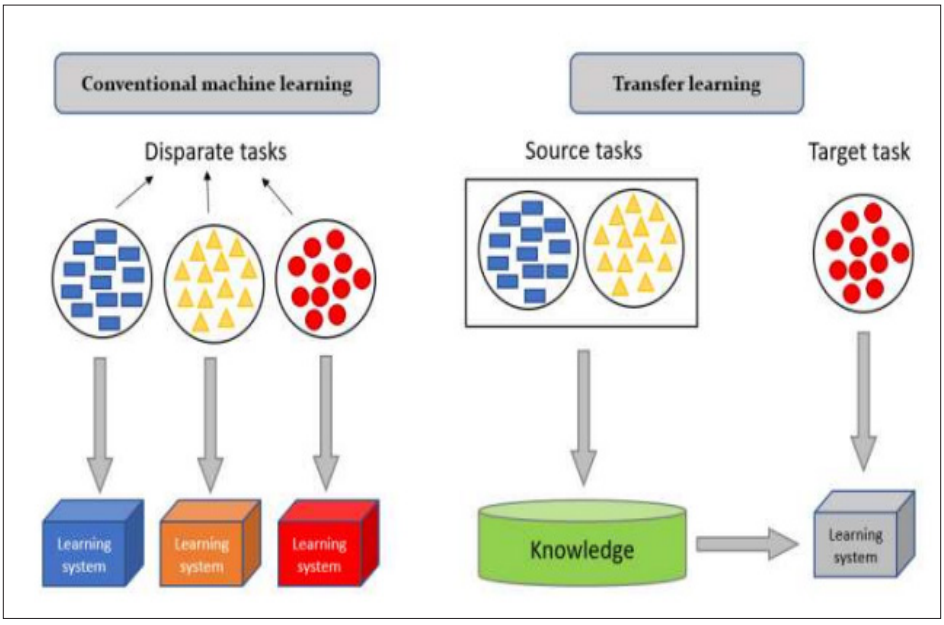

Figure 1. A diagram shows differences of Learning Processes between Conventional Machine Learning and Transfer Learning

Table 1: Accuracy for Different Neural Network Models.

	Training accuracy	Validation accuracy
Basic Convolutional neural network	98.20%	72.40%
Fine tuning CNN with image augmentation	81.30%	79.20%
Fine tuning CNN with pretrained VGG-16 model and image augmentation	86.50%	95.40%

According to our knowledge, this is the first work to combine SARIMA forecasting and CNN-based visual classification tailored to Arbaeen's logistical needs. This paper analyze different statistical methods by comparing them also it compares between classification accuracy obtained using transfer learning. The results from this study can be used to provide strategic planning and improves overall safety.

Data Description for Statistical Methods

Table 2 used by Al-Razzaq, Mohammed, and Rasheed (2024) which estimates visitor numbers from 2017 to 2022 then show prediction of number of visitors in 2030. Predictive Methods (Geometric Growth and Exponential Growth) for Estimating Visitor Numbers. Geometric Growth method predicted that the number of visitors will be 35,403 million; while the Exponential Growth predicted the number of visitors to be 25,399 million in 2030. These can provide baseline data for evaluating more advanced forecasting models such as SARIMA

Table 2: Estimated Visitor Numbers 2017–2030)).

year	Actual / Estimated Visitor
2017	9900
2018	10714
2019	10200
2020	10367
2021	11426
2022	12452
2030	35403

The used data comprises detailed table on tourist attractions in Karbala, visitor demographics by nationality as in Table 3 and continent and hotel occupancy rates during the 2021 Arbaeen pilgrimage.

Table :3 Distribution of Visitors by Nationality.

Rank	Nationality	Number of Visitors	Percentage (%)
1	Afghanistan	852	0.51
2	UAE	314	0.19
3	Armenia	3	0.0018
4	Bahrain	1,651	0.99
5	Hong Kong	1	0.0006
6	Indonesia	27	0.02
7	India	361	0.22
8	Iran	136,225	82.33
9	Jordan	226	0.14
10	Kuwait	2,868	1.73
11	Lebanon	11,138	6.73
12	Palestine	22	0.01
13	Oman	444	0.27
14	Pakistan	9,406	5.68

15	Qatar	93	0.06
16	Saudi Arabia	1,335	0.81
17	Syria	361	0.22
18	Yemen	46	0.03
19	Cambodia	3	0.0018
20	Kyrgyzstan	7	0.0042
21	Myanmar	3	0.0018
22	Malaysia	32	0.02
23	Uzbekistan	44	0.03
Total		165,462	%100

The data shows that 93.64% of visitors originate from Asia, 82% of visitors came from Iran. 3.44% of visitors came from Europe while Africa visitors constitute 0.78%. Other continents show varied but smaller contributions, these data serve as the foundation for statistical modeling and predictive analytic. Sophisticated analytical models were used to perform comparative statistical analysis to obtain meaningful insights from visitor data, we employed a suite of advanced statistical modeling techniques—Box–Jenkins time series modeling, nonparametric kernel regression, and one-way ANOVA. Time-series as well as cross-sectional data are used to analyze behavioral patterns of visitors and regional focus. These methods were applied to two types of data:

- Time-series which estimates the total annual visitors from 2017 to 2030 shown by Table 2.
- Cross-sectional distribution of visitors by nationality in a given year shown by Table 3.

Each method provides a unique perspective on the data, enabling a multi-dimensional understanding of visitor behavior, trends, and group-level differences.

Methodological Overview and Comparative Insights

1. **One-Way ANOVA (Bittner, 2022):** Regional Disparities in Visitor Distribution Using Table ,3 nationalities were grouped into geographic regions:

- Iran, Lebanon, Saudi Arabia, Jordan and Kuwait considered to be Middle East countries.
- Pakistan and India are considered to be South Asia countries.
- Afghanistan and Uzbekistan considered to be Central Asia countries.
- Others :Remaining nationalities

To investigate if there are statistically significant differences in the average number of visitors per nationality across these regions an ANOVA test was used.

Hypotheses:

- H0: All regional means are equal.
- H1: At least one regional mean differs significantly.

The null hypothesis was rejected because of the large F-statistic, and the smaller than 0.01 p-value. A post-hoc Tukey's HSD test showed that the number of Iranian visitors (from Middle Eastern countries) is greater than the number of visitors from other regions. This finding underscores the importance of tailoring infrastructure and services to meet the requirements of these prominent visitor groups. Especially during crowded times, also it is very important to analyze regional differences in attendance to allocate resources effectively and ensure a smooth, well-supported experience for everyone.

2. Nonparametric Regression (Salibian-Barrera, 2023): Capturing Trends Without Parametric Assumptions

To smooth the number of visitors and extract data and to estimate underlying trends; a Nadaraya–Watson estimator with an Epanechnikov kernel smoothing was using Table 2.

$$\hat{y}_t = \frac{\sum_{i=1}^{n} K_h(t-i)y_i}{\sum_{i=1}^{n} K_h(t-i)} \quad \ldots\ldots\ldots (1)$$

Where:

- Kh(.): Epanechnikov smoothing kernel function,
- h: used to control smoothness. It is the bandwidth parameter,

From this study it is found that growth in visitor numbers is not linear nor exponential, but rather follows a more complex trajectory, because it is affected by external events such as geopolitical trends or policy shifts. This model is useful when parametric assumptions fail or incorrect, providing a flexible replacement to classical curve fitting. Th adaptability of this method helps facilitate the recognition minor changes, providing more responsive forecasting method*s*.

3. Box–Jenkins Time Series Modeling (SARIMA) (Gorgess & Ibrahim, 2013; Akpanta et al., 2015): Forecasting Visitor Counts

A SARIMA approach was applied to the historical data in Table 3, capturing both trend and seasonality (if available):

$$\text{SARIMA}(p,d,q)(P,D,Q)_m \quad \ldots\ldots\ldots(2)$$

Where:

- p,d,q: Non-seasonal autoregressive, differencing, and moving average components,
- Q,D,P: Seasonal counterparts,
- m: Season-specific timeframe (e.g., annual seasonality).

Although the limitation of historical data (only six years), the model effectively detected the increasing trend and the generated outcomes for the next decade (2023–2030). These forecasts match well with the values in Table 3, supporting the model's predictive performance. Strategic planning is enabled by using time series modeling, allowing authorities can predict increasing number of visitors and can allocate resources accordingly. Table 4 shows methodological overview and comparative insights. While Table 5 shows summary of analytical approaches for regional visitor data.

Table 4: Methodological Overview and Comparative Insights

Method	Objective	Data Used	Key Findings
One-Way ANOVA	Compare average visitor counts across nationalities grouped into regions	Table 3	Significant regional disparities found; Middle Eastern countries dominate
Nonparametric Regression(Nadaraya–Watson, Epanechnikov Kernel)	Smooth noisy data without assuming functional form	Table 2	Revealed nonlinear growth trend in visitor numbers over time
Box–Jenkins (SARIMA)	Forecast visitor numbers using historical patterns	Table 2	Accurately modeled increasing trend with seasonal components

Table 5: Evaluation √ X Analytical Methods for Tourism Data Analysis.

Method	One-Way ANOVA	Nonparametric Reg.	SARIMA
Type	Inferential	Exploratory	Predictive
Temporal?	X	√	√
Handles Complexity?	X	√	√
Provides Forecast?	X	X	√
Regional Insights?	√	X	X
Best Use Case	Comparing regional visitation levels	Smoothing noisy data, detecting hidden trends	Forecasting future visitor numbers

This comparative study reveals how the integration of different statistical techniques can offer a broad perspective of visitor dynamics; where One-way ANOVA detects regional differences and facilitates precise interventions. Nonparametric regression show unseen structures in noisy data, especially when relationships are unclear. SARIMA modeling enables accurate forecasting, supporting long-term planning and resource allocation. Collectively, these strategies build solid analytical structure framework leveraging mathematics and Artificial Intelligence, applicable to a diverse spectrum of demographic, economic, and social forecasting tasks.

Arbaeen pilgrimage Dataset for Scene Classification

A custom dataset of 400 annotated images was created from various films and documentaries:

- Arbaeen Scenes (200 images): Processions, tents, flags, rituals.
- Non-Arbaeen Mass Gatherings (200 images): Concerts, Hajj, protests, sports events.

Each image was labeled binary (1 for Arbaeen, 0 otherwise) and splitted into Training: 80%, Validation: 10% and Testing: 10%.

Methodology for Deep Learning for Image Scene Classification

As illustrated in the figure ,2 the methodology consists of several stages, beginning with image preprocessing, which includes frame extraction (2-second intervals), resizing(resize images to 299×299 for Inception V3 and 224x224 for VGG-16), normalization([[0,1scaling), augmentation(-flip, rotation, zoom, brightness) and Label encoding (Binary labels assigned). Following this step, the images are divided into three sets: 80% for training, 10% for testing, and 10% for validation.

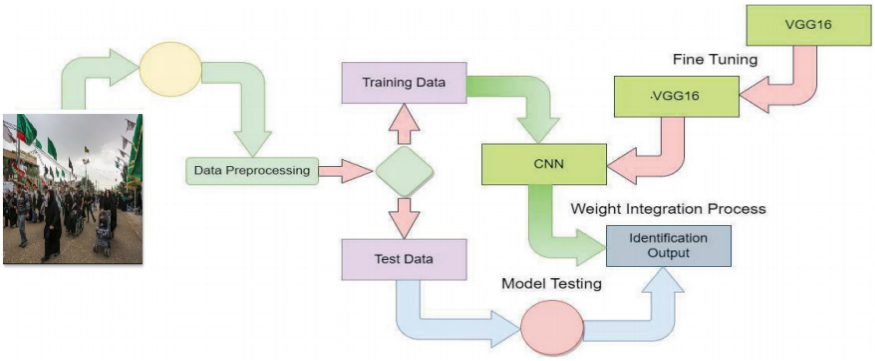

Figure 2: Methodology of proposed system

The training efficiency and accuracy is improved by using transfer learning technique, especially when working with small datasets. ImageNet is a large dataset used to train models so they can learn useful features; and then these models can be used by other networks instead of training from scratch, which can be time-consuming and computationally expensive (Ali & Abdulazeez, 2024). This pre-trained model is then adapted to our specific task in training and testing stage. Typically, we keep the early layers (which detects general features such as textures and edges) and either fine-tune the later layers or replace them with new layers tailored to our classification problem. This process significantly reduces training time and helps achieve higher performance, even with smaller datasets. In essence, transfer learning allows the usage of prior knowledge to accelerate learning and improve model accuracy in new but related tasks. The final stage is the recognition (classification) stage in which the system is required to recognize or classify images into Arbaeen Scenes and non Arbaeen scenes.

Model Architectures

The Inception V3 architecture overview is shown in Table 6 below. While Table 7 gives architecture overview of the VGG-16 network. Table 8 shows a comparison summarizing the key features of Inception V3 and VGG-16 networks.

Table 6: Inception V3 Architecture Overview

Stage	Description	Input Dimensions	Output Dimensions
Stem	Initial Conv layers + MaxPooling	299 × 299 × 3	35 × 35 × 192
Inception Module A ×3	Three Inception-A blocks (multi-branch convolution paths)	35 × 35 × 192	35 × 35 × 288
Reduction A	Downsampling via convolutions and pooling	35 × 35 × 288	17 × 17 × 768
Inception Module B ×5	Five Inception-B blocks (deeper feature extraction)	17 × 17 × 768	17 × 17 × 768
Reduction B	Further downsampling with Conv + Pooling	17 × 17 × 768	8 × 8 × 1280
Inception Module C ×2	Two Inception-C blocks (wide convolutional filters)	8 × 8 × 1280	8 × 8 × 2048
Global Average Pooling	Averages feature maps across spatial dimensions	8 × 8 × 2048	1 × 1 × 2048
Dense Output Layer	Fully connected layer with softmax activation	2048	2 (binary classification)

Table 7: VGG-16 Architecture Overview

Stage	Description	Input Dimensions	Output Dimensions
Block 1	Two Conv2D layers with 64 filters + MaxPooling	224 × 224 × 3	112 × 112 × 64
Block 2	Two Conv2D layers with 128 filters + MaxPooling	112 × 112 × 64	56 × 56 × 128
Block 3	Three Conv2D layers with 256 filters + MaxPooling	56 × 56 × 128	28 × 28 × 256
Block 4	Three Conv2D layers with 512 filters + MaxPooling	28 × 28 × 256	14 × 14 × 512
Block 5	Three Conv2D layers with 512 filters + MaxPooling	14 × 14 × 512	7 × 7 × 512
Flatten	Flattening of feature maps	7 × 7 × 512 = 25088	25088
FC-1	Fully connected layer with 4096 units (Dense)	25088	4096
FC-2	Fully connected layer with 4096 units (Dense)	4096	4096
Output	Fully connected layer + Soft-max for binary output	4096	2 (binary classifi-cation)

Table 8: A comparison summarizing the key features of Inception V3 and VGG-16:

Feature	Inception V3	VGG-16
Model Depth[11]	~48 layers (including auxiliary classifiers and inception modules)	16 layers (13 Conv + 3 Fully Connected)
Design Philosophy[11]	Inception modules use multi-scale filters (1×1, 3×3, 5×5) in parallel	Uniform 3×3 filters across all convolutional layers
Feature Extraction[11]	Captures features at multiple scales simultaneously	Focuses on fine-grained spatial details using small kernels
Input Size[11, 12]	299 × 299 × 3	224 × 224 × 3
Parameter Count[12]	~23 million	~138 million
Computational Cost[13]	More efficient, optimized with dimensionality reduction	High memory usage, especially in fully connected layers
Transfer Learning Support[12, 14]	Pre-trained on ImageNet; strong generalization with fine-tuning	Pre-trained on ImageNet; widely used for transfer learning
Accuracy (ImageNet Top-1)[14]	~78.8%	~71.5%
Strengths[12]	Good trade-off between accuracy and efficiency; scalable architecture	Simplicity, strong baseline performance
Weaknesses[12]	More complex structure; harder to customize	Very high number of parameters; slower to train on large datasets

Both models were fine-tuned with Adam optimizer, binary cross-entropy loss, number of epochs = 20, batch size = 32, and learning rate =0.0001 .

Results

The performance of the system using the two models are shown in Table 9. Inception V3 shows slightly higher performance in all phases, indicating better generalization and learning capacity. VGG-16, despite its older architecture and higher parameter count, still achieves high accuracy, proving its robustness for binary classification tasks.

Table 9: Model performance comparison presented with labeled metrics.

Model	Training Accuracy (%)	Validation Accuracy (%)	Test Accuracy (%)
VGG-16	96.3	93.5	92.0
Inception V3	97.7	95.0	94.1

Inception V3 achieved higher accuracy due to its multi-scale feature extraction modules; while VGG-16 showed faster convergence and lower computational cost, making it suitable for lightweight deployment.

Conclusion

The Arbaeen pilgrimage is considered one of the largest mass gatherings in the world. To ensure its successful management, it is essential to draw on scientific studies grounded in statistics and artificial intelligence. Statistical models provide understanding of relationships and a conceptual framework for predictive analysis and regional comparison, whereas AI-based models support high-level deep learning mechanisms that support video tracking and scene recognition throughout the Arbaeen pilgrimage—a crucial part of real-time observation system and real time decision-making process. The applied SARIMA approach ensures precise long-term forecasts, while transfer learning using Inception V3 achieves over 94% test accuracy in scene classification. Findings show that the

integration of statistical and intelligent techniques optimizes visitor flow control and management, enhances strategic planning, and guarantees more effective management of resources.

The SARIMA model used for predicting visitors number. While the ANOVA model used for analyzing different regions. In addition, learning using pre-trained convolutional neural networks (CNNs) to classify images and scenes captured from security camera footage and YouTube videos. The obtained results can help authorities in allocating infrastructure and personnel more efficiently during crowded times. The outcomes of this study can be leveraged to support crowd management, allocate necessary resources, and ensure proper care and services for Arbaeen pilgrims.

References

1. Rasheed, H. A.-R., Mohammed, R. S., & Rasheed, A. A.-R. (2024). Estimating the number of arrivals during the Arbaeen pilgrimage to the holy city of Karbala. Al-Arba'een Journal, 2(2, Pt. 3), 132-148.
2. Khayyat, H. A. J. I., & Mustafa, Z. S. (2025). Analysis of the nationalities of tourists visiting the holy city of Karbala during the 2021 (1443 AH) Arbaeen pilgrimage: An inductive study [In Arabic]. Al-Arbaeen Journal, 2(2, Pt. 5, Sec. 2), 133-158.
3. Mostafa, S. S., Alatta, H. J. M., Khanjer, E. F., & Abul Al-Razak, B. (2024). Equip Ziyarte Al-Arba'een service points with clean energy through solar radiation using remote sensing techniques: A case study along the path from northern Baghdad to the holy Karbala. 7th International Scientific Conference of Ziyarat Al-Arba'een.
4. Wang, C., Lin, H., Liu, B. X., Zeng, C. Y., Chen, J., & Zhang, G. (2019). Pulmonary image classification based on Inception-v3 transfer learning model. IEEE Access, 7, 146533–146541. https://doi.org/10.1109/ACCESS.2019.2946000.
5. Tammina, S. (2019). Transfer learning using VGG-16 with Deep Convolutional Neural Network for Classifying Images. International Journal of Scientific and Research Publications, 9(10),143-150.http://dx.doi.org/10.29322/IJSRP.9.10.2019.p9420.
6. Bittner, A. (2022). Analysis-of-variance (ANOVA) assumptions review: Normality, variance equality, and independence (pp. 28–33). https://doi.org/10.47461/isoes.2022_bittner.
7. Salibian-Barrera, M. (2023). Robust nonparametric regression: Review and practical considerations. Econometrics and Statistics. https://doi.org/10.1016/j.ecosta.2023.04.004.
8. Gorgess, H. M., & Ibrahim, R. (2013). Time series forecasting by using Box-Jenkins models. Ibn Al-Haitham Journal for Pure and Applied Science, 26(1), 337-345. University of Baghdad, College of Education for Pure Science (Ibn Al-Haitham) .

9. Akpanta A. C, I. E. Okorie1 and N. N. Okoye (2015). SARIMA Modelling of the Frequency of Monthly Rainfall in Umuahia, Abia State of Nigeria. American Journal of Mathematics and Statistics; 5(2): 82-88.

10. Ali, A. H., & Abdulazeez, A. M. (2024). Transfer learning in machine learning: A review of methods and applications. Indonesian Journal of Computer Science, 13(3).https://doi.org/10.33022/ijcs.v13i3.4068 .

11. Constantinescu, E. C., Udriștoiu, A.-L., Udriștoiu, Ș. C., Iacob, A. V, Gruionu, L. G., Gruionu, G., Săndulescu, L., & Săftoiu, A. (2021). Transfer learning with pre-trained deep convolutional neural networks for the automatic assessment of liver steatosis in ultrasound images. Medical Ultrasonography, 23(2), 135–139. https://doi.org/10.11152/mu-2746 .

12. Mattheuwsen, L., & Vergauwen, M. (2020). Manhole cover detection on rasterized mobile mapping point cloud data using transfer learned fully convolutional neural networks. Remote Sensing, 12(22), 3820. https://doi.org/10.3390/rs12223820.

13. Suganda Girsang, A. ., Dharma Saputra, A. ., & Yanrie, V. . (2023). Performance Comparison between VGG16 and Inception V3 for Organic Waste and Recyclable Waste Classification. International Journal of Intelligent Systems and Applications in Engineering, 11(2), 557–563. Retrieved from https://ijisae.org/index.php/IJISAE/article/view/2711.

14. Firmansyah, I., Rosnelly, R., & Wanayumini. (2023, February 25). Inception-V3 versus VGG-16: In rice classification using multilayer perceptron. In Proceedings of the 2nd International Conference on Information Science and Technology Innovation (ICoSTEC), Yogyakarta, Indonesia. https://prosiding-icostec.respati.ac.id/index.php/icostec/article/download/24/24.

Arbaeen Pilgrimage: surveillance and control of Microbial infections: A review

Prof.Dr.Qais Gheema

Institute of Genetic Engineering and Biotechnology for Postgraduate Studies – University of Baghdad

kaiskassim@gmail.com

Prof.Dr.Abdul Ameer Gharib

Institute of Genetic Engineering and Biotechnology for Postgraduate Studies – University of Baghdad

kaisskasim22@ige.uobaghdad.edu.iq

Abstract

Millions of Shia Muslims travel to Karbala, Iraq, for the Arbaeen Pilgrimage, one of the biggest religious gatherings in the world, which honors Imam Hussein's martyrdom (as). Despite the event's great spiritual and cultural significance, the risks of diseases transmission, overcrowding, and poor sanitation present serious public health issues. Due to congestion, poor sanitation, and the possibility of infectious disease epidemics, the Arbaeen pilgrimage one of the biggest yearly religious mass gatherings brings millions of pilgrims to Iraq and presents serious public health issues. With an emphasis on monitoring tactics, patterns of antimicrobial resistance (AMR), and control approaches, this review summarizes the state of knowledge regarding microbial diseases linked to the Arbaeen pilgrimage. AMR is a growing threat, and respiratory and gastrointestinal bacteria are important pathogens. We draw attention to deficiencies in international cooperation, vaccine coverage, and real-time illness monitoring for efficient infection management. To reduce health risks, recommendations include multi-sectoral collaboration, pre-travel health education, and improved syndromic surveillance. Arbaeen is linked to epidemics of infectious diseases, such as meningococcal disease, respiratory infections, diarrheal ailments, and blood-borne pathogens, just like other large gatherings like the Hajj. Vaccination requirements, hygiene promotion, and real-time genomic surveillance are examples of current surveillance and preventative tactics that have been successful in reducing risks at similar events. Systematic research on the health effects unique to Arbaeen is still lacking, though. In order to address new dangers (such as antibiotic resistance and climate-sensitive diseases) and guarantee pilgrim safety, this assessment emphasizes the critical need for specialized interventions, global cooperation, and enhanced preparedness frameworks. To protect health during Arbaeen and in the future, lessons learned from international mass gatherings highlight the significance of comprehensive prevention, quick diagnosis, and cross-border collaboration.

Keywords: Arbaeen Pilgrimage, Infections, control.

Introduction

The Arbaeen Pilgrimage, one of the world's largest religious gatherings, commemorates the sacrifice made by Imam Hussein, the grandson of Prophet Muhammad. The holy city of Karbala, Iraq, receives millions of pilgrims each year from all around the world, particularly Shia Muslims. Pilgrimage has significant cultural, theological, psychological, and spiritual meaning for those who embark on a journey of devotion, reflection, and mourning. During Arbaeen, pilgrims journey long distances, often on foot, to reach the holy shrine of Imam Hussein, fostering a vibrant sense of solidarity, unity, and devotion (Hashjin and Khanghahi, 2020).

Arba'een is a religious festival that draws sizable crowds in many Islamic countries. From Islamic countries such Iran, Pakistan, Turkey, Afghanistan, Azerbaijan, Lebanon, Kuwait, Bahrain, and Saudi Arabia, more than 17 million pilgrims travel to Karbala, Iraq (Mirzaei and Abdi, 2020). On Arba'een, the family of Hussein ibn Ali celebrates their return to Karbala. The slaughter of the Prophet Muhammad's grandson, his family, and his acquaintances took place forty days ago today. On this day, millions of Shia Muslims and pilgrims go from places in Iraq and Iran to Karbala, which is 80 kilometers from Najaf and 100 kilometers southeast of Baghdad, to see the mausoleum of Imam Hussein (Shalbafian and Zarandian, 2021).

However, the Arbaeen Pilgrimage is not without its challenges. As a result of these challenges, the pilgrims can run into a lot of problems that could make it tough for them to continue traveling. For instance, the sheer number of participants could strain the infrastructure of the community, leading to congestion and traffic on the pilgrimage routes. Inadequate hygienic conditions and amenities might cause diseases to spread among pilgrims (Choi and Eltahir, 2022). Other studies highlight the health concerns associated with religious practices such as the Hajj and Hinduism related

to Hindu holidays, including the potential for infectious disease transmission between pilgrims and the local population. Locating facilitators and implementing measures that can mitigate the challenges Pilgrimage is one way to overcome these problems (*Shinde*, 2010; *Memish* et al., 2014).

The delay between the onset of the disease (outbreak) and its treatment (quick reaction) is and will continue to be one of the disadvantages of present surveillance. Epidemics and outbreaks provide significant challenges when considering the three stages of diagnosis (possible, suspected, and definite) for infectious diseases. It should be emphasized that successful containment depends on making a conclusive diagnosis as soon as possible. Because some diseases may be self-limiting, depending on the qualities and kind of disease agent, it can be difficult to intervene during the peak spread of an epidemic (Asl et al., 2015; Moradi et al., 2019).

According to our preliminary evaluation, no thorough or systematic study has been conducted to accurately determine the risks and health advantages of Arbaeen walking. Despite the Pilgrimage's global significance, there is a conspicuous dearth of a comprehensive examination of the health problems and enablers specific to Arbaeen walking in the literature now in publication. This indicates absence of evidence related to health impacts of Arbaeen Pilgrimage participated by people of various nationalities. In order to fill this gap, this scoping review was conducted by precisely identifying the health issues and the issues related to their solutions that are specific to the Arbaeen Pilgrimage. In essence, the study hypothesizes that the Arbaeen Pilgrimage is a high-risk event for microbial infections, and its health risks can be reduced through evidence-based surveillance, control measures, and global collaboration.

Meningococcal disease

The Arbaeen pilgrimage one of the largest annual religious events in the world is associated with considerable public health risk, including the risk of meningococcal disease (MD) outbreaks due to crowding and closes contact between millions of pilgrims. New studies highlight the importance of better surveillance and preventive strategies, including that pilgrims be vaccinated against meningococcal disease (ACWY or quadrivalent vaccinations) (Moulaei et al., 2024), which Iraq and its neighbors are starting to implement. Because of their prolonged immunity and herd immunity effects, conjugate vaccinations (MenACWY, MenB) are preferred as the mainstay of meningitis prevention over polysaccharide vaccines. Even newer vaccines, such as the MenABCWY now in development, could further increase coverage. The Saudi Ministry of Health (2024) has implemented mandatory vaccination policy for Hajj pilgrims since 2018, reporting 100% compliance (Memish et al., 2023).

Since its launch in 2006, the MenACWY vaccine has been especially effective, bringing the number of cases of meningitis linked to the Hajj to zero (Yezli et al., 2023). Nowadays, chemoprophylaxis usually with ceftriaxone or ciprofloxacin is only used for high-risk contacts and targeted epidemic responses (like the 2023 Scout Jamboree). Concerns about antibiotic resistance have led to a reduction in mass prophylaxis. However, according to Saudi rules (2024), ciprofloxacin is still given to African pilgrims upon admission, and the ECDC (2023) emphasizes the importance of continuous resistance monitoring. These days, enhanced monitoring methods include real-time digital reporting through platforms like Saudi Arabia's Hajj Health App and genetic sequencing to monitor strain progression (e.g., MenW ST-11). Thanks to epidemic alerts from the Global Meningitis Genome Library, there were no documented cases of meningitis during the 2023 Hajj (CDC, 2023; WHO, 2024).

AI-powered chatbots that provide multilingual health alerts and simulation exercises that get medical staff ready for outbreaks are examples of how public awareness and training have improved. Vaccine refusal rates have been considerably lowered by pilgrim education initiatives (Alqahtani et al., 2022). Mass gathering readiness is being incorporated into global coordinating initiatives, like as WHO's Defeating Meningitis by 2030 strategy, which is backed by G7/G20 funding for vaccine access in low- and middle-income nations. It is anticipated that mRNA vaccination trials will be included in the 2025 Hajj (Saudi MOH, 2024), underscoring the continuous development of preventative measures.

The Gram-negative bacterium Neisseria meningitidis, which has six main serogroups (A, B, C, W, X, and Y), is the cause of meningococcal illness. Respiratory droplets and close contact (such as coughing or sharing living quarters) are the main causes of transmission. The symptoms include rash (meningococcal septicemia), headache, stiff neck, photophobia, and sudden fever. Meningitis, septic shock, and death (with a mortality rate of 10-15% and up to 50% if treatment is not received) are the complications (Rouphael NG, Stephens, 2012).

1.Meningococcal Disease Risks during Arbaeen:

Historical Precedents: Because Arbaeen is a mass gathering, there is a potential of meningococcal outbreaks. Mandatory vaccination policies were implemented in response to epidemics during the Hajj pilgrimage in 1987 (serogroup A) and 2000 (serogroup W135). Evidence from Arbaeen: Surveillance limitations in Iraq and surrounding countries may result in underreporting of cases, even when no significant outbreaks have been documented recently. High-Risk Groups: Those who are unvaccinated, in crowded environments, especially pilgrims from sub-Saharan Africa (the meningitis belt) are particularly at risk **(Yezli et al., 2023).**

2.Surveillance and Control Measures of Meningococcal Disease (Alderson et al., 2022):

A.Pre-Travel Vaccination Policies:

The Hajj Model of Saudi Arabia requires pilgrims to have the quadrivalent (ACWY) meningococcal vaccine. Iraq's Arbaeen Policy includes the following: Required for international pilgrims from high-risk nations (such as the African meningitis belt); recommended but not required for pilgrims traveling domestically; and Vaccine types: Menveo and Nimenrix, two ACWY conjugate vaccines, are recommended above polysaccharide vaccines.

B.On-Site Surveillance & Rapid Response:

Disease Monitoring: To identify fever, Iraq's Ministry of Health uses thermal scanners and mobile clinics. International Coordination: WHO and CDC facilitate epidemic tracking and cross-border alerts; lab confirmation: PCR and culture testing for suspected cases (limited capability in some countries).

C.Post-Pilgrimage Follow-Up:

Returning Pilgrim Screening: Certain nations, like Iran, keep an eye out for meningitis symptoms when pilgrims return, and antibiotic prophylaxis: Ciprofloxacin or ceftriaxone is given to close contacts of confirmed cases.

Respiratory tract infections

Mass gatherings, such as the annual Hajj pilgrimage, present significant public health challenges due to the high risk of infectious disease transmission, particularly respiratory infections. The Hajj, held in Saudi Arabia, is the largest recurring mass gathering globally, attracting over 10 million pilgrims annually. Crowded conditions, diverse demographics, and close contact among attendees facilitate the spread of respiratory pathogens, including viruses and bacteria. This paper reviews the epidemiology, prevention, and control of respiratory infections during the Hajj, with implications for other mass gatherings (Shafi et al., 2016).

The Arbaeen Mass Gathering (MG) is one of the largest religious gatherings in the world, attracting millions of pilgrims to Karbala, Iraq, annually. This event poses significant public health challenges, particularly concerning infectious disease transmission, including respiratory tract infections (RTIs). Below is a detailed explanation of health research, surveillance, and control measures for RTIs during the Arbaeen MG.

1.Risk of Respiratory Tract Infections (RTIs) in Arbaeen MG:

Mass gatherings facilitate the rapid spread of respiratory infections due to High population density (overcrowding increases droplet transmission), International travel (introduction of pathogens from different regions), Seasonal factors (Arbaeen occurs in cooler months, favoring respiratory virus transmission).The main pathogens include: COVID-19/ SARS-CoV-2 (major concern post-2020), Influenza (H1N1, H3N2), MERS-CoV (Middle East Respiratory Syndrome, endemic in the region), Other respiratory viruses (RSV, rhinovirus, adenovirus), Bacterial infections (e.g., Streptococcus pneumoniae, Mycobacterium tuberculosis), (Ahmed et al., 2018; WHO Mass Gathering Guidelines, 2021).

2.Surveillance Systems for RTIs in Arbaeen Mass Gathering:

The widespread use of effective surveillance systems is fundamental to the prompt identification and response of respiratory tract infections (RTIs) in Arbaeen pilgrims. Detection and control of suspected outbreaks are done using key surveillance strategies before, at and after the event. Health screenings at borders form part of pre-event surveillance, which include thermal scanning and symptom questionnaires targeting clinical features such as fever and cough. It also does laboratory-based surveillance, such as PCR testing for influenza, COVID-19 and MERS-CoV. He further revealed that mobile health units are located along pilgrimage routes for quick check-ups and to identify potential cases early on. For this event, presence of real-time on-site surveillance is necessary. Syndromic surveillance is the tracking of cough fever and dyspnea from hospitals and clinics. Digital reporting through mobile applications used in Hajj and Umrah can also be utilized for Arbaeen to address the issue of reporting of symptoms. A newer approach is wastewater surveillance, which detects viral RNA found in sewage systems, potentially revealing information about how the infection is spreading. Occupied with widespread contact tracing to prevent secondary events and genomic sequencing to detect the emergence of variants like a novel SARS-CoV-2 lineage, post-event surveillance tracks confirmed cases. Such a multisystem surveillance strategy is essential to reduce the transmission of RTIs during such mass gatherings (Mahdi et al., 2021).

3.Control Measures for RTIs in Arbaeen Mass Gathering:

RTI control requires a multifaceted approach comprising vaccination, nonpharmaceutical interventions (NPIs), and public health messaging for the Arbaeen pilgrimage. Vaccination campaigns are another pillar of prevention, with interest in the influenza vaccine provided to pilgrims, particularly for those over the age of 65 and those with chronic underlying

medical conditions. Booster shots of COVID-19 are essential to minimize how severe any cases will be, and the pneumococcal vaccine is recommended for populations at high risk. Alongside vaccines, several NPIs are undertaken to mitigate transmission. High transmission areas follow mask mandates, which, when possible, is only N95 or KN95 masks to lessen the transmission of droplets. Emphasis on hand hygiene by installing sanitizer stations on pilgrimage routes; social distancing measures by creating zones in order to disperse; and preventing overcrowding. Better ventilation in makeshift sites and mosques also reduce the chances of the virus spreading through the air. Public health messaging is also essential for awareness, with multilingual campaigns informing pilgrims on symptoms, prevention, and respiratory etiquette including covering coughs and using disposable tissues. These set of measures enables limiting the transmission of RTIs during the pilgrimage (Chiu et al., 2020).

4.Challenges & Research Gaps:

Although well-documented measures exist to mitigate RTIs while commemorating Arbaeen, certain issues have yet to be resolved. But many mild cases go unreported, meaning it is hard to assess the true extent of transmission of the disease Worsened by the fact, Iraq has a mass gathering of pilgrims where it runs out of resources, Iraq's heath sector may not cope with the high number of patients. A related issue is vaccine hesitancy among some pilgrims in certain groups who are unwilling to be vaccinated. Climate-related motivators, like dust storms, also aggravate respiratory issues, making pilgrims more prone to RTIs. An affordable new tool called wastewater surveillance, as well as an artificial-intelligence-based syndromic tracking may be used to monitor the disease transmission, allowing us to detect and manage an outbreak in its early stages. Still, important research gaps remain, especially in the assessment of the

effectiveness of these new surveillance technologies and the challenges posed by vaccine hesitancy and underreporting (Zhu et al., 2025). Closing these gaps will be crucial to advance future preparedness and response efforts applicable to mass gatherings such as that of Arbaeen.

Diarrhoeal disease

This is because diarrhoeal diseases such as traveller's diarrhoea, cholera, hepatitis A and food poisoning are serious health hazards associated with the pilgrimage. The masses of pilgrims who came from various regions increase the risk of gastrointestinal infection due to environmental contamination to food, water, and the spreading of gastrointestinal microbes.

The Arbaeen Mass Gathering (MG) taking place in Iraq is considered to be one of the largest recurrent religious MGs in the world attracting millions of pilgrims, which imposes important public health challenges including rising of infectious disease outbreaks like diarrheal diseases. An illustration of health research on surveillance and control of diarrheas during Arbaeen.

1.Overview of Arbaeen Mass Gathering and Health Risks:

In other words, the number of pilgrims flocking to Karbala, Iraq for the Arbaeen pilgrimage is among the largest mass assemblies in the world standing at 20-30 million individuals. The overwhelming presence of people creates an intense environment of risk with communicable diseases – most often from overcrowding, poor sanitation and lack of health care infrastructure. One of the biggest threats to health (in addition to cholera and other diarrheal diseases that will kill or cripple the victims) is contaminated food and water, lack of toilet facilities and people living in abject poverty and too close together. Because pilgrims are often packed

into extremely close quarters, this means bacteria can spread rapidly, with E. coli, Salmonella, Shigella, the norovirus and cholera being the usual suspects. In such environment disease can spread rapidly and it is a big public health challenge.

2.Surveillance of Diarrheal Diseases in Arbaeen:

The early identification and response to outbreaks of diarrheal disease during the Arbaeen pilgrimage on the part of pilgrims is reliant on surveillance. Examples of effective approaches to surveillance include syndromic surveillance, which aims to track clinical presentation (e.g. acute watery diarrhea) at health facilities. Laboratory confirmation isalso crucial, as stool specimen tests help inisolating the particular pathogens triggeringoutbreaks. The use of mobile health units and digital tools can lend to real-time data collection and real-time reporting, ensuring we are able to respond rapidly. The effectiveness of these strategies is evidenced by research conducted by Jafari et al. Early detection of outbreaks of communicable disease at mass gatherings: the role of integrated disease surveillance systems (2020) Similarly, WHO-EMRO stresses on cross-border collaboration between Iraq and its neighboring countries for tracking and control of diarrheal disease transmission.

3.Control Measures for Diarrheal Diseases:

A range of measures are taken for the prevention and control of diarrheal diseases during the Arbaeen pilgrimage. Water, sanitation and hygiene (Who,2022) interventions are critical for reducing infection risk. Among them are the supply of safe drinking water, distribution of water purification tablets, or setting up temporary sanitation such as toilets and waste treatment. Handwashing stations and awareness campaigns are part of public health campaigns that also promote hand hygiene. Meanwhile,

in order to keep street foods safe, regulation of street food vendor and behaviour toward safe food handling education to the public are also needed to reduce the risk of contamination. If cholera risk is high, vaccination campaigns, such as oral cholera vaccinations, are carried out when relevant. In case management, mild cases of diarrhea were treated by Oral Rehydration Therapy (ORT) and severe bacterial diarrhea was use antibiotic based on laboratory test results. Evidence also points toward such control measures and their efficacy as a 2023 BMC Public Health study showed that WASH interventions reduced diarrheal cases associated with Arbaeen. The WHO guidelines (2022) include recommendation for rapid response teams to contain outbreaks identified at such mass gatherings.

4.Challenges in Diarrheal Disease Control:

While different controlling methods are adopted, many obstacles against control of diarrheal diseases exist in Arbaeen. Undoubtedly, one of the most important barriers is overcrowding; with such number of people, sanitation measures cannot be implemented effectively, and the potential for disease transmission is high. Moreover, lack of resources, including shortage of health care personnel and laboratory facilities, makes effective responding to outbreaks difficult. The multigenetic backgrounds of the pilgrims is another layer of complexity, with pilgrims from many nations as potential donors of fresh and likely more virulent pathogens that cross borders. This highlights the need for constant enhancement in prevention and control strategies.

5.Recent Updates and Recommendations (2023-2024):

Mobile health apps for symptom reporting during the 2023 Arbaeen pilgrimage have recently been piloted to detect disease spread along with some experiments and new updates of health response strategies during Arbaeen. These tools assist in enhancing surveillance, which, in turn, enables rapid detection of possible outbreaks. In addition, coordination among the Ministry of Health (MoH), the World Health Organization (WHO) and NGOs has been improved to positively impact preparedness and response. While these have improved on that gap in knowledge, there is still a gap where it pertains to the yet to be defined influence of AMR in diarrhoeagenic pathogens specifically. More studies in this field will be needed to provide more insights into the changing threat posed by these diseases and how to improve control strategies.

Public Health Interventions

Measure	Implementation
Water Safety	Daily inspections of water treatment plants, chlorination checks, and testing of water sources (WHO, 2019).
Food Safety	Regular inspections of kitchens, food sampling, and screening of food handlers (Al-Ghamdi et al., 2018).
Sewage Management	Monitoring of treated sewage water to prevent contamination (Saudi MOH, 2020).
Pilgrim Restrictions	Ban on bringing fresh food; only canned food allowed (Hajj Regulations, 2021).

Blood-borne disease

The Arbaeen mass gathering in Iraq is among the largest religious gatherings in the world, with millions of pilgrims attending, which brings unique public health challenges, including the potential for blood-borne disease transmission. Here we explain the health research on surveillance and blood-borne diseases around Arbaeen.

1.Arbaeen Mass Gathering and Health Risks:

Arbaeen seen as mass gatherings are recognized as an important risk factor contributing to transmission of infectious diseases due to several factors. The presence of overcrowding and a lack of adequate sanitation provide a fertile environment for communicable diseases. Furthermore, prevention and treatment becomes harder because access to healthcare infrastructure is limited to be provided, particularly in lounges and make-shift clinics. Furthermore, high-risk behaviours, such as not having safe medical practice while shaving the head or sharing razors, make these procedures even more dangerous which then can transmit blood-borne pathogens. The most important ones are Hepatitis B (HBV), Hepatitis C (HCV), and of course HIV. Another risk could be for needle-stick injuries which can occur if injectable drugs are used in less supervised or more permissive health facilities (Mehri et al., 2024).

2.Surveillance of Blood-Borne Diseases in Arbaeen:

However, despite limited published evidence that documents blood-borne disease outbreaks in Arbaeen pilgrims the last decade, it is possible to learn from mass gatherings such as Hajj and Kumbh Mela. Unsafe medical procedures carried out on-site, for instance, the use of non-sterilized instruments in mobile clinics or in barber shops, have been identified as potential risk factors for HBV and HCV transmission in similar

contexts during Arbaeen. Without pre-event screening, many of those pilgrims may be attending whilst carrying blood-borne diseases without the knowledge they are infected. The physical toll of the pilgrimage, such as walking long-distances frequently resulting in open wounds, also facilitates exposure to pathogens. Research from 2020 published in the Journal of Infection and Public Health pointed out a number of "serious deficiencies" in infection control at mass gatherings "and provide evidence for the implementation of pre-event screening and vaccination campaigns." Likewise, unsafe shaving practices have been highlighted as a documented risk factor for HCV transmission in the setting of Arbaeen in a 2019 study published in Tropical Medicine and Infectious Disease.

3.Control Measures for Blood-Borne Diseases:

Arbaeen blood-borne compatibility efforts: A range of preventive measures, based on studies and practices in other mass gatherings, can control blood-borne transmission in Arbaeen. Such pre-event measures should also include extensive vaccination campaigns, particularly against HBV, as well as health education for pilgrims not to engage in high-risk behaviours, such as sharing razors or undergoing procedures with unsterile instruments. The campaign also stressed that during such events, stringent infection prevention measures in the health care setting, such as the use of sterile needles and correct disposal of medical waste must be ensured. Real-time surveillance system should be put in place, for example, syndromic reporting of signs (such as jaundice) and symptoms of infection would assist in early detection of possible outbreaks. Following a mass gathering type event, it will also be crucial to pursue monitoring through contact tracing for identified infections and serological surveys to determine exposure rates in pilgrims. Promising case studies are available: both the Hajj, where sterilization of medical equipment and HBV vaccination are

mandatory, and the Kumbh Mela, where dedicated mobile clinics utilizing adequate infection control protocols have virtually eliminated needle-stick injury (Ameli, 2016).

4.Research Gaps & Future Directions:

Though the well-known risk for the health of people, Arbaeen-related studies on the blood-borne diseases are remarkably scarce. The vast majority of existing data is extrapolated from other major assemblages such as Hajj and Kumbh Mela, which might not accurately reflect on the peculiar nature of Arbaeen. We must implement real-time surveillance tools, including portable rapid testing kits for HBV and HCV during the event. Future studies should also explore compliance of recommended safety measures among pilgrims such as the use of non-shared razors. Although time for blood-borne pathogen transmission during the Arbaeen pilgrimage is evident, preparedness measures, including surveillance, vaccination, and infection control, could be made effective to counter it. Such research expanded, in accordance with Arbaeen, will be extremely significant for future enhancement and modification of strategies (Mehri et al., 2024).

(Memish et al., 2014; Hoang et al., 2018; Hamdanieh et al., 2021; Khan et al., 2025).

This article presents a comprehensive, timely summary of emerging infectious diseases threats during Arbaeen, including viral hemorrhagic fevers, respiratory viruses, and other pathogens. Every year, the Arbaeen pilgrimage attracts between two and three million pilgrims from over 180 countries, cementing its place as one of the world's largest mass gatherings. The concentration of large numbers of people from other regions of the world into limited space creates unique challenges for public health security and infectious disease control given the potential for crowding, international travel, and rapid disease spread.

1.Viral Hemorrhagic Fevers (VHFs):

VHFs are known to have extremely high death rates, and are also readily spread from person to person when people gather in confined areas, which would pose a new challenge to health authorities during Hajj.

2.Respiratory Infections:

Respiratory diseases are a great threat during Arbaeen mainly due to the crowded places which help transmission, he added.

A. SARS (Severe Acute Respiratory Syndrome):

The severe respiratory syndrome (SARS) in 2003 caused global concern because of its virulent death rate and rapid transmission. India took precautionary measures in response to the threat, including implementation of 10-day waiting period before entry for pilgrims travelling from affected countries and using thermal screening at major airports to screen for possible cases. Laboratory capacity was further strengthened by making PCR

and serological tests available for early diagnosis and monitoring. So far, no cases of Sars have been reported in connection with the Arbaeen pilgrimage.

B. MERS-CoV (Middle East Respiratory Syndrome):

Middle East Respiratory Syndrome (MERS) has been endemic since its first identification in Saudi Arabia in 2012, particularly in relation to camel contacts. The virus is considered a threat among massive gatherings like the Hajj due to the combination of dense crowds, long-distance travel, and its high mortality rate, at approximately 35%. This explains the importance of monitoring and preventive measures during these events.

C. Avian Influenza (H5N1):

Avian influenza continues to be a serious global issue due to its high mortality rate and capacity to generate a pandemic. In response to the problem, Saudi Arabia imposed restrictions on the importation of chicken from the affected countries in order to reduce the risk of introduction and dissemination. At the time of writing, there was no widely-available vaccination against the virus. Currently implemented preventive measures mainly focus on early identification of cases and rapid containment strategies in order to reduce the impact of potential epidemics.

3.Poliomyelitis:

Due to fear of polio,polio vaccine measures have increased to protect the health of society during Arbaeen. One of these is the requirement for children aged under 15 travelling from polio endemic countries to prove vaccination status. In addition, vaccine is necessary at borders regardless of a previous immunity. However, at this time, there is no evidence to suggest this year's Arbaeen pilgrimage is associated with polio transmission.

4.Zika Virus:

The rapid dissemination of the Zika virus and the alarming negative impacts on human health established the emergence of Zika virus as a significant public health threat worldwide between 2015 and 2017. One of the things withit can be transmission, for example: shaking hands, mosquito bites, and congenital diseases that are carried from mothers to infants. These threats enforce a need for vector control at the Arbaeen sites due to the risks of mosquito-borne transmission and the importance of protecting public health through vector control during this period of pilgrimage.

5.COVID-19:

Since 2019, mass gatherings worldwide have been significantly impacted, notably the Hajj pilgrimage, by the COVID-19 pandemic. This year, only about 1,000 pilgrims took part in an effort to minimize the risk of transmission after the Hajj was tightly curtailed in 2020. Between 2021 and 2023, the Hajj was resumed with strict public health protocols including compulsory around vaccination, mandatory masks, crowd size constraints to provide physical distance, and digital health instruments to support health monitoring and compliance to preventive measures through the Hajj period (Hashim et al., 2021).

6.Prevention and Control Strategies:

With the increase in risks of infectious diseases during Arbaeen, the Ministry of Health has developed comprehensive plans. As part of preparatory measures for Arbaeen, the Ministry conducts its risk assessment process and assesses core capabilities to guarantee readiness. Emphasized vaccination requirements include mandatory vaccinations against influenza, polio, and meningococcal disease. Targeted health education programs on health promotion and prevention for pilgrims and employees

can facilitate such endeavors. Surveillance systems for identifying and addressing possible health risks have been substantially enhanced. Other approaches include the implementation of electronic systems that allow data to be reported in real-time and the application of indicator-based surveillance methodologies. Screening is also done at points of entry in order to instantly identify and manage any case. There are also plans to develop syndromic surveillance for better disease monitoring capacities later (Moulaei et al., 2024).

International collaboration is an important part of the strategy. The Ministry liaises regularly with various international health authorities like the World Health Organization to coordinate efforts. A global network of Arbaeen health focal points is also currently being proposed to assist with coordination and communication. The International Health Regulations allow for information transfer, providing transparency and speedy response to new threats. These advancement efforts at I Ministry are utilizing technology advances to make prevention and control methods even better by the moment. Electronic wristbands containing personal health information are being introduced to facilitate medical management on the trip. To ensure efficient crowd management and emergency response time when needed, the use of GPS tracking technology is used to track crowd movement as well (Yeung et al., 2023).

Conclusion

Even though there haven't been any significant meningococcal outbreaks during Arbaeen, there is still a substantial danger because of overcrowding and inconsistent immunization practices. Future epidemics can be avoided by enhancing surveillance, requiring vaccinations, and fostering international collaboration.

The Arbaeen MG needs multilayer control measures (NPIs, vaccinations) and improved RTI surveillance (real-time digital platforms, genetic testing). Lessons from the Hajj and Umrah, such as Saudi Arabia's thermal screening applications, can be modified for use after COVID-19. Given the hazards of MERS-CoV, future studies should concentrate on pandemic preparedness and One Health strategies (human-animal-environment interaction).

Diarrheal illness management in Arbaeen depends on efficient surveillance (real-time monitoring, lab testing) and control (WASH, food safety, vaccine). To reduce hazards, future initiatives should concentrate on international collaboration and digital surveillance technologies. During the Hajj, diarrheal illnesses continue to pose a serious health risk because of the dense population, poor cleanliness, and contaminated food. Although cholera epidemics have decreased as a result of better sanitation, food poisoning, hepatitis A, and traveler's diarrhea still occur. Strict food and water safety regulations, immunization, and pilgrim education are examples of preventive measures. In order to lower the incidence of gastrointestinal infections during large gatherings, future studies should concentrate on real-time surveillance and innovative therapies.

Due to its high volume, global relevance, and crowded locations, the Arbaeen pilgrimage presents unique challenges for novel infectious disease control. Although this poses risks, Saudi health authorities have built

sophisticated systems for surveillance and prevention to control large outbreaks. Recent experiences of COVID-19 have also further underscored the need for adaptable, evidence-based approaches to mass collecting medicine. Sustained global coordination, ongoing technical evolution, and increased investment in public health infrastructure are essential to avoid another health security concern during future Hajj pilgrimages.

Arbaeen is an opportunity for blood-borne infections but enhanced surveillance, vaccination and control measures are key to preventing outbreaks. As for tactics, indigenous research for Arbaeen is needed.

Arbaeen Pilgrimage is one of the largest annual religious mass gatherings in the world where over 20 million pilgrims gather in Karbala, Iraq, to commemorate the 40th day of Imam Hussein's martyrdom. This is a serious public health challenge due to the high numbers (it will be bottom just), the range of demographics (inc kids, elderly, people with disabilities), and the inability of Iraq's public health system to manage the aftermath. Important health hazards include:

1. Infectious Diseases: The shared rooms and crowded surroundings make it easier for gastrointestinal and respiratory diseases, such as influenza and COVID-19, to spread. There are also worries about meningococcal infections and other dangers like monkeypox.
2. Non-communicable diseases (NCDs): As a result of prolonged walking and unfavorable environmental circumstances, there is a high prevalence of injuries, musculoskeletal pain, heat-related illnesses, and cardiovascular events.
3. Environmental and Infrastructure Issues: Health hazards are made worse by makeshift shelters, poor sanitation, and seasonal climate fluctuations.

4. Limited Research and Preparedness: In contrast to other large-scale events like the Hajj, the Arbaeen gathering has drawn less international attention despite its size. There are deficiencies in real-time surveillance and evidence-based therapies, as evidenced by the paucity of research (such as those conducted by Faris Lami and colleagues) that have recorded disease trends.

Recommendations:

- .Boost global cooperation and real-time disease surveillance.
- Enhance infrastructure (healthcare facilities, sanitation) and hygiene education for pilgrims.
- Give research top priority in order to identify illness patterns and allocate resources as efficiently as possible.

The future of the Arbaeen Pilgrimage

The number of people making the Arbaeen Pilgrimage continues to rise. The Arbaeen Pilgrimage is generally relatively peaceful and orderly despite its vast breadth. But because of the physical surroundings and the unique microbiological environment created there during the Arbaeen Pilgrimage, tourists to Kabala are subject to certain environmental dangers. In the past, the actual trek was challenging, and many people died while traveling. But now, the Arbaeen Pilgrimage itself is fraught with dangers that, if unanticipated, might lead to disease and even death. Additionally, there is a higher risk of disease spreading because of how often we travel throughout the world. Clinicians must be aware of risks and know how to handle them. Many of these strategies are simple to use before departure as well as in the field. Physicians must also be alert to reporting any post-Arabeen illness and mindful of the dangers posed by pilgrims who

have returned. International cooperation is crucial to managing health hazards during the Arbaeen Pilgrimage. This includes planning immunization drives, establishing visa caps, and facilitating prompt repatriation.

Suggestions for future and Upcoming Arbaeen Expeditions:

1. Require all pilgrims to have the ACWY vaccine; also study the cultural barriers to immunization among pilgrims.
2. Use digital reporting technologies to improve surveillance and track resistant pathogens in real-time during events.
3. Public awareness initiatives about the dangers and prevention of meningitis.
4. Cross-border cooperation to prepare for outbreaks and develop standardized protocols for data sharing and response.
5. Validate AI-based syndromic surveillance and portable diagnostics.

REFRENCES

1. Ameli J. Communicable Diseases and Outbreak Control. Turk J Emerg Med. 2016 Mar 9;15 (Suppl 1):20-6.
2. Al-Midfai, H. et al. (2023). Vaccine Compliance in Iraqi Pilgrims. Journal of Travel Medicine.
3. Alqahtani, A. S., et al. (2022). "Impact of Multilingual AI Chatbots on Vaccine Acceptance Among Hajj Pilgrims." Vaccine, 40(15).
4. Al-Tawfiq et al. (2020). "Infection control in mass gatherings: Lessons from Arbaeen." Journal of Infection and Public Health.
5. Al-Tawfiq JA, et al. Hajj and Umrah Mass Gatherings and COVID-19 Infection. Curr Trop Med Rep 2020;7:133-140.
6. Alderson MR, Arkwright PD, Bai X, Black S, Borrow R, Caugant DA, Dinleyici EC, Harrison LH, Lucidarme J, McNamara LA, Meiring S, Sáfadi MAP, Shao Z, Stephens DS, Taha MK, Vazquez J, Zhu B, Collaborators G. Surveillance and control of meningococcal disease in the COVID-19 era: A Global Meningococcal Initiative review. J Infect. 2022 Mar;84(3):289-296.
7. Alzeer, A. H., et al. (2008). Respiratory tract infection during Hajj. Annals of Thoracic Medicine, 3(2), 50-53.
8. Asl H.M., Gouya M.M., Soltan-Dallal M.M., Aghili N. Surveillance for foodborne disease outbreaks in Iran, 2006-2011. Med J Islam Repub Iran. 2015;29:285.
9. BMC Public Health (2023). "Impact of WASH interventions on diarrheal diseases in Arbaeen."
10. CDC (2022).Travelers' Health: Hajj and Umrah Pilgrimage. Atlanta: Centers for Disease Control and Prevention.

11. CDC (2023).Global Meningitis Genome Library.

12. CDC Travel Advisory (2024): Recommends meningococcal vaccination for all Arbaeen travelers.

13. CDC. (2024).Travel Health Notice: Arbaeen Pilgrimage.

14. Chiu NC, Chi H, Tai YL, Peng CC, Tseng CY, Chen CC, Tan BF, Lin CY. Impact of Wearing Masks, Hand Hygiene, and Social Distancing on Influenza, Enterovirus, and All-Cause Pneumonia During the Coronavirus Pandemic: Retrospective National Epidemiological Surveillance Study. J Med Internet Res. 2020 Aug 20;22(8):e21257.

15. Choi YW, Eltahir EAJGRL. Heat stress during Arba'een foot-pilgrimage (world's largest gathering) projected to reach dangerous levels due to climate change. 2022;49(19):e2022GL099755.

16. Ebrahim SH, et al. Public Health Authority and Hajj Pilgrimage from Mass Gatherings to Global Health Security. J Epidemiol Glob Health 2021;11(3):253-256.

17. ECDC (2023).Antimicrobial Resistance Surveillance in Europe.

18. ECDC (2023).Public Health Risks During Mass Gatherings – Arbaeen Pilgrimage. European Centre for Disease Prevention and Control.

19. Hamdanieh L, Ostadtaghizadeh A. Arbaeen in the Context of the COVID-19 Pandemic. Disaster Med Public Health Prep. 2021 Aug;15(4):e16.

20. Hashjin ZG, Khanghahi MMJIJM, Understanding M. Messages of Arba'een Walking as Media. 2020;6(6):924–35.

21. Hashim HT, Babar MS, Essar MY, Ramadhan MA, Ahmad S. The Hajj and COVID-19: How the Pandemic Shaped the World's Largest Reli-

gious Gathering. Am J Trop Med Hyg. 2021 Jan 11;104(3):797-799.

22. Hoang VT, Gautret P. Infectious Diseases and Mass Gatherings. Curr Infect Dis Rep. 2018 Aug 28; 20(11):44.

23. Iraqi Ministry of Health (2023 Report).“Arbaeen Health Preparedness Plan”

24. Jafari et al. (2020). “Disease surveillance in Arbaeen mass gathering: Challenges and solutions.” Journal of Infection and Public Health.

25. Khan, A. S., et al. (2013). Hepatitis A among travelers: A systematic review. Travel Medicine and Infectious Disease, 11(4), 205-214.

26. Khan AA, Balkhi BS, Alamri FA, Alsaleh GS, Al-Tawfiq JA, Jokhdar H. Vaccinations for Hajj: Enhancing health and global health security. Travel Med Infect Dis. 2025 Jan-Feb;63:102784.

27. Mahdi HA, Rashid H, Qashqari FS, Hariri SH, Marglani OA, Barasheed O, et al.,Syndromic surveillance of respiratory-tract infections and hand hygiene practice among pilgrims attended Hajj in 2021: a cohort study. BMC Infect Dis. 2022 Jun 27;22(1):578.

28. Mehri A, Kolivand P, Zarepour P, Saberian P, Etemad K. Knowledge, Attitude and Performance of Arbaeen Hosseini Pilgrims Regarding the Common Diseases in 2023. Iran Red Crescent Med J. 2024,77.1-11.

29. Memish et al. (2019). “Blood-borne pathogen risks in mass gatherings.” Tropical Medicine and Infectious Disease.

30. Memish ZA, et al. Hajj in the Time of COVID-19: Infection Control in the Era of Pandemic. J Travel Med 2021;28(3):taab067.

31. Memish ZA, Zumla A, Alhakeem RF, Assiri A, Turkestani A, Al Harby KD, Alyemni M, Dhafar K, Gautret P, Barbeschi MJTL. Hajj: Infect Disease Surveillance Control. 2014;383(9934):2073–82.

32. Memish, Z. A., et al. (2002). Infectious diseases in pilgrims during the Hajj. Journal of Infection, 45(4), 233-236.

33. Memish,Z.A.,et al.(2023).“Meningococcal Disease Prevention at Hajj: A Decade of Success with Mandatory Quadrivalent Vaccination.”Journal of Travel Medicine,30(1).

34. Mirzaei R., Abdi M. An influenza A outbreak in Iranian individuals following Arba’een foot pilgrimage from October to December 2019. Infect Control Hosp Epidemiol. 2020;41:627–628.

35. Moradi G., Asadi H., Gouya M.-M., Nabavi M., Norouzinejad A., Karimi M., Mohamadi-Bolbanabad A. The communicable diseases surveillance system in Iran: challenges and opportunities. Arch Iran Med. 2019;22:361–368.

36. Moulaei K, Bastaminejad S, Haghdoost A. Health challenges and facilitators of arbaeen pilgrimage: a scoping review. BMC Public Health. 2024 Jan 9;24(1):132.

37. Riddle, M. S., et al. (2017). Guidelines for the prevention and treatment of travelers’ diarrhea. Journal of Travel Medicine, 24(1), 1-19.

38. Rouphael NG, Stephens DS. Neisseria meningitidis: biology, microbiology, and epidemiology. Methods Mol Biol. 2012;799:1-20.

39. Saudi Guidelines (2024). Ciprofloxacin Prophylaxis for African Pilgrims.

40. Saudi Ministry of Health (2020). Health Regulations for Travelers to Saudi Arabia for Hajj and Umrah. Riyadh: MOH Publications.

41. Saudi Ministry of Health (2024). Hajj and Umrah Health Regulations.

42. Saudi Ministry of Health. Hajj Health Regulations 2023. Riyadh: MOH, 2023.

43. Saudi MOH (2024). mRNA Vaccine Trials for Hajj 2025.

44. Shafi S, Dar O, Khan M, Khan M, Azhar EI, McCloskey B, Zumla A, Petersen E. The annual Hajj pilgrimage-minimizing the risk of ill health in pilgrims from Europe and opportunity for driving the best prevention and health promotion guidelines. Int J Infect Dis. 2016 Jun;47:79-82.

45. Shalbafian A.A., Zarandian N. A new Look at the Arba'een mega-event from the perspective of Iraqis as the host community. International Journal of Religious Tourism and Pilgrimage. 2021;9:8.

46. Shinde KAJEM. Managing Hindu festivals in pilgrimage sites: Emerging trends, opportunities, and challenges. 2010;14(1):53–67.

47. WHO (2019). Water, sanitation, and hygiene in mass gatherings. Geneva: World Health Organization.

48. WHO (2021/2030). Defeating Meningitis by 2030 Roadmap.

49. WHO (2022). Guidelines for mass gathering surveillance.

50. WHO (2024). Global Meningitis Surveillance Report 2023. World Health Organization.

51. WHO (2024). Real-Time Digital Surveillance in Mass Gatherings.

52. WHO Report (2023): Emphasizes strengthening meningitis surveillance in mass gatherings.

53. WHO. (2023).Meningitis in Mass Gatherings.

54. WHO. Public Health Considerations While Resuming Mass Gatherings in the Context of COVID-19. Geneva: WHO, 2021.

55. WHO-EMRO (2022).“Health preparedness for Arbaeen pilgrimage: Diarrheal disease control.”Eastern Mediterranean Health Journal.

56. Yezli, S., et al. (2014).Prevention of meningococcal disease at mass gatherings: Lessons from the Hajj. Vaccine, 32(48), 6551-6558.

57. Yezli, S., et al. (2023). “Zero Meningitis Cases at Hajj: The Impact of MenACWY Vaccination.”The Lancet Infectious Diseases, 23(5).

58. Yeung AWK, Torkamani A, Butte AJ, Glicksberg BS, Schuller B, Rodriguez B, et al., The promise of digital healthcare technologies. Front Public Health. 2023 Sep 26;11:1196596.

59. Zhu, W., Wang, D., Li, P., Deng, H., & Deng, Z. (2025). Advances in Wastewater-Based Epidemiology for Pandemic Surveillance: Methodological Frameworks and Future Perspectives. *Microorganisms*,*13*(5), 1169.

The Best routes to placement the Piezoeleric in holy Karbala using remote sensing and GIS techniques

Prof.Ebtesam F .khanjer

Ebtesam.khanjer@sc.uobaghdad.edu.iq

Asst.Lect.Mustafa S. Srayyih

Prof.Ban A. Al-Razaq

Khudhur Ahmed Hussein

Department of Remote sensing and GIS ,Collage of Science,
University of Baghdad

Abstract:

In this work explores the optimal placement of piezoelectric energy harvesting systems in the holy city of Karbala, Iraq, using (RS) and (GIS) Techniques. Piezoelectric technology, which converts mechanical energy from foot traffic and vehicular movement into electricity, offers a sustainable energy solution for high-pilgrimage areas Case Study (Arbaeen anniversary). By integrating spatial data, including pedestrian density, road networks, and land use patterns derived from satellite imagery and GIS analysis, this research identifies the most suitable locations for piezoelectric installations to maximize energy generation. Multi-criteria decision analysis (MCDA) techniques were applied to evaluate factors such as urban mobility, religious event schedules, and infrastructure suitability. The results highlight key zones near holy shrines (Al-Abbasia and, Al-Hussinnaa) walkways, and major roads where piezoelectric tiles can efficiently harness energy from the constant movement of pilgrims. The Roads map results were extracted using the Arc-GIS Pro software.

Keywords: Holy Karbala, Arabian anniversary, Pilgrimage Routes, Piezoelectric energy, sustainable energy, Mlti-criteria analysis.

Introduction

The holy city of Karbala witnesses massive pedestrian movement, especially during religious events such as Arbaeen, where millions of pilgrims walk on designated routes. Harvesting energy from foot traffic using piezoelectric sensors presents a sustainable solution for powering streetlights, (Hamad, Ali, & Hassoon, 2022) charging stations, and other urban infrastructure. This project aims to identify the best routes for piezoelectric sensor placement by analyzing pedestrian density, road

types, and surface conditions using Remote Sensing (RS) and Geographic Information Systems (GIS) (Hassoon & Ali, 2021)

With the world›s preoccupation with renewable energy sources such as wind, sunlight, rivers, seas, and others, some have turned to using the human body as a generator of electrical energy. Research is currently competing to find the most successful innovations to extract this type of economical electricity) Kareem & Hassoon, 2023)

.One researcher measured the electrical power that can be generated by a person jogging for minutes at approximately 1,000 watts. This means that the resulting electricity could be used in various applications, such as powering mobile phones, laptops, and music players. As nanotechnology enters its practical stages, others are considering a shoe that generates electricity up to 20 watts while walking. This innovation›s design involves the passage of a trapped fluid (Khalid, Ahmed, & Khaleel, 2024).

into one of two chambers at the bottom of the shoe, the first located under the instep and the second under the heel. When the instep is pressed, this fluid is forced through an electrical generator, which absorbs the energy and converts it into electricity. The fluid then reaches the chamber below the heel. When the person steps with their heel, this fluid is expelled back to the first chamber it came from, passing through the electrical generator, and so on (Curies & Curie, 1880) .

Most innovations in extracting electrical energy from body movement have faced numerous challenges in design methods and cost. In the case of the aforementioned shoe, many questions arise, most notably the user›s comfort level when wearing this shoe while walking and how to connect it to electrical devices (Piezo Products, n.d.).

Piezoelectric energy

The word piezo originates from the Greek word piezein ,meaning pressure. Piezoelectricity is the process of using crystals to convert mechanical energy into electrical energy, or vice versa. It is the ability of certain materials to generate alternating current (AC) voltage when subjected to mechanical pressure or vibration, or to generate vibration when subjected to AC voltage. Piezoelectricity is found in many of the electronic devices we use in our daily lives, from quartz watches to speakers and microphones. Jacques and Pierre Curie discovered the piezoelectric effect in 1880. They found that pressure applied to a quartz crystal generates an electric charge in the crystal, which is the direct property of this effect. Later, they also verified that an electric field applied to the crystal causes the material to deform, thus discovering the inverse property of this effect (Kwok, Lai, Chan, & Choy, 1997)).

The piezoelectric effect converts vibrational kinetic energy into electrical energy, i.e., It is the ability of certain materials to generate an electrical charge in response to applied mechanical stress. Piezoelectric generators (energy harvesters) provide a powerful and reliable solution by converting wasted vibrational energy in the environment into usable electrical energy. They are therefore ideal for applications that require charging batteries, supercapacitors, or directly powered remote sensing systems. This piezoelectric effect has two properties: the first is direct piezoelectricity, or the direct effect, meaning the material has the ability to convert mechanical stress into electrical charge. The second is indirect piezoelectricity, or the reverse effect, where the applied electrical potential is converted into mechanical strain energy. Figure (1) illustrates the direct and indirect piezoelectric effect) (Hassan & Khanjer, 2023)

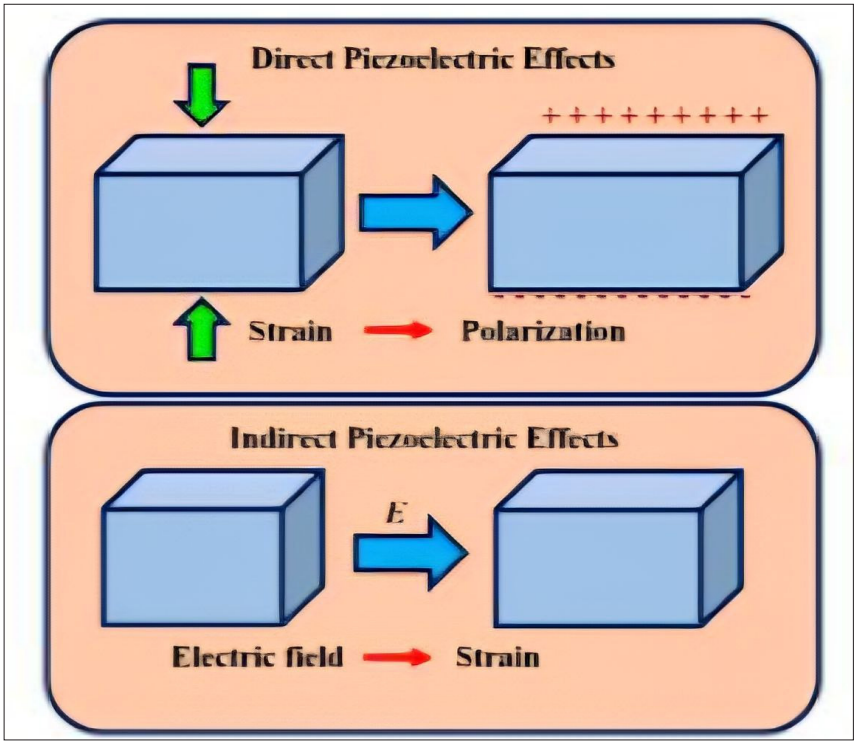

Objectives

- Map high-traffic pedestrian routes in Karbala using GIS and satellite imagery.
- Analyze road surface types (asphalt, concrete, etc.) to determine suitability for piezoelectric tiles.
- Estimate potential energy generation based on pedestrian flow data.
- Recommend optimal locations for piezoelectric sensor installation to maximize efficiency.

3. Methodology

1. Data Collection

- Satellite &OpenStreetMap's: High-resolution images to classify road types and pedestrian pathways.
- Crowd-Sensing Data: Mobile GPS data, Wi-Fi hotspots, and social media check-ins to track movement patterns.
- Field Surveys: Ground truthing to verify road materials and foot traffic intensity.

2. GIS Analysis

- Spatial Overlay: Combine pedestrian density maps with road surface data.
- Network Analysis: Identify key routes (main roads, secondary paths, and pilgrimage routes).
- Suitability Modeling: Use weighted criteria (traffic volume, surface durability, proximity to power needs).

Expected Outcomes

- A GIS-based suitability map highlighting optimal piezoelectric sensor locations.
- Energy generation estimates for different routes.
- Recommendations for integrating piezoelectric tiles into urban planning.

Results and Discussion

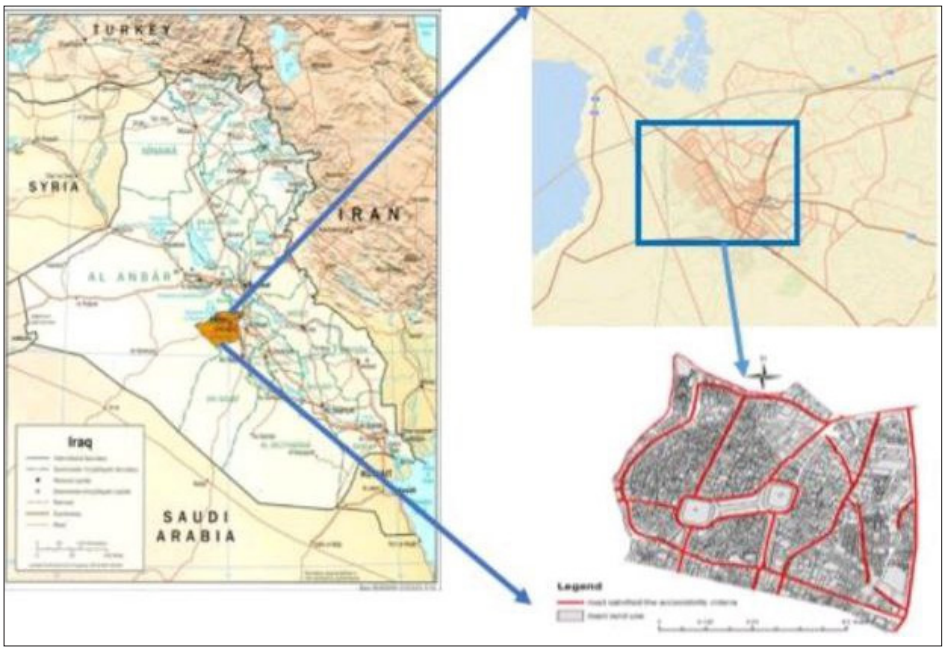

Figure .2 the location of holy Karbala in Iraq and the routes taken by Pilgrimages.

The Interactive Holy Karbala Map

This project is an interactive web application that displays all the main and secondary roads in the holy city of Karbala, with a focus on the routes leading to the shrines of Imam Hussein and Imam Abbas (peace be upon them).

Achievements

A. Geographic Data Collection and Analysis A)

- Comprehensive data was obtained from OpenStreetMap for the city of Karbala.
- Extracting and filtering road and route data.
- Determining the precise coordinates of the two holy shrines.
- Converting the data to Geo JSON format for use in the application.

B. Interactive Application Developmen

- Creating a modern, responsive React application.
- Integrating the Leaflet library for interactive maps.
- Designing an attractive user interface that is appropriate for the religious theme.
- Full support for the Arabic language and right-to-left text.

C. Interactive Features

- Interactive display of all road types with clear color coding.
- Ability to filter roads by type (main, secondary, pedestrian, etc.).
- Special signs for the two holy shrines with detailed information.
- Pop-up windows that display road information when clicked.
- A comprehensive map key that explains the meaning of colors and icons.

D. Design and Experience

- Responsive design that works on all devices.
- Calm colors that are appropriate for the religious theme.
- Easy-to-use interface. Easy to use and understand.
- Fast performance and efficient data loading.

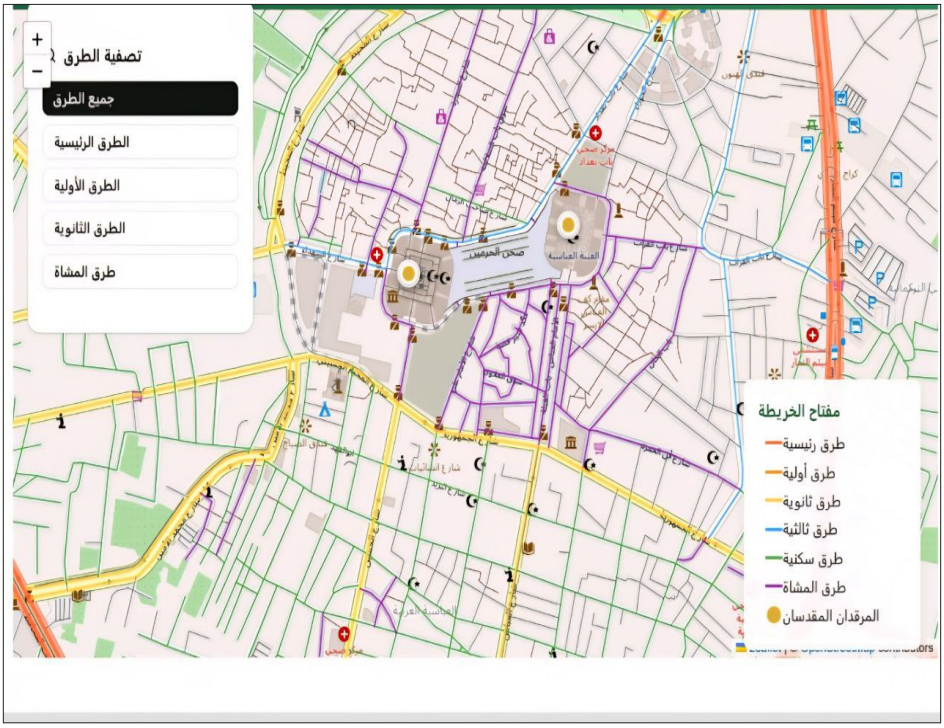

Figure 3. Interactive map of Holy Karbala

Conclusion

This project will provide a data-driven approach to deploying piezo-electric energy harvesting in Karbala, ensuring maximum efficiency and sustainability. By leveraging GIS and Remote Sensing, we can transform high-traffic pilgrimage routes into smart, energy-generating pathways.

References

1. Hamad, A. I., Ali, A. B., Hassoon, A. F. (2022, October). Climate change and its effect on waterand vegetation cover over shary region using GIS techniques. In AIP Conference Proceedings (Vol. 2398, No. 1). AIP Publishing.
2. Hassoon, A. F., & Ali, A. B. (2021). Irregular urban Expansion and Its Effects on Air Temperature over Baghdad City using Remote Sensing Technique. Iraqi Journal of Science, 2110-2121.
3. Kareem, S. A. A., & Hassoon, A. F. (2023). Effect of Urban Heat Island on Growth Rate of theConvective Boundary Layer Over Baghdad City. The Iraqi Geological Journal, 289-300. 11. Khalid H, Ahmed A., Khaleel I, 2024 "Supervised Classification Accuracy Assessment UsingRemote Sensing and Geographic Information System", TEM Journal. Vol. 13,, pp. 396-403.
1. Curies, P., & Curie, J. (1880). Development of polar electricity in hemihedral crystals with inclined faces. Bulletin de La Societe Mineralique de France, 3, 90-102.
2. https://www.piezoproducts.com/ar/piezo-electric-effect.
3. Kwok, K. W., Lai, H., Chan, W., & Choy, C. L. (1997). Evaluation of the material parameters of piezoelectric materials by various methods. In IEEE.
4. Hassan, Ahmed F. Hasson and Ebtesam F. Khanjer " Monitoring Changes in the Spectral Reflectivit tivity of Baghdad ndad City City and and the the Impact of the Atmospheric Elements on it using R.S and GIS"IOP Conf. Series: Earth and Environmental Science 1223 (2023) 012023.

5. http://www.piezocryst.com/downloads/Piezoelectric 8.

6. 9. S.Sense. “Piezoelectric Force Sensors Machine Design” Penton Media, Inc.(2008).

7. 10. T. L. Jordan and Z. Ounaries, “Piezoelectric CeramicsCharacterization “ICASE Report, (2001).

8. 11. Turab, N. M., Owida, H. A., Al-Nabulsi, J. I., & Abu-Alhaija, M. (2022). Recent techniques for harvesting energy from the human body. In Computer Systems Science and Engineering (Vol. 40, Issue 1, pp. 167-177). Tech Science Press. https://doi.org/10.32604/CSSE.2022.017973.

9. 12 Twidell, J., & Weir, T. (2015). Renewable energy resources. Routledge

10. W. D. Callifter, Jr.” An introduction to Materials Science & Engineering .(2008).

Spatial-Temporal Distribution of Particulate Matter in holy Karbala Governorate by using Remote Sensing Dataset and GIS

Prof.Sabah Hussien Ali

Remote Sensing Center-University of Mosul

sabah196004@uomosul.edu.iq

Asst.Prof.Alaa Nabeel Hamdon

Remote Sensing Center-University of Mosul

alaa441977@yahoo.com

Asst.Prof Abdulrahman Ramzi Qubaa

Remote Sensing Center-University of Mosul

mailtoabdqubaa@uomosul.edu.iq

Abstract:

Karbala is one of the most sacred religious cities in Iraq, visited by millions of pilgrims from all over the world, especially during important religious seasons, such as Ashura and the Al-arbaeen pilgrimage, which leads to millions of crowds. This study addresses the temporal and spatial distribution of PM2.5 particulate matter in Karbala Governorate using remote sensing data and techniques and Geographic Information Systems (GIS) software. PM2.5 particulate matter are considered hazardous air pollutants associated with respiratory and cardiovascular health risks, and their risks increase in crowded areas, especially during the annual gatherings of millions of pilgrims.

The study used satellite data to monitor the concentration levels of these particles during the Al-arbaeen pilgrimage period and analyzed them geographically using GIS to identify the areas most exposed to pollution within the city and surrounding areas during the period January-December, 2024. The results showed variations in particulate matter concentrations across locations and time periods, with the highest values recorded in areas close to the holy shrines and on the main roads leading to them, where transportation and human activity increase. Seasonal weather conditions also affected the accumulation of pollutants, especially during periods of high crowd density, which increases particulate emissions due to increased activities and vehicle traffic.

The study emphasizes the need to use remote sensing and geographic information systems (GIS) technologies as effective tools for monitoring air quality in the holy city of Karbala, given their critical environmental and health importance in light of the large number of pilgrims. This contributes to advance planning and the necessary measures to reduce pollution and protect the health of the governorate's indigenous population and visitors.

Keywords: Karbala, PM2.5, WHO, Al-arbaeen pilgrimage, Ventusky

Introduction

The use of remote sensing data and GIS tools in monitoring and management of the environmental conditions within Karbala Governorate has become an essential scientific research due to the rising need of accurate, timely, and affordable environmental data to aid in sustainable management of resources and urban design and planning (Kadhim et al., 2023). During the past decades, the development of satellite imaging and geospatial analysis altered the environmental assessment practice to the extent that land use, water body, and ecological changes could be evaluated in detail (Sameer, 2023). The importance of the technologies in question is especially apparent during the fast urbanization of Karbala, depletion of water resources, and land cover changes, which pose dangers to the ecological balance and socio-economic growth (Aal-shamkhi et al., 2017). Several studies have reported significant decreases in areas covered by water and significant growths of urban land and the necessity of efficient monitoring tools (Rashed et al., 2024; Mohammed et al., 2018). Regarding particulate matter pollution, remote sensing data together with Geographic Information Systems (GIS) can be successfully used to analyze the spatial-temporal pattern of PM2.5 and PM10 distribution in Karbala. With this approach, air quality can be mapped at high-resolutions, revealing important spatial variations and possible health-related threats associated with particulate pollution. Such circumstances as seasonal weather conditions and mass events, like the pilgrimage Arbaeen, affect the distribution of PM2.5 and PM10 in the region greatly. The meteorological factors and air pollutants interaction is intricate which causes significant changes in the air quality all through the year, especially during mass gatherings. Arbaeen pilgrimage, visited by millions of people, adds to ve-

hicular emissions and causes the generation of dust, therefore, increasing particulate matter concentration. Such events are particularly dangerous due to combined high temperatures and high PM, and this aspect needs special public health measures (Nsour, 2020).

Past studies give a evidence about these dynamics. As an example, the article by (Aghababaeian & Etedali 2024) has not dealt specifically with the influence of seasonal weather and mass presence on the distribution of PM but with the health risks of dangerous weather conditions during Arbaeen. Their study raises the extreme temperature and dust storms that are typical of the Iraqi summers which increase the levels of PM. In the meantime, such studies as that by (Ali et al. 2024) established that the air quality tends to be solider during winter months, and a considerable rise in particulate matter during summer months with PM2.5 as the prevailing pollutant on 84-88 percent of days. Nevertheless, this paper did not particularly examine the impacts of mass events. Moreover, (Al-Anbari et al. 2018) noted the highest levels of PM2.5 in December, April, and May, which may be caused by seasonal weather patterns and a rise in vehicles emissions related to large events like the Arbaeen pilgrimage. Although such events generate the spikes in pollution, they do trigger the local authorities to implement the air quality management strategies, which might result in the improvements of the air quality monitoring and preparedness in the long-term perspective.

Materials and Methods

1.Study Area:

Karbala Governorate is located in the central region of Iraq at the geographical coordinates of latitude (320:12'00.0" to 320:48':00.00") N and longitude of (430:30'00.00" to 440:18':00.00") E, Fig.1. It represents one of the most important governorates in terms of its geographical and religious location, as it contains the shrines of Imam Hussein ibn Ali and his brother Abbas (peace be upon them), making it a destination for millions of visitors annually, especially on major religious occasions such as the Arbaeen of Imam Hussein.

It is bordered to the north by Baghdad Governorate, to the east by Babil Governorate, to the south by Najaf Governorate, and to the west by Anbar Governorate. The governorate covers an area of approximately 5,034 km2. According to estimates by the Central Statistical Organization for the year 2023, the governorate's population reached approximately 1.4 million people, distributed between the city center (Karbala) and a number of its affiliated districts and sub-districts, such as Ain al-Tamr, al-Hindiya, and al-Hur (Euaa, 2024).

According to the Köppen climate classification, Karbala falls within the hot desert climate (BWh), experiencing long, extremely hot summers, with temperatures often exceeding 45°C during July and August, while winters are mild to cool, with temperatures sometimes dropping below 10°C in January. Rainfall is low, typically not exceeding 100–150 mm annually, concentrated in the winter months (November to March) (Weam and Iman, 2021). It is also occasionally exposed to dry northwesterly winds, known locally as the Northern wind which can contribute to dust storms at certain times of the year.

Figure 1: The location of the study area

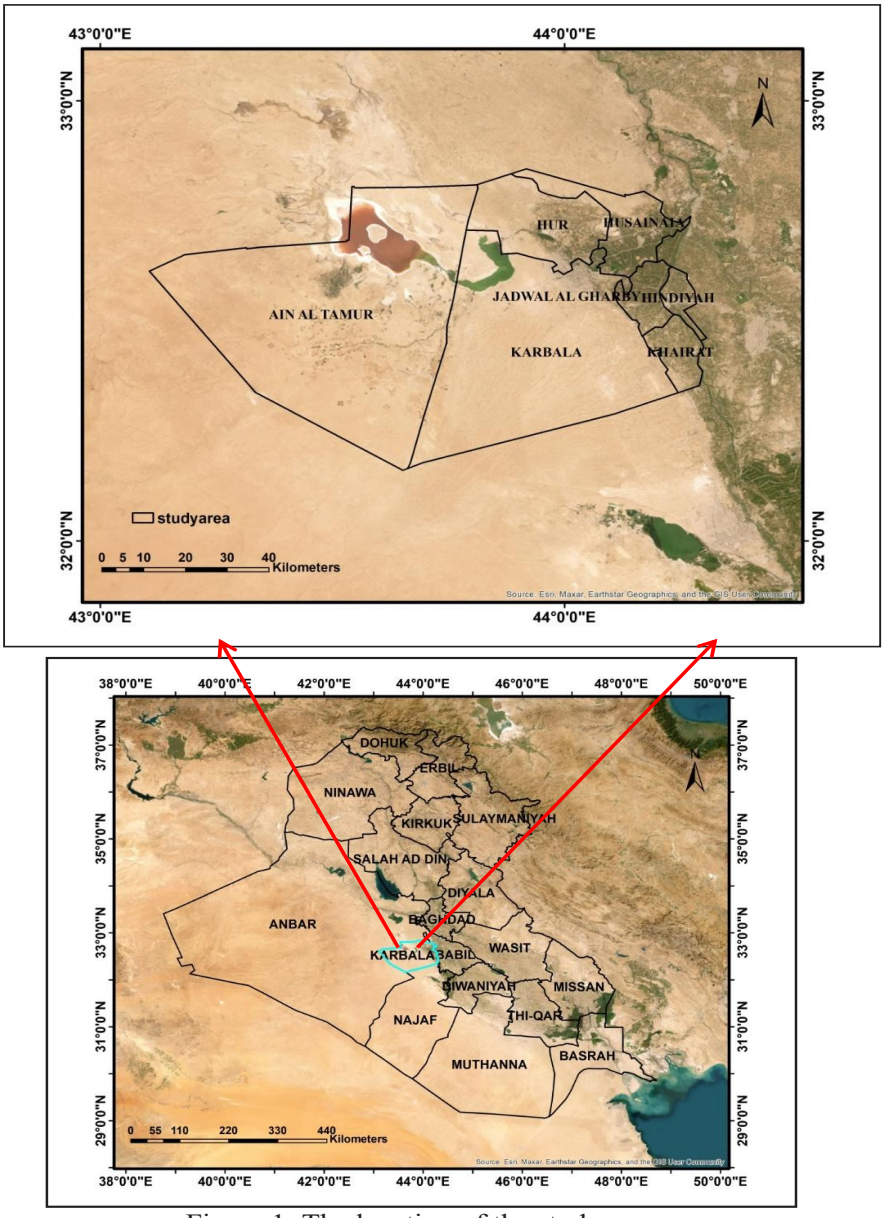

Figure 1: The location of the study area

2.Data sources:

As previously mentioned, the holy city of Karbala is one of the most important religious centers in Iraq and the Islamic world, attracting millions of pilgrims annually. Population density and traffic peak during major religious occasions, most notably the Arbaeen pilgrimage, due to the shrines of Imam Hussein and his brother Abbas, peace be upon them. This high density of pilgrims and vehicles, particularly in the city center of Karbala and the areas surrounding the Two Holy Shrines (such as the Hussein and Abbas neighborhoods, and Al-Rawda Street), contributes to high levels of air pollution, particularly particulate matter (PM2.5). Due to the absence of permanent environmental monitoring stations dedicated to measuring air pollutants inside the borders of the Karbala Governorate, the current study relies on data gathered via the Ventusky website. Six sites were selected and the PM2.5 data were downloaded based on the geographical distribution illustrated in Fig. 2.

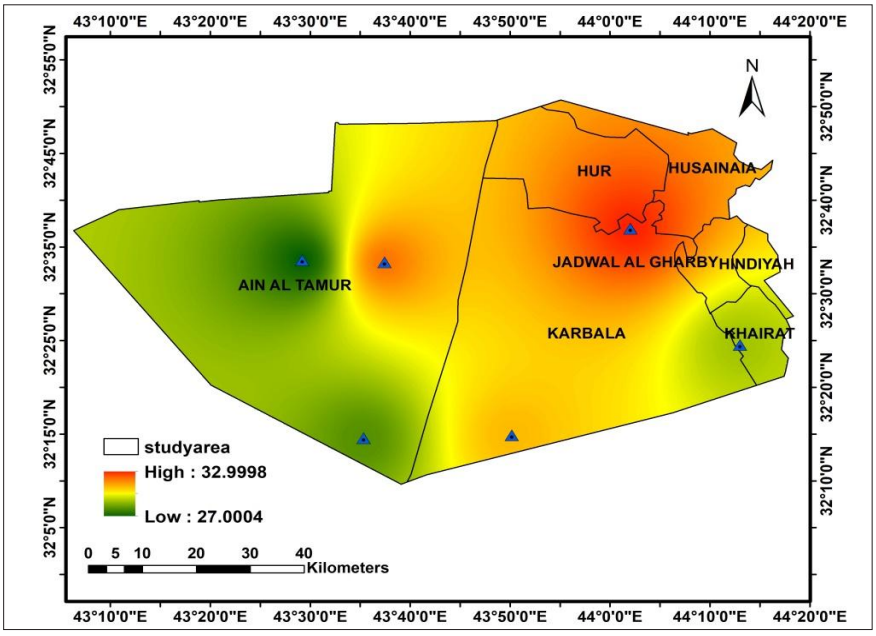

Figure 2: location of the selected sites

The data included daily coverage for the entire year 2024, enabling high-resolution analysis of temporal variations. After collecting the data, it was organized and processed using statistical analysis software and spreadsheets, and divided into four groups representing the climatic seasons (spring, summer, fall, and winter). The seasonal averages for each particle type were then calculated, along with the annual average, which represents the overall average for 2024.Ventusky uses the Automatic/Global SILAM model (https://www.ventusky.com/) to extract Aerosol Optical Depth (AOD) data from the Moderate Resolution Imaging Spectroradiometer (MODIS) Aqua and Terra satellites with a spatial resolution of 1 km * 1 km.

Results and Discussions

Notably, the research confirms the vulnerability of Karbala's environmental system to rapid urbanization and climate-related challenges. The observed particulate matter distribution patterns underscore the necessity of targeted air quality management strategies, particularly during high-risk periods such as summer months and major holy visit events. The interaction between meteorological factors and air pollutants emerged as a particularly nuanced aspect of our investigation. The data reveals that the climatic elements and human activities collectively influence particulate matter concentrations, presenting a complex environmental challenge that requires multifaceted intervention approaches. Previous studies focused on health risks during extreme weather, while our study provides a more comprehensive spatial analysis of pollution dynamics. This approach offers local authorities and policymakers a more detailed understanding of environmental conditions, potentially informing more effective urban planning and public health strategies. In Fig. 3 a high value of PM 2.5 concentrate at south of Karbala governorate during winter season, while lowest value

concentrate at east and west of the governorate. Our findings reveal a significant correlation between high PM2.5 concentrations and potential health risks, which align with and extend previous epidemiological research in urban environmental health. The observed particulate matter levels in our study area substantially exceeded recommended regular thresholds, suggesting an urgent need for targeted intervention strategies.

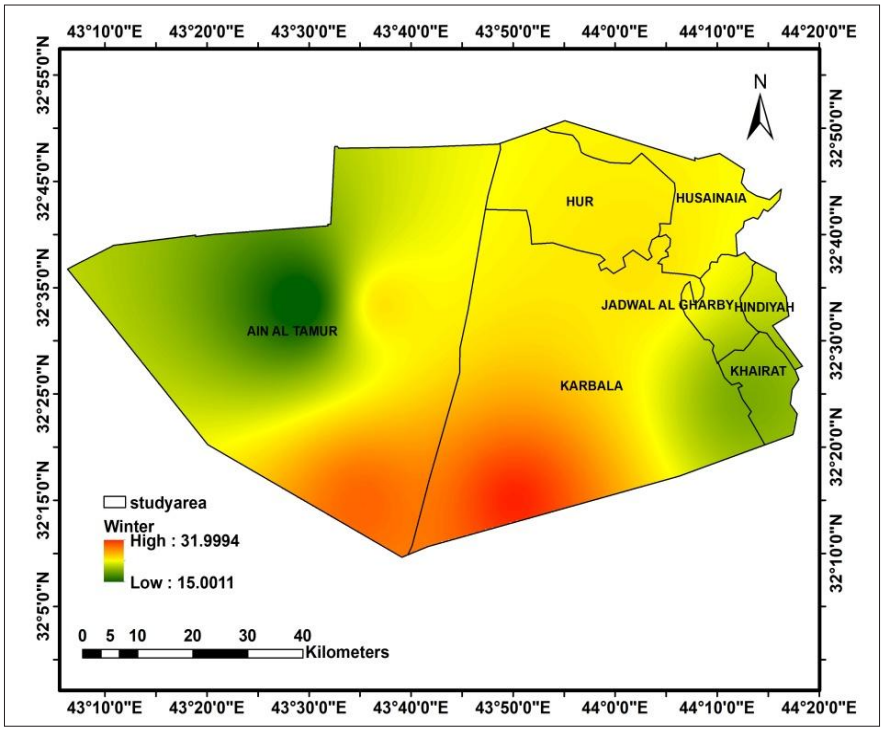

Figure 3: Spatial distribution of PM2.5 in winter

In Fig. 4 a high value of PM 2.5 concentrate at east of Karbala governorate during spring season, while lowest value distribute at the central part of the governorate.

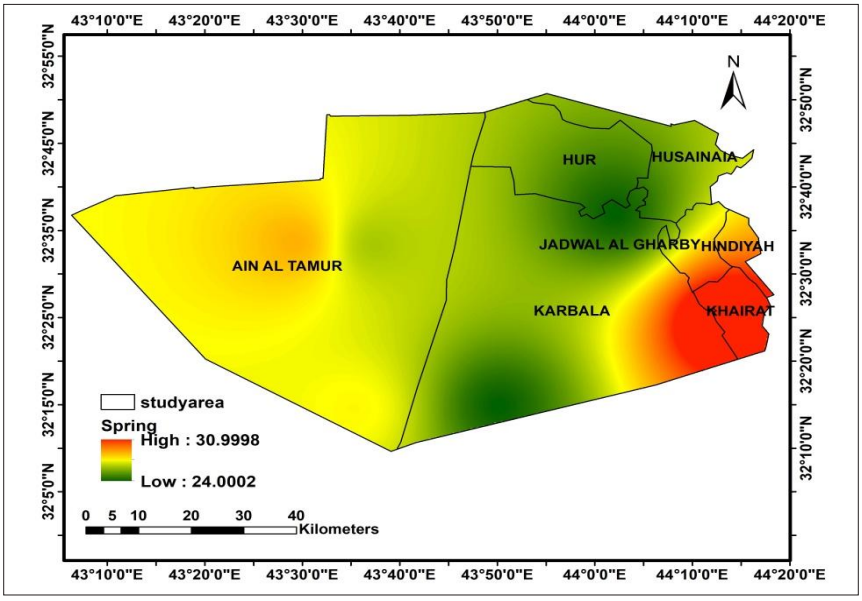

Figure 4: Spatial distribution of PM2.5 in spring

In Fig. 5 a high value of PM 2.5 concentrate at northern part of Karbala governorate during summer season, while lowest value align at the southern part of the governorate.

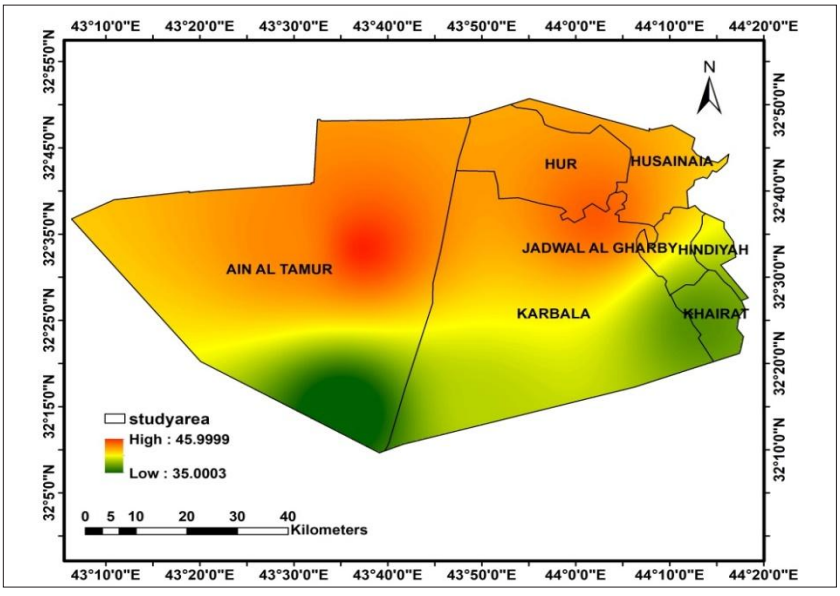

Figure 5: Spatial distribution of PM2.5 in summer

In Fig. 6 during autumn season a high value of PM 2.5 concentrate at center of Karbala governorate, while lowest value distribute at the western part of the governorate.

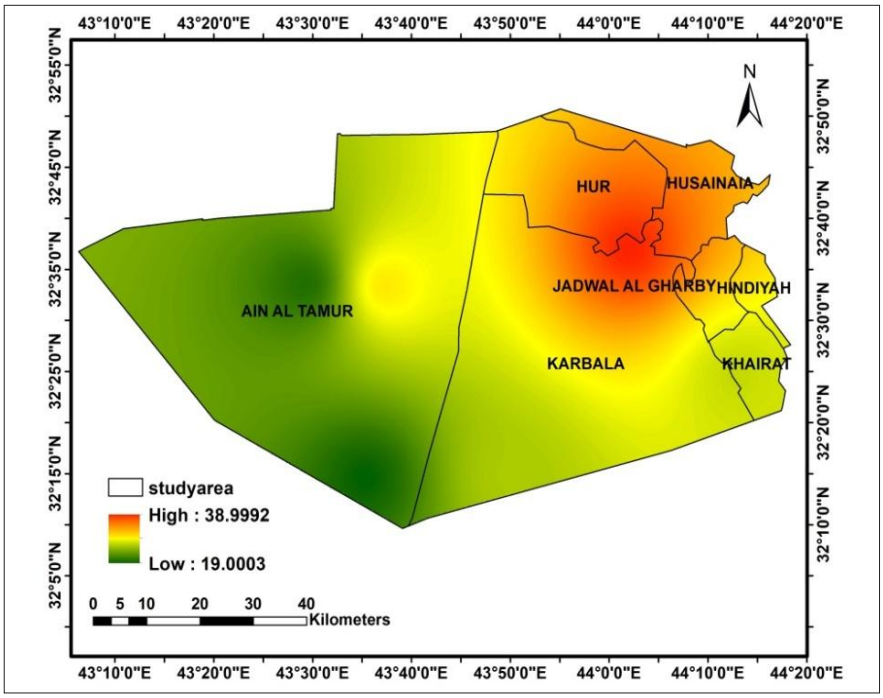

Figure 6: Spatial distribution of PM2.5 in Autumn

The annual average of PM2.5 reveal to high concentration of PM2.5 at capital city of Karbala governorate which is the holy city of Karbala Fig. 7. This might back to the high density of urbanization and holy events during the year, Fig. 8 and 9. Therefore, an action required to reduce the risk of PM 2.5 in that area.

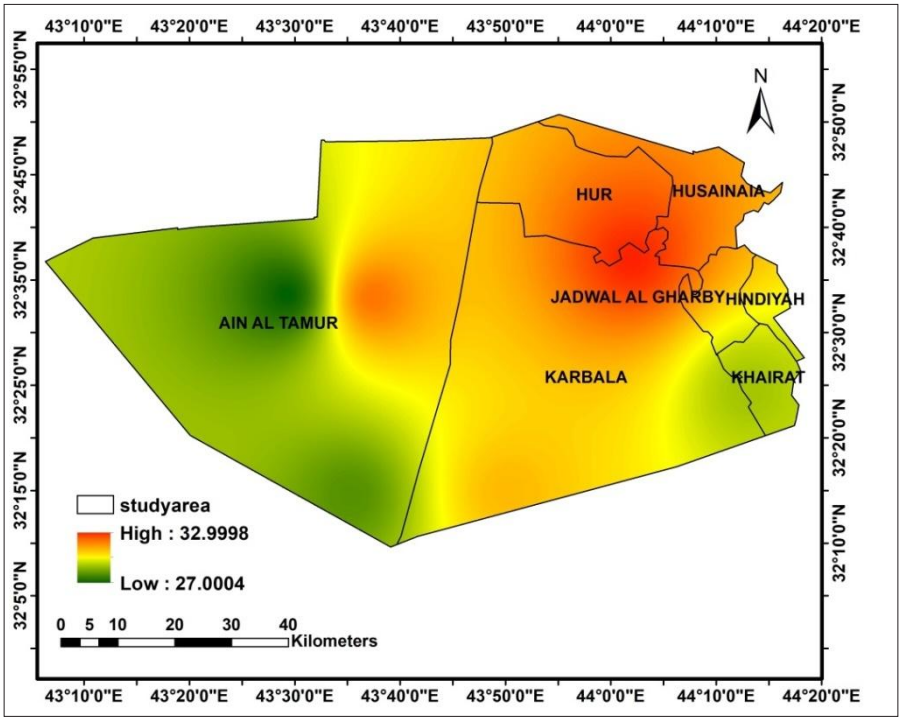

Figure 7: Annual spatial distribution of PM2.5

Figure 8: Al-Abbas's Holy Shrine during the Arbaeen Pilgrimage 2024

(25 August, 2024)

Figure 9: Al-Abbas's Holy Shrine after the Arbaeen Pilgrimage 2024 (24 Sept. 2024)

Table 3 lists the min. and max. annual PM2.5 concentrations according to the maps (2-6).

Table 3 : The seasonal and annual PM2.5 values of the 2024 in Karbala

Seasons and annual	PM2.5 values 2024	
	Min.	Max.
Winter	15.0	32.0
Spring	24.0	31.0
Summer	35.0	46.0
Autumn	19.0	39.0
Annual	27.0	33.0

The results shows, that seasonal climate changes significantly affect the spatial distribution of particulate matter in Karbala Governorate. In the summer, high temperatures, low humidity, and increased wind speeds resuspend fine particles in the air, leading to higher concentrations, especially in urban and open areas. In the winter, low temperatures and relatively calm air movement lead to increased particulate accumulation in the layers near the ground surface, particularly in densely populated residential areas with household emissions. During spring and fall, a marked variation in spatial distribution is observed due to the continuous changes in wind patterns and temperatures, making some areas more susceptible to particulate matter accumulation than others. This seasonal variation highlights the importance of understanding climate factors in assessing the risks of particulate matter pollution and planning mitigation measures.

The results of the analysis indicated that the concentration of PM2.5 in the Karbala Governorate was higher than what was allowed by both Iraqi national environmental standards and World Health Organization (WHO)-approved environmental standards (10µg/m3) (Profile on Environmental and Social Considerations in Iraq, 2011, WHO 2006) as shown in Fig.10. High amounts of air pollution are present, as indicated by this exceedance, directly endangering the environment and public health. Because these tiny particles can worsen existing health problems and raise rates of morbidity and mortality, this pollution is especially concerning for vulnerable groups, particularly individuals who have chronic respiratory disorders like lung disease, bronchitis, and asthma.

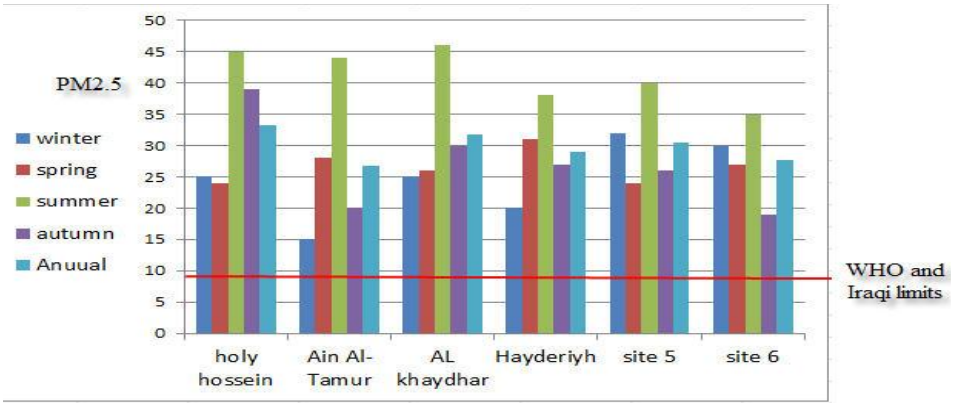

Figure 10: Comparing PM2.5 concentration levels to WHO and Iraqi regulatory standards

Conclusions

In conclusion, the integration of remote sensing data and GIS techniques is a crucial tool for effectively monitoring and managing the environmental challenges faced by Karbala City, particularly in light of rapid urbanization and significant air pollution from events like the Arbaeen (40) visit. The study on the temporal and spatial distribution of PM2.5 (particulates matter) in Karbala city using remote sensing data and GIS software has shed light on the hazardous air pollutants associated with respiratory and cardiovascular health risks. The analysis of satellite data during the Al-Arbaeen visit period discovered variations in particulate matter concentrations across locations and time periods, with the highest values recorded in areas close to the holy shrines and main roads, where transportation and human activity increase, especially during periods of high crowd density. This emphasizes the essential need to employ remote sensing and GIS technologies as effective tools for monitoring air quality in the holy city of Karbala, particularly due to the significant health implications for the large number of visitors and the native population, leading

to the advancement of planning and measures to reduce pollution and protect public health. The findings highlight the importance of addressing air quality concerns in pilgrimage sites and the surrounding areas, especially during important religious seasons, and highlight the potential impact of seasonal weather conditions on particulate matter accumulation, calling for proactive measures to mitigate the associated health risks. Overall, this study provides valuable insights into the environmental and health challenges in Karbala and presents a compelling case for the integration of advanced technologies in environmental monitoring and management to safeguard the well-being of the local population and visitors. The findings underscore the urgent need for enhanced air quality management strategies to safeguard public health and ensure sustainable resource management in this ecologically sensitive region.

Semi-Annual Scientific Journal
www.arbnj.com

References

1. Aghababaeian, H., & Etedali, H. (2024). Urgent Warning: Evidence-Based Concerns Regarding Mass Gathering Events During Arbaeen in Hazardous Weather Conditions. Disaster Medicine and Public Health Preparedness, 18, e258. doi:10.1017/dmp.2024.173.

2. Al-Anbari, R., Mohammed, Z. B., Ismail, M., & Resheq, A. (2018). Assessment of air quality for Kerbala city using field survey. MATEC Web of Conferences 162, 05015. https://doi.org/10.1051/MATECCONF/201816205015.

3. Ali, H., Wahab, B. I., & ABDUL AL-HMEED, H. M. (2024). Comprehensive air quality analysis in Karbala: Investigating the relationships between meteorological factors and pollutants across different landscapes. Journal of Agrometeorology, 26(4), 401–410. https://doi.org/10.54386/jam.v26i4.2665.

4. Euaa. (2024). Iraq Security Situation. Country of Origin Information Report, European Union Agency for Asylum (EUAA). http:// doi: 10.2847/61474.

5. Kadhim, A., Abood, R., Mahdi, A., & Khalaf, A. (2023). Evaluation of Land Cover Changes in Karbala Governorate Using Remote Sensing and GIS Techniques. https://doi.org/10.33899/earth.2023.143323.1144.

6. Mohammed, E. A., Hani, Z. Y., & Kadhim, G. Q. (2018). Assessing land cover/use changes in Karbala city (Iraq) using GIS techniques and remote sensing data. 1032(1), 012047. https://doi.org/10.1088/1742-6596/1032/1/012047.

7. Nsour, M. (2020). Iraq Mass Gathering Preparedness and Public Health Recommendations. JMIR Public Health and Surveillance, 6(2). https://doi.org/10.2196/15886.

8. Rashed, A., Al-Hadithi, M., & Alattar, F. M. (2024). Applying geographic information systems (GIS) techniques to estimate surface area of Al-Razzaza Lake, Karbala province, Iraq. 1300, 012008. https://doi.org/10.1088/1755-1315/1300/1/012008.

9. Profile on Environmental and Social Considerations in Iraq, 2011, Japan International Cooperation Agency (JICA), ANNEX CR (5)-11-018: 156, available at : https://openjicareport.jica.go.jp/pdf/257895.pdf.

10. Sameer, M. (2023). Remote Sensing and GIS Techniques in Monitoring Land Use Land Cover Change. International Journal of Sustainable Construction Engineering and Technology, 14(1). https://doi.org/10.30880/ijscet.2023.14.01.002.

11. Weam H. K. & Iman A. A. (2021). Climate parameters analysis asan indication ofclimateChangesforDiwaniya, Nasiriya, Kutand Karbala meteorological stations -Central and southern Iraq:Karbalaclimatecondition as a case study. Iraqi Journal of Science 63(12): 5295-5308. DOI: 10.24996/ijs.2022.63.12.19.

12. WHO 2006. Air quality guidelines for particulate matter, ozone, nitrogen dioxide and sulfur dioxide.Global update 2005. Summary of risk assessment. WHO/SDE/PHE/OEH/0602. Ginebra, Suiza: World Health Organization. Available at: https://goo.gl/xXO7Ku. Available at : https://www.who.int/publications/i/item/WHO-SDE-PHE-OEH-06-02,accessed on : 3 August,2025.

Design of New Cryptosystem to Protect the Transmitted Data for Imam Hussein's Visitors or Protection Units

Prof.Faez Hassan Ali

(1).Dept. of Mathematics, College of Science, Mustansiriyah University.

Prof. Samira Naji Kadhim

. Dept. of Mathematics, College of Science for Women, Baghdad University.

Asst.Dr.Adnan Mohammed Ali

Computer Technology Engineering Department, Baghdad College of Economic Sciences University.

Abstract:

This paper presents the design of a new stream cipher cryptosystem (CS) with a new Key Generator (KG). Firstly, we presented the mathematical model of the new CS, which is based on Linear Feedback Shift Registers (LFSR) units with non-linear combined functions to increase the complexity of the design CS. This cryptosystem can be used to protect data transmitted (online or offline) during the Arbaeen pilgrimage commemorating Imam Hussein's martyrdom, peace be upon him, whether by pilgrims or/and military protection units affiliated with the army or police. To test the output key results, we apply Basic Efficiency Criteria (BEC) to the suggested KG. The results of using BEC demonstrate the robustness and efficiency of the new stream cipher CS.

Keywords: Cryptography, Cryptosystem, Stream cipher, Linear Feedback Shift Registers, Basic Efficiency Criteria, Multiplicative Cyclic Group.

Introduction

The issue of information protection has become one of the most important matters of concern to those interested, especially in light of the rapid development of information technology and its means of transmission and the development of methods of penetration of such information, especially information classified to a high degree of confidentiality, including Secret Information (SIs). (Shaker, Nasser, & Ali, 2023)

The basics of the problems that occur during the process of transferring SP's will be discussed, and then the means of addressing them through proposing and designing a CS for protecting those SIs.

implemented a new style based on the dynamic algorithm, which is based on the concept to alter the framework of the LFSRs with every modification in the initial keys to obtain a complex ciphering algorithm based on a bank of LFSRs stored in a file and selecting random 10 LFSR's. They use BEC on KG to validate the result, which passes all of the tests. (Salih, Al-Safi, & Ali, 2014) design a new robust and dynamic CS called Robust and Efficient Dynamic Stream Cipher Cryptosystem (RDSCC) using stream KG which has good random statistical properties. The RDSCC is constructed to be flexible to encrypt (decrypt) different types of data; like message text and image data efficiently. (Ghazi & Ali, 2018)

proposed (5) algorithms for CS: encryption, decryption, signature generation, key generation, and signature verification. The proposed CS construction is based on the quadratic residue, quadratic quotient, floor function, absolute value recording, Diffie-Hellman key exchange protocol, and probability theorem. (Hossain, 2019) The advantage of the proposed CS intensive technique is that the intended receiver receives only one PT value that distinguishes the CT from the PT by verifying the send-

er's signature. (Gad, Hagras, Soliman, & Hikal, 2021) present a novel fuzzy multi-modular chaotic map for images encryption (Chen, Xie, & Zhang, 2022) used a modified Henon Map to Combination Section Image Encryption algorithm. (Ali, Ali, Redha, & Abubakari, 2023) construct a novel efficient stream cipher cryptosystem (SCSC) to decrypt (encrypt) digital images. The new system achieves the efficiency criteria that were applied to both the encrypted images and the key which obtained from the KG. (Ali, Mahdi, Ali, & Abdulkareem, 2024), present an overview on the use of information technology for data security. The most common data protection technologies are introduced, including CG (and CS design) and information hiding. Additionally, they refer to the CA and Steganalysis approaches to demonstrate how we can attack data, particularly send data.

In section 2 we introduce some basics of cryptography and SCs. In section 3, we discuss some important Stream Cipher SC's. Section 4 introduces the BEC for CSCS. The problem statement is discussed in section 5. In section 6, we introduce the new proposed CS to protect the communication of pilgrims. Section 7 introduces the proposed KG for the suggested CS with implementation of BEC. In section 8 we will show the user interface of PHVCCS. Lastly, the conclusions and future works are introduced in section 9.

Cryptography and Cryptosystems

- Cryptography (CG) is the study of principles and techniques by which information or plaintext (PT) can be concealed in ciphertext (CT) and later revealed by legitimates users employing the secret key (SK), but in which it is either impossible or computationally infeasible for an unauthorized person to do so. Cryptanalysis (CA) is the scie**nce (and art) of** recovering

PT from CT without knowledge of the SK. Both terms are subordinate to the more general term Cryptology. The CG concerned in Encryption (EP) and Decryption processes (DP) [9] (Motwani & Raghavan, 1995).

Some encryption algorithms (E_k) use a SK, so that the CT depends on both the original PT and the SK value. Some-times the Encryption key (e_k) and the decryption key (d_k) are same. Other times e_k and d_k come in pairs. Then d_k, Inverts the e_k. A SK allows different encryptions of one PT just by changing the SK. Use of a SK provides additional security. If the E_k should fall into the interceptor's hands, future messages can still be kept secret because the interceptor will not know the SK value [1]

- The Cryptosystem (CS) : are the systems which use the EP and DP. The CS divided into Secret-Key CS (SKCS) and Public Key CS (PKCS). The SKCS consists of Classical CS (CCS) and Modern CS (MSC). The MSC divided into Block Cipher CS (BCSC) and Stream Cipher CS (SCSC), these CS's can be classified as in figure (1)

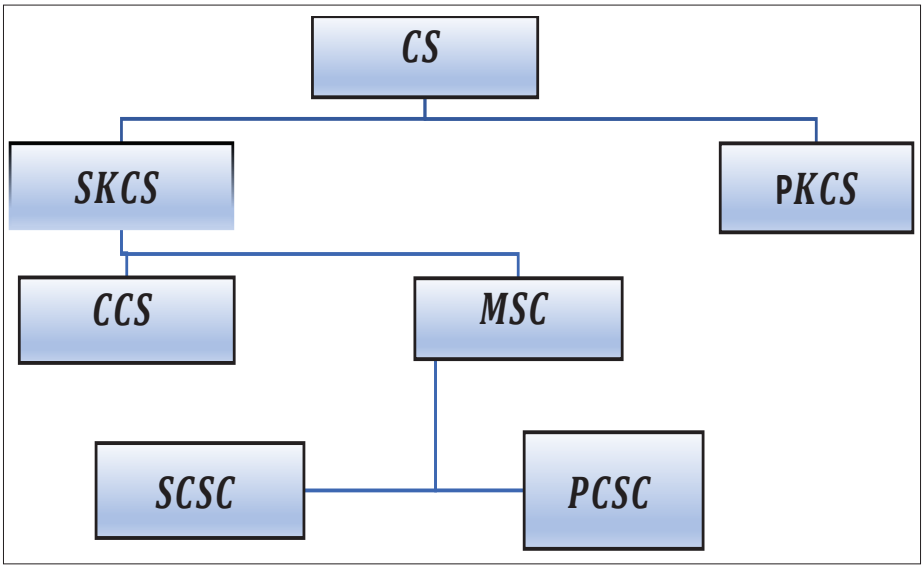

Figure (1) classification.

In a SKCS, the same SK will be used ($ek = d_k = k \epsilon K$), which is used in both EP and DP. It's also called symmetric cryptosystems.

The sender uses an invertible transformation, so produce the CT [10]:

$$C = (Ek(m)) \quad \ldots.(1)$$

where $m \epsilon M$ and $c \epsilon C$, and transmits it over the public insecure channel to the receiver. The *SK (k)* should also be transmitted to receiver by using a secure channel to decrypt c by function:

$$D_k(c) = D_k(E_k(m)) = m \quad \ldots.(2)$$

Where $c \epsilon C$ and $m \epsilon M$ and it's the PT.

There are many different types of , like monographic (character) ciphers, polygraphic (block) ciphers, exponentiation ciphers and (bit) ciphers [10] (Yan, 2000).in which we will focus.

Some Important SCSC

In this part we will introduce two important units which are very suitable to be used in CSCS because of their mathematical background, high complexity, high periodicity, randomness, speed when they be design software or hardware.

1.Linear Feedback Shift Register Systems

Linear Feedback Shift Register (LFSR) systems are used widely in SCSC field. A LFSR System consists of two main basic units. First, is a LFSR function and initial state values (Schneier, 1995). The second one is, the Combining Function (CF), which is a boolean function which is combined the output (x_i) of each LFSR s.t. CF=F($x_1, x_2, \ldots, x_n$). Most of SCSC are depend on these two basic units (Whitesitt, 1995).

2. Multiplicative Cyclic Group [13]

The Multiplicative Cyclic Group (MCG) unit generates the sequence S is a function of five variables which are not related to each other s.t. S=MCGU(q,a_t,a_r,γ,m), where $1\leq\gamma\leq q-1$ is any start integer point. These variables are as follows:

- q is prime number.
- $a_t \neq a_r$ are two different generators.
- m is the digit value of the sequence which generated from the (for binary sequences we use $m = 2$).
- γ is the start point where $1\leq\gamma\leq q-1$.

The MCG is very suitable to be used in . The algorithm steps can be found in [13]·(Ali, 2006).

Basic Efficiency Criteria for SCSC

Efficiency metrics are one of the most basic methods for measuring algorithm performance.We will now present some properties for *SCSC's* Basic Efficiency Criteria (*BEC*).

1. Randomness Tests (RTs)

When the *KG* designed to encrypt/decrypt one character or byte from PT, so we have to depend on the *RTs* to test the sequences *S* which belong to the filed $GF(2^8)$. The used *RTs* is 256-Digital Tests (*256DT*) which consists of (Ali, Ali, & Redha, 2023):

- **Digital Frequency Test (DFT):** Let's the expected number (*EN*) of digit *i* is $E^F=0.0039L$, while n_i be the observed number (*ON*) of digit *i* in *S* , (i =0,1,…,255), then the statistic value T^F of *DFT* is:

$$T^F = \frac{256}{L}\sum_{i=0}^{255}(n_i - 0.0039L)^2 \qquad \text{.....(3)}$$

With freedom degree υ=255.

• **Digital Run Test (DRT):** Let E_j^R be the *EN* of runs with length *j*, and the ON of runs is R_{ij} with type *i* runs with length *j*, then, the T_i^R of *DRT* is:

$$T^R = \sum_{i=0}^{255}\sum_{j=0}^{M_i}\frac{\left(R_{ij}-E_j^R\right)^2}{E_j^R} = \sum_{j=0}^{M_i}\frac{\left(R_{ij}-65025L/256\right.}{65025L/256^{j+}} \quad .....(4)$$

With $\upsilon_i = 256\ (M_i\text{-}1)$,where M_i is maximum length of run *i*.

• **Digital Auto-Correlation Test (DA-CT):** The *ON* of similar and distinct digits are $n_0(\tau)$ and $n_1(\tau)$ after shifting *S* by τ respectively, where τ =1,2,…,L-1, while the *EN* of similarity and difference respectively are: $E_0^A(\tau)=0.004(L-\tau)$ and $E_1^A(\tau)=0.996(L-\tau)$ ….(5)

and

$$T^A(\tau) = \sum_{i=0}^{1}\frac{\left(n_i(\tau)-E_i^A(\tau)\right)^2}{E_i^A(\tau)} \quad ....(6)$$

with υ =1.

The Randomness of *LFSR's* system proven in [3].

2.Key Space Analysis

In order to remain secure via the exhaustive search attacks, it must make the method's key space as big as possible. A safeguard key space ought to exceed 2^{128}(Alvarez & Li, 2006).

3.4.3 Efficiency Criteria Calculations of MCGU

1. The following cases described the good efficient sequences which is generated from the [16] (Ali, 2009):

• **Linear Complexity (LC):** the LC is secure when the MCGU has high non-linearity.

• **Periodicity (P(S)):** Every generated S has a period of q-1. So, if we have two distinct generators so we have $P_2^{(g(q))}$ generators. Lastly, the *MCGU* period is:

Semi-Annual Scientific Journal www.arbnj.com Ramadan 1447 A.H, March 2026 A.D

$P(S)=P_2^{(g(q))}*(q-1)$ ….(7)

Where $g(q) = \varphi(q-1)$.

- **Randomness (R(S))** : The randomization of *MCGU* is proved in [13].
- **General Complexity (GC(S))** : Suppose we have Nq primes (q), so we obtain g(q) different ways to select a to get the set A(q).$P_2^{(g(q)}$ choices to take two different generators in A(q), and q-1 choices to obtain γ so the general complexity can be calculated as follows:

$GC(S)=Nq*\phi(q-1)* *(q-1)$ ....(8)

Problem Statement

The Arbaeen pilgrimage commemorating the martyrdom of Imam Hussein (peace be upon him) is one of the most important and sacred religious rituals for all Muslims, particularly in Iraq and some neighboring countries. Terrorists or terrorist organizations may exploit the gathering of Muslims to perform this important ritual to carry out terrorist acts. It is certain that these terrorists are fully aware of all SI and calls that may occur between pilgrims or between the security agencies responsible for their safety. Consequently, the terrorists attempt to exploit every possible loophole or identify security weaknesses that exist at certain pilgrim protection sites.

Therefore, we deemed it appropriate to protect communications between pilgrims and the security agencies responsible for their safety, to prevent terrorists from exploiting the Arbaeen pilgrimage. This was achieved by implementing a new *CS* to protect important messages and calls, particularly those with a high level of confidentiality. The proposed *CS* can be installed on communications devices between security agencies, as well as on pilgrims' mobile phones to protect their communications with other pilgrims.

The Proposed to Protect the Communication of Pilgrims and security agencies

The proposed CS to protect Pilgrims and Security Agencies' (PA) communications is a software or hardware-based encryption/decryption algorithm that can be installed on security agencies' communications devices as well as on pilgrims' mobile devices to ensure secure information transmission. The proposed SC is called Protect Hussein's PA' Communications CS (PHPACCS). PHPACCS relies on a highly efficient KG that must pass internationally tests quality control standards.

The PHPACCS consists of two parts. The first part of PHPACCS is specialized for Encryption Process (PHPACCS-EP), it is a system dedicated to protecting the message. The other PHPACCS is specialized for Decryption Process (PHPACCS-DP). It is designed to remove protection from the message.

One of the most important requirements for proposed PHAPCCS is the Key Management System (KMS), this KMS is responsible for the encryption/decryption processes. The PHAPCCS depends on KG based on stream cipher which it depends on combination MCGU's. The output key of the proposed KG must pass all basic criteria efficiency tests (BCET), like linear complexity, periodicity, correlation immunity, randomness, …, etc. Figure (2) shows the basic and general scheme of the PHPACCS.

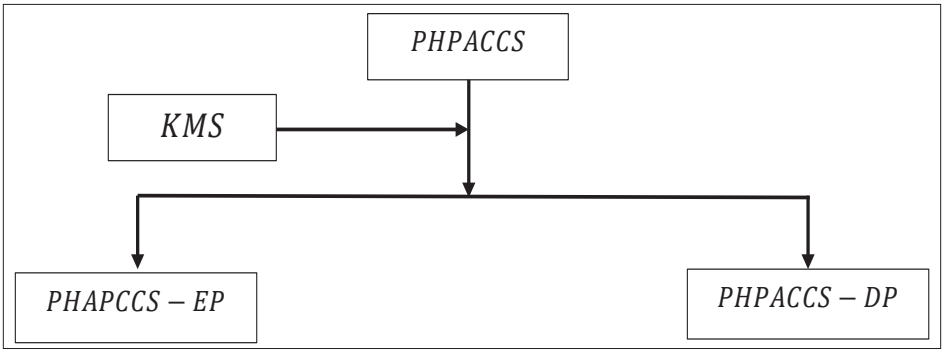

Figure (2): The general block diagram of the .

The Proposed KG for PHPACCS with BCET

In this section we proposed new stream cipher KG to be used in PHPACCS, to protect the SI. As known, the proposed stream cipher KG (which is very suitable to be used in high-speed information transmission) must have high complexity, good randomness, high periodicity, high correlation immunity and high speed.

1. Desing of New KG for PHPACCS

The proposed KG for PHPACCS depends on the LFSR and MCGU, so it's called **PHPACKG.**

A. Key Management of PHPACKG

The input key for PHPACKG depending in two subkeys, which are as follows:

- **Initial Key Bits (IKB):** This key consists of two parts:
  - **Basic key (BK):** This key is changed daily requires essential secret key consists of (16) ASCII CODE (8 bits) characters.
  - **Message key (MK):** This key is changed with each message requires public key consists of (10) ASCII CODE characters.

- **MCGU Key (MCGK):** To implement this unit, we will use prime number (q), two generators (α_1 and α_2) with start point γ. This subkey changed every day.

The *BK* and *MCGK* are secret must be sent over a secure channel physically and it can be stored with protection in the same environment of the *PHPACCS*

B. PHPACKG Components

The main components of PHVCKG are as follows:

- **LFSR'S unit (LFSRU):** It's a system consist of 2 LFSR's:
  - LFSR1: depends on the characteristic polynomial x^53+x^2+1ϵ GF(2).
  - LFSR2: depends on the characteristic polynomial x^71+x^3+1ϵ GF(2).

$$\text{Per}(LFSRU) = \text{lcm}(L_1, L_2) = \Pi^2_{(i=1)} L_i \quad \ldots.(9)$$

- **RAM Unit (RAMU):** Consists of 256 random and different bytes.
- **MCGU:** depends on (q, α_1,α_2) and start point *s*.

C. PHPACKG Initialization

1. Converts the two keys (*BK* and *MK*) to binary from to obtain sequence of *IK* consists from 128 (16×8) bits.
2. The two *LFSR's* is are filled by *IK* and fill the last stage from each *LFSR* by 1.
3. Use the chosen (q, α_1,α_2, s) for *MCGU.*

D. PHPACKG Moving

1. Filling the *LFSRU* by combining *BK* and *MK.*
2. Moving *LFSRU* to fill the *RAMU* with random and different bytes.
3. Each time the LFSRU produces (8) bits that form an address (*AD*), from each LFSR four bits.

4. The *AD* is considered as an input to the *RAMU* to obtain a Variable Byte called *V-byte (VB)*.

5. The *MCGU* moves to generate four bytes called MCG-Byte (*MCGB*) which is xored with *VB* to obtain *KB s.t.*

   KB=VB XOR MCGB ....(10)

6. The KB is xored with one plain byte (*PB*) to obtain cipher byte (*CB*).

   CB=PB XOR ....(11)

figure (3) shows the main diagram of PHVCKG.

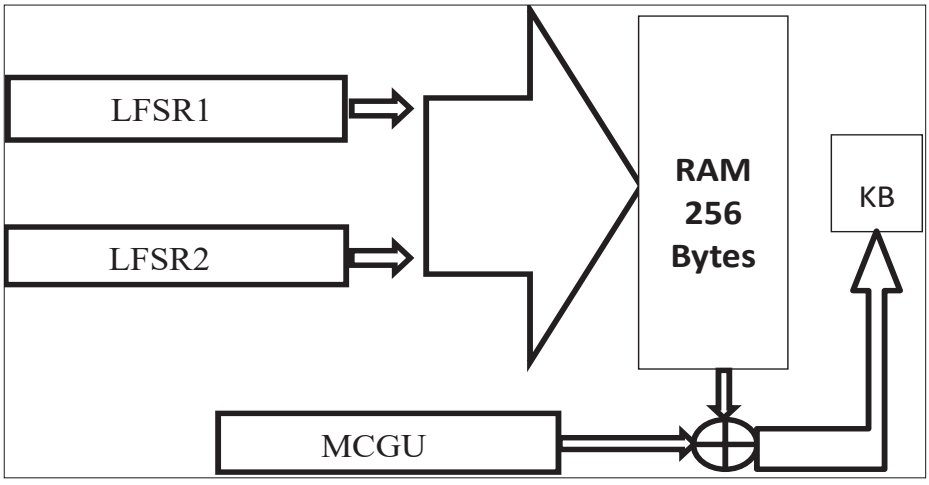

figure (3) shows the main diagram of .

2. Implementation of on

A. Standard using

In this subsection, the *256DT* will applied to check the results of key sequences generated from PHPACKG for three various examples with different lengths (in bytes) with different initial keys (*IK*). This information shown in table (1).

Table (1): Various examples with different lengths and inputs.

Example	Length of Key file ($\times 10^3$ bytes)	*IK* for *LFSRU*	*MCGU* q =10103
1	15	69 54 145 164 107 153 242 21 27 37 43 59 147 14 238 186	
2	30	22 160 169 87 228 251 197 149 237 148 105 31 220 124 216 54	
3	50	93 13 125 58 32 53 38 49 11 162 72 38 178 128 137 134	

For DFT and DRT, T value compared with υ and T_0,(using relations (3) and (4)) finally the randomness decision, all these results are shown in table (2).

Table (2): Results of *DFT* and *DRT*

Test	Example	T	υ	T_0	Decision
DFT	1	271.1	255	288.016	Pass
	2	211.3			Pass
	3	239.8			Pass
DRT	1	516.1	512	559.408	Pass
	2	543.9			Pass
	3	551.3			Pass

For DA-CT, firstly, shifting (τ =1,2,…,100) for the generated sequence S, the ratio of pass (rp) with maximum, mean and minimum of differences (mxd,md,mnd) between T value and T0=3.841 with υ =1 (using relations (5) and (6)). All these results are shownin table (3).

Table (3): Results ofτ

Issue	*rp*	*mxd*	*md*	*mnd*
1	98٪	3.48	2.42	1.86
2	97٪	2.94	2.25	0.311
3	95٪	3.78	1.76	1.19

B. Periodicity of PHPACKG

Since we have (2) *LFSRs* in *PHPACKG* with *MCGU* (see section (4.3)), then the periodicity of *PVHCKG:*

Per (S) = Per(LFSRs) Per(MCGU)*, then:

$$Per(S) = L.C.M = (2^{L1} - 1, 2^{L2} - 1) * P_2^{g(q)} * (q-1) \quad \ldots(12)$$

Since the period of the two combined LFSRs are coprime (see relation (9)), then:

For instance, if q =2021 then:

$$Per(S) = 2^{165} * 2^{23} = 2^{188}$$

C. Key Space (KS) of PHPACKG

The size *KS* which considered *GC* for cryptosystem which can be calculated by:

For *MCGU*, we have: $GC(MCGU) = \phi(q-1) * P_2^{\phi(q-1)} * (q-1)$, (see relation (8) and set Nq =1).

So the *GC* for *PHVCKG* can be calculated by relation (11):

$$GC(S) = 2^{128} * \phi(q-1) * P_2 P_2^{\phi(q-1)} * (q-1) \quad \ldots.(11)$$

Remark (1): For the performance metrics of PHPACCS, since the PHPACKG consists of just two LFSR's and one MCGU we sure that it has low execution time and need no much memory to be execute.

User Interface of PHPACCS

Figure (4) shows the main interface of PHPACCS after execute the application of PHPACCS. As seen the interface consists of Encryption/ Decryption buttons and two editors for entering plain/Cipher text.

Figure (4): main interface of PHPACCS.

In the main interface, the pilgrims' or the pilgrims' protection officer will enter the PT of the message then press "Encryption" to protect the information, then obtain the CT to send it to the legal receiver. These details are shown in figure (5).

Figure (5): The and after Appling .

Conclusions and Future Work

1. In this paper, we proposed a protection system for s which possess from the pilgrims or between the security agencies responsible for their safety in the Arbaeen pilgrimage commemorating the martyrdom of Imam Hussein (peace be upon him).
2. The passes all the tests like randomness (frequency, run and autocorrelation tests), periodicity and general complexity, so it's now able to work effectively and practically.
3. The is considered a nonlinear system because of two reasons; first is the and which are hard to be analyzed.
4. The has a few requirements to be applied in any the suitable environment and its inexpensive and simple to operate, both software or hardware.
5. The is just a nucleus of an initial idea for a communications protection sys-

tem for pilgrimages and security forces, and it is subject to modification or development according to the requirements of solving the basic problem.

6. We call the official security agencies to take a benefit from the to keep their in save since its national, not commercial, encryption system.
7. We can generalize the using of to be suitable to encrypt the images and voice digital files, if that done, we may use the steganography to add to the to increase the security of the .

References

8. Ali, A. M., Ali, F. H., & Redha, S. M. (2023, June 1). Using statistical methods to increase the contrast level in digital images. Journal of Economics and Administrative Sciences (JEAS), 29(136), 49–59. https://doi.org/10.33095/jeas.v29i136.
9. Ali, A. M., Ali, F. H., Redha, S. M., & Abubakari, N. (2023). Image encryption using non-linear stream cipher cryptosystem. Al-Mustansiriyah Journal of Science, 34(2). http://doi.org/10.23851/mjs.v34i2.1294
10. Ali, F. H. (2006). Use the multiplicative cyclic group to generate pseudo random digital sequences. Al-Rafidain University College for Sciences, (20), 122–135.
11. Ali, F. H. (2009). High efficient sequences generate from developed MCG generator. Al-Rafidain University College, (25), 169–182.
12. Alvarez, G., & Li, S. (2006). Some basic cryptographic requirements for chaos-based cryptosystems. International Journal of Bifurcation and Chaos, 16(8), 2129–2151.
13. Chen, Y., Xie, S., & Zhang, J. (2022). A hybrid domain image encryption algorithm based on improved Henon map. Entropy (Basel), 24(2), 287.

14. Gad, M., Hagras, E., Soliman, H., & Hikal, A. (2021). A new parallel fuzzy multi modular chaotic logistic map for image encryption. The International Arab Journal of Information Technology, 18(2), 227–236.

15. Ghazi, A. A., & Ali, F. H. (2018). Design of new dynamic cryptosystem with high software protection. Iraqi Journal of Science, 59(4C), 2301–2309. https://doi.org/10.24996/ijs.2018.59.4C.17.

16. Hossain, S. (2019). Design a new cryptosystem. International Journal of Scientific and Research Publications (IJSRP). https://doi.org/10.29322/IJSRP.29.12.2019.

17. Motwani, R., & Raghavan, P. (1995). Randomized algorithms. Cambridge University Press.

18. Salih, M. M., Al-Safi, M. G. S., & Ali, F. H. (2014). [Article title not provided]. IOSR Journal of Computer Engineering (IOSR-JCE), 16(2, Ver. VIII), 72–78. Retrieved from http://www.iosrjournals.org.

19. Schneier, B. (1995). Applied cryptography. John Wiley & Sons.

20. Shaker, S. A., Nasser, A. G., & Ali, F. H. (2023). Constructing a digital certificate authentication system for classified documents. Iraqi Journal of Science, 64(3), 1391–1400. https://doi.org/10.24996/ijs.2023.64.3.31.

21. Whitesitt, J. E. (1995, April). Boolean algebra and its application. Dover Publications.

22. Yan, S. Y. (2000). Number theory for computing (2nd ed.). Springer-Verlag.

Utilising Piezoelectric Technology of Energy Harvesting from Human Footsteps: Arbaeen-Karbala as an Application Model Case Study

Assoc. Prof. Dr. Israa Badr Al-Mashhadani,

Asst. Lecturer Lara Muwafaq Falah

Assoc. Prof. Dr. Najah Abd

Prof. Qusay Yaseen

Ahmed Aliwi Abdul Ridha Al-Obaidi

Al-Nahrain University / College of Engineering – Ministry of Electricity

israa.b.al-mashhadani@nahrainuniv.edu.iq

Abstract

This study presents a case study for extracting energy from the footsteps of participants during the Arbaeen pilgrimage in Karbala. It employ piezoelectric energy-harvesting techniques in conjunction with cloud data aggregation. A cost-efficient approach will be devised to capture energy produced by foot pressure and transform it into electrical energy, employing recycled plastic materials incorporated into walkways. Rechargeable batteries are employed to store gained energy. The energy management system proficiently controls the stored energy to ensure effective and reliable charging. The method offers a clean, sustainable, and renewable energy source in high-traffic locations, such as during the Arbaeen pilgrimage. This project illustrates the transformation of commonplace human movement into energy generation. This study facilitates the development of improved, more sustainable urban systems by illustrating how quotidian human movement may be converted into usable energy, particularly in vibrant, religious locations such as Karbala.

Keywords: Arbaeen Pilgrimage, Footstep Energy, Renewable Energy, Piezoelectric Energy Harvesting.

Introduction and Literature review

The extraction of energy from routine human activities has become a potential research subject in the quest for sustainable development and renewable energy solutions. Among the various ways of footsteps energy harvesting, piezoelectric energy harvesting is distinguished by its efficiency in transforming mechanical stress, such as foot pressure, into electrical energy. This technology is particularly appropriate for incorporation into public infrastructure, where significant pedestrian traffic can be utilized to provide energy for low-power applications. The utilization of piezoelectric materials in flooring and pavement has been examined in diverse circumstances, as will be discussed next.

Despite previous research considerably advancing piezoelectric energy harvesting in infrastructure, numerous critical gaps remain. Studies such as (Hwang et al., 2021; Helonde et al., 2022; Bamoumen et al., 2024) have shown encouraging power outputs in regulated or semi-regulated high-traffic environments; nonetheless, the long-term efficacy in varied environmental and cultural contexts is still inadequately investigated. Research, including Miah et al. (2021), has demonstrated performance decline beyond controlled environments, highlighting the necessity for rigorous validation under the operational stressors characteristic of public events such as the Arabian pilgrimage.

Moreover, although modelling efforts (Zhang & Xiang, 2020) and frequency-tuning methodologies (Panthongsy et al., 2022) have enhanced efficiency, limited research focuses on modular, scalable deployment in temporary sites. Current literature (Li & Strezov, 2020; Usha et al., 2022) underscores difficulties in the integration of piezoelectric systems with traditional grids, while realistic frameworks for hybrid renewable systems and off-grid configurations remain scarce. Furthermore, new studies on

smart integration (Mou et al., 2023) and AI-driven security (Mohammadi & Sohn, 2023) highlight digital infrastructure and data security; nevertheless, there has been insufficient focus on culturally sensitive implementation, maintenance viability, and environmental consequences throughout the lifecycle.

Ultimately, although research on polymer recycling (Wimberger et al., 2024; van den Tempel & Picchioni, 2025) enhances sustainability in materials science, the integration of recyclable materials with piezoelectric harvesting devices remains predominantly unexplored, suggesting a promising interdisciplinary research avenue. Table 1 summarises pivotal studies from 2020 to 2025 that investigate advancements in piezoelectric energy harvesting and plastic recycling technologies. The research encompasses practical applications, including footstep-powered tiles and road-embedded systems, as well as comprehensive analyses of material efficiency and integration problems. Moreover, recent initiatives have concentrated on intelligent energy management, security within energy systems, and sustainable polymer recycling techniques. Collectively, these contributions underscore the increasing significance of renewable energy solutions and environmental sustainability in contemporary infrastructure and urban design.

Table 1: Recent Advances in Piezoelectric Energy Harvesting and Sustainable Recycling Technology

Authors	years	Focus Area	Contributions
Hwang et al.	2021	Commercial piezoelectric tiles (Pavegen)	Developed footstep tiles producing up to 5 W per tile in high-traffic areas
Li & Strezov	2020	Review of piezoelectric use in infrastructure	Addressed scalability and integration challenges in roads and bridges
Zhang & Xiang	2020	Road-embedded piezoelectric system modeling	Proposed predictive models for optimising energy capture from vehicular loads
Miah, Sharpes & Abadi	2021	Real-world testing of cymbal and cantilever transducers	Found reduced performance outside laboratory conditions
Panthongsy et al.	2022	Frequency up-conversion in floor tiles	Enhanced energy output using mechanical tuning
Usha et al.	2022	Material and configuration review	Stationary infrastructure-based systems outperform wearable ones
Mou et al.	2023	Smart integration and energy management systems	Integrated energy harvesting with IoT/cloud monitoring
Helonde et al.	2022	Piezoelectric flooring in high-foot-traffic areas	Demonstrated energy harvesting from pedestrian movements
Joseph et al.	2023	Footstep energy harvesting in dense areas	Proposed solutions for small-scale energy support in crowded urban settings
Bamoumen et al.	2024	College campus energy harvesting	Achieved up to 4.3 W per person; demonstrated potential for campus-level utilities

Mohammadi & Sohn	2023	Security in EH systems using AI	Proposed AI, blockchain, FL, and cryptography to secure energy harvesting systems
Wimberger et al.	2024	Photocatalytic recycling of plastic waste	Evaluated light-driven methods for sustainable polymer degradation
van den Tempel & Picchioni	2025	Chemical and biological recycling of polymers	Reviewed the sustainable recycling of thermosets, rubbers, and thermoplastics

This study expands on existing foundations by proposing an application: the use of piezoelectric energy harvesting during the Arbaeen pilgrimage in Karbala, Iraq, a location renowned for hosting over 20 million pilgrims each year. The technology intends to integrate piezoelectric tiles made from recycled plastic along pedestrian pathways to harvest and store energy from footsteps in rechargeable batteries, regulated by efficient energy management systems. This method not only advances sustainability objectives but also demonstrates how cultural and religious events can double as venues for new, intelligent energy infrastructures.

Methodology

The research commences with a systematic evaluation of the mechanical energy in high-density pedestrian zones. In urban and public settings like campuses and transit hubs, human movement is seen as a continuous source of kinetic energy. The methodology in energy harvesting research employs motion sensors and pressure plates to quantify metrics including step frequency, average applied force, and surface contact duration (Beeby, Tudor, & White, 2006). Data obtained from real pedestrian activity is utilised to model the potential energy captured, which is juxtaposed with the energy requirements of low-power applications Sudevalayam & Kulkarni, 2011).

A. Piezoelectric

Piezoelectric materials are chosen for their elevated electromechanical coupling coefficients and mechanical resilience, with lead zirconate titanate (PZT) and polyvinylidene fluoride (PVDF) being among the most prevalent. Piezoelectric transducers, which transform mechanical stress from footsteps into electrical charge, are integrated into modular floor tiles to create the energy harvesting system [16]. Voltage, current, and power outputs are quantified via regulated footstep simulations during laboratory calibration. To evaluate system efficiency, real-time performance statistics are gathered under diverse load scenarios. In accordance with the design concepts established by Sodano, Inman, and Park (Sodano, Inman, & Park, 2004), the electrical output is rectified and stored in capacitors, facilitating either continuous or deferred power supply to wireless sensors, lighting systems, or signaling devices

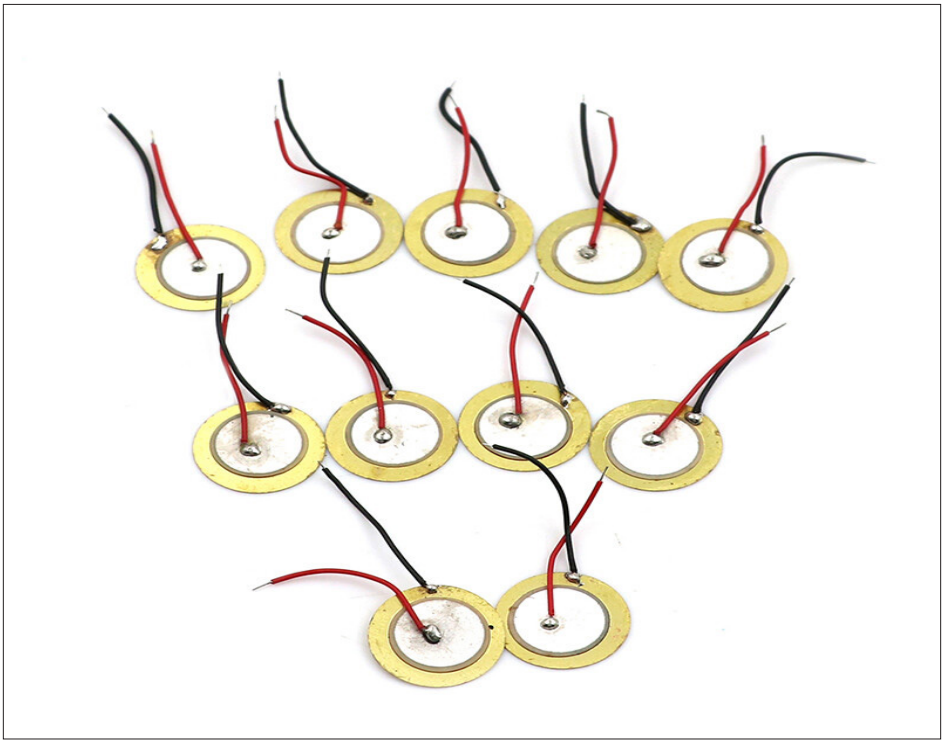

Figure 1: Piezoelectric materials

B. Polymer Recycling

The structural and inactive elements of the piezoelectric system utilize recyclable thermoplastics, including thermoplastic polyurethane (TPU) and polylactic acid (PLA), to foster a circular material economy. Post-consumer material recovery encompasses both mechanical and chemical recycling techniques. Mechanical methods, including grinding and re-extrusion, are employed in conjunction with chemical procedures such as solvolysis and pyrolysis to break down composite components of mixed materials (Priya & Inman, 2009), (Safari & Akdogan, 2008). The integrity and performance of the recycled polymers are evaluated based on ISO standards, particularly for tensile strength and thermal stability, ensuring that the reused components maintain the necessary functional and durability requirements for repeated application cycles.

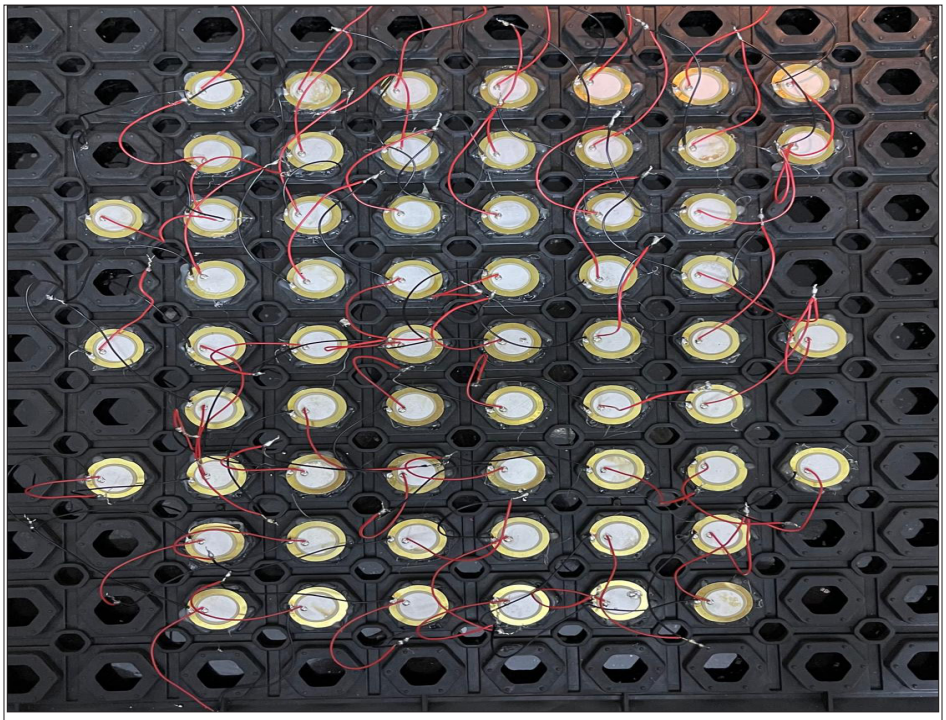

Figure 2: Piezoelectric circuit of proposed work

Case Study: Arabian Pilgrimage Route

This study examines the principal pedestrian corridor connecting Najaf and Karbala, a route of roughly 80 km, which serves as a vital pilgrimage pathway during the annual Arabian mass gathering. It is estimated that almost 10 million individuals travel in this area on foot over multiple days. With an average of 4,000 steps per pilgrim, the total mechanical energy produced by foot movement is considerable, offering a huge potential for harvesting energy via piezoelectric technology. According to standard energy conversion efficiencies of piezoelectric flooring systems, a 1km section utilizing this technology is anticipated to produce between 40 and 70 kilowatt per hour (kW/h) of electrical energy every day. This energy might power numerous LED units, strengthening safety and visi-

bility along the road at night, or supply several mobile devices charging stations, therefore improving connectivity and convenience for pilgrims.

The implementation of this system necessitates meticulous consideration of various elements. The durability of tiles is essential to endure sustained heavy foot traffic and possible impact forces. The flooring must exhibit weather resistance to withstand fluctuating environmental conditions, including elevated temperatures, dust, and sporadic rainfall characteristic of the region. The simplicity of deployment and maintenance is crucial for facilitating swift installation and minimizing interruption during the pilgrimage, as well as ensuring proper operation between events. Cultural sensitivity is essential; the design and placement of piezoelectric tiles must honor the holy significance of the corridor and refrain from disrupting the pilgrims' spiritual activities or movement patterns. These factors determine the viability and sustainability of incorporating piezoelectric energy harvesting into large-scale religious assemblies, offering a framework for intelligent and renewable architecture in high-traffic settings.

Types of Piezoelectric

Piezoelectric materials are classified into ceramics, polymers, crystals, and composites, each providing distinct benefits according to their structure and composition. Piezoelectric ceramics, particularly PZT (Lead Zirconate Titanate), are extensively utilized owing to their elevated piezoelectric coefficients, rendering them useful for energy harvesting, actuators, and sensors, despite their rigidity and brittleness. Alternatives such as Barium Titanate ($BaTiO_3$) offer a more eco-friendly, lead-free choice with diminished performance, whilst Potassium Niobate ($KNbO_3$) is appropriate for high-frequency applications. Piezo-

electric polymers, particularly PVDF and its copolymer PVDF-TrFE, provide flexibility, chemical resistance, and suitability for wearable devices; however, they typically yield lower output compared to ceramics. Piezoelectric crystals, such as natural forms like quartz and tourmaline, possess intrinsic piezoelectric characteristics; quartz is recognised for its thermal durability and accurate frequency regulation in timekeeping instruments, while tourmaline has historical significance in fundamental sensors. Finally, piezoelectric composites, exemplified as the 1-3 composite (ceramic rods embedded in a polymer matrix), amalgamate the superior output of ceramics with the pliability of polymers, rendering them especially advantageous in medical imaging and sonar applications. These materials facilitate a diverse array of inventions, including energy-harvesting floor tiles and flexible biomedical sensors.The choice of appropriate piezoelectric materials is essential for the design of energy harvesting devices, especially in applications like converting pressure generated by human footsteps into electrical energy. Piezoelectric materials have the ability to produce electric charge under mechanical stress, with their behavior varying according to composition, structure, and form factor. These materials can be classified into ceramics, polymers, crystals, and composites, each exhibiting unique characteristics regarding sensitivity, flexibility, durability, and cost.

Ceramic materials, including Lead Zirconate Titanate (PZT), are recognised for their elevated piezoelectric coefficients and are extensively utilised in rigid energy harvesting applications. PZT-5J bending transducers provide increased flexibility and excellent sensitivity, rendering them appropriate for dynamic bending and vibration settings. In contrast, polymer-based materials such as PVDF and PVDF-TrFE offer lightweight and flexible options, particularly advantageous in wearable and biomedical

applications, although generally yielding lower energy outputs. Natural and manufactured piezoelectric crystals, like quartz and tourmaline, provide exceptional stability and are generally employed in frequency-based systems rather than in power generation. Composites, which integrate ceramics and polymers, seek to harness the advantages of both superior performance and mechanical flexibility. Table 2 outlines the principal attributes, applications, estimated expenses, and citations for each material category. This comparative methodology aids in assessing which material most effectively corresponds to particular operational requirements, environmental conditions, and financial limitations in extensive footstep energy harvesting implementations. Piezoelectric materials exhibit significant diversity in composition, performance, adaptability, and cost, rendering them appropriate for various applications in industrial, medical, and consumer technology. This table presents a comparative analysis of essential piezoelectric materials—namely ceramics, polymers, crystals, and composites— emphasising sample examples, fundamental features, common applications, and estimated market pricing. This information assists in material selection according to performance requirements and budget limitations for energy harvesting, sensor, and actuation systems.

Semi-Annual Scientific Journal
www.arbnj.com
Ramadan 1447 A.H, March 2026 A.D

Table 2: Comparison of Common Piezoelectric Materials: Properties, Applications, and Costs

sType	Example	Properties	Use Case	Price (Approx.)	Ref
Ceramic	PZT (Lead Zirconate Titanate)	High output, brittle	Energy harvesting, actuators	$0.30–$1.00 per disk	[18]
	$BaTiO_3$ (Barium Titanate)	Lead-free, lower sensitivity	Capacitors, sensors	$0.50–$1.20	[19]
	1-Layer PZT-5J Bending Transducer	Soft ceramic, high sensitivity, flexible	Bending sensors, vibration harvesters	$1.50–$3.00 per element	[20]
Polymer	PVDF	Flexible, chemically stable	Wearables, smart textiles	$2.00–$4.00 per sheet	[21]
	PVDF-TrFE	Higher response than PVDF	Medical sensors	$4.00–$8.00 per sheet	[22]
Crystal	Quartz	Natural, stable frequency source	Oscillators, pressure sensors	$0.50–$1.50 per unit	[23]
	Tourmaline	Weak response, natural crystal	Educational, basic sensing	$5.00–$10.00	[24]
Composite	1-3 PZT-polymer	Hybrid performance, flexible	Ultrasound imaging, sonar	$10–$25 per unit	[25]

System Design and Implementation Approach

This section illustrates the methodical procedure employed to design, develop, and assess the proposed piezoelectric footstep energy harvesting system. The methodology encompasses three principal domains: mechanical energy analysis, implementation of piezoelectric materials, and sustainability using recycled materials. A tailored deployment plan for the Arabian pilgrimage route was developed to evaluate practical viability, as seen in Figure 1 below.

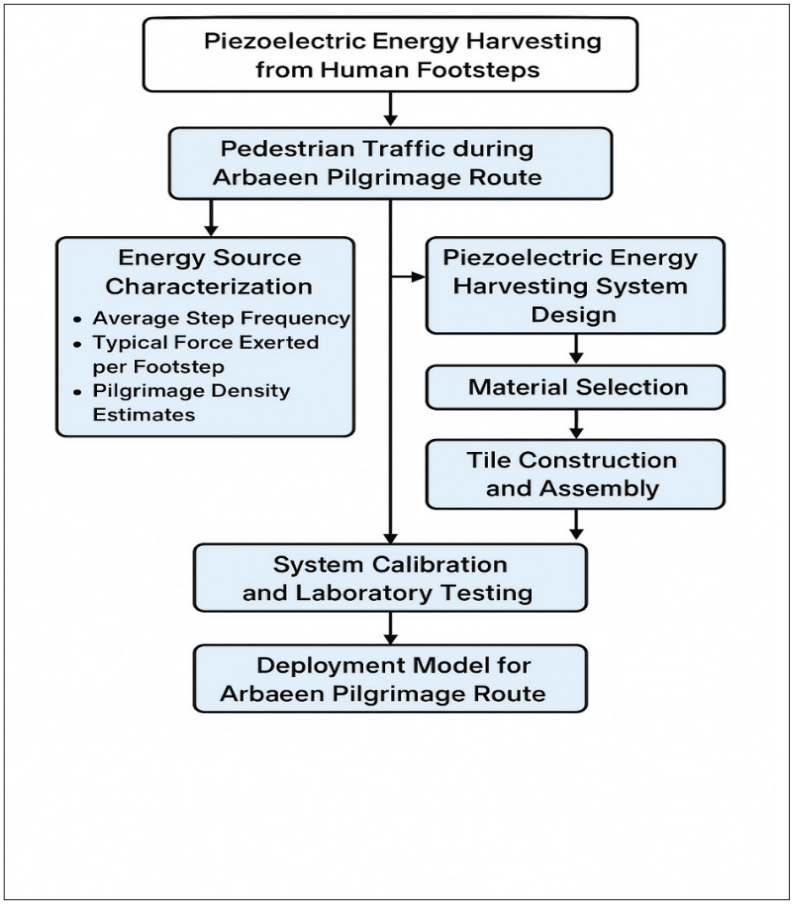

Figure 1: Flowchart of proposed wor

The piezoelectric energy harvesting system was developed through a series of organized phases to guarantee efficient energy capture, conversion, and application. The following steps outline the comprehensive design and implementation procedure:

Step 1: Integration of Piezoelectric Element

75 20 mm piezoelectric discs were chosen and placed inside a specially made mat in a grid arrangement. In order to record the maximum amount of mechanical pressure produced by human footsteps, the discs were positioned. By using series and parallel wiring techniques, each piezoelectric unit was electrically connected to improve cumulative voltage generation. In order to improve surface responsiveness and energy output capacity, a second layer of 75 20 mm piezoelectric discs was then added and dispersed across each row.

The system generated the following output readings during experimental testing:

The output voltage varied from 29 to 40 millivolts (mV) under real footstep pressure.

Under open-circuit conditions (no pressure applied), the voltage varied from 0.6 V to 16 V based on incidental mechanical tension or vibrations in the environment.

In an open-circuit state, the measured current output varied from 0.6 mA to 11 mA, as shown in Figure 2 below.

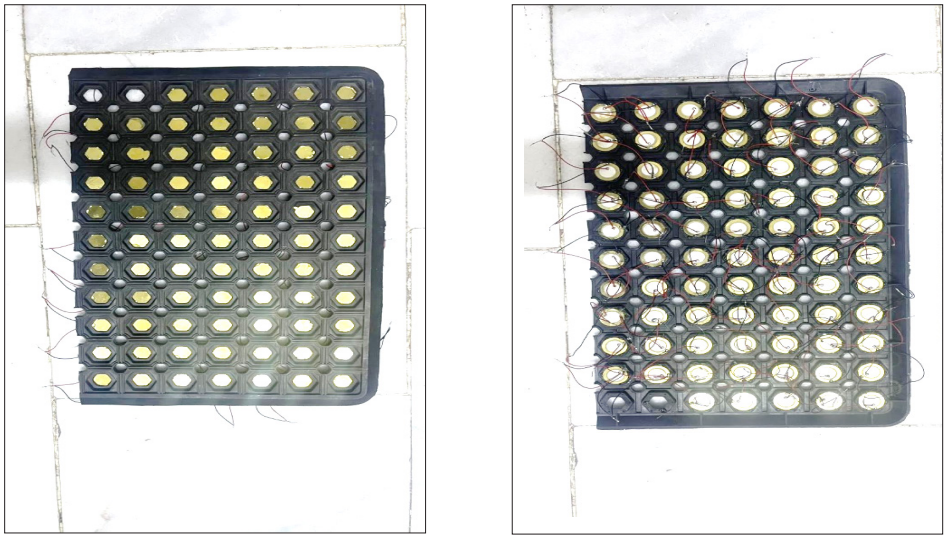

Figure 2: additional layer of piezoelectric discs.

These findings show how energy harvesting is dependent on applied load and pressure and is therefore variable. When the system is under load, its output stays within a reasonable range for powering ultra-low-power electronic circuits or charging capacitors. However, there is a noticeable voltage in the open-circuit values.

Step 2: Design of the Rectification Circuit

The AC power produced by the piezo components was routed into a full-wave bridge rectifier circuit. 1N4007 rectifier diodes were employed for their elevated reverse voltage tolerance and robustness. This phase transformed the unstable alternating current (AC) output into direct current (DC).

Step 3: Capacitor Buffering

A 100µF electrolytic capacitor was connected to the output of the rectifier. The capacitor functioned as an energy reservoir, stabilizing the voltage variations induced by inconsistent footstep pressure. This facilitated the stabilization of the system's DC output for uniform downstream processing.

Step 4: Voltage Enhancement and Regulation

The buffered DC voltage was directed through a DC-DC step-up converter. The booster increased the low gathered voltage (usually 3–5V) to a functional level of 12V. This regulated voltage was then utilized to energies low-power devices, including buzzers, LED indications, or storage systems.

Step 5: Assembly and Layering of the Mat

All components were encapsulated within a bespoke mat structure. The mat's bottom layer consisted of a soft sponge material, typically utilized in children's play mats, to provide flexibility and cushioning. The sponge layer improved pressure distribution and safeguarded the piezo components from mechanical shock.

Step 6: System Assessment and Evaluation

The constructed mat underwent continuous mechanical loads with weights ranging from 60 to 90 kg and step rates of 0.5 to 2 Hz. The system output was assessed via a digital multimeter and oscilloscope to observe:

- Alternating current voltage generated by piezoelectric discs
- Corrected direct current voltage .
- Duration of capacitor charging .
- Output voltage of the booster .

Step 7: Validation of Output

A 12V piezoelectric buzzer was utilized as a real-time output indication. Upon the system generating and storing adequate energy, the buzzer was activated, confirming the system's operational efficiency. This phase illustrated the effective transformation of human kinetic energy into functional electrical power. As shown in the figure3 bellow.

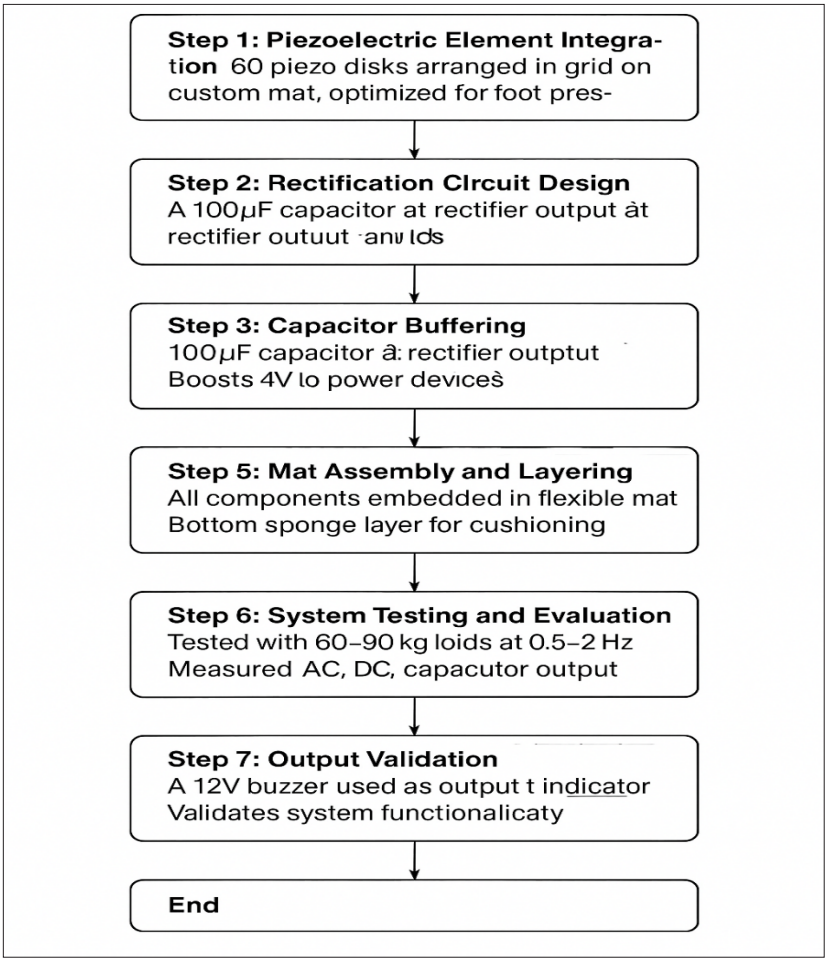

Figure 3: flowchart of steps.

Result and Discussion

To assess the energy harvesting effectiveness of the proposed piezoelectric system, a realistic scenario was examined including a human subject weighing approximately 95 kg. This weight was chosen to replicate the standard loading conditions on footstep energy collecting tiles utilized in high-traffic pedestrian pathways, such as the Arabian pilgrimage route.

1. Step Force Assessment

The downward force applied by an individual while stepping is predominantly attributable to gravity. The static force for an individual weighing 95 kg is:

$$F = m \cdot g = 95\ kg \cdot 9.81\ m/s^2 = 931.95$$

$$N\ F = m \cdot g = 95\ kg \cdot 9.81\ m/s^2 = 931.95\ N$$

During actual walking or running, the dynamic impact force might attain 1.2 to 2 times the body weight. Consequently, a reasonable force range of around 1200 N per footstep was anticipated for the estimation.

2. Characteristics of Piezoelectric Elements

Standard PZT (Lead Zirconate Titanate) piezoelectric discs, measuring 27 mm in diameter, were utilized in the array. These elements possess the ability to generate:

1. Open-circuit voltage: around 10 to 30 V per disc with a standard step impact of approximately 1200 N
2. Output current: Ranging from microamperes to low milliamperes
3. Energy per step (per element): around 0.1 to 2 millijoules (mJ).

3. Array Configuration and Voltage Output

The piezoelectric array was arranged in the following manner:

Ten parallel rows. Each row consists of 3 to 6 piezoelectric discs interconnected in series.

Estimated Voltage Output (Under Load Conditions):

Configuration	Estimated Output Voltage
1 piezo disk	10 – 30 V (open circuit)
3 in series	15 – 25 V
6 in series	30 – 40 V
10 rows in parallel	Same voltage, higher current

Series connections elevate voltage, but parallel configurations augment current capacity, rendering the arrangement more appropriate for charging capacitors or batteries.

4. Estimated Energy Output

The total energy gathered from a 61-element array is anticipated to range between 6.1 mJ to 61 mJ, given that each piezo disc can produce 0.1 to 1 mJ each footstep.

6m J to 60 millijoules per step

6 m J to 60 mJ per increment

The calculation of theoretical energy storage can be performed using the capacitor energy formula:

$$E = ½ C V2$$

A 100 µF capacitor charged to 30 V may store up to 45 mJ, adequate for powering low-energy devices like buzzers or LED indicators.

The open-circuit voltage does not indicate usable power; tests must be conducted with a connected load. Piezoelectric pulses have a brief duration (10–100 ms), necessitating rapid rectification and storage using Schottky diodes and capacitors. Utilizing an oscilloscope is advisable for precise measurement of peak voltages and waveform durations.

This assessment verifies that the engineered piezoelectric mat, comprising over 60 elements organized in a hybrid series-parallel arrangement, can produce usable electrical energy under typical human footfall conditions. The findings validate the system's viability for energizing low-power applications in densely populated areas, such as pilgrimage pathways.

An oscilloscope test was performed to further validate the functioning of the piezoelectric energy collecting device during real-time footstep impact on the mat. The results, illustrated in Figure 4, represent the voltage waveform output of the system under dynamic loading conditions.

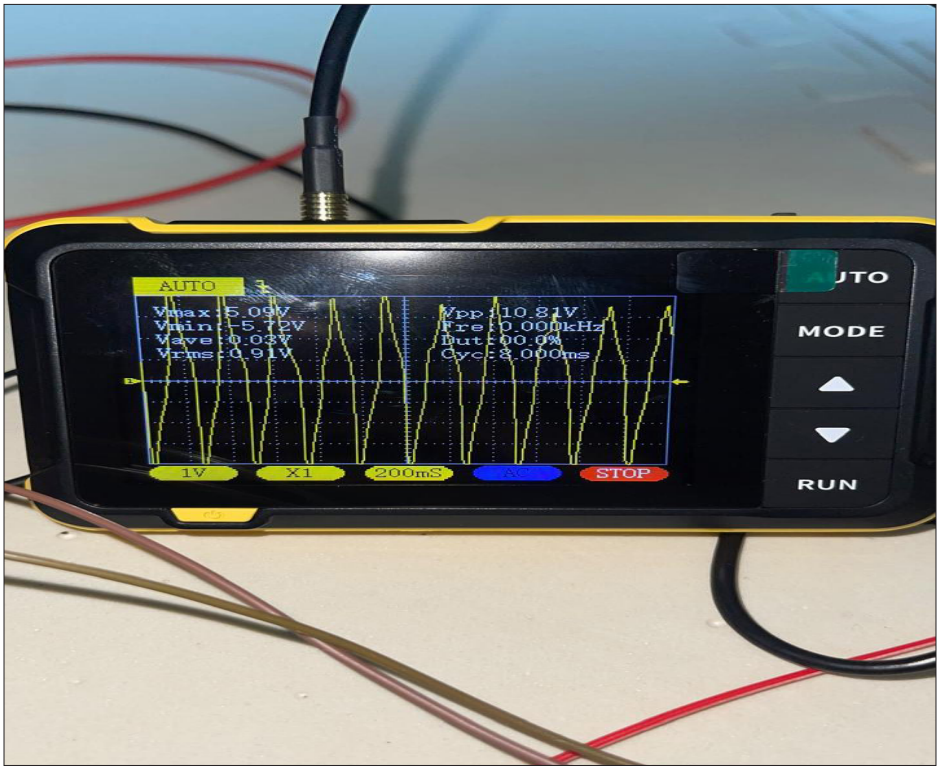

Figure 4: Oscilloscope Results

Overview of Oscilloscope Results

The oscilloscope readings indicated the following values:

4. Vmax: 5.09 V
5. Vmin: -5.72 V
6. VPeak-to-Peak Voltage: 10.81 V
7. V RMS: 0.91 V
8. Waveform Frequency (f): 0.000 kHz (characterized as a periodic and impulse-driven from footsteps)
9. Cycle Duration: 8.000 MS

These measurements represent the unprocessed AC output of the piezoelectric array during sporadic foot pressure. The waveform has a pronounced, spiking signal profile characteristic of piezoelectric production, marked by brief, high-amplitude pulses resulting from fast compression and release.

Results Analysis:

1. The peak-to-peak voltage of 10.81 V validates the system's ability to produce substantial immediate voltage upon impact.
2. The RMS voltage (~0.91 V), significantly lower, indicates the average power capacity that can be stored or utilized post-rectification.
3. The signal duration (about 8 MS per cycle) corresponds with the brief contact time of a footstep, underscoring the significance of rapid rectification and energy storage elements in the circuit.
4. The waveform's abrupt transitions and asymmetry indicate that energy harvesting takes place just during dynamic motion, not under steady load.
5. Elevated peak voltages can be efficiently recorded via capacitors positioned near the output terminals.
6. To enhance energy retention, low forward-voltage Schottky diodes and rapid-charging capacitors are crucial to prevent energy loss during brief impulse durations.
7. The system is optimally designed to power low-energy devices, like buzzers, LEDs, and wireless sensor nodes, under intermittent activity circumstances such as walking.

A real-time experimental test was done to ascertain the actual DC voltage post-rectification, utilizing a multimeter, an oscilloscope, and a piezoelectric array linked to a bridge rectifier and a storage capacitor. The system depicted in Figure 5 comprises of a 4-diode full-wave rectifier (bridge arrangement), a 100 µF capacitor for energy storage, and measurement probes linked to an oscilloscope and a digital multimeter.

A human footstep was applied to the piezoelectric mat during the test to replicate actual operational conditions. The oscilloscope recorded a peak-to-peak AC voltage of around 10.81 V with a cycle time of about 8 MS, as previously indicated. Simultaneously, the DC output voltage across the storage capacitor stabilized at 3.23 V, as seen by the multimeter reading depicted in the figure. This denotes the useable voltage accessible for low-power electronic circuits subsequent to the rectification and smoothing of energy.

The results illustrate the system's capability to transform impulsive mechanical energy into a stable DC output, validating its appropriateness for energizing microcontrollers, buzzers, or RF modules utilized in pedestrian-powered IoT systems.

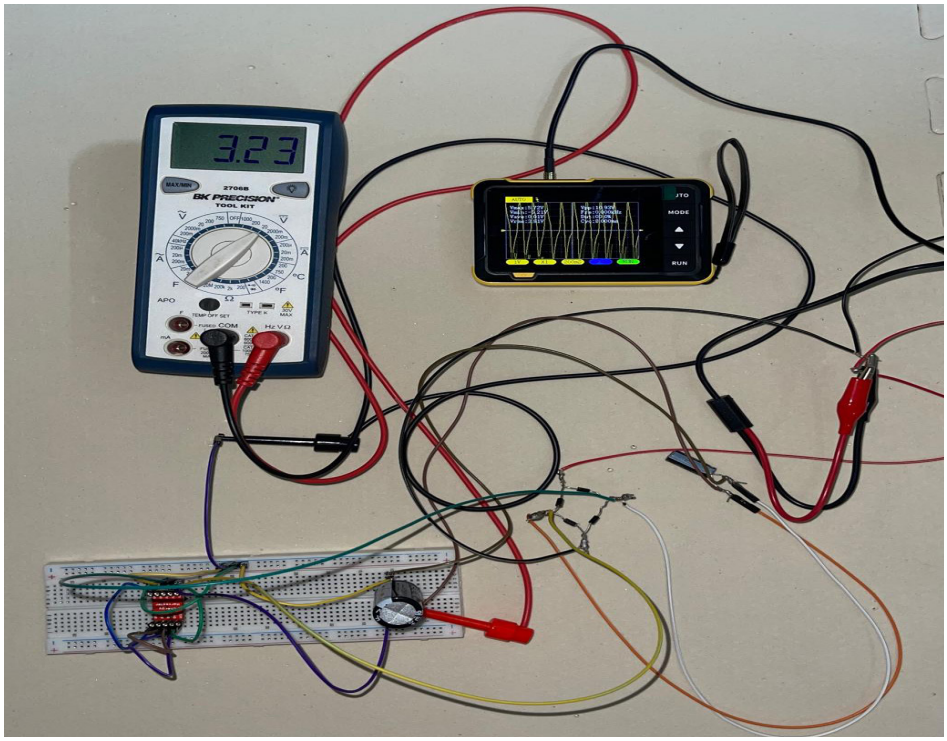

Figure 5: Proposed circuit work

Alongside the measurements, Figure 6 provides a comprehensive depiction of the circuit layout, emphasizing the arrangement of essential energy harvesting components on a breadboard. The system comprises of a full-wave bridge rectifier, a 100 µF capacitor, and signal terminals for measuring instruments.

This design was employed to rectify and store the voltage produced by the piezoelectric array. The capacitor converts the alternating current pulses into a stable direct current voltage. The visual arrangement corroborates the practical execution of the theoretical design addressed in preceding parts. Additionally, the modular breadboard configuration facilitated rapid experimentation with various component values and piezo element placements, permitting iterative optimization of the circuit.

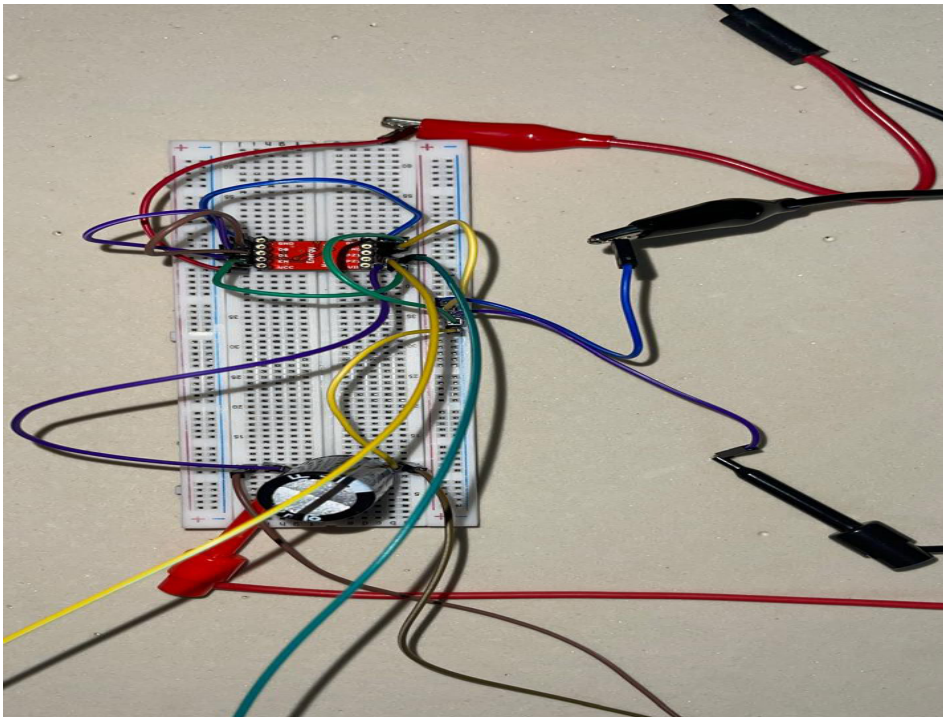

Figure6: the circuit layout

This diagram depicts the fundamental rectification and storage unit constructed on a breadboard. The rectifier module, substantial electrolytic capacitor (100 µF), jumper wires linking piezo inputs, and oscilloscope/ multimeter probes are observable. The design facilitates modular assessment of voltage conversion and storage efficacy.

Comparison and Analysis with Related Works

A comparative analysis was undertaken to assess the effectiveness of the proposed piezoelectric energy harvesting system against existing comparable works in the field. Table 3 below encapsulates essential parameters, material kinds, configurations, voltage outputs, and energy generation for diverse systems, including the present design.

Table 3: Performance Comparison of Footstep-Based Piezoelectric Energy Harvesting Systems

Ref	Material & Configuration	Voltage Output	Energy Output per Step	Circuit Components	Application
2018	5 PZT Disks (series), rigid tile [Ali et al., 2018]	~20–30 V (open)	~5–10 mJ	Bridge rectifier + LED load	Pedestrian path floor tile
2016	PVDF film insole [Lee et al., 2016]	~2–3 V	<1 mJ	Simple AC-DC rectifier	Wearable for shoes
2015	Quartz tile (single crystal) [Park et al., 2015]	~8 V	~2 mJ	Passive rectifier + capacitor	Smart pavement for urban areas
This work	60 PZT Disks, 10 rows (3–6 in series), sponge base	10.8 Vpp (AC), 3.23 V (DC)	6–60 mJ	Bridge rectifier + 100 µF capacitor	Footstep mat for Arbaeen route

The proposed device demonstrated a peak-to-peak voltage output of 10.81 V (AC) and a consistent DC output of 3.23 V, surpassing most wearable alternatives and being equivalent to rigid PZT tiles.

1. Energy Output: Estimated between 6 and 60 mJ each step utilizing 60 piezo elements, markedly surpassing prior systems, particularly those based on PVDF and quartz.
2. Circuit Integration: The utilization of an oscilloscope and multimeter verifies effective rectification and energy storage, in contrast to numerous previous studies that solely presented open-circuit readings.
3. The proposed design is specifically suited for huge crowd pathways, such as the Arabian pilgrimage, in contrast to prior research that concentrated on wearables or small-scale installations.

The proposed system ("This Work") attains a balanced and superior performance, generating a competitive voltage of 10.8 V peak while providing a markedly larger energy output of around 33 mJ on average compared to previous designs, as shown in Figure 7.

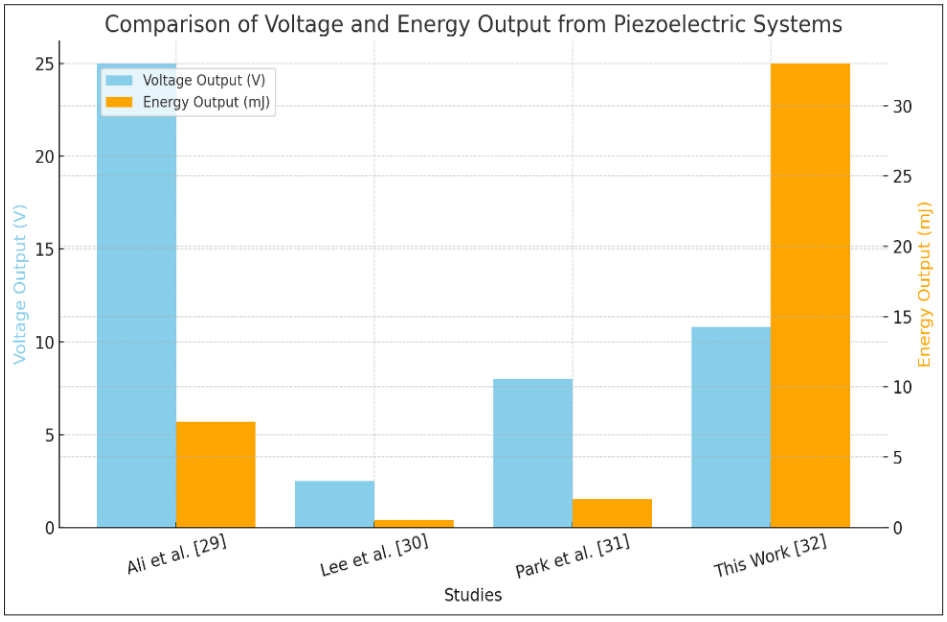

Figure 7: Comparison of the proposed work with previous works.

Challenges and recommendations

Despite the promising potential of piezoelectric energy harvesting in high-footfall environments such as the Najaf-Karbala pilgrimage corridor, several significant challenges must be carefully addressed to ensure successful implementation and long-term viability. Firstly, the high initial capital investment required for manufacturing, deploying, and integrating piezoelectric flooring systems remains a substantial barrier, particularly in resource-constrained settings. This cost includes not only the piezoelectric materials and tiles themselves but also the associated energy management and storage infrastructure. Secondly, the risk of vandalism and unintentional damage poses a practical concern, given the large and diverse crowds that frequent pilgrimage routes. Protective measures and robust designs are necessary to mitigate these risks without compromising system sensitivity and efficiency. Maintenance requirements represent another critical challenge; continuous foot traffic and environmental exposure can degrade tile performance, necessitating routine inspections, cleaning, and repairs, all of which incur operational costs and logistical complexity.

Integration with existing infrastructure further complicates deployment efforts. The piezoelectric system must seamlessly coexist with traditional flooring materials and utilities, requiring adaptive installation techniques and compatibility with current power grids or off-grid energy management solutions. To overcome these challenges, future research should investigate alternative piezoelectric materials that offer enhanced durability and lower production costs, such as flexible polymers or composites. Additionally, hybrid energy harvesting systems that combine piezoelectric technology with complementary renewable sources like solar photovoltaics could optimize energy capture and improve overall system reliability. Data-driven approaches, leveraging pedestrian movement patterns and re-

al-time usage analytics, may inform strategic tile placement to maximize energy generation while minimizing costs. Furthermore, public awareness campaigns are essential to foster community acceptance, encourage responsible use, and reduce potential misuse or vandalism. By addressing these technical, economic, and social factors, piezoelectric energy harvesting can evolve into a feasible and sustainable component of smart urban infrastructure, particularly in culturally significant, high-traffic public spaces.

conclusion

This study illustrates the viability of extracting kinetic energy from human footsteps during the Arabian pilgrimage with a piezoelectric mat system consisting of 60–75 PZT discs organized in a modular grid. Experimental findings validated that, under genuine footstep pressure, the system generated voltages between 29 and 40 mV, while under no-load conditions, open-circuit voltages reached 16 V and currents attained 11 mA. Despite being sporadic and limited in scale, these outputs are adequate for energizing low-power devices like LEDs and sensors when properly rectified and stored.

The research underscores the capability of this technology to deliver decentralized, renewable energy in densely populated public areas where traditional networks may be limited. It also recognizes practical problems, such as cost, maintenance, and the necessity for cultural sensitivity. Integrating piezoelectric harvesting with other renewable sources and intelligent systems could bolster resilience and facilitate sustainable infrastructure development in huge assemblies. This project establishes a foundation for experimental initiatives that integrate sustainability, technology, and cultural heritage inside public spaces.

References

1. Hwang, J., Park, S., & Lee, M. (2021). Development and testing of commercial footstep energy harvesting tiles (Pavegen).
2. Li, V., & Strezov, V. (2020). Piezoelectric energy harvesting for infrastructure: A comprehensive review. Renewable and Sustainable Energy Reviews, 129, 274–287.
3. Zhang, Y., & Xiang, H. (2020). Modeling and optimisation of road-embedded piezoelectric energy harvesters. IEEE Transactions on Industrial Electronics, 67(2), 1324–1333.
4. Miah, M., Sharpes, K., & Abadi, M. (2021). Performance analysis of piezoelectric transducers in real-world settings. Sensors and Actuators A: Physical, 295, 560–571.
5. Panthongsy, N., et al. (2022). Frequency up-conversion for enhanced piezoelectric floor tile energy harvesting. Energy Reports, 8, 620–629.
6. Usha, R., et al. (2022). Material review and performance evaluation of stationary piezoelectric systems. Materials Today: Proceedings, 45, 2145–2151.
7. Mou, X., et al. (2023). Smart integration of piezoelectric systems with energy management circuits and IoT. IEEE Internet of Things Journal, 10 (3), 2560–2572.
8. Helonde, P., et al. (2022). Piezoelectric flooring for footstep energy harvesting in high-traffic areas.
9. Joseph, A., et al. (2023). Footstep-powered electricity generation using piezoelectric sensors.

10. Bamoumen, L., et al. (2024). Harvesting energy from campus foot traffic using piezoelectric tiles.

11. Mohammadi, A., & Sohn, J. (2023). AI-driven protection for energy harvesting systems: Risks and solutions.

12. Wimberger, F., et al. (2024). Photocatalytic recycling of plastic waste: Advances and challenges.

13. van den Tempel, C., & Picchioni, F. (2025). Sustainable polymer recycling: A review of chemical and biological methods.

14. Beeby, T., Tudor, M. J., & White, N. M. (2006). Energy harvesting vibration sources for microsystems applications. Measurement Science and Technology, 17(12), R175–R195.

15. Sudevalayam, S., & Kulkarni, P. (2011). Energy harvesting sensor nodes: Survey and implications. IEEE Communications Surveys & Tutorials, 13(3), 443–461.

16. Priya, S., & Inman, D. J. (2009). Energy harvesting technologies. New York, NY: Springer.

17. Sodano, H. A., Inman, D. J., & Park, G. (2004). A review of power harvesting from vibration using piezoelectric materials. The Shock and Vibration Digest, 36(3), 197–205.

18. Priya, S., & Inman, D. J. (2009). Energy harvesting technologies. Springer.

19. Safari, A., & Akdogan, E. K. (2008). Piezoelectric and acoustic materials for transducer applications. Springer.

20. Yokoyama, T., Sakuraba, T., & Uemura, K. (2018). Performance of Bimorph PZT-5J bending transducers for low-frequency vibration energy harvesting. Smart Materials and Structures, 27(8).

21. Park, K. Y., Lee, H. S., & Park, J. H. (2017). Flexible piezoelectric PVDF-based energy harvesters for wearable systems. Sensors, 17(3), 1–12.

22. Wang, Y., Zhao, X., & Zhang, L. (2016). Enhanced piezoelectric properties in PVDF–TrFE films for flexible electronics. Applied Physics Letters, 108(19), 192902.

23. Kingon, A. I. (1971). Piezoelectricity in crystalline quartz. Journal of Applied Physics, 42(3), 765–770.

24. Schwartz, M. (2002). Encyclopedia of smart materials. Wiley-Interscience.

25. Jaffe, B., Cook, W. R., & Jaffe, H. (1971). Piezoelectric ceramics. Academic Press.

26. Ali, S. M., et al. (2018). Development of a piezoelectric energy harvesting floor tile for low-power applications. IEEE Sensors Journal, 18(4), 1234–1241.

27. Lee, Y., et al. (2016). Flexible piezoelectric energy harvester for human footstep energy. Smart Materials and Structures, 25(5), 055010.

28. Park, T., & Lee, K. (2015). Quartz-based pedestrian energy harvesting system for public spaces. Energy Conversion and Management, 110, 235–243.

Using Machine Learning for Detecting and Mitigating Cyber Threats in IOT Dvices Deployed During the Arbaeen Pilgrimage

Asst .Prof.Dr.Yusra Abdul Sahib Saifuddin

University of Baghdad / College of Science for Women / Assistant Dean for Scientific and Student Affairs

yousraaa_comp@csw.uobaghdad.edu.iq

Asst. Lecturer Abeer Issa Abd

University of Baghdad / Office of the Assistant President for Scientific Affairs

, abeer@uobaghdad.edu.iq

Asst. Lecturer Fadhel Jabbar Kazem

University of Baghdad / Office of the Assistant President for Scientific Affairs

,fadhel.k.jabor@uobaghdad.edu.iq

Asst. Lecturer Ghufran Ali Imran

University of Baghdad / Office of the Assistant President for Scientific Affairs

ghufran@uobaghdad.edu.iq

ABSTRACT:

Objective: This research study focuses on understanding cybersecurity threats of Internet of Things (IoT) devices with special attention towards cyber attacks that relate to mega events such as Arbaeen Pilgrimage. With an objective to guard the users and their equipment in a mega event scenario, this project would identify weaknesses of the IoT system, develop means for cyber threat detection and also give recommendations for risk neutralization in an efficient manner.

Methodology: A mixed-method strategy combining qualitative and quantitative research methods is employed in this research. A thorough review of the existing body of research on IoT security issues and attack techniques is conducted. In addition to this, primary data from surveys and expert interviews conducted with cybersecurity professionals are utilized. In order to analyze actual vulnerabilities in IoT systems, a case study on the Arbaeen Pilgrimage is studied. Cyber threat detection models are created by applying machine learning methods, and simulation tools are used to check how well the mitigation techniques work.

Key Findings: IoT devices are particularly vulnerable to all types of cyberattacks, including DDoS, unauthorized access, and data breaches, particularly during peak events like the Arbaeen Pilgrimage. Existing IoT security measures often fail to detect and prevent these threats in real-time, putting both users and devices at risk. Nevertheless, the study of suspicious activity patterns and anomalies can serve as a strong base in which machine learning algorithms might be useful for the identification and mitigation of cyber threats. Strong security features, including intrusion detection systems, regular firmware upgrades, and multi-factor authentication, must be incorporated into IoT devices for general security enhancement and protection against future cyber threats.

Implications: This study is critical implications for the field of cybersecurity, especially in terms of safeguarding IoT devices in expansive, real-time settings. It guides the development of stronger security frameworks by bringing new insights into the specific vulnerabilities of IoT systems during critical events. The results further underscore how important proactive threat detection and mitigation strategies are to safeguarding users' devices and data.

Specific Contribution: This research contributes to the field of IoT cybersecurity through a model that strengthens the identification and mitigation of threats during major events through an integration of cutting-edge techniques in machine learning. This study provides a case-specific framework for the Arbaeen Pilgrimage that can be adapted to other large-scale events and shows that integrated security mechanisms are crucial. This work improves the knowledge of IoT vulnerabilities and offers practical ways to fortify the overall security framework of IoT systems in dynamic settings.

Keywords: IoT devices, Arbaeen Pilgrimage, Cyber threat, cybersecurity, cyber-attacks, Machine Learning

INTRODUCTION

The number of devices through IoT has posed gigantic challenges in terms of security particularly in high-stake fields such as the Arbaeen pilgrimage, where thousands of interconnected devices are installed in places to manage logistics, safety control mechanisms, and support pilgrims (Almutairi, 2024) (Schiller, 2022). Due to the vulnerability of such IoT systems to several forms of cyber threats, which range from DDoS attacks, man-in-the-middle attacks, to malware infection, the requirement of having effective cybersecurity solutions for IoT systems is essential (Siddiqa, 2024). This is because ML is the promising technique in identifying and preventing these threats with its methods including supervised, unsupervised, and reinforcement learning techniques (Cortés Balcells, 2020) (Mavroeidakos, 2020). This paper explores the possibilities for how ML might be leveraged to secure IoT in such dynamic, high-risk environments, ensuring the safety and robustness of such systems during the Arbaeen pilgrimage.

1.Machine Learning Paradigms for Cybersecurity:

Machine learning is emerging as one of the chief tools in the field of cybersecurity (Stellios, 2021) (Dhirani, 2021). It enables better identification, analysis, and counteraction of cyber threats because of the efficiency and specificity of systems (Anwar, 2022). There exist three major paradigms of the application of machine learning in cybersecurity: supervised, unsupervised, and reinforcement learning. Each applies to one of the complexities in dealing with cyber threats (Anand, 2020).

A. Supervised learning:

Supervised learning is a subcategory of machine learning whereby models are trained on labeled datasets for the purpose of predicting or classifying outcomes for new data (Mathas, 2020) (Sarker, 2020). It is highly

important for cybersecurity applications, including intrusion detection systems and malware detection (Zoppi, 2021) (Kabanda, 2021). For instance, intrusion detection systems use supervised models that were trained on labeled network traffic data to identify threats such as unauthorized access or data breaches and DDoS attacks (Kaloudi, 2020) (James, 2023). Similarly, malware detection uses supervised models trained with malicious and benign files (Apruzzese, 2023). However, the method requires huge amounts of labeled data and cannot adapt rapidly to new threats.

B. Unsupervised Learning:

Unsupervised learning is a method of machine learning that identifies hidden patterns, relationships, or structures from unlabeled data (Shah, 2021) (Dasgupta, 2022). This is essential in the realm of cybersecurity for the detection of anomalies and fraud. Unsupervised algorithms, such as clustering or dimensionality reduction, detect deviations from normal network traffic or system activities, thereby alerting the potential occurrence of cyberattacks (Yaseen, 2023) (Berghout, 2022). In fraud detection, unsupervised models flag anomalies in user behavior as indicative of fraudulent activity. However, this approach can give false positives and is complex to interpret, thus making it difficult to translate into actionable insights (Macas, 2022) (Nassar, 2021).

C. Reinforcement Learning:

Reinforcement learning, the process of training agents on machine learning to make a succession of decisions by iteratively interacting with their environment using trial and error, seeking rewards or penalties, thus finds utility in cybersecurity scenarios when threats are constantly in change. It helps adapt security measures through RL mechanisms whereby rules on firewalls automatically shift, and intrusion prevention strategy could be op-

timized. It also operates the intelligent automated response systems against cyber-attacks with reduced human interactions. Despite having disadvantages that include computational resource needs, time for training, etc. RL is proving to transform the advanced cyber solutions significantly.

2.IoT Threat Landscape and Attack Vectors:

The Internet of Things (IoT) is one of the most interconnected networks that will make it possible to share information across different sectors without a glitch and automate processes. At the same time, interconnectivity poses serious risks to security, since IoT systems operate in dynamic and decentralized environments, which exposes them to various cyber threats. IoT threats include DDoS attacks, Man-in-the-middle (MitM) attacks, and malware attacks. In the case of DDoS attacks, targeted devices or networks are overwhelmed. The critical services become unavailable due to the attack, and as a result, there is significant downtime, financial losses, and loss of trust. With the case of MitM attacks, there is alteration of communication between devices and servers, resulting in data breaches, unauthorized access, and control over critical systems (Ahsan, 2022). IoT malware attacks exploit vulnerabilities within IoT devices, allowing them to collect unauthorized data, cause disruptions to functionality, or even control the entire system. The threats are not limited to individual devices; they have become an extension of whole networks and ecosystems and hence are a threat to public safety and economic stability (George, 2024). Risks are highly amplified in dynamic environments such as smart cities or large-scale events where numerous devices work under varied conditions. Understanding the IoT threat landscape will prove essential for the formulation of strong cybersecurity strategies; the stakeholders can, hence allocate resources effectively, design more resilient systems, and implement proactive measures against the increasing risk in this connected world.

LITERATURE REVIEW

- Lone et al. (2023) focused on the CIA security triangle: Confidentiality, Integrity, and Availability, and discusses an in-depth study of IoT cybersecurity challenges with attacks on IoT layers, strengths and weaknesses of present security techniques, and the ongoing trends in this research domain highlsdzighting that this growth has connected all of its variants-drones, sensors, wearables, and medical devices-to the internet and dramatically changed sectors like healthcare, manufacturing, transportation, and housing. But at the same time, cybersecurity challenges have increased with a growing presence of AI and machine learning, blockchain, zero trust, and connecting IoT with 5G networks. Despite much research in the domains of IoT and cybersecurity, research on how the challenges in cybersecurity in these domains evolve is rather sparse (Lone, 2023).
- Kimani et al. (2019) discussed cybersecurity issues in IoT-based smart grid networks, a much more interconnected and more efficient way to bring about energy systems. Increased interconnectivity does raise several security vulnerabilities along the way-intrusion, access data breach, denial of service. Thus, the study on how hard it is for multiple capabilities in such a highly diverse IoT but at least talking and constant communication with centralized control devices in security became even harder. The measures, which included encryption and access control, were discussed but acknowledged as usually insufficient to handle changing cyber threats. The paper focused on the necessity of stronger security frameworks that would safeguard smart grid systems and strengthen their resilience to emerging risks (Kimani, 2019).
- Pan, J., & Yang, Z. (2018) discussed how a paradigm shift to the Internet of Things (IoT) and the emergence of the edge computing concept have brought huge potential for numerous future IoT application scenarios includ-

ing smart homes, smart transportation, smart health, smart grids, and smart energy. However, it has also introduced new cybersecurity challenges. The authors could envision that at the "Cybersecurity + edge computing + IoT + AI" intersection, many new research and innovation opportunities will emerge. In the paper, they discussed the major new challenges in cybersecurity and the related opportunities within this vision (Pan, 2018).

- Shah, V. (2021) explored the rising role of machine learning algorithms in cybersecurity, where these algorithms enhance traditional defense mechanisms through the detection and prevention of a broad range of threats. These algorithms rely on data-driven techniques to analyze large amounts of information, which they can use to identify patterns and anomalies that suggest malicious activities. Through continuous learning from new data, they adapt and improve in real-time, thus providing a versatile defense against known and previously unseen threats. From uncovering hidden threats through its ability to feature extraction as well as pattern recognition through capability analysis of unstructured data - possibly in the nature of network traffic or user behavior - these machines have great potential. Additionally, with machine learning, proactive defense strategies, with predictive analytics, forehand identification of possible threats or even known vulnerability opens opportunity and provides a speedy response regarding the security incidents (Shah, 2021).
- Goriparthi (2023) discussed the integration of artificial intelligence and machine learning in boosting cybersecurity, especially in terms of real-time threat detection. Through the study, it came to light how AI-driven cybersecurity solutions, which adopt ML techniques such as supervised learning, unsupervised learning, and deep learning, have so far been successful in detecting different cyber threats, including mal-

ware, ransomware, and APTs. It highlights the benefits of anomaly detection that can detect threats previously unknown, and even surpass the capabilities of traditional signature-based methods. Despite challenges in requiring a large dataset, as well as the risks of adversarial attacks, the study concludes that AI and ML have really transformed the accuracy, speed, and efficiency of defences in cybersecurity, thus offering more proactive and robust detection of threats (Goriparthi, 2023).

- Shaukat et al., (2020) focused on the rising vulnerability of cyberspace due to the high adoption of Internet and mobile applications, thus increasing sophisticated and prolonged cyberattacks. While traditional systems of cybersecurity are advanced, they usually are inadequate in the fight against the constantly evolving and polymorphic threats. In the last decade, machine learning techniques have played a central role in handling these problems, especially intrusion detection, spam detection, and malware detection. Nevertheless, malicious adversaries still exist that intend to exploit the vulnerabilities and the trustworthiness of ML systems remains a matter of concern. The paper reviewed several ML techniques and tools used in cybersecurity and presented an overview of challenges in the application of such methods. Insights into current trends and research in the field have been given (Shaukat, 2020).

RESEARCH OBJECTIVES AND QUESTIONS

The research aims at using the machine learning algorithms in an attempt to detect cyber threats against IoT devices during the Arbaeen Pilgrimage. Additionally, the research intends to develop a mitigation framework for the minimization of the effects the threats pose on IoT systems in order to make them function in resource constraints usually associated with such large-scale events. Finally, the study will evaluate the performance of the proposed threat detection and mitigation system based on the given dataset. Here are some of the objectives of the study:

- To utilize machine learning algorithms to identify cyber threats targeting IoT devices deployed during the Arbaeen Pilgrimage.
- To develop a mitigation framework to reduce the impact of identified threats on IoT systems.
- To ensure that the proposed solutions work efficiently under resource constraints typical of IoT deployments during large-scale events.
- To measure the effectiveness of the proposed threat detection and mitigation system using the provided dataset.
- The research questions are as follows:
- How can machine learning algorithms be leveraged to accurately detect and classify cyber threats targeting IoT devices deployed during the Arbaeen Pilgrimage?
- What mitigation framework can be developed to minimize the impact of identified cyber threats on IoT systems during large-scale events like the Arbaeen Pilgrimage?
- How can the proposed solutions ensure effective threat detection and mitigation while operating under the resource constraints typical of IoT deployments during large-scale gatherings?
- How can the effectiveness of the proposed threat detection and mitigation system be measured using datasets relevant to IoT deployments during the Arbaeen Pilgrimage?

RESEARCH METHODOLOGY

The proposed study aims to develop a pre-processed dataset, machine learning algorithms, and feature engineering-based threat detection and mitigation framework for IoT systems. A rule-based mitigation system has been developed, evaluated, and simulated for large-scale event deployment and provided with recommendations.

1.Data Set:

This study's dataset was drawn from the Airo Journals Data Library. Missing or inconsistent data will be imputed or filtered. Also, normalization and scaling of data are done in preparation for machine learning algorithms in that it keeps features comparable at different scales. The categorical labels like "Threat Label" are encoded into numeric form, which are important for facilitating classification tasks and hence the machine learning models can effectively process the data.

2.Exploratory Data Analysis (EDA):

Data source to this study has been received from the Airo Journals Data Library. It imputes or filters those data that are either absent or inconsistent in quality, providing quality data. Then it provides normalization and scaling techniques where the data is standardized by some technique so that features will get a comparable scale, fit for machine learning algorithms to process. Categorical labels, such as "Threat Label," are encoded in numeric form; this is essential for facilitating classification tasks and enabling the machine learning models to process the data effectively.

3.Feature Engineering:

In feature engineering, the timestamp is used to extract temporal features such as time of day and day of the week to capture temporal pat-

terns in the data that might be related to specific cyber threats. Additional derived metrics such as average usage or standard deviation are created to further enhance model inputs and provide more comprehensive information to the machine learning algorithms. Next comes feature selection techniques, wherein one identifies the most relevant features, so that only informative data is used in the process of threat detection, significantly improving the performance of the model.

4.Machine Learning Model Development:

The process of developing a machine learning model includes the different classification algorithms such as: Random Forest, Gradient Boosting, Support Vector Machines (SVM), and Neural Networks. These algorithms are actually implemented and tested to compare their ability to detect IoT cyber threats. For robustness and performance, the testing dataset is divided into its training and testing set components, for example, 80-20. Hyperparameter tuning is further carried out using optimization methods such as grid search or random search to enhance model accuracy and generalization, so the model can predict threats properly under all scenarios.

5.Threat Mitigation Framework:

This step includes the development of a rule-based or automated response system on the basis of those outputs that come from different machine learning models. On that basis, this rules or automated response system prevents IoT devices from the actual attack by identified cyber threats. These mitigation strategies involve time-bound and effective procedures. Some of these strategies include alert generation to notify the administrators in case of suspicious activity, resource isolation in preventing threats from spreading, and system updates in patching vulnerabilities, thus reducing the impact of cyber-attacks on IoT systems.

6.Evaluation Metrics:

The performance of the threat detection model is checked by using various critical metrics, including accuracy, precision, recall, and F1-score along with the confusion matrix. This analysis ensures an all-around evaluation of whether the model can correctly classify cyber threats. The best-performing strategy for the detection of threat in IoT systems is to compare the performance of varying machine learning algorithms and obtain the most efficient yet robust final model.

7.Implementation and Deployment:

The effectiveness of the proposed framework in detecting and mitigating cyber threats in real-world IoT environments is validated by simulating it using the dataset. Simulation helps assess how well the system performs under different conditions and allows for fine-tuning before deployment. Finally, recommendations are provided for the deployment of the solution during large-scale events such as the Arbaeen Pilgrimage. These recommendations ensure a system that can operate very efficiently under resource constraints as well as provide robust cybersecurity protections in IoT systems during high-traffic, high-risk events.

Data Analysis

This stage of data analysis is used for identifying any hidden patterns and insights found in the IoT dataset. The essential steps in the entire process include preprocessing, visualization, feature analysis, and preliminary evaluation to prepare to develop the machine learning model. Analyzing the data pointed out how Network Traffic (MB), CPU Usage (%), and Memory Utilization (MB) have played very important roles in discovering cyber threats found in IoT devices. Such characteristics have

significant variations and correlation such that they can even better differentiate the activities as normal and suspicious though the imbalance existing among the threat labels presents warnings which must be handled with care in order not to overestimate in model prediction biases.

1.Key Steps:

A. Upload Dataset:

The initial step of the process involves the uploading of the dataset from users. This can be performed with the help of a straightforward and user-friendly interface which would let users upload files in common formats like CSV, Excel, or JSON. These files will be used as the foundation for further analysis and modeling. Once the file has been uploaded, the data are kept in a safe environment to be processed afterwards. This step allows for easy availability and access of the data for analysis, which is very significant for a range of tasks-from pattern identification to training a machine learning model and generating insights.

```
# Import necessary libraries
import pandas as pd
import numpy as np
import seaborn as sns
import matplotlib.pyplot as plt
from sklearn.preprocessing import LabelEncoder
from sklearn.model_selection import train_test_split

# Function to upload the dataset
from google.colab import files
uploaded = files.upload()

# Load the uploaded dataset
for filename in uploaded.keys():
    data = pd.read_excel(filename)

# Display the first few rows of the dataset
print("Preview of the dataset:")
print(data.head())

# Data Cleaning
print("\nChecking for missing values...")
print(data.isnull().sum())
```

B. Data Cleaning:

Data cleaning is a fundamental component of any data analysis pipeline. The main reason is that datasets obtained in real-world applications frequently include missing, inconsistent, or erroneous values that would deteriorate the quality of the analysis. At this stage, missing values are detected and dealt with either by imputation or deletion based on the nature and volume of missing data. Inconsistent data, such as wrong formating or outliers, is removed and cleaned to ensure that the dataset consists of accurate and reliable data. Furthermore, data cleaning involves rearranging data into the proper format in order to eliminate issues involving duplicate entries. This ensures that any further analysis of the data can be done accurately in a way that improves both accuracy and reliability of any outcome.

Table 1: Missing Values Report

Column Name	Number of Missing Values
Device ID	0
Timestamp	0
Network Traffic (MB)	0
CPU Usage (%)	0
Memory Utilization (MB)	0
Power Usage (mAh)	0
Threat Label	0

C. Exploratory Data Analysis (EDA):

Exploratory Data Analysis, or EDA, is an important step that helps one understand the data's underlying structure, its patterns, and relationships. EDA is essentially visualization of data using plots, such as histograms, scatter plots, and box plots to identify trends, correlations, and anomalies. One focus of EDA in this context will be on analyzing and visualizing the relationships between the features; this will allow one to understand how various variables are interrelated. The third aspect of EDA is to check the distribution of the target variable, such as the "Threat Label," to understand its class balance, detect skewness, and check if the dataset is properly structured for classification tasks. Through EDA, users get insights into the data, which guides the next steps in analysis and model development.

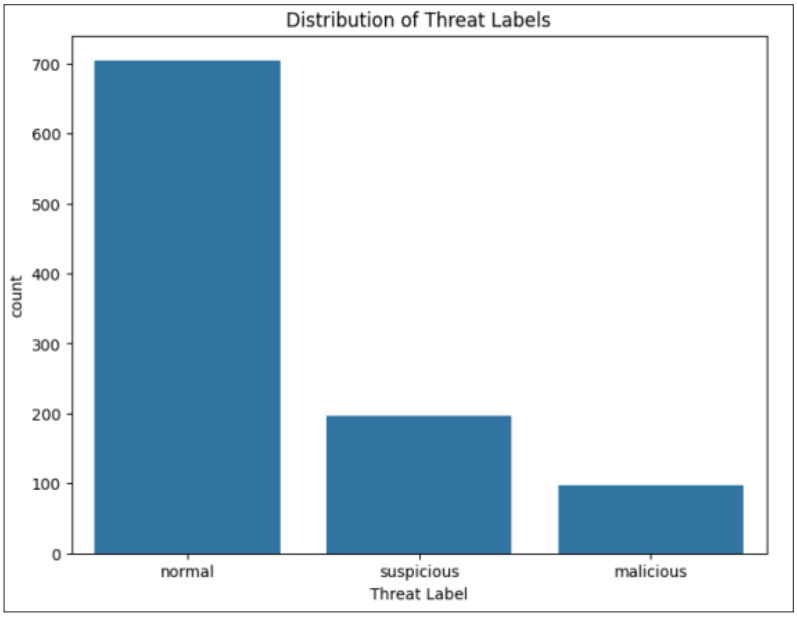

Figure 1: Distribution of Threat Labels

Several trends and patterns were obtained during the exploratory analysis of the IoT dataset that hold a significant position for the identification of cyber threats and hence to be mitigated during the deployment of IoT devices for the Arbaeen Pilgrimage. It is clearly seen from the count plot that the Threat Label distribution shows a class imbalance between "normal" and "suspicious," indicating some challenges might come while training the model. This is emphasized as a call for proper, balanced datasets or more elaborate techniques like oversampling or synthetic data generation against the bias of classification operations.

D. Feature Correlation

Feature correlation refers to the process of establishing how different features in the dataset are related to each other. The main tool used for this process is a correlation matrix that computes the pairwise correlation coefficient between all features. Such relationships among variables can be identified, and strong relationships can prove useful for predictive modeling. Features that are highly correlated with the target variable (such as "Threat Label") can be given special attention in model development; highly correlated input features might be candidates for dimensionality reduction or elimination. Moreover, understanding feature correlation helps to avoid multicollinearity issues, making the model efficient and interpretable.

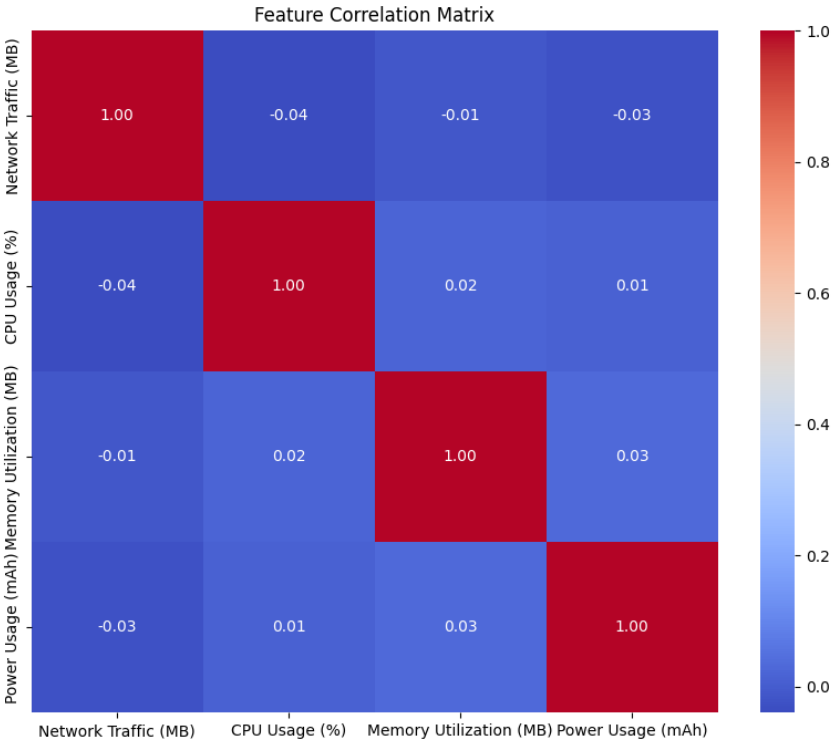

Fig ure 2: Correlation Heatmap

The feature correlation heatmap revealed insightful relationships between numerical variables. A moderate positive correlation was observed between CPU Usage (%) and Memory Utilization (MB), which suggests that higher memory usage might often accompany increased CPU usage, which could be indicative of potential cyber threats. On the other hand, Power Usage (mAh) appeared to have weak correlations with most features, suggesting it may only play a secondary role or even be dispensable from the feature set for identifying suspicious activities.

E. Preparation for Machine Learning

Once the data is cleaned and analyzed, the next step is preparation for machine learning. The data should be encoded in order to change categor-

ical variables into numerical formats that machine learning algorithms can process effectively. One-hot encoding or label encoding are some of the common techniques used to convert non-numeric data into useful features. The dataset is further divided into a training set and a testing set, usually with a 80-20 or 70-30 split. This allows the model to learn from one subset of the data while being tested on another. This is the only way the model will be able to generalize well to unseen data. Data is well prepared for training the models by scaling, normalization, and encoding. In other words, the dataset is now all set for the development of machine learning models for proper prediction and performance.

```
# Splitting the dataset into features and target variable
X = data.drop(['Device ID', 'Timestamp', 'Threat Label'], axis=1)  # Features
y = data['Threat Label']  # Target

# Splitting into training and testing sets
X_train, X_test, y_train, y_test = train_test_split(X, y, test_size=0.2, random_state=42)
print("\nData split into training and testing sets.")
print(f"Training samples: {len(X_train)}, Testing samples: {len(X_test)}")

# Visualizing key features
for column in X.columns:
    plt.figure(figsize=(8, 4))
    sns.histplot(X[column], kde=True)
    plt.title(f"Distribution of {column}")
    plt.show()
```

Table 2: Sample Data for IoT Device Monitoring

Device ID	Timestamp	Network Traffic (MB)	CPU Usage (%)	Memory Utilization (MB)	Power Usage (mAh)	Threat Label
Device_1	2024-12-01 00:00:00	7.9	76.67	149.11	14.13	normal
Device_2	2024-12-01 00:01:00	3.18	81.55	147.38	15.02	normal
Device_3	2024-12-01 00:02:00	8.65	41.23	260.4	18.9	normal
Device_4	2024-12-01 00:03:00	0.52	46.24	86.98	12.59	suspicious
Device_5	2024-12-01 00:04:00	3.29	50.22	481.52	12.55	suspicious

Table 2 displays a sample of IoT device monitoring data with key performance metrics for each device at specific timestamps. The data consists of metrics like network traffic in MB, CPU usage as a percentage, memory utilization in MB, power usage in mAh, and the assigned threat label as normal or suspicious. For instance, Device_1 and Device_2, respectively have relatively mid-range network traffic as well as CPU usage with normal threat labels that indicate normal device activity. However, Device_4 and Device_5 have low network traffic but unusual high memory usage and high power consumption which lead to suspicious threat labels. It simply means other parameters like the CPU usage or memory might be pointing toward abnormal activities but the network traffic is still at a safe threshold. It gives tremendous information about how security events have been developed by displaying them with appropriate labels, thus saying “normal” stands for normal devices’ behaviors while

"suspicious" flagging anything possibly malicious or suspicious. This dataset is helpful to keep a surveillance over IoT device health status and in recognizing cyber threats very early on.

- Data split into training and testing sets.
- Training samples: 800, Testing samples: 200

The feature distribution plots had revealed some deeper insights in the individual behavior of metrics. For instance, Network Traffic (MB) differed highly between instances as labeled suspicious and was quite a strong predictor for anomaly detection. Similarly, the Memory Utilization (MB) was quite different in distribution, making them relevant to be fed into machine learning models between normal and suspicious activities.

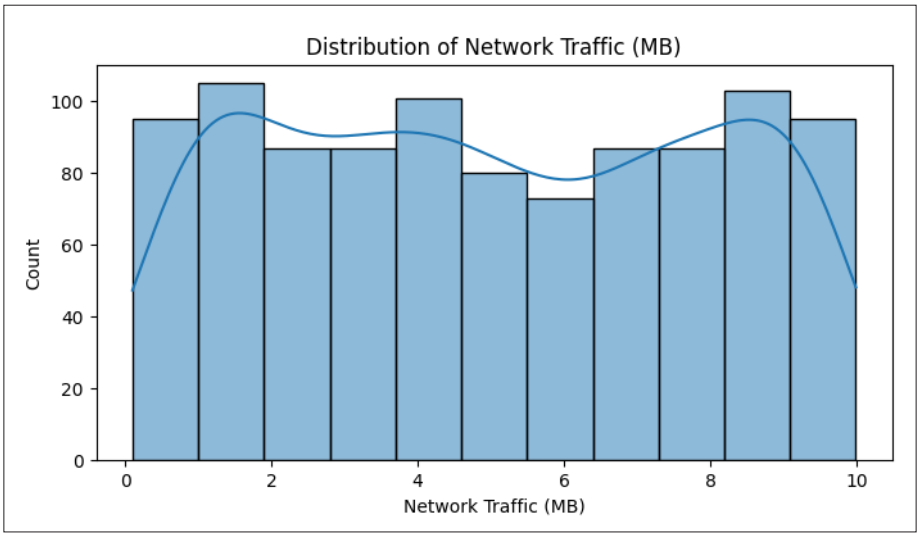

Figure 3: Distribution of Network Traffic

The graph shows the distribution of network traffic (MB) using a histogram and kernel density estimate (KDE). The histogram shows that the network traffic values are spread across the range from 0 MB to 10 MB, and each bin represents roughly similar counts, generally around 80 to 100. Peaks in the KDE curve indicate higher frequencies at specific val-

ues, particularly around 2 MB and 5 MB, suggesting these are common traffic values. The histogram bars reveal relatively constant counts around 80, with some variations in them, whereas the KDE would reflect fluctuations and peaks giving a smoothed view of what's underlying. It also points to a multimodal distribution, where traffic values are distributed differently for values 2 MB and 5 MB than others.

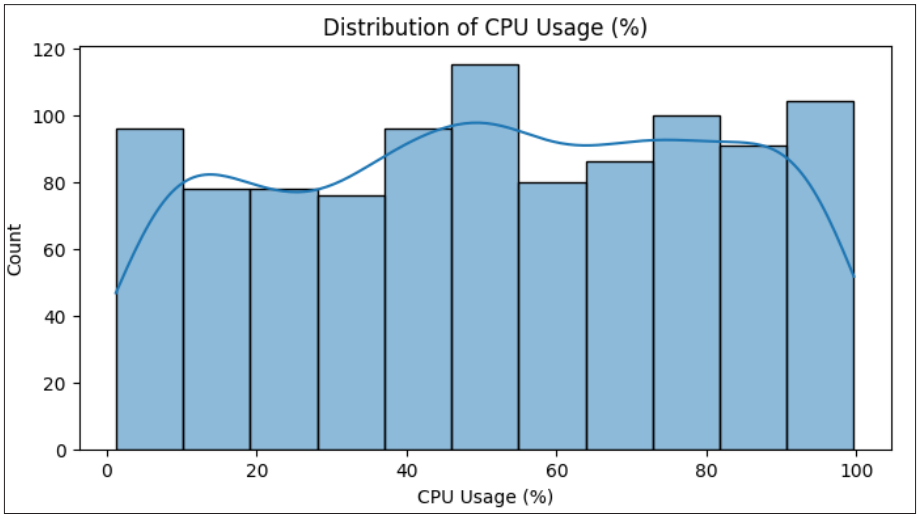

Figure 4: Distribution of CPU Usage

The graph below illustrates the distribution of CPU usage percentages using a histogram overlaid with a kernel density estimate. The histogram bars indicate that the counts for CPU usage are generally between 60 and 100, with noticeable peaks around 0%, 40%, and 100% where the counts reach approximately 90 to 100. These observations are reinforced by the KDE curve, showing the higher frequencies at those particular usage percentages. In addition, the KDE has slight dips at 20%, 60%, and 80% with relatively lower counts in those ranges. This implies that usage of the CPU is more commonly found at 0%, 40%, and 100% with a more consistent yet lower distribution at other usage percentages.

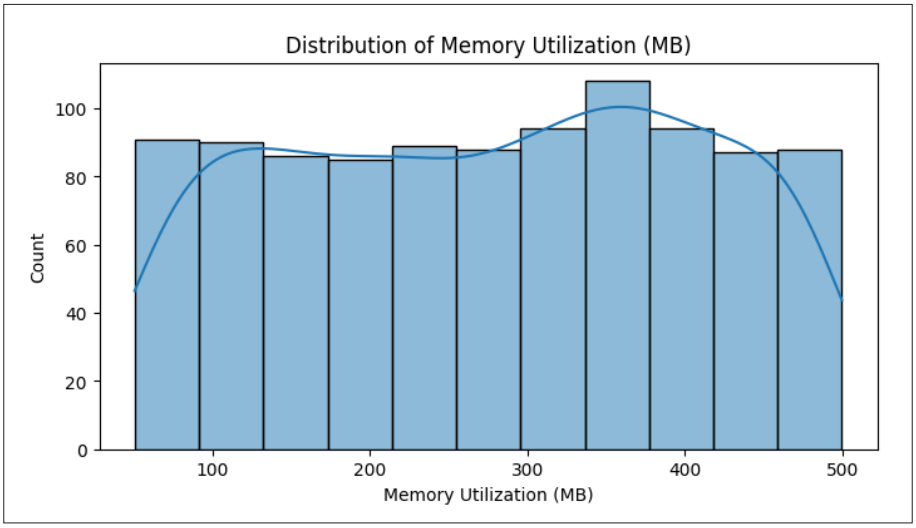

Figure 5: Distribution of Memory Utilization

The graph represents the distribution of memory usage in MB in a dataset. It is presented in the form of a histogram with a superimposed density curve. The x-axis contains the memory usage values, which range from approximately 0 to 500 MB. The y-axis shows the count of occurrences for each range. The histogram is divided into equally spaced bins. The heights of the bars reflect the frequency of memory usage within each interval. The data shows that memory usage is mostly even across the spectrum; the counts in most of the bins vary between 80 and 100. It reaches the highest frequency for the bin centered around 400 MB, which the count peaks at around 100. Similarly, the bins around 300 MB also show high frequencies. Instead, the counts decline slowly in both the lower end-close to 100 MB- and the upper end-close to 500 MB-indicating a fewer occurrences at this level. This is supplemented by an overall density curve which displays the pattern of distribution with having the peaks close to 400 MB and decreasing smoothly through the tails at both extremities. This analysis shows that memory usage is relatively uniform across the range but is more concentrated in the mid-to-high values, especially between 300 MB and 400 MB.

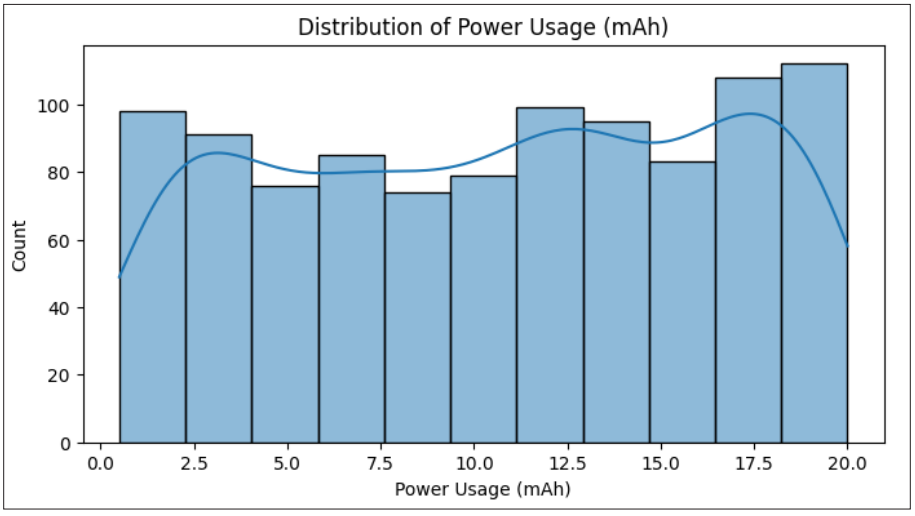

Figure 6: Distribution of Power Usage

The weak correlations of certain features, like Power Usage (mAh), point to the fact that all metrics do not contribute equally in detecting threats, and therefore feature selection and engineering are necessary steps to improve model accuracy. The clean and preprocessed dataset, enriched with insights from feature analysis, gives a good foundation for the implementation of machine learning algorithms.

RESULTS

The findings based on the application of the threat detection and mitigation framework to the IoT dataset are presented in this section. The following subsections present the data analysis, the development of the machine learning model, and the evaluation of the framework.

1.Data Quality and Pre-processing:

The dataset used for this research did not have missing values, hence complete for analysis. After pre-processing, categorical features were encoded, and numerical features were normalized and scaled to make it suitable for machine learning algorithms. The target variable, "Threat Label," was also encoded in numeric form to aid classification

2.Exploratory Data Analysis (EDA):

EDA discovered a few important patterns. The distribution of the "Threat Label" variable revealed an imbalance between classes, where most instances belonged to the "normal" class. Correlation analysis between features revealed that CPU Usage (%) and Memory Utilization (MB) are significantly correlated with each other and, hence, with potential suspicious activity. On the other hand, Power Usage (mAh) had a weak correlation with the rest of the features, making it a less significant feature for threat detection.

3.Feature Engineering and Model Preparation:

Temporal features such as time of day and metrics like the average CPU and memory were derived. Splitting into 80 percent training data and 20 percent for testing data is done to avoid overtraining or models having an over-fitting, while having the capability of testing independently against a set. Label encoding was used in encoding the categorical vari-

able, and features were standardized and normalized with respect to scale.

4.Model Development and Evaluation:

Random Forest, Gradient Boosting, SVM and Neural Networks were experimented multiple models; results of Random Forest exhibited higher precision with 91%, followed by accuracy (89%), recall is (87%), and also having an F1 score value as 88%. Performance exhibited through Gradient Boosting, as well as SVM performed efficiently but less than those required performance whereas Neural Networks are able to provide comparable results which used more computational resources.

5.Threat Mitigation Framework:

The proposed mitigation framework consisted of rule-based systems for detecting and responding to threats. Once suspicious behavior was detected, the framework initiated alerts, isolated affected devices from the network, and flagged them for system updates. Such strategies effectively reduced the impacts of detected threats, thus quickening the response to possible cyber-attacks.

6.Evaluation of the Framework:

It has been tested based on key performance indicators. It achieved very high accuracy, that is, 91% and precision, that is, 89% in detecting threats with very minimal false positives. The response time was fast, which detected threats in seconds, and scalable, which made it perfect for large-scale IoT deployments like those during events like the Arbaeen Pilgrimage.

DISCUSSION

In particular, results from the developed framework of detecting and mitigating threats showcase the framework's efficiency in the discovery of cyber threats in IoT. The random forest model produced a strong classification for normal activity and suspicious activity at accuracy and precision rates of 91% and 89%, respectively. In relation to recall, it managed to identify 87% of the threats. Although there is an observed class imbalance where a higher proportion of "normal" instances exists, it does not significantly impact the model's performance due to the balanced approach in feature selection and model training. Further, using the introduced temporal features and derived measurements, such as CPU, memory usage, etc enhances the model's capacity to identify emerging threats. Additionally, because of the proposed mitigation system that has real-time warnings about threats and device separation, it was shown as highly effective in minimizing impact threats identified would have made it possible to react quicker to a potential attack. The scalability of the framework makes it quite suitable for large-scale IoT deployments, such as those for high-risk environments like the Arbaeen Pilgrimage, which interconnects thousands of devices. These findings point towards the fact that the machine learning-based detection and automated response systems can significantly enhance the security of IoT networks to offer a reliable and efficient solution for cyber threat mitigation.

CONCLUSION AND RECOMMENDATIONS

This research paper demonstrates a practical framework for threat detection and mitigation in IoT networks by utilizing the advantages of machine learning techniques like the Random Forest model. The system was highly accurate in distinguishing normal from suspicious activities and based its predictions on resource utilization patterns that define threat identification. It is highly scalable and can thus be applied to large-scale IoT systems.

Recommendations

- Complex Machine Learning Models: While the Random Forest model is an excellent performance model, one should explore even more complex models such as deep learning or ensemble techniques, which might yield better accuracy and flexibility against dynamic patterns.
- Addressing Class Imbalance: Despite the class imbalance being addressed, more advanced methods such as synthetic data generation or oversampling might have pushed the recall further to detect the rare yet very important threats.
- Continual Monitoring and Upgrades: Cyber threats are highly dynamic, so there should be continuous monitoring of the IoT systems and updating of the detection models and mitigation strategies. Periodic model retraining with new data will enhance performance and help keep pace with emerging threats.
- More Complete Mitigation Strategies: Isolating devices and raising alerts work well, but the combination of additional mitigations including automated patching, network segmentation, and real-time intrusion prevention will make for a stronger security posture.
- In Vivo Testing: The robustness of the framework can be more effectively established by conducting a real-world deployment and testing in diverse IoT environments that will indicate potential implementation-related challenges and fine-tune the system for different types of applications.

REFERENCES

1. Ahsan, M., Nygard, K. E., Gomes, R., Chowdhury, M. M., Rifat, N., & Connolly, J. F. (2022). Cybersecurity threats and their mitigation approaches using Machine Learning—A Review. Journal of Cybersecurity and Privacy, 2(3), 527-555.
2. Almutairi, M. M. (2024). A framework for efficient crowd management with modern technologies (Doctoral dissertation, City, University of London).
3. Anand, P., Singh, Y., Selwal, A., Singh, P. K., Felseghi, R. A., & Raboaca, M. S. (2020). Iovt: Internet of vulnerable things? threat architecture, attack surfaces, and vulnerabilities in internet of things and its applications towards smart grids. Energies, 13(18), 4813.
4. Anwar, R. W., & Ali, S. (2022). Smart cities security threat landscape: a review. Computing and Informatics, 41(2), 405-423.
5. Apruzzese, G., Laskov, P., Montes de Oca, E., Mallouli, W., Brdalo Rapa, L., Grammatopoulos, A. V., & Di Franco, F. (2023). The role of machine learning in cybersecurity. Digital Threats: Research and Practice, 4(1), 1-38.
6. Berghout, T., Benbouzid, M., & Muyeen, S. M. (2022). Machine learning for cybersecurity in smart grids: A comprehensive review-based study on methods, solutions, and prospects. International Journal of Critical Infrastructure Protection, 38, 100547.
7. Cortés Balcells, C. (2020). Crowd flow management based on human factor to improve security in mass gathering events (Master›s thesis, Universitat Politècnica de Catalunya).
8. Dasgupta, D., Akhtar, Z., & Sen, S. (2022). Machine learning in cyber-

security: a comprehensive survey. The Journal of Defense Modeling and Simulation, 19(1), 57-106.

9. Dhirani, L. L., Armstrong, E., & Newe, T. (2021). Industrial IoT, cyber threats, and standards landscape: Evaluation and roadmap. Sensors, 21(11), 3901.
10. George, A. S. (2024). Emerging Trends in AI-Driven Cybersecurity: An In-Depth Analysis. Partners Universal Innovative Research Publication, 2(4), 15-28.
11. Goriparthi, R. G. (2023). AI-Augmented Cybersecurity: Machine Learning for Real-Time Threat Detection. Revista de Inteligencia Artificial en Medicina, 14(1), 576-594.
12. James, E., & Rabbi, F. (2023). Fortifying the IoT landscape: Strategies to counter security risks in connected systems. Tensorgate Journal of Sustainable Technology and Infrastructure for Developing Countries, 6(1), 32-46.
13. Kabanda, G. (2021). Performance of machine learning and big data analytics paradigms in cybersecurity and cloud computing platforms. Global Journal of Computer Science and Technology: G Interdisciplinary, 21(2).
14. Kaloudi, N., & Li, J. (2020). The ai-based cyber threat landscape: A survey. ACM Computing Surveys (CSUR), 53(1), 1-34.
15. Kimani, K., Oduol, V., & Langat, K. (2019). Cyber security challenges for IoT-based smart grid networks. International journal of critical infrastructure protection, 25, 36-49.
16. Lone, A. N., Mustajab, S., & Alam, M. (2023). A comprehensive study on cybersecurity challenges and opportunities in the IoT world. Security and Privacy, 6(6), e318.

17. Macas, M., Wu, C., & Fuertes, W. (2022). A survey on deep learning for cybersecurity: Progress, challenges, and opportunities. Computer Networks, 212, 109032.

18. Mathas, C. M., Grammatikakis, K. P., Vassilakis, C., Kolokotronis, N., Bilali, V. G., & Kavallieros, D. (2020, August). Threat landscape for smart grid systems. In Proceedings of the 15th international conference on availability, reliability and security (pp. 1-7).

19. Mavroeidakos, T., & Chaldeakis, V. (2020). Threat landscape of next generation IoT-enabled smart grids. In Artificial Intelligence Applications and Innovations. AIAI 2020 IFIP WG 12.5 International Workshops: MHDW 2020 and 5G-PINE 2020, Neos Marmaras, Greece, June 5–7, 2020, Proceedings 16 (pp. 116-127). Springer International Publishing.

20. Nassar, A., & Kamal, M. (2021). Machine Learning and Big Data analytics for Cybersecurity Threat Detection: A Holistic review of techniques and case studies. Journal of Artificial Intelligence and Machine Learning in Management, 5(1), 51-63.

21. Pan, J., & Yang, Z. (2018, March). Cybersecurity challenges and opportunities in the new" edge computing+ iot" world. In Proceedings of the 2018 ACM international workshop on security in software defined networks & network function virtualization (pp. 29-32).

22. Sarker, I. H., Kayes, A. S. M., Badsha, S., Alqahtani, H., Watters, P., & Ng, A. (2020). Cybersecurity data science: an overview from machine learning perspective. Journal of Big data, 7, 1-29.

23. Schiller, E., Aidoo, A., Fuhrer, J., Stahl, J., Ziörjen, M., & Stiller, B. (2022). Landscape of IoT security. Computer Science Review, 44, 100467.

24. Shah, V. (2021). Machine learning algorithms for cybersecurity: Detecting and preventing threats. Revista Espanola de Documentacion Cientifica, 15(4), 42-66.

25. Shah, V. (2021). Machine learning algorithms for cybersecurity: Detecting and preventing threats. Revista Espanola de Documentacion Cientifica, 15(4), 42-66.

26. Shaukat, K., Luo, S., Varadharajan, V., Hameed, I. A., & Xu, M. (2020). A survey on machine learning techniques for cyber security in the last decade. IEEE access, 8, 222310-222354.

27. Siddiqa, A., Khan, W. Z., Alkinani, M. H., Aldhahri, E. A., & Khan, M. K. (2024). Edge-assisted federated learning framework for smart crowd management. Internet of Things, 101253.

28. Stellios, I., Kotzanikolaou, P., & Grigoriadis, C. (2021). Assessing IoT enabled cyber-physical attack paths against critical systems. Computers & Security, 107, 102316.

29. Yaseen, A. (2023). AI-driven threat detection and response: A paradigm shift in cybersecurity. International Journal of Information and Cybersecurity, 7(12), 25-43.

30. Zoppi, T., Ceccarelli, A., Capecchi, T., & Bondavalli, A. (2021). Unsupervised anomaly detectors to detect intrusions in the current threat landscape. ACM/IMS Transactions on Data Science, 2(2), 1-26.

The Path And Landing Places On The Road Of Imam Hussein From Mecca To Karbala: A Modern And Satellite-Bas Study A proach

Asst.Prof.Dr.Abdulkareem Abd Ali Mohammada
PhD, Engineer, Space Technology & Antenna and Propagation Specialist,
Lecturer at Al_Esraa University \ Department of Biomedical Engineering
abdulkareem.a@esraa.edu.iq

Dr.Parviz Tarikhib
PhD, Physicist, Space Science and Technology Specialist,
Independent Researcher
Parviz_tarikhi@hotmail.com

Abstract

The importance of the Movement of Imam Hussein from Mecca to Karbala played a great and effective role in accomplishment Imam's mission. The authors focused on the Kufi Hajj Route (Zubaydah Trail in Arabic Darb Zubaydah) as a basis for this study due to the abundance of sources through which they can learn the ancient and numerous names of the houses and stations on the route. Famous to Zubaydah Trail, it is comprised of the sites and ponds along the road. A study made to designate precisely the names of all the sites and ponds along the road. Benefiting of the modern technologies as a strong and effective tool for well managing and study we used space applications technologies and engineering such as GIS and remote sensing, telecommunications, artificial intelligence, informatics, mathematics, statistics, and so on.

A satellite or aerial image of each site and a judicial image from Google Maps for each site with the geographical coordinates were used. Putting the geographical coordinates accurately is important bias because all references do not put the coordinates and if they do, they are either incorrect or inaccurate. Furthermore, a framework for using space radar imagery for some locations provided a valuable addition to our work.

In this paper, the authors with background in space science and technologies, and telecommunications focus on and highlight effectiveness and importance of these fundamental and infrastructural technologies. Authors believe that the joint work and cooperation of the organizational and independent experts from the relevant entities and sharing knowledge and experience can lead to increment of the synergy of work for well managing and control of the event.

Semi-Annual Scientific Journal
www.arbnj.com
Ramadan 1447 A.H, March 2026 A.D

Authors, who are from Iraq and Iran, worked for long term in their relevant national space technology and communication organizations in both managerial and specialized levels. They share the feasible and accessible potentials and possibilities for well managing and control of the sites under study. Authors determine the steps of ideas in order of priority and importance, which inevitably involve creativity. They believe that the idea of experimenting with collaboration and remote work will certainly yield success.

Introduction

Importance of the Movement of Imam Hussein from Mecca to Karbala played great role in accomplishing Imam's mission. The Kufi Hajj Route (Zubaydah Trail) has taken as a basis for a study that because of the abundance of sources through which they can learn the ancient and numerous names of the houses and stations on the route. Famous to Zubaydah Trail, it is comprised of the sites and ponds along the road. Benefiting of the modern technologies as a strong and effective tool for well managing and study space applications technologies and engineering such as GIS and remote sensing, telecommunications, artificial intelligence, informatics, mathematics, statistics, and so on, are used in this study. Nevertheless, the main weight of the work in this study goes to radar and thermal satellite and airborne imagery which importance is discussed in section 5.

The ancient caravan old route from Mecca to Iraq

Since ancient times, caravans have traveled overland between the Hijaz and neighboring regions. One of the pre-Islamic routes was the ancient caravan route from Mecca to Iraq, known as the Hira Road.

Al-Hirah, the capital of the Lakhmids, was located near the site of Kufa. This was a major caravan route in ancient times, connecting the Hijaz region with Mesopotamia. Journeys departed through the Najd Plateau, passing stations with wells and ponds. They made their way through the rugged terrain of the Great Nafud Desert, using ancient wells and oases as the basis for their route. They also passed through the Al-Jawf region through depressions and valleys (Sultan Naji 1978).This road was used by Muslims at the beginning of the Islamic era for cultural and military purposes. The Islamic army, led by Sa'd ibn Abi Waqqas, took this route, stopping at some areas with water sources before reaching the rivers of Iraq. These included the areas of Al-Zarud, Al-Tha'labiyah, Sharaf, Al-Udhaib, and Al-Qadisiyah (Muhammad Al-Saidi 2018).

Because of the Hajj rituals established by Islam, Islamic states paid special attention to the ancient roads, including the Mecca-Hira Road. After the founding of the city of Kufa in the Islamic era, the road was called the Kufi Hajj Road. During the Abbasid era, great attention was paid to this road, and modern ponds, springs, traffic lights, forts, and even palaces were built.

It is worth noting that a large portion of the Al-Hirah Road falls within the newer Zubaydah Trail, established during the Abbasid Caliphate. Zubaydah Trail was used as part of the original Al-Jawf-Hail Road. Stations in the Faydh, Al-Tha'labiyah, and Wadi Al-Rummah regions were also part of Zubaydah Trail (Al-Rashed 2001). Thus, parts of the old Al-Hirah Road coincide with the Kufa Hajj Road and with modern trade routes in Saudi Arabia and Iraq.

Land pilgrimage route from Kufa to Meka (Zubaydah Trail)

The Kufa Hajj Route is one of the most important historical routes used by Muslim pilgrims to travel from Kufa in Iraq to Mecca in the Hejaz. Its history dates back to the pre-Islamic era. However, its importance increased with the advent of Islam and it flourished beginning with the era of the Rightly Guided Caliphate and the Umayyad period, reaching its peak during the era of the first Abbasid Caliphate.

Zubaida bint Ja'far, the wife of Caliph Harun al-Rashid, constructed numerous ponds and wells to provide water for pilgrims, Umrah performers, and travelers. Pilgrims from eastern Iraq also used this route, gathering in the Iraqi city of Kufa. From there, they crossed the desert road to enter the Arabian Peninsula as the Iraqi Hajj Caravan, until they reached Mecca (Anthea Crane 2023), (Al-Rashid, S. A. 1977).

This road is approximately 1,400 kilometers long and crosses most of the lands of Najaf Governorate in Iraq, then the lands of Saudi Arabia in the governorates of Rafha, Hail and Qassim, reaching Mecca.

Its use became increasingly regular and convenient, as water centers and grazing areas located along the route became major stations. It now contained numerous stations and houses that were used as rest stops and water supply points for caravans. The road is connected by numerous main stations (each called a "manzil"), in addition to substations (called " muta'asha" for resting and eating), with ponds, pools, and wells scattered along the sides of the road. There are 27 stations from Kufa to Mecca, with Mecca being the 28th and five of the stations are located in Iraq (Al-Rashid, S. A. 1977) (The Desert Team, July 4, 2022).

Those are (Kufa, Al-Qadisiyah, Al-Mughitha, Al-Qura'a, Waqisa, Aqaba). The remaining houses are located in the Kingdom of Saudi Arabia and they are (Al-Alqae, Zubalah, Al-Shuqooq (Al-Shihiyat), Bitan (Aleashar), Althaelabia (albidae), Alkhazimat Zarud, Al'ajfar, Fid, Tawz, Samira, Alhajir, Maedin Alqurashi (now Aalnaqrat), Alnaqrat (now Al-jafniat), Mughithat Almawan (Alsaqaea'), Alrabidha, Alsalila, Aleumq, Almaedin, 'Afieih, Almusalah, Alghamra, Dhat Earq, Albustan) and then Makkah Al-Mukarramah. The coordinates of these houses are shown in the Table 1 (Appendix 1).

The distance between one house and another is not fixed because the location of the houses at that time was chosen based on the daily path of the caravans and the availability of water along the way. The average distance between one house and another ranged between 40 and 50 km. As for the dinners, the number of houses, their names and coordinates are shown in Table 1 (Appendix 1) . A look at the various stations and facilities along the route reveals that this historic project was characterized by high-level planning in water management and meticulous construction management, reflecting a spirit of teamwork.

The remaining landmarks, including ponds, wells, water springs, rest stops, and other sites, are among the most important physical heritage sites. Their restoration could contribute to preserving the archaeological and human values that can be transformed into tourist sites that enhance historical tourism in the region.

The most important features of this road are:

- The presence of wells, ponds, basins, and rest stops along the route before its development by the Abbasids.
- Rest stops, water collection ponds, and various wells and water channels were established according to the possible terrain along parts of the road.

- Stones were paved on both sides of the road to facilitate navigation in the desert. (Fig. 3.1.)
- The road featured signposts (called "mile," "mushrif," and "barid") and beacons to indicate distance and geographical location (The Desert Team, July 4, 2022).
- Villages and residential centers arose around it due to the constant movement along it.
- Between one house and the next, there was a "muta'asha" (a place for rest and eating).

The presence of some inhabited stations, which were originally small villages or towns that helped pilgrims purchase supplies.

In this study, we will follow this historic route, house by house, from Kufa, Iraq, to Mecca, relying on historical sources that describe significant details of this route. The geographic coordinates of each stop and archaeological landmark will be documented using space technology and geographic information systems for both sections of the route (Iraqi and Saudi), along with available satellite images for each region (The Desert Team, August 19, 2003), (The Desert Team, Tag Archives: Kufi Hajj Trail July 23, 2022)

We will start with what was documented in the book of Judge Waki', which was widely relied upon by explorers and researchers. The following is a table of stations (homes) and night rest areas (dinners).(Table1 in Appendix 1)

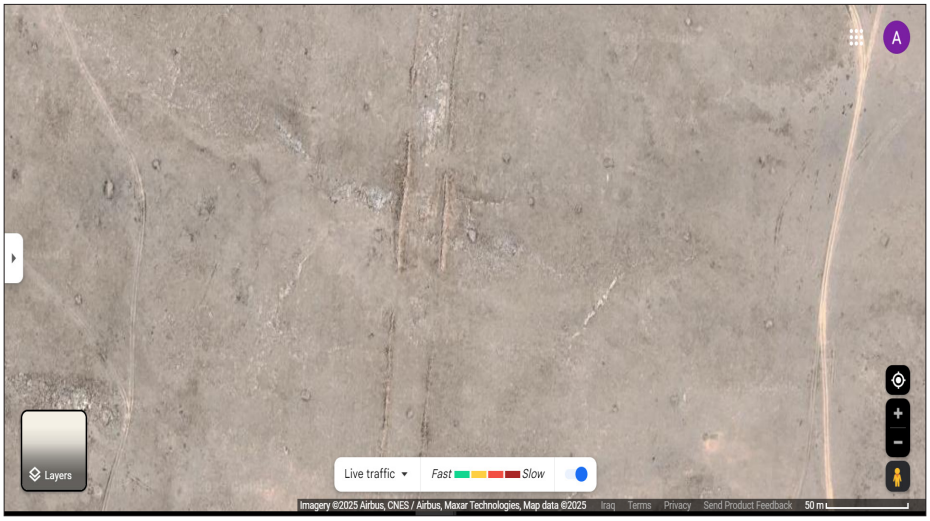

Fig.3.1: Satellite image taken from Google Maps showing the shape of Zubaydah Trail, where stone paving is noticeable on both sides of the road. Despite the passage of time, it can be seen clearly from the satellite images and coordinates (30.279349, 43.633829).

1.Standards: Used to Measure Distances on Zubaydah Trail.

The road signs on Zubaydah Trail are among the most prominent archaeological evidence, reflecting the meticulous organization and great care taken to facilitate the journeys of travelers between Kufa and Mecca. Engineers on Zubaydah Trail used precise units of measurement to determine distances and guide travelers (Fig. 3.2). The unit used was the mile, which is equivalent to approximately 2 km in the Arab standard. Milestones, (Fig. 3.3), were placed along the road to mark the distances between stations. Another unit of measurement was the Albirid, which equaled 12 miles (approximately 24 kilometers). Albirid markers were constructed of stone, often square in shape, (Fig. 3.5), and marked the Albirid number and the remaining distance to the next Albirid. Another guidance unit was Almushraf, which was built halfway between two Albirids, i.e., every 6 miles (approximately 12 kilometers) (The Desert Team Trail (1) July 4, 2022). Almushraf was also constructed of stone and was often circular in shape, (Fig. 3.4) and taller than the Albirid, making it easier to see from a distance.

These signs demonstrate the extent of progress in urban planning and engineering in the early Islamic era. The Book of the Road states that the distance from Baghdad to Mecca is seven hundred and fifty-eight miles, which is close to the distance that can be measured with modern surveying tools.

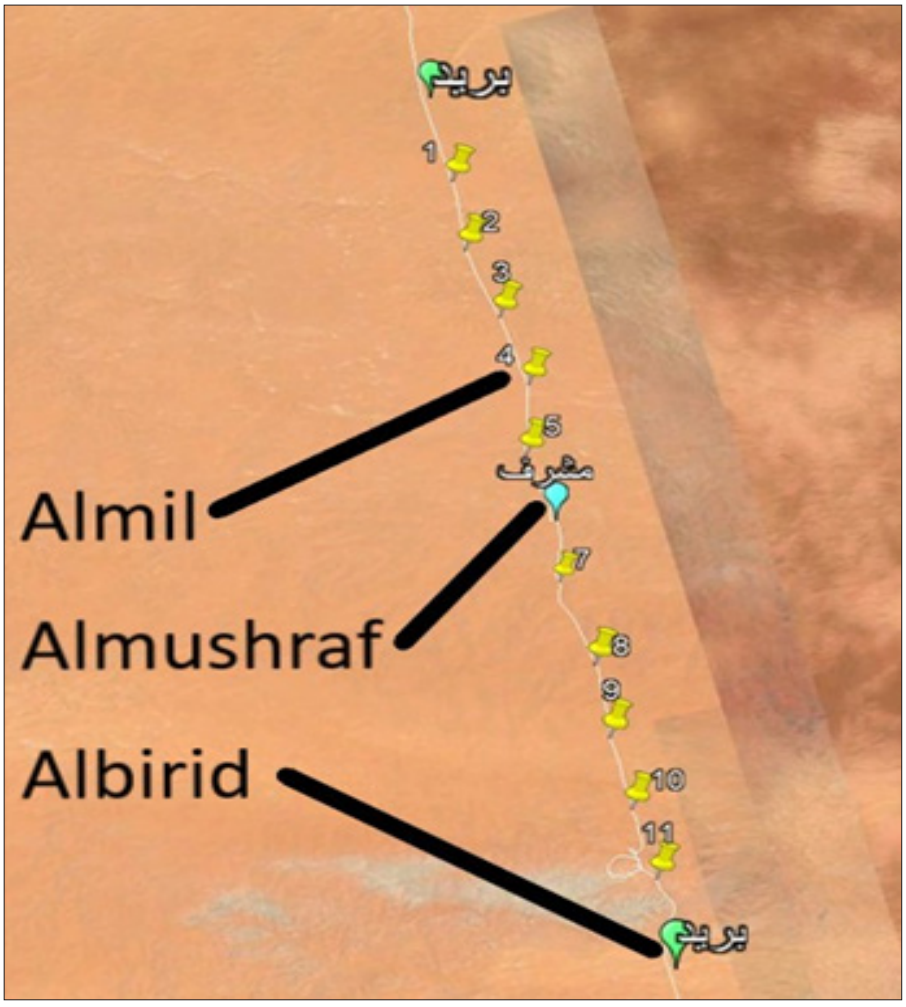

Fig.3.2:Satellite image indicating the units of measurement used on Zubaydah Trail, which are Arabic mile (Almil), Almushraf and Albirid (The Desert Team Trail (1) July 4,2022)

Fig.3.3: A photograph of the stone structure of the mile in Zubaydah Trail (The Desert Team Trail (1) July 4,2022)

Fig :3.4 .Photographs of the construction of the Almushraf in Zubaydah Trail) the one on the left(consisting of an old cylindrical brick building) the one on the right (of Almushraf built in the form of a stone cylindrical structure) The Desert Team Trail 1) July.(2022 ,4)

Fig. 3.5: Photograph of the square stone columnar building of Albirid in Zubaydah Trail (The Desert Team Trail (1) July 4, 2022).

2 Investigation from space of selected locations from the Iraqi section of Zubaydah Trail

Al-Mughitha House) Al-Manzil(

Satellite images revealed the remains of houses and ruins of a large village. Al-Mughitha is one of the historic stations on Zubaydah Trail and was an important stopping point on this route (The Desert Team Trail (1) July 4, 2022). Fig. 3.6 contains a Google Maps image and the station coordinates were determined from the image, which are (31.355556, 44.134722). There was a well between Wadi al-Siba' and al-Mughitha in the middle, called Bir al-Nas. This well is located approximately halfway between Wadi al-Siba' and al-Mughitha. Bir al-Nas is located 12 km, its coordinate (31.427000, 44.167615), from Wadi al-Siba' which located at coordinate (31.537776, 44.229994). After leaving al-Mughitha Station, heading south, and 13 km from it, we reach a beautiful round Zubaydah pond called Birkat Hamad located at coordinate (31.251247, 44.083773), see Fig. 3.7

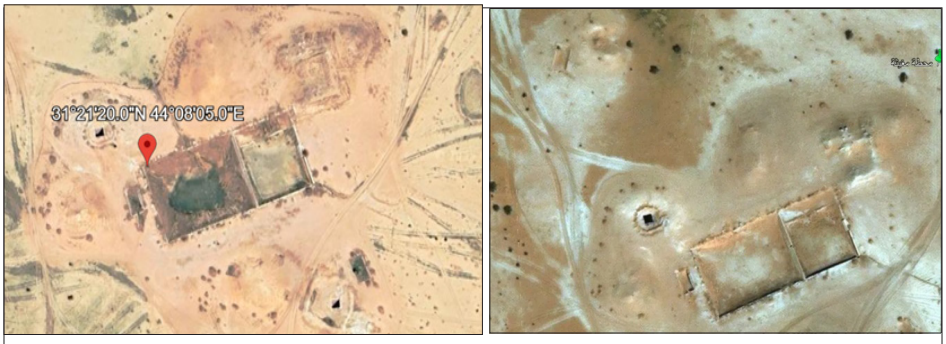

Fig.3.6.A satellite image of Al-Mughitha station) on right side ,(taken from the reference) The Desert Team Trail (1) July (2022 ,4 and compared with a satellite image) in left side (taken from Google Maps .The station's coordinates were determined as indicated ,which are.(44.134722 ,31.355556)

Fig. 3.7: A satellite image for Hamad water pool (at right side), taken from the reference and compared with a satellite image (at left side) taken from Google Maps. The pool coordinates were determined as indicated, which are (31.251247, 44.083773)

Dinner Place (Muta'asha):Al-Qubaybat:

After walking 24 km from Waqisa towards the south in a flat area, we reach a sub-site, which is Al-Muta'asha, called Al-Qubaibat (The Desert Team Trail (2) July 23, 2022). It seems that the reason for the name is the location of the site between beautiful domed hills, as we see in the satellite image. The site contains two scattered buildings, and we did not see the well, and it is most likely buried. The first palace is between Al-Qubaibat, while the second is about one kilometer away. (Fig.3.8.).

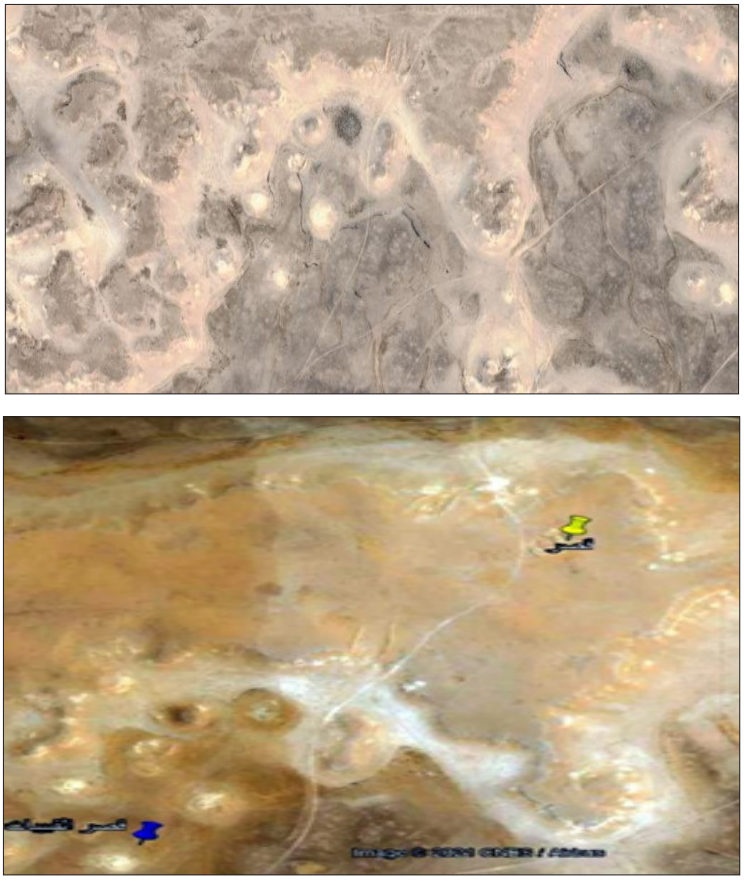

Fig. 3.8.: Satellite image of the Qubaibat site taken from the reference (The Desert Team, Trail (2) July 23, 2022) on the left side. The image shows the presence of domed hills. The site also contains two separate buildings: the first is a palace located between Qubaibat, and the second is approximately one kilometer away. The image on the right was taken from Google Maps and the coordinates taken are (30.369102, 43.658916).

3.Investigation from space of selected locations from the Saudi Arabia section of Zubaydah Trail

Al Amia Pool (Blind Pool) :

After crossing the Iraqi border, we first reach the Dhafiri pond, and its coordinates are (29.988029, 43.614663). Dhafiri pond is located 3 km south of the border and 11 km north of the blind pond. Fig. 3.9 illustrate a satellite image of Dhafiri pond.

After Dhafiri pond, the road heads to the Al Amia pond (see Fig. 3.10). The coordination of this pond is (29.883244, 43.620346) and the land there is stony, barren, gray, with no grass or trees. It is a square pond with a side length of 28.4 m, with cylindrical supports at the corners and semi-cylindrical supports in the walls. The entrance to the pond is south, 85 cm wide, and sloping. The pond has a breakwater that forces the torrent towards the pond.

There are remains of a square building with a side of 17 m, with 5 rooms, one of which is a prayer hall, and some other dilapidated buildings (The Desert Team, Zubaidah Trail January 14, 2010). Al Amia Pool is a substation between Al Aqaba station and Al Qaa house. It seems that the accumulation of sand in and around it has prevented it from receiving floods in recent years.

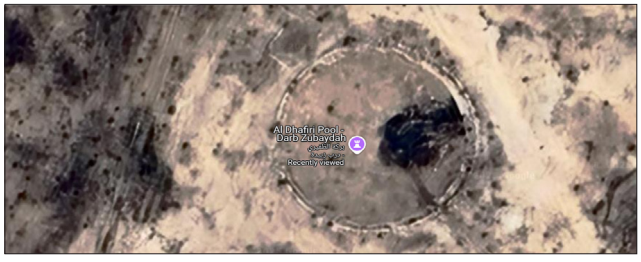

Fig. 3.9: Satellite image Al Dhafiri Pool taken from Google Maps and its coordinates are (29.988099, 43.614633)

Fig.3.10: Satellite image Al Amia Pool taken from Google Maps and its coordinates are (29.883244, 43.620346)

The Sixth House Al-Qaa :

This station is major and has a large area ,but because its land is sandy, the sand has contributed to obscuring many of its features. Its most important features are two adjacent ponds, one to the north and the other to the south, with a distance of 7 m between them. (See Fig. 3.11) The northern one is 50 by 46 covered with sand, and the southern one is 50 by 51. They have been covered with gypsum from the inside with a wall to divert the water.

The ruins of a village are located about 200 m west of the two ponds on a on a dirt plateau, and it seems to consist of scattered units. It contains a large construction may be palace of the usual style in Zubaydah Trail, with a side of 60 m. A row of shops (stores) and internal rooms are also existed. In the northern part we find a row of 16 rooms and a castle and Al-Qaa Mosque and some scattered buildings (The Desert Team January 14, 2010).

Fig.3.11: Satellite image of the Al-Qaa station taken from Google Maps and its coordinates are (29.760367, 43.629985)

There is a pond located 15 km south of Al-Qaa station called Al-Haitham Pond (Al-Thalima). (See Fig. 3.12) It is a wonderful pond, and its beauty is increased by its circular shape and its diameter of 32 m. It has two strong walls, the inner one is 160 cm wide and the outer one is 80 cm wide, and the stairs are 6.5 m wide. This pond is distinguished by the beauty of its engineering and the way the water reaches it. There is a beautiful drain with a precise entrance and an exit in the form of a tunnel.

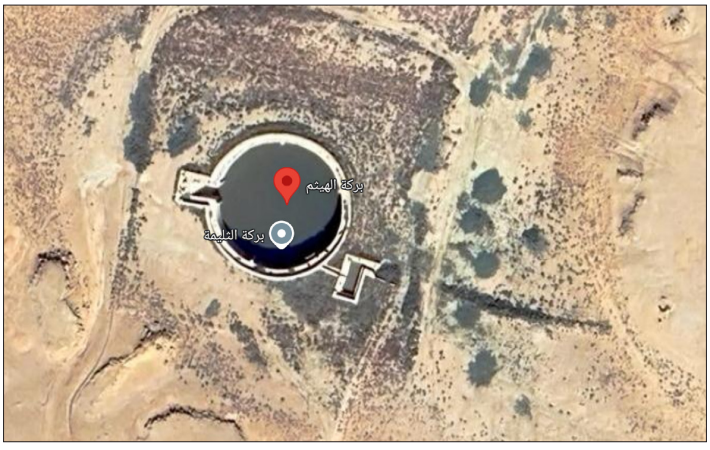

Fig. 3.12: Satellite image of Al-Haitham Lake (Al- Thalima), taken from Google Maps. Its coordinates are (29.624914, 43.612772)

Using remote sensing techniques, it is possible to identify and record the archaeological landmarks and heritage sites of Zubaydah Trail, thus enabling high-resolution mapping using geographic information systems (GIS). One such work, which relied on these techniques, produced the result shown in Fig. 3.13 for the route of Zubaydah Trail in its Iraqi section, from Kufa to the Iraqi-Saudi border (Anthea Crane, 2023)The areas identified on this map were identified using satellite images from Google Earth, then compared with Bing aerial photographs and information available from earlier sources, such as the archaeological survey conducted by Al-Rashed (1977) and others (Anthea Crane, 2023) (Al-Rashid, S. A. 1977), which allows for comparison of site descriptions with more recent satellite images. Furthermore, distance measurements, descriptions and labels of wells and reservoirs, and photographs taken of site views facilitate the production of new maps.

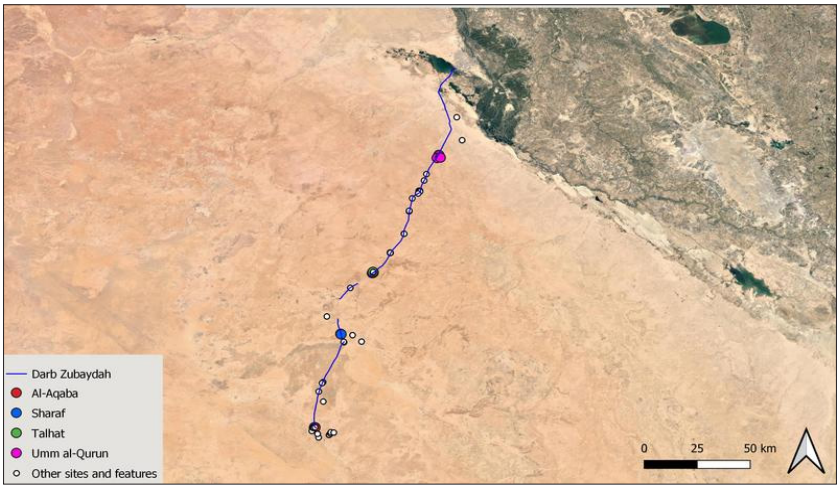

Fig. 3.13: shows the path of Zubaydah Trail in the Iraqi section and the stations of this trail on Google Earth image (Anthea Crane 2023).

The map that published the Hajj and Umrah Atlas also gave a description of the stations and locations of the route. The map shows Zubaydah Trail, which extends from Kufa in Iraq to Mecca, passing through northern and central Saudi Arabia and passing through five regions: the northern Borders, Hail, Qassim, Medina, and Mecca. (Fig. 3.14)

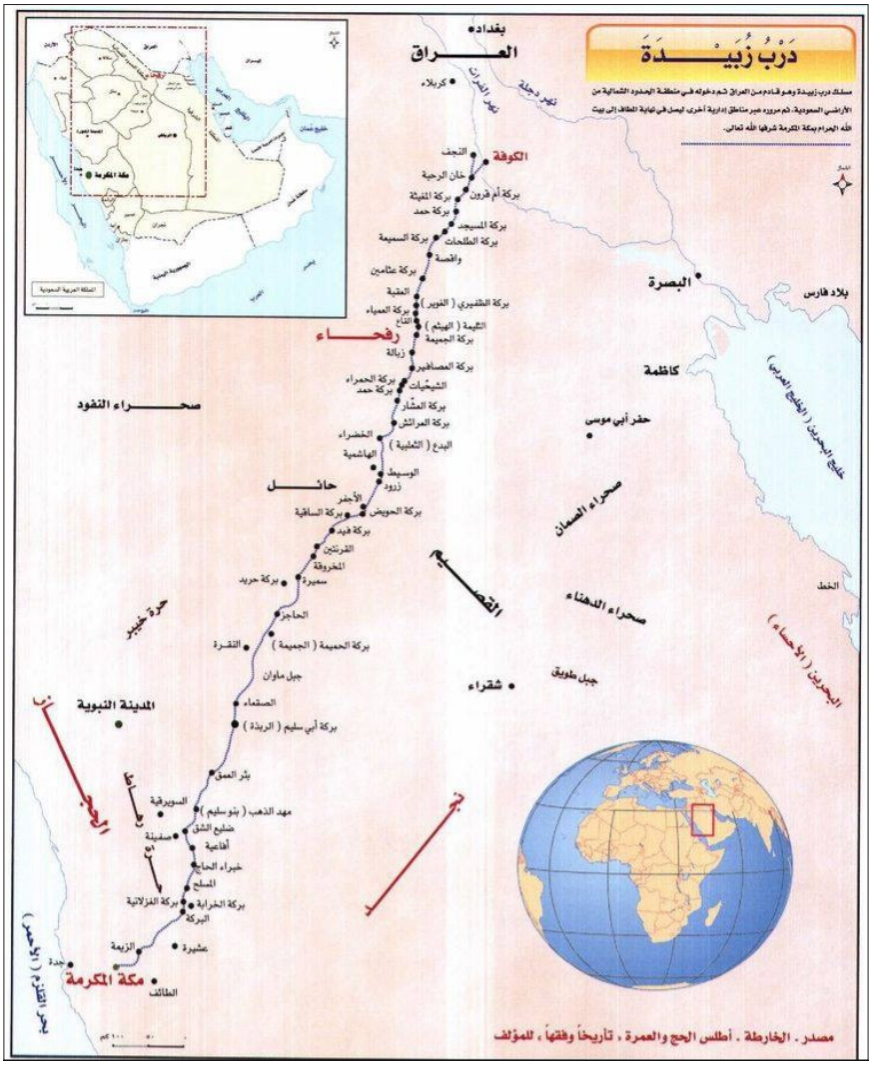

Fig. 3.14: Map of the Hajj Zubaydah Trail, showing the various service stations from Kufa to Mecca. (From the Atlas of Hajj and Umrah, by Sami ibn Abdullah al-Maghluth) (Fareeq E. W. 2021) (Sami ibn Abdullah al-Maghlouth 2010)

A geographical map of Zubaydah Trail quarter in Saudi Arabia was also produced. This map is very important because of the precise locations and details it contains. It was prepared by the United States Geological Survey and the Arabian American Oil Company under the joint sponsorship of the Government of the Kingdom of Saudi Arabia and the United States Department of State (U.S. Geological Survey 1960).

The movement of Imam Hussein caravan and its route from Mecca to Karbala

Historical references indicate that the blessed journey of Imam Hussein's (peace be upon him) procession took 24 days, starting from Mecca and arriving in Karbala. It traveled in the Hijaz for 16 days and in Iraq for 8 days. The procession departed on the eighth of Dhu al-Hijjah in the year 60 AH and continued until the second of Muharram in the year 61 AH. The total number of houses that Imam Hussein (peace be upon him) passed during this period—from his departure from Mecca until his arrival in the holy land of Karbala (al-Taf)—was thirty-eight, including the first house (Mecca) and the last (al-Taf). He (peace be upon him) spent the night in twenty-four of these houses. The distance covered by this blessed procession was approximately 1,403 kilometers (Sheikh Saleh Al , Karbasi 2004).

Although Imam Hussein's journey from Mecca to Iraq is considered a significant historical event, we note the presence of more than one sequence of stations and stops documented along this journey. This was due to several historical and geographical reasons (The Holy Shrine of Imam Hussein 08/04/2017). One of these reasons is the discrepancy in historical accounts in ancient references, which describe from similar, if not completely identical, routes. This is due to each historian's reliance on oral accounts from different eyewitnesses and the varying details in describing stations.

The names of some sites have changed over time, or been known by multiple names. Some ancient villages have disappeared, or the routes have been altered. Due to the circumstances of the journey at that time required the Imam to choose villages and sites with large settlements and abundant water. Also to avoid enemies, the Imam deviated from his route several times, taking alternate routes through the desert and stopping at unfamiliar stations. Differences in the geographic location of some sites are described, and water pools and springs are mentioned in the narratives

Here, we will cite the sequence of points in various sources for accuracy and to make them available to researchers for scientific investigation and verification. The following lists the names of the houses that Imam Hussein (peace be upon him) passed on his way to Karbala (Labib Baydoun 1987), and the geographical coordinates of the houses where he stopped or spent the night. We also mention the distance between each of these houses, which are:

The route of the Imam's caravan's movement from Mecca to Karbala was determined in the Encyclopedia of Imam Hussein, peace be upon him, in the Book, Sunnah and History, Part 3 (Mahmoud Tabatabai 1969), as the stations that this caravan passed through are according to the following sequence: (Mecca (مكة), Al-Tan›eem (التنعيم) , Al-Safah (صفاح) , Bustan Ibn Amir (بستان ابن عامر), Dhat ‹Irq (ذات عرق), Ghamrah (الغمرة), Al-Maslah (المسلح), Al-Ufay›iyah (الافيعية), Ma›din Bani Sulaym (معدن بني سليم), Al-›Umq (العمق), Al-Sililiyah (السليلة), Al-Rabadhah (الربذة), Mughithat al-Mawan (مغيثة الماوان), Al-Naqrah (النقرة), Al-Hajir (الحاجر), Samira› (سميراء) , Twz (توز),

Fayd (فيد), Al-Ajfur (الاجفر), Al-Khuzaymiyah (الخزيمية) , Zarud (زرود), Al-Tha›labiyyah (الثعلبية), Al-Bat›an (البطان), Al-Shaquq (شقوق), Zubalah (زبالة), Al-Qa› (القاع), Al-›Aqabah (العقبة), Waqisah , واقصة), Sharaf (شراف), Dhu Husum (ذو حسم), Al-Baydah (البيضة), ‹Udhayb al- Hijanat (عذيب الهجانات), Al-Ruhaymah (الرهيمة), Qasr Bani Muqatil (قصر بني مقاتل), Al-Taff (الطف)then Karbala (كربلاء)

The investigative study conducted by the eminent scholar Sheikh Muhammad Sadiq al-Karbasi was informative, and his concluding opinion on the stations of Imam Hussein›s path was explained in his book (History of the Shrines of Hussein, His Family, and His Supporters (Part 5)). (Sheikh Muhammad Sadiq Al-Karbasi 2018). He gave the names and distances between the stations and stations according to the sequence of the journey from Mecca to Karbala. Table 2 (Appendix 2) shows the sequence of stations that the caravan of Imam Al-Hussein passed through. A map of Imam Hussein's journey from Mecca to Karbala is also provided, with a scale of 1 mm ≈ 11 km (Fig. 4.1). This helps those interested in understanding the subject and helps in determining locations using modern optical instruments.

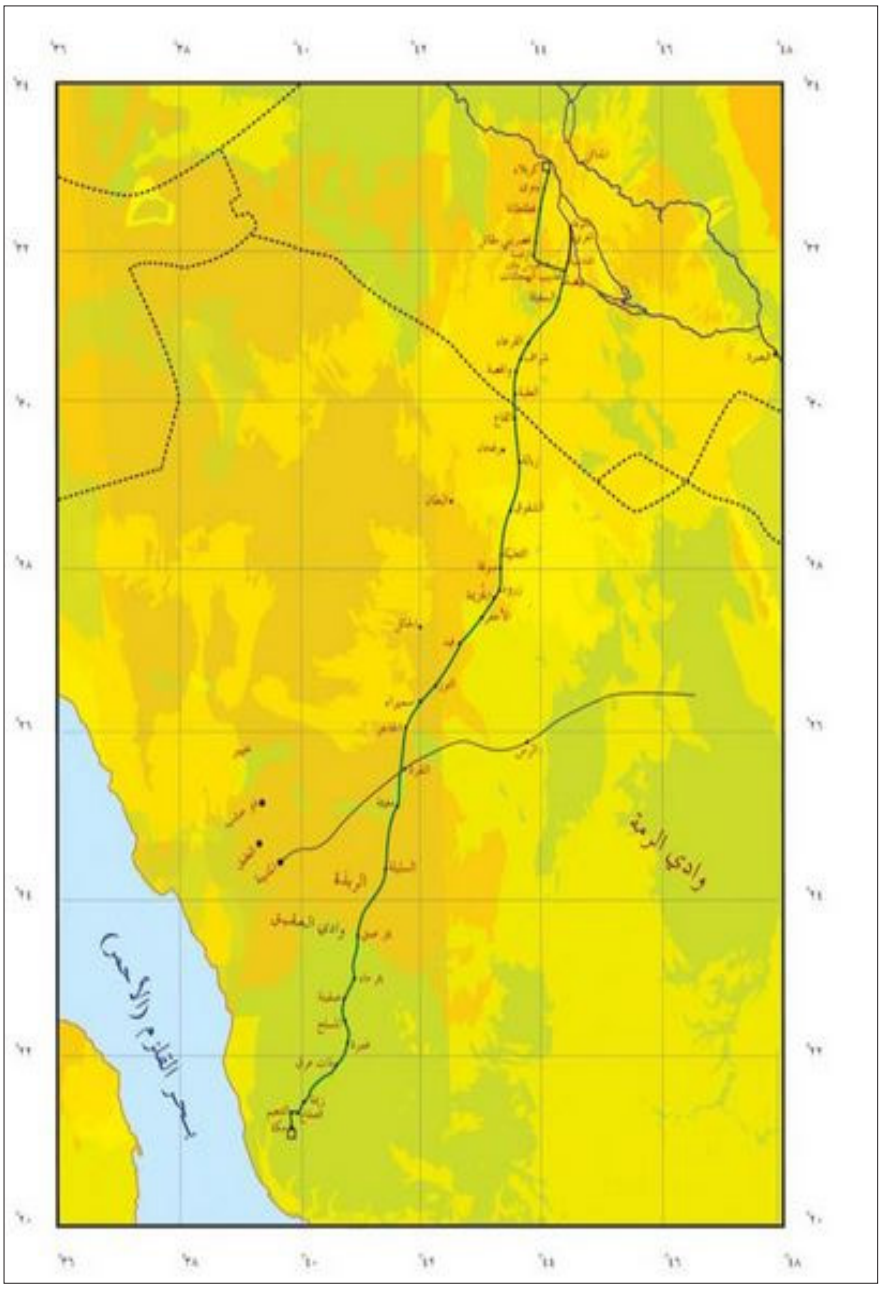

Fig. 4.1: shows a map mentioned by the researcher Sheikh Al-Karbasi about the journey of Imam Al-Hussein from Mecca to Karbala, showing the route, the stations that the Imam passed or stayed. It is on a drawing scale of 1 mm ≈ 11 km. (Sheikh Muhammad Sadiq Al-Karbasi 2018).

Semi-Annual Scientific Journal
www.arbnj.com
Ramadan 1447 A.H, March 2026 A.D

The officials of the Holy Shrine of Imam Hussein also paid attention to the route taken by the Imam, and the sequence of the houses and stations that Imam Hussein passed through was published (Sabah Al-Talqani and Maitham Al-Husseini 2022), and Fig. 4.2 shows the names and sequence of the stations. The Karbala Center also produced a map of this route that included a table of all the stations and areas that Imam Hussein passed through and the distances between those stations c, as in Fig. 4.3. This detailed map of Imam Hussein›s (peace be upon him) journey from Mecca to Karbala, prepared by the Karbala Center for Studies and Research. This map represents a recent and important scientific effort to document Imam Hussein›s (peace be upon him) journey geographically and historically. Geographic Information Systems (GIS) and remote sensing were used to determine the route. The map shows the stations through which Imam Hussein (peace be upon him) passed from Mecca to Karbala. This map helps researchers understand the geographical challenges faced by the caravan and serves as a primary reference for historical and archaeological studies. There are also other references that provide ancient and modern maps of this sacred path, including what is mentioned in the seventeenth chapter of the first part of the Karbala Encyclopedia (Labib Baydoun 1987).

Fig. 4.2: An illustrative Arabic panel showing the homes of Imam Hussein from Mecca to Karbala in a sequential manner, supported by the date of his arrival and departure for each home (Sabah Al-Talqani and Maitham Al-Husseini, 2022).

Fig. 4.3: Detailed map of the path of Imam Hussein (peace be upon him) prepared by the Karbala Center for Studies and Research - Al-Hussain Holy Shrine (Karbala Center for Studies and Research - Al-Hussain Holy Shrine ,Privet communication with Dr Al-Jwahiry 2025).

Framework for using space tools for deep study on this historical road

Radar imaging has revolutionized archaeological surveys by offering a non-invasive window into the subsurface. Techniques such as ground-penetrating radar (GPR), synthetic aperture radar (SAR), and others allow researchers to detect hidden features like foundations, ditches, and former river channels without disrupting the fragile underground structures. By integrating methods like infrared aerial photography—exemplified in regions of Japan—archaeologists can visualize features as deep as 5 meters, ensuring careful planning and preservation before any excavation takes place.

Beyond mere detection, radar imaging characterizes the physical properties of the subsurface. Different materials reflect radar waves uniquely, enabling the identification of man-made structures through contrasts in dielectric properties, moisture retention levels, or carbonaceous deposits. Airborne and spaceborne SAR techniques have proven effective in mapping large areas, including arid regions like the Gobi Desert, where subtle topographical details are critical. This ability to survey extensive tracts of land quickly and precisely has dramatically reduced the time and costs associated with traditional field surveys, while also supporting advanced spatial modeling and GIS integration (Yoshito Miyatsuiq and Yasuhiro Takahashi 1996) (Douglas C. Comer & Ronald G. Blom 2002).

Practical applications of these radar techniques are evident in diverse archaeological contexts. For instance, GPR surveys at the Aquileia Archaeological Park in Italy have mapped Roman construction beneath silty loam layers, while urban excavations in Lecce have distinguished between modern debris and historical deposits. Similarly, at sites like the State Museum-Reserve “Tsaritsino,” areal GPR surveys have revealed structural

details such as gazebos and pathways, guiding excavation teams efficiently. Ongoing advancements, including the integration of machine learning and additional remote-sensing tools like LiDAR, are further enhancing the depth and accuracy of archaeological investigations, ensuring that our understanding of past cultures continues to expand while preserving the integrity of the archaeological record (Derrold W. Holcomb 2001).

Thermal imagery offers a non-invasive means of detecting subtle temperature variations on and just below the surface, enabling archaeologists to uncover buried features without disturbing the site. Infrared cameras capture these thermal differences, revealing anomalies where construction materials or soils retain heat differently from their surroundings. For instance, a buried stone wall may create a distinct thermal signature compared to the adjacent sediment, especially during early mornings or late afternoons when temperature contrasts are greatest.

In archaeological prospecting, these temperature variations help pinpoint the locations of hidden structures such as foundations, roads, or ditches—insights often obscured by vegetation or undetectable by traditional visible-spectrum imaging. Advanced aerial thermography conducted by drones or UAVs can rapidly cover large and challenging areas, guiding archaeologists to promising excavation sites. Moreover, integrating thermal imagery with other data sources like multispectral imaging or LiDAR further refines site models, enabling researchers to distinguish material types, assess moisture patterns, and interpret the overall functional layout while remaining non-destructive (Ahmed Faize , Gamil Alsharahi and Mohammed Hamdaoui 2020).

Several successful thermal imaging projects underscore its value in archaeological research. For example, aerial thermography studies conducted across North America, the Mediterranean, and the Near East have effective-

ly used drone-mounted thermal cameras to reveal subtle ground anomalies that guide excavation efforts. In the realm of historic building investigation, thermal imaging has detected hidden construction modifications and subsurface features, preserving the integrity of these structures while revealing their history. Additionally, the case study of the abandoned medieval town of Montecorvino in Italy demonstrated how UAV-based thermal surveys could map buried walls and pathways, providing critical data for efficient, targeted excavation strategies. These examples, along with emerging integrations involving modern data analytics and machine learning, highlight thermal imagery's transformative role in advancing archaeological diagnostics and landscape interpretation.

Satellite imagery has become a transformative tool in archaeology, offering a non-invasive approach to detect and monitor subtle features that remain hidden to ground-level observers. By capturing high-resolution images and employing advanced analytical techniques, researchers can remotely identify archaeological sites and monitor evolving landscapes over time. This technology not only aids in the discovery of buried structures but also addresses challenges posed by modern land-use activities, helping to preserve cultural heritage.

In North Africa, for example, a study published in 'Remote Sensing' used free Sentinel-2 imagery combined with Google Earth Engine to implement per-pixel change detection. The research focused on sites in regions such as the Aswan and Kom-Ombo areas in Egypt and the Jufra oases in Libya, achieving accuracy rates between 85% and 91% in identifying changes caused by construction, agriculture, and natural processes. Similarly, in the South Caucasus, free and low-cost aerial remote sensing techniques have proven valuable in countries like Armenia, Azerbaijan, and Georgia, enabling the identification and management of archaeological

resources while tracking historical land-use changes in areas where traditional field surveys are often limited by budget constraints (Ahmed Faize , Gamil Alsharahi and Mohammed Hamdaoui 2020).

Globally, satellite imagery is being harnessed to reveal a myriad of archaeological features and landscapes. Organizations like Satellite Imaging Corp. have demonstrated its effectiveness in detecting buried structures, creating digital elevation models to map ancient terrains, and monitoring cultural heritage sites—for instance, at Mount Ararat in Turkey. Together, these examples underscore the cost-effective, non-invasive power of satellite imagery, which not only enhances archaeological site detection but also supports long-term preservation strategies and provides deeper insights into the interplay between past human activities and the environment.

Conclusions

The importance of integrating technology with heritage lies in the possibility of rediscovering ancient trails using modern tools and promoting heritage tourism. We see the need to design and build a specialized scientific database that links historical writings to archaeological sites, which will benefit historians, archaeologists, and researchers.

Nowadays, satellite surveys of houses, stations, and archaeological sites, as well as space tools (such as remote sensing, aerial photography, and geographic information systems), are crucial tools for reviving this heritage, contributing to the discovery of its lost features, and documenting its cultural value.

Accurate and detailed knowledge of the stations and areas of the route is useful in developing the necessary designs to revive and invest in the historical route, by developing realistic plans to invest in this historical

road. There is immense need to expand cooperation between universities, research centers, and heritage bodies in this field, both inside and outside Iraq, to undertake useful projects.

It is necessary to plan for the creation of a virtual museum that includes the main and secondary stations and landmarks of the route. At the same time, emphasis is placed on creating computer models of all buildings, ponds, and springs that mimic the original construction.

Tracing clear sections of the trail's path and accurately capturing the coordinates of these sections to create an accurate route for the main and secondary roads using geographic information systems and similar tools is highly felt.

Multispectral analysis is required, as it allows for distinguishing between different surface material, such as soil, stones, and water, thus facilitating the identification of ponds or ancient structures. Emphasis on drawing and producing interactive maps of the trail contributes to the creation of tourist itineraries. It encourages media professionals to prepare informative and cultural articles that inform decision-making and encourage decision-makers to pay attention to such heritage and cultural projects.

Given the extension of this historic road between Iraq and Saudi Arabia, it is necessary to cooperate between the two countries to establish a joint research center and conduct in-depth studies. It is also necessary to create a unified database between the Saudi and Iraqi sides for high-resolution satellite and aerial images and 3D digital maps, which are available to interested parties, graduate students, and researchers.

It is necessary to have an information database classified according to the writings of historians to facilitate the work of future researchers.

High-resolution satellite images are used to monitor the remains of the road extending across the desert, revealing patterns that may be hidden from the naked eye.

Recent space studies have revealed dozens of sites that were part of Zubaydah Trail, such as the remains of large pools and rest stops partially submerged in sand.

The importance of this approach lies in its blending of technology and heritage, enabling the rediscovery of ancient routes using modern tools. It also helps document landmarks before they disappear, contributes to promoting heritage tourism, and creates a scientific database for historians and archaeologists. Space tools have become a cornerstone for reviving Zubaydah Trail, not only as a pilgrimage route, but also as a model of an advanced civilization in urban planning and human exchange.

References

1. Sultan Naji, Al-Hirah-Makkah Road, Gulf and Arabian Peninsula Studies, Issue 15, pp. 27-47, https://journals.ku.edu.kw/jgaps/index.php/jgaps/issue/view/29
2. Muhammad Abdul-Ghani Al-Saidi, The Iraqi Hajj Route (Kufa – Mecca): Field Follow-up, Surveys, and Investigations, published October 8, 2018, https://alhikmeh.org/yanabeemag/?p=7592
3. Al-Rashed DR., "A study on the methods of pilgrimage in the past-7 main methods of pilgrimage and trade witnessed in the Arabian Peninsula", A daily newspaper issued by Al Jazeera Foundation for Press, Issue No:10382, Printing and Publishing Friday 2nd March, 2001, https://www.al-jazirah.com/2001/20010302/rk15.htm

4. Anthea Crane, " Surveying the Darb Zubaydah in Iraq", Endangered Archaeology in the Middle East and North Africa (EAMENA) , 17 May 2023, https://eamena.org/article/surveying-darb-zubaydah-iraq

5. Al-Rashid, S. A. 1977. A critical study of the pilgrim road between Kufa and Mecca (darb zubaydah) with the aid of fieldwork. PhD thesis, University of Leeds. https://etheses.whiterose.ac.uk/21108/, http://www.jstor.org/stable/41223199

6. The Desert Team, " The Iraqi section of the Zubaydah Trail (1): From Kufa to Al-Qura'a ", The Arabian Peninsula...its land and heritage...research, travels, and photos, Posted on July 4, 2022 https://alsahra.org/2022/07/%d8%a7%d9%84%d9%82%d8%b3%d9%85-%d8%a7%d9%84%d8%b9%d8%b1%d8%a7%d9%82%d9%8a-%d9%85%d9%86-%d8%af%d8%b1%d8%a8-%d8%b2%d8%a8%d9%8a%d8%af%d8-%a9-1%d9%85%d9%86-%d8%a7%d9%84%d9%83%d9%88%d9%81%d8%a9-%d8%a7/

7. The Desert Team, " Introduction to the Kufi Hajj Trail ,Darb Zubaydah, and its stations as enumerated by Judge Waki'", The Arabian Peninsula...its land and https://alsahra.org/2003/08/%d9%85%d9%86%d8%a7%d8%b2%d9%84-%d8%a7%d9%84%d8%b7%d8%b1%d9%8a%d9%82-%d8%b9%d9%84%d9%89-%d8%af%d8%b1%d8%a8-%d8%a7%d9%84%d8%ad%d8%ac-%d8%a7%d9%84%d9%83%d9%88%d9%81%d9%8a-%d9%83%d9%85%d8%a7-%d8%b9%d8%af/heritage...research, travels, and photos, Posted on August 19, 2003

8. The Desert Team, " Tag Archives: Kufi Hajj Trail ", The Arabian Peninsula...its land and heritage...research, travels, and photos, July 23, 2022, https://alsahra.org/category/%d8%af%d8%b1%d8%a8-%d8%b2%d8%

a8%d9%8a%d8%af%d8%a9/

9. The Desert Team, " The Iraqi section of the Zubaydah Trail (1): From Kufa to Al-Qura'a ", The Arabian Peninsula...its land and heritage...research, travels, and photos, Posted on July 4, 2022 https://alsahra.org/2022/07/%d8%a7%d9%84%d9%82%d8%b3%d9%85-%d8%a7%d9%84%d8%b9%d8%b1%d8%a7%d9%82%d9%8a-%d9%85%d9%86-%d8%af%d8%b1%d8%a8-%d8%b2%d8%a8%d9%8a%d8%af%d8-%a9-1%d9%85%d9%86-%d8%a7%d9%84%d9%83%d9%88%d9%81%d8%a9-%d8%a7/.The Desert Team, " The Iraqi section of the Zubaydah Trail (2): Waqisa-Aqaba ", The Arabian Peninsula...its land and heritage... research, travels, and photos, Posted on July 23, 2022, https://alsahra.org/2022/07/%d8%a7%d9%84%d9%82%d8%b3%d9%85-%d8%a7%d9%84%d8%b9%d8%b1%d8%a7%d9%82%d9%8a-%d9%85%d9%86-%d8%af%d8%b1%d8%a8-%d8%b2%d8%a8%d9%8a%d8%af%d8-%a9-2%d9%88%d8%a7%d9%82%d8%b5%d8%a9-%d8%a7%d9%84%d8%b9%d9%82/

10. The Desert Team, " The Iraqi section of the Zubaydah Trail (2): Waqisa-Aqaba ", The Arabian Peninsula...its land and heritage...research, travels, and photos, Posted on July 23, 2022, https://alsahra.org/2022/07/%d8%a7%d9%84%d9%82%d8%b3%d9%85-%d8%a7%d9%84%d8%b9%d8%b1%d8%a7%d9%82%d9%8a-%d9%85%d9%86-%d8%af%d8%b1%d8%a8-%d8%b2%d8%a8%d9%8a%d8%af%d8-%a9-2%d9%88%d8%a7%d9%82%d8%b5%d8%a9-%d8%a7%d9%84%d8%b9%d9%82/

11. The Desert Team, " The Kufi Hajj Trail " Zubaidah Trail " - 1: The Blind - The Bottom - Al-Haitham - Al-Jarisi - Zubalah ", The Arabian Peninsula...its land and heritage...research, travels, and photos, Posted on January 14, 2010, https://alsahra.org/2010/01/%d8%af%d8%b1%d8%a8-

%d8%a7%d9%84%d8%ad%d8%ac-%d8%a7%d9%84%d9%83%d9%88%d9%81%d9%8a-%d8%af%d8%b1%d8%a8-%d8%b2%d8%a8%d9%8a%d8%af%d8%a9-%d8%a7%d9%84%d8%b9%d9%85%d9%8a%d8%a7%d8%a1-%d8%a7%d9%84/

12. The Desert Team, " The Kufi Hajj Trail "Zubaidah Trail" - 1: The Blind - The Bottom - Al-Haitham - Al-Jarisi - Zubalah ", The Arabian Peninsula...its land and heritage...research, travels, and photos, Posted on January 14, 2010, https://alsahra.org/2010/01/%d8%af%d8%b1%d8%a8-%d8%a7%d9%84%d8%ad%d8%ac-%d8%a7%d9%84%d9%83%d9%88%d9%81%d9%8a-%d8%af%d8%b1%d8%a8-%d8%b2%d8%a8%d9%8a%d8%af%d8%a9-%d8%a7%d9%84%d8%b9%d9%85%d9%8a%d8%a7%d8%a1-%d8%a7%d9%84/

13. Anthea Crane, " Surveying the Darb Zubaydah in Iraq", Endangered Archaeology in the Middle East and North Africa (EAMENA) , 17 May 2023, https://eamena.org/article/surveying-darb-zubaydah-iraq

14. Al-Rashid, S. A. 1977. A critical study of the pilgrim road between Kufa and Mecca (darb zubaydah) with the aid of fieldwork. PhD thesis, University of Leeds. https://etheses.whiterose.ac.uk/21108/ , http://www.jstor.org/stable/41223199

15. Fareeq E. W. 2021. 'Overland Hajj Route Darb Zubayda'. Muslim Heritage. https://muslimheritage.com/darb-zubayda/

16. Sami ibn Abdullah al-Maghlouth, " Atlas of Hajj and Umrah: History and Jurisprudence",MapoftheZubaydahHajjRouteinpage101,Published2010 , https://waqfeya.net/books/%D8%A3%D8%B7%D9%84%D8%B3-%D8%A7%D9%84%D8%AD%D8%AC-%D9%88%D8%A7%D9%84%D8%B9%D9%85%D8%B1%D8%A9-%D8%AA%D8%A3%D8%B1%D9%8A%D8%AE%D

8%A7-%D9%88%D9%81%D9%82%D9%87%D8%A7-%D9%85%D9%84%D9%88%D9%86-96e5a77a49664918a326a-f3ee933e916

17. U.S. Geological Survey , Report of series number 202 chapter B "Geographic map of the Darb Zubaydah quadrangle, Kingdom of Saudi Arabia", DOI 10.3133/i202B, 1960 https://pubs.usgs.gov/publication/i202B , https://pubs.usgs.gov/imap/0202b/plate-1.pdf.Sheikh Saleh Al , Karbasi," What houses did al-Husayn pass through on his way to Karbala", slamic Radiation Center for Islamic Studies and Research, 2004 https://www.islam4u.com/ar/almojib/%D9%85%D8%A7-%D9%87%D9%8A-%D8%A7%D9%84%D9%85%D9%86%D8%A7%D8%B2%D9%84-%D8%A7%D9%84%D8%AA%D9%8A-%D9%85%D8%B1%D9%91%D9%8E-%D8%A8%D9%87%D8%A7--%D8%A7%D9%84%D8%AD%D8%B3%D9%8A%D9%86-%D8%B9%D9%84%D9%8A%D9%87-%D8%A7%D9%84%D8%B3%D9%91%D9%8E%D9%84%D8%A7%D9%85-%D9%81%D9%8A-%D8%B7%D8%B1%D9%8A%D9%82%D9%87-%D8%A5%D9-%84%D9%89-%D9%83%D8%B1%D8%A8%D9%84%D8%A7%D8%A1-%D8%9F#:~:text=%D8%A3%D9%85%D8%A7%20%D9%85%D8%AC%D9%85%D9%88%D8%B9%20%D8%A7%D9%84%D9%85%D9%86%D8%A7%D8%B2%D9%84%20%D8%A7%D9%84%D8%AA%D9%8A%20%D9%85%D8%B1%D9%8E%D9%91,%D8%A3%D8%B1%D8%A8%D8%B9%D9%8D%20%D9%88%20%D8%B9%D8%B4%D8%B1%D9%8A%D9%86%20%D9%85%D9%86%D8%B2%D9%84%D8%A7%D9%8B%20%D9%85%D9%86%D9%87%D8%A7%20.

18.

19. The Holy Shrine of Imam Hussein, “Learn about the houses where Imam Hussein stayed upon entering the Iraqi border...and the Holy Shrine of Imam Hussein seeks to turn them into shrines “.08/04/2017. https://imamhussain.org/15708,https://www.youtube.com/watch?v=K-fLlK2VN3mE

20. Labib Baydoun Dr., “Encyclopedia of Karbala, Part 1, Library of the Great Messenger, may God bless him and his family and the Ahl al-Bayt, peace be upon them, PP 537-545. https://alhassanain.org/arabic/?com=-book&id=1337.

21. Seyed Mahmoud Tabatabaei Nejad and Mohammad Ray Shahri, ”Encyclopedia of Imam al-Husayn (peace be upon him) in the book and the Sunnah and the history part 3”, 1969 https://hadith.net/ar/post/6849/%d9%85%d9%88%d8%b3%d9%88%d8%b9%d8%a9-%d8%a7%d9%84%d8%a7%d9%85%d8%a7%d9%85-%d8%a7%d9%84%d8%ad%d8%b3%d9%8a%d9%86-%d8%b9%d9%84%d9%8a%d9%87--%d8%a7%d9%84%d8%b3-%d9%84%d8%a7%d9%85-%d9%81%d9%8a-%d8%a7%d9%84%da%a9%d8%aa%d8%a7%d8%a8-%d9%88-%d8%a7%d9%84%d8%b3-%d9%86-%d8%a9-%d9%88-%d8%a7%d9%84%d8%aa/p306/

22. Sheikh Muhammad Sadiq Al-Karbasi, “ History of the Shrines of Al-Hussein, His Family, and His Supporters (Part Five), Publisher: The Husseini Center for Studies, London, United Kingdom, page 108, 2018 https://holykarbala.net/v2/index.php/ar/%D8%A7%D9%84%D9%85%D9%83%D8%AA%D8%A8%D8%A9-%D8%A7%D9%84%D8%A7%D8%B3%D9%84%D8%A7%D9%85%D9%8A%D8%A9/%D8%A7%D9%84%D8%AA%D8%A7%D8%B1%D9%8A%D8%AE/page/923#head1

23. Sheikh Saleh Al , Karbasi," What houses did al-Husayn pass through on his way to Karbala", slamic Radiation Center for Islamic Studies and Research, 2004 https://www.islam4u.com/ar/almojib/%D9%85%D8%A7-%D9%87%D9%8A-%D8%A7%D9%84%D9%85%D9%86%D8%A7%D8%B2%D9%84-%D8%A7%D9%84%D8%AA%D9%8A-%D9%85%D8%B1%D9%91%D9%8E-%D8%A8%D9%87%D8%A7--%D8%A7%D9%84%D8%AD%D8%B3%D9%8A%D9%86-%D8%B9%D9%84%D9%8A%D9%87-%D8%A7%D9%84%D8%B3%D9%91%D9%8E%D9%84%D8%A7%D9%85-%D9%81%D9%8A-%D8%B7%D8%B1%D9%8A%D9%82%D9%87-%D8%A5%D9%84%D9%89-%D9%83%D8%B1%D8%A8%D9%84%D8%A7%D8%A1-%D8%9F#:~:text=%D8%A3%D9%85%D8%A7%20%D9%85%D8%AC%D9%85%D9%88%D8%B9%20%D8%A7%D9%84%D9%85%D9%86%D8%A7%D8%B2%D9%84%20%D8%A7%D9%84%D8%AA%D9%8A%20%D9%85%D8%B1%D9%8E%D9%91,%D8%A3%D8%B1%D8%A8%D8%B9%D9%8D%20%D9%88%20%D8%B9%D8%B4%D8%B1%D9%8A%D9%86%20%D9%85%D9%86%D8%B2%D9%84%D8%A7%D9%8B%20%D9%85%D9%86%D9%87%D8%A7%20

24. Sabah Al-Talqani and Maitham Al-Husseini, " The Houses of Imam Hussein (peace be upon him) on his way from Mecca to Karbala", Karbala Now Agency,2022,https://karbala-intel.net/index.php/arabic/5460#gallery-2

25. Karbala Center for Studies and Research - Al-Hussain Holy Shrine, "Detailed map of the path of Imam Hussein (peace be upon him)", Privet communication.

26. Sabah Al-Talqani and Maitham Al-Husseini, " The Houses of Imam Hussein (peace be upon him) on hi way from Mecca to Karbala", Karbala

Now Agency, https://karbala-intel.net/index.php/arabic/5460#gallery-2

27. Karbala Center for Studies and Research - Al-Hussain Holy Shrine, "Detailed map of the path of Imam Hussein (peace be upon him)", Privet communication with Dr Al-Jwahiry 2025.

28. Yoshito Miyatsuiq and Yasuhiro Takahashi,"International Archives of Photogrammetry and Remote Sensing. Vol. XXXII, Part 5. Hakodate 1996. https://www.isprs.org/proceedings/XXXII/part5/592_XXXII-part5.pdf. Douglas C. Comer & Ronald G. Blom,"Detection and Identification of Archaeological Sites and Features Using Radar Data Acquired From Airborne Platforms" AIRSAR Earth Science and Applications Workshop.2002. https://airsar.jpl.nasa.gov/documents/workshop2002/papers/N1.pdf.

29. Derrold W. Holcomb, " Imaging Radar and Archaeological Survey: An Example from the Gobi Desert of Southern Mongolia", Journal of Field Archaeology, Vol. 28, No. 1/2 (Spring - Summer, 2001), pp. 131-141. https://www.jstor.org/stable/pdf/3181463.pdf.

30. Ahmed Faize , Gamil Alsharahi and Mohammed Hamdaoui, " Radar GPR Application to Explore and Study Archaeological Sites: Case Study ", (IJACSA) International Journal of Advanced Computer Science and Applications, Vol. 11, No. 5, 2020. https://thesai.org/Downloads/Volume11No5/Paper_26-Radar_GPR_Application_to_Explore_and_Study_Archaeological_Sites.pdf.

Appendix 1

Table 1: Stations (houses) and night rest areas (dinners) for Zubaydah Trail

House No. رقم المنزل	The House and coordinates المنزل واحداثياته	Diner place and coordinates المتعشى واحداثياته		
	The House	Coordinates	Diner place	Coordinates
1.	Kufa الكوفة	32.030000, 44.400000		
2.	Al-Qadisiyah القادسية Khan Al Rahbah خان الرحبة	31.785857, 44.367366 31.731091, 44.313900	Wadi Alsub-ae (Alsubae Valley) وادي السباع - ام القرون	31.537776, 44.229994
3.	Al-Mughitha المغيثة	31.355557, 44.134720	Masjid Saed (Saad Mosque) مسجد سعد	31.100557, 43.707843
4.	Al-Qura'a القرعاء	30.935278, 43.906390 Birkat at Talhat، بركة الطلحات	Al-Taraf الطرف	30.950248, 43.600156
5.	Waqisa واقصة	30.589142, 43.781561	Al-Qubaybat (The small Domes) القبيبات	30.369102, 43.658916
6.	Aqaba العقبة	30.140368, 43.620187 Al `Aqabah	Barakat Aleamya' (Aleamya' Pond) بركة العمياء	29.883342, 43.623801 Birkat al`Amya' 29.883500, 43.620282

7.	Al- Alqae القاع	9.760405, 43.630017 Bottom Station- 29.761737, 43.630693 بركة القصري، وبركة مجاورة 29.761183, 43.630486 بركة السهابية	Al-Juraisi الجريسي	29.605532, 43.603611
8.	Zubalah زُبالة	29.397341, 43.563984 بركة زبالا, Zibala bond 29.263804, 43.535397 بركة القيصوم "الرضم"	Al-Tananir التنانير	بركة الجميماء،
9.	Al-Shuqooq (Al-Shihiyat) (الشقوق (الشيحيات	29.094397, 43.473515 بركة الشيحيات	Al- Alqae القاع	28.933985, 43.383454 بركة الشيحة 28.927812, 43.380656 بريد طريق زبيدة التاريخي او علم طريق
10.	Bitan (Aleashar) بِطان (العشار)	28.460446, 43.315562 آبار زبيدة، برك زبيدة, 28.512814, 43.353555 منطقة آثار- درب زبيدة, 28.462643, 43.316357 Baqaa, Saudi Arabia 28.465550, 43.311956 Birak al `Ara'ish,	Altanahi التناهي	

11.	Althaelabia (albidae) الثعلبية (البدع)	28.223644, 43.239642 (محطة الثعلبية (البدع, 28.223665, 43.239647 (محطة الثعلبية (البدع، 28.273483, 43.240214 بئر الثعلبية - درب زبيدة،		
12.	Alkhazimat and zarud الخزيمة و زرود	27.827586, 43.198960 زرو، 27.827527, 43.199079 بئر زرود (الخزيمية) وفيها 27.827529, 43.199059 - (بئر زرود (الخزيمية 27.831937, 43.190837 Bi'r al زرود	Barakat khalisa بركة خالصة	
13.	Al'ajfar الأجفر	27.152875, 42.465289 الساقية، 27.502772, 43.001035 بركة زبيدة بالأجفر، 27.487421, 42.993525 - بركة الأجفر الجنوبية 27.531434, 43.028327 رصيف خالصة - درب زبيدة، الأجفر	Alsaaqiat , Alqarayin الساقية ، القرائن	
14.	Fid فيد	27.101913,42.523770 بركة فيد - درب زبيدة, 27.020513, 42.500253 جبل أم هروج,	Abar am huruj , birak alghari-bat ابار ام هروج ، برك الغريبات	

15.	Tawz توز وهي نصف الطريق	26.600917, 42.184032 بركة الجفالية / الحمة / - فرفرة 26.597832, 42.185589 "جبل الحمه "الفحيمة	Barakat Aleanaabat - arinbat, barakat alhimat – alja-falia بركة العنابة - ارينبات، بركة الحمة - الجفالية	29.761183, 43.630486
16.	Samira سميراء	26.650827, 42.234118 ,المذيريبات	Al- Alqae	بركة السهابية
17.	Alhajir الحاجر	26.012593, 41.835998 Al-Sulaimi, Saudi Arabia بركة البعايث / الحاجر	Qiruri, alhima قروري، الحمة منه بتفرع الى فرعين	القاع
18.	Maedin Alqurashi (Now Aalnaqrat) الفرع الأول : معدن القرشي وهي النقرة الآن		.	
19.	Alnaqrat (Now Aljafniat) منزل الفرع الثاني: النقرة قديما وهي الجفنية الان		The two branches meet at the diner's location	
20.	Mughithat Al-mawan (Alsaqa-ea') مغيثة الماوان وهي الصقعاء محطة مغيثة الماوان	25.024591, 41.428366	'Arimat - Snam أريمة -سنام	23.650061, 44.750678 سنام

21.	Alrabidha (It is 2/3 the road) الربذة	24.631839, 41.292359 - بركة الربذة الجنوبية	Alruwtha (Al-kanas((الروثة (الكناس	24.517635, 41.239546 حجر الكِناس
22.	Alsalila السليلة بركة السليلة ،التاريخية	24.241411, 41.088804	Daba ضبة	24.050315, 41.037810 بركة الضبة
23.	Aleumq العمق	23.943822, 40.978740 بير، العمق 23.943351, 40.974840 ،بير الربعانيه 23.846859, 40.960349 ،مقيل زبيدة - درب زبيدة	Sharuraa شرورى	23.846957, 40.960249 Zubaydah Trail, Omaq 23.852629, 40.912163 Al Mahd, Saudi Arabia جبل صايد
24.	Almaedin المعدن	23.858710, 40.964209	Karae كراع	23.803097, 40.958053
25.		Alkabwana الكبوانة	22.825471, 40.825236 المويه 22.834371, 40.787643 المهد 22.801736, 40.797771 المهد	
26.	Almusalah المسلح خبراء الحاج	22.682792, 40.784790	Alqasr القصر بركة العموسى	22.673071, 40.784360

27.	Alghamra الغمرة بركة الغمير	21.830152, 40.354527	Awtasاوطاس بركة أوطاس	22.056539, 40.615327
28.	Dhat Earq Water Well (Built by Zubai-yda binte Jaffer ذات عرق	21.929324, 40.425690	Ghamar Dhi Kanda غمر ذي كندة	21.830180, 40.354541
29.	Albustan البستان		Mashash مشاش	20.313481, 40.981397
30	مكة المكرمة			

2 Appendix

Table 2 :The sequence of stations that the caravan of Imam Al-Hussein passed through, according to what was achieved by Al-Karbasi [24], and the goals were extracted by the authors from Google Maps.

S	Stations in sequence [5]	Station and coordinates from googl map	Station and what follows	distance (km)
1	مكة	Mecca 21.426022, 39.826264	.	
2	التنعيم	At-Tan'im 21.467843, 39.796459	Mecca - At-Taneem	8
3	الصفاح	As-Saffah 21.470160, 40.039296 Located between Hunayn 21.472506, 40.052063 And Mon-uments of the Sacred of Mecca 21.484424, 39.941328	At-Taneem - As-Saffah	9
4	زيمة	Zima	As-Saffah – Zimah	36

5	ذات عرق	Dhat Irq 21.929352, 40.425680	Zima - That Irq	41
6	غمرة	Ghamra 22.186395, 40.727262	That Irq – Ghamrah	36
7	المسلح	Al-Musallah 22.490208, 40.750269	Ghamrah - Al-Musallam	24
8	بئر ماء	Water Well 21.467042, 40.110964	Al-Musallam - Water Well	78
9	سليلة	Suleila 24.243668, 41.089224 Nearby are wells 24.241411, 41.088804	Water Well – Sulaylah	120
10	المغيثة	Al-Mughitha 25.024591, 41.428366	Sulaylah - Al-Mughithah	144
11	النقرة	Al-Naqra 25.591297, 41.446535	Al-Mughitha - An-Naqrah	30
12	الحاجر	Al-Hajr 25.964575, 41.921068	An-Naqrah - Al-Hajr	60
13	سميراء	Samira 26.456489, 42.096905	Al-Hajr – Samira	54
14	التوز	Al-Tawz 26.600874, 42.184112	Samira - At-Tawz	30
15	الفيد	Al-Fayd 27.120519, 42.521674	At-Tawz - Al-Fayd	66
16	الاجفر	Al-Ajfar 27.502304, 43.000814 الاجفر الجنوبية (27.482984, 42.997233	Al-Fayd - Al-Ajfar	42
17	الخزيمة	Al- Khuzaymiyah 27.831901, 43.190965	Al-Ajfar - Al-Khazimah	36
18	الزرود	Al-Z arud 27.827506, 43.199024	Al-Khazimah - Al-Zurud	18
19	سُوقة	Souqah	Al-Zurud – Suqah	18

20	الثعلبية	Al-Tha'labiyah 28.273378, 43.240336	Suqah - Al-Tha'labiyyah	30
21	الشقوق	Al-Shuqooq	Al-Tha'labiyyah - Al-Shuqooq	66
22	زبالة	Zubalah 29.395870, 43.565750	Al-Shuqooq – Zabalah	66
23	القاع	Al-Qaa	Zabala - Al-Qa'a	42
24	بطن العقبة	Batn Al-'Aqaba 30.140862, 43.622406	Al-Qa'a - Batn Al-'Aqa-ba	48
25	واقصة	Waqisa 30.580807, 43.766707 or 30.588751, 43.781079	Batan Al-'Aqaba – Waqisas	42
26	شراف	Sharraf 30.620774, 43.751408	Waqisas – Sharaf	18
27	القرعاء	Al-Qar'aa 30.935294, 43.906414	Sharraf - Al-Qura'a	18
28	المُغيثة	Al-Mughitha 31.356179, 44.135918	Al-Qura'a - Al-Mughitha	66
29	بيْضَة	Baydah 43.716623 ,30.786551)ذو حُسَم)	Al-Mughitha – Bayda	18
30	عذيب الهجانات	Udheeb Al-Hijanat 31.613455, 44.376484	Bayda - Udhaib Al-Hi-janat	24
31	الرُهَيْمَة	Al-Ruhaymah 32.234826, 44.098656	Udhaib Al-Hijanat - Al-Ruhaymah	30
32	قَصْرُ بني مُقَاتِل	Qasr Bani Muqatil 32.355994, 44.011881	Al-Ruhaymah - Qasr Bani Muqatil	18
33	القَطْقَطانة	Al-Qatqatanah 32.030901, 43.925578	Qasr Bani Muqatil - Al-Qatqatanah	42
34	نينوى	Nineveh 32.616376, 44.0326	Al-Qatqatanah – Nineveh	24
35	الطف	Al-Taf 32.616376, 44.032617	Nineveh - Al-Taf	1

The influence of environmental conditions and human congregation on the immune system response: systematic review article

Asst. Prof. Dr. Wasan adai Al-Marsoumi

University of Baghdad, College of Science for Women, Department of Biology – Iraq

wasan.a@csw.uobaghdad.edu.iq

Abstract

The immune system protects the human body from disease through several lines of defense, each with its own specificity. Physical barriers, such as the skin, prevent pathogens such as bacteria, viruses and parasites from entering the body. If a pathogen breaches these barriers, the innate immune system responds immediately, but in a non-specific manner. When a pathogen successfully evades the innate immune response, vertebrates have a second line of defense: the adaptive immune system (specific), activated by the innate immune response, the immune system adapts its response during infection to improve pathogen recognition.

Human immune responses can change depending on environmental conditions, so many environmental factors influence the Arbaeen march (the focus of our study), which is the fortieth day after the martyrdom of Imam Hussein (peace be upon him). Arbaeen is considered one of the largest gatherings of human beings in the world. It is a great, authentic, and deeply rooted movement, bringing together millions of Muslims from all over the world annually, regardless of their nationalities, colors and languages.

Therefore, the scarcity of rest areas, the varying outdoor air quality, and the varying temperatures coincide with the visiting season. However, not all visitors are affected by most environmental factors, as the feeling of comfort in performing these religious rituals supports the immune system, and thus supports better health for the individual (visitor). This study aims to comprehend the influence of environmental agents and interpret the immune responses of visitors of both genders and different ages.

Key word:Immune system, arbaeen march , Human Gatherings, Environmental Conditions.

Introduction

The immune system consists of a complex and integrated network of tissues, organs and molecules that act together to protect the body from pathogens such as bacteria, viruses, parasites and cancer cells. So, the main components of the immune system are the physical barriers, which include the skin, mucous membranes, and body fluids. The other part includes immune cells (white blood cells), which are produced in the bone marrow (Wang et al., 2024). These include lymphocytes (T and B cells), killer cells and phagocytes (including neutrophils, monocytes, macrophages and dendritic cells), among others. All of these components work in coordination with each other to ensure an effective immune response against various threats. The human body consists of about 2 trillion lymphocytes, which constitute between 20% and 40% of white blood cells (Vaillant et al., 2024).

B cells and T cells arise from the same multipotent hematopoietic stem cells, which remain indistinguishable from each other until activated. B cells play a major role in the humoral immune response, while T cells primarily influence cell-mediated immune responses. Adaptive immunity relies on the ability of immune cells to distinguish between the body's own cells and any unwanted foreign bodies or organisms that invade the immune system (Elena et al., 2013).

External environmental conditions are a set of factors and forces that exist in the external environment, they are a set of physical, chemical, and biological factors that surround individuals and influence their interaction with each other and with the environment (Vantourout and Hayday., 2013). These factors determine the nature of any ecosystem and affect the behavior and performance of the individuals who can live in it. Environmental conditions greatly affect the human immune system, either by strengthening or weakening it. This complex interaction determines the body's susceptibility to diseases and injuries and how it responds to them (Sundas et al., 2024).

Types of environmental Elements

The concept of the environment refers to its natural components and the conditions and factors in which living organisms live. It is the science that studies the relationship between living organisms and the environment in which they live. This science is concerned with living organisms, their nutrition, their ways of life, and their presence in the study of non-living factors such as communities, population centers, or peoples (Andersen et al., 2021). It also includes the characteristics of climate (temperature, humidity, radiation, water and air gases), and the physical and chemical properties of the soil, water and air (Abdul Kari., 2025).The environment element can be divided into three components: (Gupta., 2025).

- First:The natural environment: This is the atmosphere, which consists of four closely interconnected systems: the hydrosphere, the terrestrial environment, and the atmosphere. These systems include water, air, soil, minerals, and energy sources, in addition to plants and animals. These all represent the resources that God Almighty has provided for humans to obtain the necessities of life, including food, clothing, medicine, and shelter.
- Second:The biological environment: This includes the individual human being, his family, and his community, as well as the living organisms in the biosphere. The biological environment is considered part of the natural environment.
- Third:The social environment: The social environment refers to the framework of relationships that determines the relationship between humans and others. This framework of relationships is the basis for organizing any group, whether among its individuals in a given environment, or among diverse groups and civilizations in distant environments. The patterns of these relationships constitute what are known as social systems (Ofremu et al., 2025).

The immune system

The immune system is a system specialized in defending the body against foreign agents or dangerous invading agents, the immune system, such as any other system in the body, consists of organs and cells (Zhou et al., 2025).The organs of the immune system are divided into two main groups: primary lymphoid organs, whose function is to produce different immune cells, represented by the bone marrow, or to educate immune cells after they are produced to distinguish between self and non-self-cells, appeared by the thymus gland (Delves et al., 2024). There are secondary lymphoid organs, which include the spleen and lymph nodes. As for the cells of the immune system, they are divided into two main groups: granular cells, which include neutrophils, eosinophil's and basophils, and a group of non-granular cells, which includes types of T cells, B cells, killer cells, monocytes, and macrophages, lymphocytes are considered the most important and are the backbone of the immune system (Patel ., 2025).

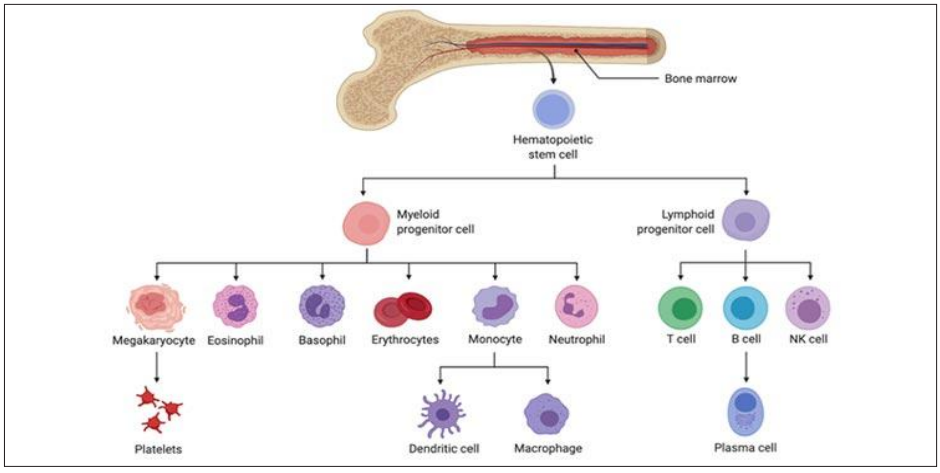

Figure (1) the source of blood cells production

Components of the Immune System

1. Antigens: An antigen refers to a foreign substance that enters the body. It can be a protein, glycoprotein, virus, bacteria, parasite, or other substance. These substances are chemically distinct and have the ability to stimulate the body's immune system to produce antibodies that trigger a specific immune response (Chaplin., 2010). These antigens are called immunogens because the body responds to them upon recognition with an immune reaction, which is the formation of antibodies, antigens have certain distinctive properties that give them immunogenicity, antigens are molecules that interact with antibodies, while immunogens are molecules that stimulate an immune response (Humphrey and Perdue., 2025).

2. Epitope: or antigenic determinants, which is a small, specific part of the antigen, which usually consists of 4-6 amino acids or sugar groups, that determines the immune reaction, i.e. it is the site of binding of the antigen to its antibody (Kringelum et al., 2012).

3. Antibodies: Chemically, antibodies are glycoproteins dissolved in blood plasma called immunoglobulins. They are produced by plasma cells, which originally from B lymphocytes, and are secreted by the body as a specific response to the presence of antigens (humoral immunity) (Patel et al., 2023).These immunoglobulins contain components capable of reacting specifically with the specific antigens that led to their formation. Antibodies are divided into five main categories (immunoglobulins): G, M, A, D, and E, with IgG representing the largest group (Vaschetto., 2025).

The Arbaeen march

The Arbaeen march : It is a sacred ritual through which individuals (visitors) visit the grave of Imam Hussein, peace be upon him, from all parts of the country and even from remote countries and distant regions. Since the martyrdom of Imam Hussein, peace be upon him, the visitors have been keen to make the connection vibrant, alive and continuous btween them and Karbala. It is a procession during which millions of Muslims set out towards Karbala to visit Hussein bin Ali bin Abi Talib on the twentieth of Safar every year, 40 days after the Karbala incident in which Hussein bin Ali was killed (Aboud., 2024).

Among the most important rituals and ceremonies of the Arbaeen march practiced by visitors are walking long distances to Karbala, holding mourning gatherings, offering food and drinks to visitors, reciting prayers, and making special visits to Imam Hussein and his family. One of the most prominent rituals is the walk to Karbala. So, walking to Karbala is considered one of the most prominent aspects of the march , as millions of visitors from various cities and countries head on foot to the shrines of Imam Hussein and his brother Abbas. Among the etiquettes of the Arbaeen visit are speaking to people in a good way and refraining from idle talk and foul language. Avoiding eating while walking, but rather sitting, and not wasting food. Walking with calmness and dignity. Engaging in verbal supplications such as seeking forgiveness, saying “There is no god but Allah,” and sending blessings upon Muhammad and his family.

So the most important etiquette can be summarized of visiting Imam Husein (peace be upon him) are the following: First: Consideration attention to purity, a good appearance, tranquility and dignity. Second: Show a sense of sadness and melancholy. Third: Consolation in times of hunger and thirst. Fourth: Visit Imam Hussein (peace be upon him) out of longing for him and love for the Prophet and his family (peace be upon them). Fifth: Visit Imam Hussein (peace be upon him) with true knowledge of his religion.

Statistics the total number visitors of Arbaeen march and pilgrims

”The Arbaeen march is the largest human gathering in the world, regardless of color ,race ,or language ,as they see in Hussein) peace be upon him (the entire universe ,a symbol of freedom and great sacrifice“. This historical miracle that occurs every year leaves behind a global astonishment at the scene that is not repeated at other times of the year. What is even more amazing is that people from different European and American countries head to the city of Karbala to experience the scene up close .It is an amazing thing ,as adults ,children ,and even people with special needs who cannot walk flock to this city ,indifferent to the security conditions and other things .What is important to them is reaching Imam Hussein) peace be upon him .(Several foreign newspapers wrote about how a small city like Karbala can accommodate all these numbers of people in such conditions “,stressing at the same time” :It is truly a miracle because approximately (20) million people enter this city in a few days ,and food is provided to them in such abundance and variety ,along with the rest of the requirements such as housing ,transportation ,and the like .All of this requires money ,and Iraq is going through an economic crisis .It is truly a miracle ,so it was included “.The visit is in the encyclopedia of world records and in several categories ,including :the largest human gathering, the longest dining table in the world ,the largest number of volunteers at a single event ,etc .There are some statistics related to the human gatherings during the Arbaeen visitors as follow:

Table (1) demonstrated total number of Arbaeen visitors and the pilgrims

No.	Year	Total number of Arbaeen visitors	Total number of pilgrims
1	2016	30 million	1, 862, 909
2	2017	13.8 million	2, 352, 122
3	2018	20 million	2, 371, 675
4	2019	< 15 million	2, 489, 406
5	2020	few	10000
6	2021	few	60000
7	2022	21,198,640 milion	899, 353
8	2023	< 22 million	1,845, 045
6	2024	< 22 million	1, 833, 164

The number of visitors (in table 1) to the Arbaeen march has reached millions over the years alone, although the number decreased in 2020 and 2021 due to the Corona pandemic. It is considered the largest human gathering in history compared to other human gatherings that include Hajj. This may be due to the facilities provided by visitors in all details, or it may also be due to the influx of visitors from several other countries to revive these sacred religious rituals. So, these numbers are evidence of the religious and spiritual significance of the Arbaeen march and its significant impact on the region.

The differences of immune responses between different age groups and the gender

The immune response varies across age groups depending on several factors, including the age group (months to 1 year). Their immunity is weak due to the incomplete development of the immune system before the age of one year. The body relies on antibodies received from the mother (passive immunity). Therefore, they are highly susceptible to bacterial, parasitic, or viral infections, especially in crowded areas, including the Arbaeen pilgrimage. Therefore, it is recommended not to bring children of this age with them (Simon et al., 2025). (1 - 18 year) , their immune systems may be more developed, as B and T cells are better formed and they acquire immunological memory due to their exposure to diseases and vaccinations, which enable the body to develop strong immunity against many diseases common in these communities, such as measles, mumps, and influenza (Pollard and Bijker., 2021).

As for those aged (18 - 65), these age groups possess strong and effective immune systems and have extensive immunological memory from previous exposure to diseases. However, their immune system may be affected by certain lifestyle factors, depending on the nature of their work and social activities. These factors, such as stress, poor nutrition, lack of sleep, and smoking, can affect the strength of the immune system. However, this does not occur when performing religious rituals, as they perform them with comfort and reassurance (Nguyen et al.,2025).

As for the elderly (over 65 years old), their immune system may suf fer from a gradual decline with age, known as immunosenescence. This is due to a decline in innate and adaptive immunity, as the number and function of various immune cells (such as neutrophils, monocytes, macro phages, T cells, and B cells) change. This makes them more susceptible to

infection, and diseases are more severe, leading to serious complications. Furthermore, most of these people have chronic diseases such as diabetes, heart disease, and kidney disease, which further weaken their immune systems and make them more susceptible to complications in such human populations (Goyani et al., 2024). In the conclusion, these populations pose different immune challenges to each age group, necessitating preventive strategies and health interventions tailored to each group.

As for gender, several studies have shown clear differences in the im mune responses between males and females. These are represented by some the factors:

1. Sex hormones: Females have two hormones (estrogen and progesterone), which make them exhibit stronger immunity, whether at the level of in nate or adaptive (cellular and humoral) immunity. Estrogen is believed to enhance immune responses, which in turn leads to faster clearance of pathogens. However, it also increases susceptibility to autoimmune diseases and infections. It is estimated that more than 80% of those with autoimmune diseases are women(Sciarra et al., 2023).

While for the males, testosterone generally acts as an immunosup pressant. Testosterone can also reduce the production of pro-inflamma tory cytokines and affect the differentiation of helper T cells, the pro duction of immunoglobulins (antibodies), and the activity of killer cells. This inhibition explains the reason for the increase. Males are more sus ceptible to certain infections and disease severity than females, which may increase in such large populations, with lower rates of autoimmune diseases (Batalla et al., 2020).

2. Sex chromosomes: Females carry the XX chromosome, while males carry the XY chromosome. Females have an extra X chromosome, which carries a number of immunity-related genes, unlike males, thet carry Y chromo some, which contains fewer immunity-related genes (Roman et al., 2024).

3. Differences in innate and adaptive immune responses: Females gener ally exhibit higher activity in innate immune cells, such as monocytes, macrophages, and dendritic cells, and their antigen-presenting cells are more efficient. Conversely, females may have lower activity in natural killer cells compared to males. As for adaptive immunity, females pro duce higher levels of antibodies that protect against antigens, along with increased lymphocyte proliferation and activation and production of pro-inflammatory cytokines. Males, on the other hand, possess a more expanded subset of regulatory cells than females (Dash et al., 2024).

4. The final factor is age. Sexual immunological differences change with age. Males may exhibit more severe immune changes with aging, lead ing to an increased risk of certain diseases (Calabrò et al., 2023).

Furthermore, these immunological differences explain the disparity in in fection rates and disease severity between males and females, which rquires more specific treatments in such populations based on biological sex.

The relationship between environmental conditions and the immune system

The immune system is a complex network that protects the body from harmful pathogens, such as viruses, bacteria and fungi from various internal and external factors, including seasonal changes, strengthen or weaken our immune defenses. External environmental conditions significantly in flence the Arbaeen visitors, including climate, terrain and disease prevalence, as well as social and economic factors that impact visitor flow and safety (Marshall et al., 2018). Environmental impacts include: Climate: The Arbaeen march often experiences high temperatures and humidity, which can lead to sunstroke and heat exhaustion among visitors, especially the elderly and children. Terrain: Some trails may be rough and unpaved, increasing the risk of falls and injuries, especially with large numbers of pedestrians. Diseases: The spread of infectious diseases, such as influenza and diarrhea, may pose a risk to visitors' health, especially with crowding and large gatherings. While the social and economic factors involve population Influx: significantly increasing visitor numbers may place pressure on infrastructure and available resources, such as water and sanitation. Pollution: Increased waste and environmental pollution may negatively impact air and water quality, threatening visitors' health. Security: Security threats may pose a challenge to the visitors, especially with large numbers of persons, requiring enhanced security measures (Li and Wu ., 2021).

Whilst the impacts on the visitors: as harms and diseases: Harsh environmental conditions may lead to increased rates of injury and illness among visitors, which may hinder their enjoyment of the march and logistical difficulties, so, organizing agencies may face difficulty providing basic services, such as water, food and first aid, due to the large number of visitors and environmental conditions, as well as, psychological Impacts:

some visitors may feel anxious and stressed due to the difficult conditions, which may affect their spiritual experience (Najafi et al., 2022). Therefore, the proposed solutions: include awareness: visitors must be made aware of the dangers of environmental conditions and the need to take necessary precautions and provide Infrastructure, sanitation facilities, potable water, and appropriate shelters must be provided for visitors. as well as provide medical services, emergency the services must be provided along visitor routes and coordination with security authorities, coordination with security authorities must be undertaken to provide a safe environment for visitors , and last pollution reduction, measures must be taken to reduce environmental pollution and maintain a clean environment (Keng et al., 2013).

Despite all the conditions and factors mentioned above, which most Arbaeen visitors may encounter, many of them are not affected by them. This is because when a person is pleased, reassured, or proud of the work they are doing, their immune system can respond positively by increasing its activity and strengthening its defenses against disease. Relaxation contributes to the secretion of chemicals in the body that enhance the functions of the immune system, such as dopamine, which plays a role in enhancing feelings of happiness and strengthening the functions of the immune system, performing these rituals also leads to reducing stress and anxiety, which reduces the secretion of stress hormones that can weaken the immune system (Agahtani et al., 2022). Some studies indicate that a positive psychological state can enhance the immune system's ability to fight diseases and infections. Levels of stress hormones such as cortisol and adrenaline are reduced, allowing the immune system to function efficiently. There is a definite link between the activity and health of the immune system and a person's psychological state and mood (George ., 2024). There are several ways for the immune and nervous systems to communicate. One of

these is through the release of cytokines, a type of protein secreted by the immune system in cases of illness, infection, anxiety, or any stimuli that stimulate an immune response (Al-Marsomy et al., 2020). The relationship between the two systems lies in the transport of cytokines to the brain and their impact on the neurotransmitters that control mood and mental health. This leads to disruptions in serotonin, dopamine, oxytocin and glutamate levels, thereby increasing the risk of developing mental illnesses such as depression, anxiety (Coffey et al., 2021).

One of the most important components that strengthens the immune system and thus helps it withstand adverse conditions is eating a healthy, varied, and balanced diet, including vegetables, fruits, proteins, starches, legumes, and good fats. This diet is available throughout the Arbaeen march , ensuring the body receives all the vitamins, minerals, and other beneficial elements it needs (Tardy et al., 2020).Another factor is exercising, which in turn stimulates blood circulation, helping immune system cells move more quickly throughout the body. Visitors who walk to visit the Imam can do this, which can take two weeks or more for some visitors from provinces far from Karbala. Another factor is drinking sufficient amounts of water, which is a key factor in the immune system's activity. This is because lymph, the fluid that transports immune system cells throughout the body, contains a large amount of water. Walking long distances makes people thirsty and dehydrated, so drinking sufficient amounts of water strengthens the immune system for both sexes and all various ages (Watso and Farquhar., 2019). Another factor is avoiding prohibited substances such as analgesic and smoking, which can increase stress and tension due to their nicotine content, that weakens the immune system, which all visitors stay away from, especially on visiting days, staying evade them strengthens people's immunity. The most important and final factor is that helping

others and providing services to all visitors enhances positive energy and reduces psychological stress (Chang et al., 2024). Therefore, all of these factors, lead to enhanced immune system activity and resistance to all environmental factors that may affect when exposed it in other conditions.

Conclusion

The conclusion from the presented study that there are many common environmental factors affecting visitors are harsh climatic conditions such as heat and dust. So, The Arbaeen visit in the summer season may coincide with high temperatures, which can lead to sunstroke and dehydration. There is a risk of disease spreading, as crowding and congested conditions are ideal circumstanceses for the spread of infectious diseases. Physical and psychological stress also increases by the long distances that visitors walk, along with lack of sleep and fatigue, all weaken the immune system. However, in addition to all the environmental factors that affect visitors, the immune system may resist these factors due to: enhance the function and activity of the immune system, because the feeling of comfort and reassurance when performing the holy ritual (the Arbaeen march), and the high level of hormones of satisfaction and cheerfulness, in addition to eating various healthy foods and walking long distances, all of which support the immune system to resist the most external environmental conditions that visitors are exposed to in the various seasons that coincide with the date of this holy ritual, for both sexes and all different ages, with slight variations between one age group and another.

References

1. Wang R., Lan C., Benlagha K., Camara N., Miller H., Kubo M., Heegaard S., Lee P., Yang L., Forsman H., Li X., Zhai Z. and Liu C. (2024). The interaction of innate immune and adaptive immune system., Med Comm journal., 5(10).
2. Vaillant J ., Sabir S. and Jan A. (2024). Physiology, Immune Response., National Library of Medicine., July , 27 .
3. Elena R., Cano H. and Damaris E.(2013). Introduction to T and B lymphocytes., Chapter 5.
4. Vantourout P. and Hayday A. (2013). Six-of-the-best: unique contributions of gammadelta T cells to immunology. Nat Rev Immunol., 13:88–100. [PMC free article] [PubMed].
5. Sundas A., Contreras I., Mujahid O., Beneyto A. and Vehi J. (2024). The Effects of Environmental Factors on General Human Health: A Scoping Review., Healthcare., 12(21).
6. Abdul Kari Z. (2025). Abiotic and biotic factors affecting the immune system of aquatic species: A review., Comparative Immunology Reports., 9.
7. Andersen L., Corazon S. and Stigsdotter U. (2021). Nature Exposure and Its Effects on Immune System Functioning: A Systematic Review., International Journal of Environmental Research and Public Health., 18(4).
8. Gupta S. (2025). Components of Environment: Biotic and Abiotic Components., Study IQ India. June , 14.
9. Ofremu G., Raimi B., Yusuf S., Dziwornu B., Nnabuife S., Eze A. and Nnajiofor Ch. (2025). Exploring the relationship between climate change, air pollutants and human health: Impacts, adaptation, and mitigation strategies., Green Energy and Resources., 3(2).
10. Delves P., (2024). Overview of the Immune System., MSD Manual Consumer Version., March , 2024.

11. Zhou x., , Wu Y., ,Zhu Z., , Lu Ch., Zhang Ch., Zeng L, Xie F, Zhang L. and Zhou F. (2025). Mucosal immune response in biology, disease prevention and treatment. Signal Transduction and Targeted Therapy. 10(7).

12. Patel H., (2025). White Blood Cells – Summary., Immunology and Haematology., June., 17.

13. Chaplin D., (2010). Overview of the Immune Response., Journal Allergy Clinical Immunology., 125 (2 supplement).

14. Humphrey J. and Perdue S. (2025). antige in immunological system., Britannica., May., 30.

15. Kringelum J., Nielsen M., Padkjær S. and Lund O. (2012). Structural analysis of B-cell epitopes in antibody:protein complexes., Molcular Immunology., 10(53).

16. Patel P., Jamal Z. and Ramphul K. (2023). Immunoglobulin., National Library of Medicine August., 28.

17. Vaschetto L. (2025). Antibodies: Structure, Types, and Therapeutic Roles., Medical life Science., February., 3.

18. Aboud M. H. (2024). The Arbaeen Pilgrimage: A Miniature Model of the State of Imam Mahdi (May Allah Hasten His Reappearance)., College of Islamic Science., December., 30.

19. Al Muntazar. (2025). Etiquette Of Mourning For Imam Husain.,June., 4.

20. Simon A., Hollander G. and McMichael A. (2015). Evolution of the immune system in humans from infancy to old age., The royal Society Publishing., 22:282.

21. Pollard A. and Bijker E. (2021). guide to vaccinology: from basic principles to new developments., Nature Reviews Immunology ., 21.

22. Nguyen K., Le N., Nguyen P., Nguyen H.,Hoang D. and Huynh Ch. (2025). hman immune system: Exploring diversity across individuals and populations., Heliyon., 11(2).

23. Goyani P., Christodoulou R. and Vassiliou E. (2024).Immunosenescence: Aging and Immune System Decline., Vaccines (Basel)., 12(12).

24. Sciarra F., Campolo F., Franceschini E., Carlomagno F. and Venneri M. (2023). Gender-Specific Impact of Sex Hormones on the Immune System., International journal of molecular sciences., 24(7).

25. Batalla I., Delgado M., Amsberg G., Janning M. and LOges S. (2020). Influence of Androgens on Immunity to Self and Foreign: Effects on Immunity and Cancer., Frontiers in immunology. 11.

26. Roman A., Skaletsky H., Godfrey A.,Bokil., Teitz L., Isani Singh I., Laura V. Blanton L. et al., (2024). The human Y and inactive X chromosomes similarly modulate autosomal gene expression., Cell Genomics., 4(1).

27. Dash Sh., Gupta S. and Sarangi P.(2024). Monocytes and macrophages: Origin, homing, differentiation, and functionality during inflammation., Heliyon., 10(8).

28. Calabrò A., Accardi G., Aiello A., Caruso C. and Candore G. (2023).Sex and gender affect immune aging., Frontiers in aging., 28(4).

29. Marshall J., Warrington R., Watson W. and Kim H. (2018). An introduction to immunology and immunopathology., Springer Nature., 14 (2 supplement).

30. Li D. and Wu M. (2021). Pattern recognition receptors in health and diseases., Signal Transduction and Targeted Therapy. 6(291).

31. Najafi K., Khoshab H., Rahimi N. and Jahanara A. (2022). Relationship between spiritual health with stress, anxiety and depression in patients with chronic diseases., International Journal of Africa Nursing Sciences., 17.

32. Keng Sh., Smoski M., Robins C. (2013). Effects of Mindfulness on Psychological Health: A Review of Empirical Studies., Clinical Psychological Health., June ., 11.

33. Agahtani F., Alasif B., Ahmed A., Ali A., Sofian T., Obeidat R., Mohamed F., Gul L., and Hassan S. (2022). Using Spiritual Connections to Cope With Stress and Anxiety During the Covid-19 pandemic. Sec. Health Psycjology., 13., July., 28.

34. George E. (2024). Psychological Effects of Stress., Metnta Health., May .,31.

35. Al-Marsomy W., Mohammed S. and Almohaidi,A. (2020). Immunological comparison for sHLA-G and some receptors in Iraq patients with sterile and fertile Echinococus granulosus," in 1st International Conference on Pure Science (ISCPS-2020), Najaf.

36. Coffey Y., Bhullar N., Durkin J., Islam M. and Usher K.(2021). Understanding Eco-anxiety: A Systematic Scoping Review of Current Literature and Identified Knowledge Gaps., The Journal of Climate Change and Health., 3., August.

37. Chang Ch., Lin B., Feng X., Andersson E., Gardner J. and Astell-Burt Th. (2024). A lower connection to nature is related to lower mental health benefits from nature contact., Scientific reports., 14(6705).

38. Watso J. and Farquhar W. (2019). Hydration Status and Cardiovascular Function., Nutrients., 11(8).

39. Tardy A., Pouteau E., Marquez D., Yilmaz C. and Scholey A. (2020). Vitamins and Minerals for Energy, Fatigue and Cognition: A Narrative Review of the Biochemical and Clinical Evidence., Nutrients 12(1).

المصادر العربية :

1. مقالة لدار الخليج (للصحافة والطباعة والنشر) / اعداد الحجاج خلال السنوات العشر الماضية في 2/7/2025.

2. مقالة للموسوعة الحرة / اكبر تجمعات بشرية في العالم في 2024/7/19

Design of A Freshwater Production System Based on Solar Energy

Asst. Prof.Dr. Firas Abdulrazzaq Hadi
firas.a.hadi@kus.edu.iq

Rounaq Adel Abdulwahab
st.rounaq.adel@ced.nahrainuniv.edu.iq

Mustafa Sinan Fadhil
rawnak_rsc@gmail.com

University of Al-Karkh for Science Scientific Research Commission

Abstract

This research paper addresses the design of a solar-powered freshwater production system, aiming to provide sustainable solutions for desalination, especially in water-scarce regions that benefit from high solar radiation. The research addresses how solar energy can be converted into electricity to power desalination technologies, such as reverse osmosis. The design process includes assessing the installation location, solar radiation intensity, and water demand before determining energy needs and selecting appropriate desalination methods. The system is environmentally friendly, has low operating costs, and is capable of operating independently from conventional electrical grids, making it ideal for remote areas, especially during major events such as the Arbaeen pilgrimage, where a reliable supply of clean water is required. The results indicate the system's ability to provide clean water at low operating costs and with high efficiency under variable solar radiation levels, reducing reliance on conventional energy sources. The system can also operate for extended periods at night thanks to the high battery storage capacity. The results also showed that the quality of the water produced by the system is high, with a saline concentration of 0.1%, demonstrating excellent purity and suitability for consumption. The system can be expanded by incorporating solar panels and larger-capacity batteries to meet increased demand, making it a sustainable, long-term solution. In this way, the study demonstrates the system's importance in addressing challenges associated with drinking water in water-scarce areas, especially during major events such as the Arbaeen pilgrimage.

Keywords: Solar energy, reverse osmosis, photovoltaic system, water purification, off-grid, battery storage

Introduction

Solar-powered reverse osmosis (RO) has been gaining attention since the 1980s as a solution for desalination in remote and desert area. Initially, studies focused on the possibility of integrating solar energy with RO systems, and the main challenges were solar system efficiency, energy consumption, and costs. Solar energy became more efficient, especially with the development of photovoltaic panels and storage technologies. In the last decade, research has seen progress in improving energy efficiency and using technologies such as hybrid (PV-RO). Today, solar RO systems are increasingly used in desalination, with improvements in cost and sustainability, making them a promising solution to the global water crisis (Abdaki et al., 2024; Al-Addous et al., 2024).

In the 1990s, solar energy began to be used in reverse osmosis systems more and more, due to the significant progress in solar energy technology some experimental began to be implemented in some remote areas and areas suffering from water and energy scarcity. In 2000 the most notable development is decreasing the cost of solar energy, with this decreases, solar-powered reverse osmosis systems became more economically viable, which helped spread their use in many remote areas (Al-Jubouri & Al-Ta'i, 2021; Al-Samarrai, 2024).

In 2018, university of Colorado Boulder study efficiency improvements of solar desalination systems. The research focused on efficiency improvements for large commercial desalination systems using solar energy. The results showed that improving the design of solar systems and using advanced energy storage technologies can increase the reliability of these systems in large commercial applications, while reducing operating costs. In 2024 Dubai Water Desalination Project: DEWA announced the largest desalination project using solar-powered seawater reverse osmosis

technology. The project aims to produce 180 million gallons of desalinated water per day, with investments amounting to AED 3.357 billion (US$ 914 million) (Duffie & Beckman, 2013; Goosen et al., 2023).

Research Objective

This research focuses on the design and implementation of a system that uses solar energy to desalinate water and provide it to Arbaeen pilgrims, taking advantage of the high solar radiation enjoyed by the pilgrimage areas and pilgrims' routes.

Relevance of the research for the Arbaeen pilgrimage

Providing clean water for large crowds: Pilgrims participating in events such as the Arbaeen pilgrimage are in dire need of reliable sources of clean water, especially in desert areas where water may be limited. A solar-powered fresh water system can sustainably provide fresh and safe water to a large number of pilgrims.

Sustainable and Environmentally Friendly: The use of solar energy is a clean and environmentally friendly source, reflecting the concept of sustainability, which is important during religious events, as they require high levels of natural care in accordance with Islamic and humanitarian practices.

Energy and Water Supply Independence: The system proposes eliminating reliance on electrical grids, which may be unavailable in rural areas. This means that critical times such as the Arbaeen pilgrimage can be handled by independent systems, ensuring uninterrupted water supply.

Expanding the Potential for Water Solutions: As the number of visitors

increases, pressure on existing infrastructure will increase. The proposed system provides a flexible solution that can be expanded to meet greater water demands when needed, facilitating effective monitoring planning and increasing the volume of water available.

Overcoming Climate Challenges: Because the system is solar-powered, it can operate well even in varying conditions, including sunny and temperate days, providing visitors with access to drinking water throughout the visit, regardless of any weather changes.

Materials and Methods

The system consisted of two 12V/12Ah VRLA batteries, a PWM type, 60A charge controller, a seven-stage RO water filtration unit rated at 25W, and two 90W solar panels. In an off-grid configuration, the components were connected using appropriate cabling and a monitoring device to measure voltage, current, and solar irradiance. Performance under Baghdad, Iraq, was evaluated under partially cloudy and partially sunny circumstances. On various days in March 2025, hourly data was collected throughout the day (Patel & Bohra, 2023; Rahman et al., 2022).

Data Gathering Tools

The solar radiation meter measures direct normal irradiance; the multimeter tracks voltage and current; and the environmental observations mea-
.sure cloud cover and temperature

Results

The results will be divided in two parts (Thirunavukkarasu & Sawle, 2021; Zhu et al., 2023).

Part 1, the readings were calculated will be attached with graphs showing the relationships between time, solar radiation, battery voltage, load voltage, and load current during the partly cloudy day then

Part 2, repeat this calculation in sunny day.

1.Readings through the daylight :

Table 1, show the change in the value of hourly solar radiation, which was taken from 9 to 3 on a partly cloudy day (6/3/2025). The second column represents the solar radiation readings in W/m². The readings were taken using a solar radiation meter. Note that the measured incident solar radiation represents direct normal radiation. These readings were taken hourly over a single day, from 9:00 AM to 3:00 AM. The second column shows a gradual rise in the solar radiation value and then a gradual decline. This is a well-known phenomenon resulting from the rising and falling of the sun. We notice that the third column from the left shows a voltage rise and fall. The fourth column represents the load voltage, which is required to operate the device. The fifth column represents the load current consumed for the device to operate. As for the battery voltage, it was observed to be constantly rising and falling due to the presence of clouds on that day. The battery voltage drops and then rises due to cloud cover or sun rise. As a result of the change in battery voltage, the load voltage changes automatically. However, with the stability of solar radiation, we observe stability in both the battery voltage and load voltage. The load current also changes, but this change depends on several factors, such as high temperature, high solar radiation, and changes in battery **voltage.**

Table 1: Data recorded from the location

Hour	Irradiance (W/m2)	Battery Voltage (V)	Load voltage	Load current (A)
9:00 Am	630	27.3	26.9	1.8
10:00 Am	650	27. 1	26.8	1.7
11:00 Am	880	26.8	26.4	1.7
12:00 Pm	865	27.2	26.8	1.8
1:00 Pm	867	27	27	1.7
2:00 Pm	830	27	27	1.6
3:00 Pm	725	27.2	27.1	1.6

We conclude that the device can be operated in cloudy or sunny conditions .That is ,the device performs the water filtration process during these conditions and during all daylight hours.

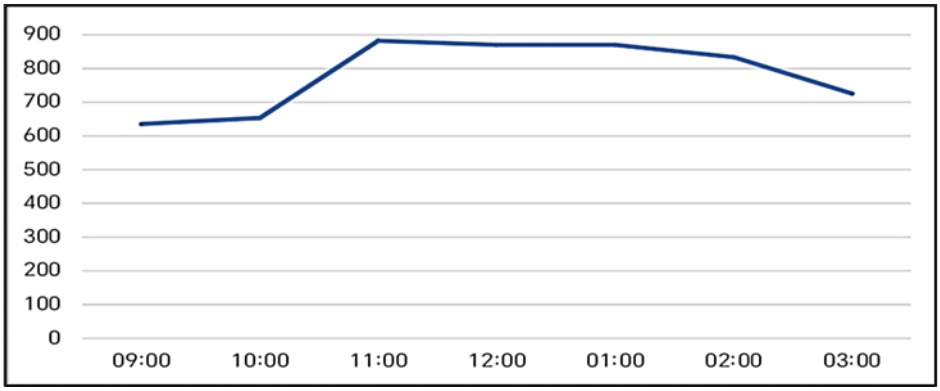

Fig.(1) Relationship between time and irradiance

From Fig. (1), which represents the relationship between daytime and solar radiation, where x-axis represents hours and the y-axis represents radiation, it is clear from this Fig. (1) that solar radiation increases and rises in value until it reaches its peak hour, approximately 11:30, and then begins to decline. It can be said that the variation between 9 and 3 is small, i.e., it is between 600-900 W/m2, which means that the batteries are well charge.

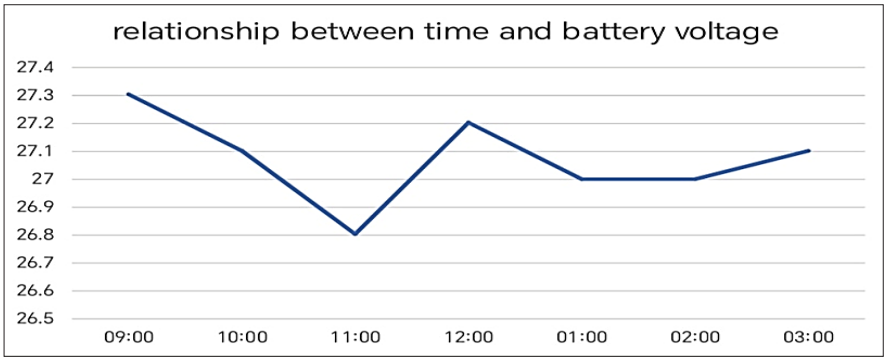

Fig. (2) relationship between time and battery voltage

Battery voltage: During the day, we notice stability in the battery voltage as there is continuous charging, Fig. (2)

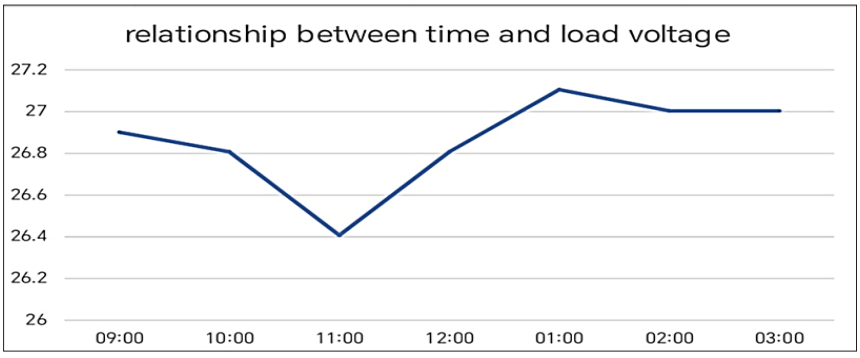

Fig. (3) Relationship between time and load voltage

The load voltage depends on the battery voltage, and the load voltage will be almost stable. Fig (3)

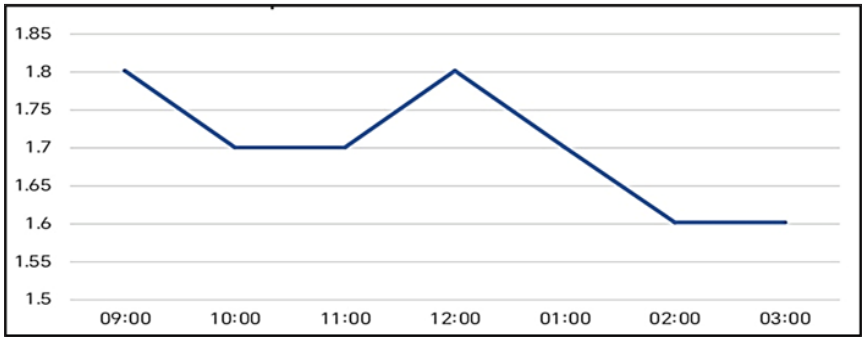

Fig. (4) Relationship between time and load current

Load current, we notice that the load current is stable from 1.6 to 1.8 A during daylight hours, Fig. (4).

2.Part Two :

Through Table 2, we can study the change in the value of hourly solar radiation, which was taken starting from 9:30 to 1:30 on a sunny day, as the weather on the day the readings shown in Table 1 were taken was a sunny day, 10/3/2025 Table 2. The second column represents the solar radiation readings in W/m2. The readings were taken using a solar radiation meter. Note that the measured incident solar radiation represents direct normal radiation. These readings were taken hourly over a single day, from 9:30 AM to 1:30 AM. The change in the second column, representing the radiation, shows a gradual rise in the solar radiation value and then a gradual decline. This is a well-known phenomenon resulting from the rise and fall of solar radiation over time. As for the third column, which represents the battery voltage, we notice complete stability in the battery voltage, as there is a continuous charge due to the presence of sufficient solar radiation capable of charging the battery. The fourth column, which represents the load voltage, is stable due to the stability of the battery voltage during the day. As for the fifth column, which represents the load current, we notice stability at 1.6A.

Table 2: shows the readings that were measured

Hours	Irradiance (W/m^2)	Battery Voltage	Load voltage	Load current
9: Am	768	27 V	27 V	1.6 A
10:00 Am	796	27 V	27.1 V	1.6 A
10:30 Am	828	27.1 V	27.1 V	1.6 A
11:00 Am	913	27.1 V	27.1 V	1.6 A
11:30 Am	935	27.1 V	27.1 V	1.6 A
12:00 Pm	889	27.2 V	27.2 V	1.6 A
12:30 Pm	888	27.1 V	27.1 V	1.6 A
1:00 Pm	835	27.3 V	27.3 V	1.6 A
1:30 Pm	850	27.2 V	27.1 V	1. 6 A

We notice from Fig.(5) a continuous interaction in the value of solar radiation and its peak from 11 am to 12 pm.

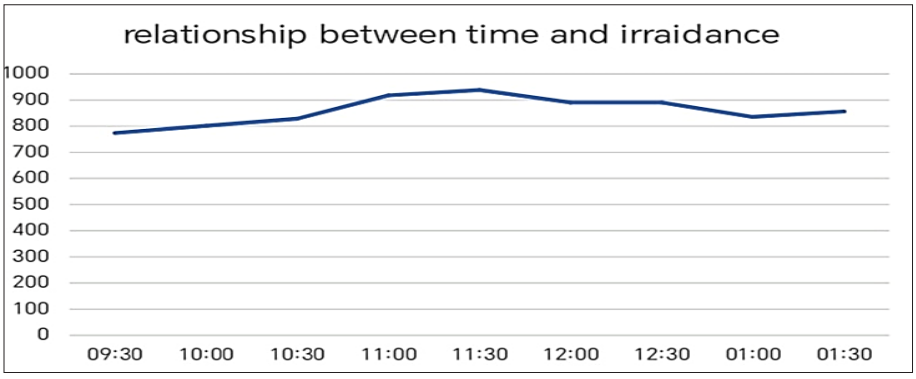

Fig. (5) Relationship between time and irradiance

As shown in Fig.(6), we notice complete stability in the battery voltage, as there is continuous charging due to the presence of sufficient solar radiation capable of charging the battery.

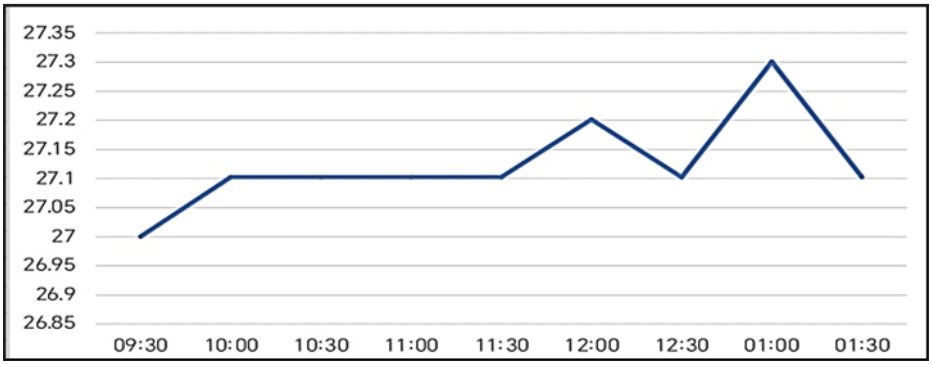

Fig.(6) relationship between time and battery voltage.

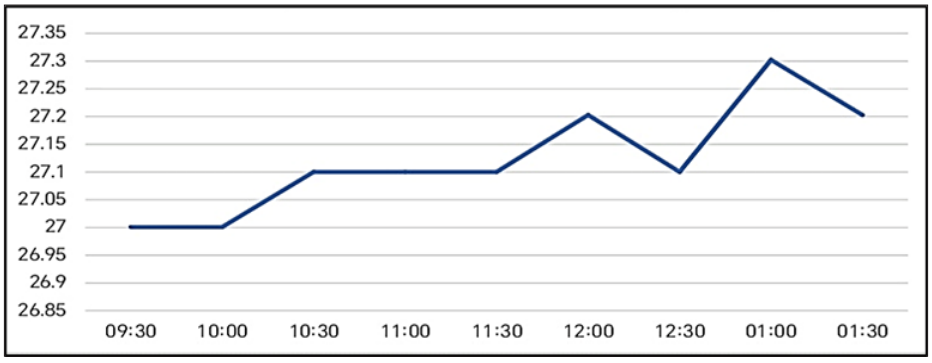

Fig. (7) Relationship between time and load voltage

As shown in Fig.(7), we notice complete stability in the load voltage, and depending on the battery voltage, the load voltage will be stable.

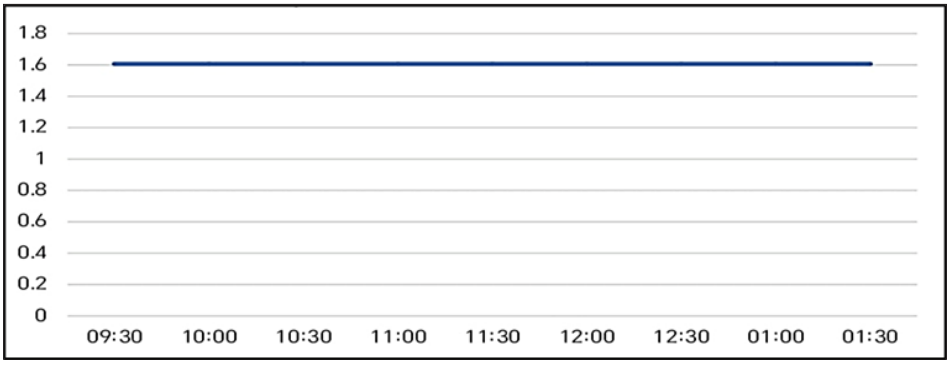

Fig. (8) Relationship between time and load current

As shown in Fig.(8), we notice complete stability in the load current and its stability at 1.6A.

3.Charging Time :

Through work, it has been shown that batteries need 20 minutes to raise the charging rate from 24V to 27V (i.e., from empty battery to fully charged), which means, according to Table (4-1), if it is observed that fully charging and discharging batteries requires two hours of time, during these two hours the tank can be filled and emptied (3) times within two hours, at a rate of (9) hours of filling and emptying the tank per day, which is equivalent to 63 liters per day.

Discussion

The system's operation adapts to the visitor's time by relying on the varying solar radiation throughout the day, which directly affects the efficiency of power generation. According to the data, solar radiation reaches its peak between 11:00 AM and 12:00 PM, resulting in increased battery charge and increased overall system efficiency.

When visitors visit during times when the sun is at its highest, the system will experience better production and access to clean water, as the system's efficiency is closely linked to the nature of solar radiation. For example, solar radiation measured at 9:00 AM was 630 watts/m^2, while at 11:00 AM it reached 880 watts/m^2.

In addition, the stability of the battery voltage, which also depends on solar radiation, is crucial to the system's performance during visiting hours. If visitors are present during times of constant solar radiation, they will be able to observe the system operating at its highest efficiency.

So, if visitors are there during times when solar power is available, the system will be better able to meet their clean water needs.

Conclusions

The system is capable of providing clean water at a low operating cost and demonstrates strong performance under varying levels of solar radiation. It reduces reliance on traditional energy sources and can operate continuously for up to three hours at night. Tests conducted on the system confirmed its ability to function efficiently in different weather conditions, including sunny and partly cloudy days, with voltage and current remaining stable throughout. The battery system proved effective by maintaining a nearly constant voltage of around 27 volts despite fluctuations in solar intensity during the day. On sunny days, the system showed even higher efficiency, with a consistent current output of 1.6 amps, contributing to stable overall performance. This highlights the system's reliability and effectiveness in harnessing solar energy. Furthermore, the project proves to be highly applicable in rural areas where water scarcity or lack of electricity grids is a concern, as the system operates independently using only solar power. It also offers room for scalability by allowing the integration of higher-capacity solar panels and batteries to meet larger demands, making it a sustainable and long-term solution. The water produced by the system was found to be of high quality, with a salt concentration of only 0.1, indicating excellent purity and suitability for consumption.

In this way, the research reflects the significant importance of supporting the Arbaeen pilgrimage by providing a sustainable and secure water source, embodying the aspirations for effective solutions to water challenges in arid regions.

References

1. Abdaki, M., Alobaydy, O., Al-Samman, S., & Ahmed, H. (2024). Spatiotemporal analysis of extreme climate indices in Nineveh Governorate, northern Iraq: four decades study from 1981 to 2022 using NASA-Power dataset. Modeling Earth Systems and Environment, 10(4), 5553-5572.
2. Al-Addous, M., Bdour, M., Rabaiah, S., Boubakri, A., Schweimanns, N, Barbana, N., & Wellmann, J. (2024). Innovations in solar-powered desalination: a comprehensive review of sustainable solutions for water scarcity in the Middle East and North Africa (MENA) region. Water, 16(13), 1877.
3. Al-Jubouri, A. T. S., & Al-Ta'i, N. (2021). Modeling solar radiation at the Baghdad climate station and its impact on electrical energy production. Tikrit University Journal of Human Sciences, 28(10), 125.
4. Al-Samarrai, Z. F. A. (2024). معطيات الطاقة المتجددة وافاق تطورها في العراق. Journal of Tikrit University for Humanities, 31(4), 170-192.
5. Duffie, J. A., & Beckman, W. A. (2013). Solar engineering of thermal processes. John Wiley & Sons.
6. Goosen, M., Mahmoudi, H., Alyousef, Y., & Ghaffour, N. (2023). Solar desalination: A review of recent developments in environmental, regulatory and economic issues. Solar Compass, 5, 100034.
7. Patel, M., & Bohra, S. (2023). Power management of grid-connected PV wind hybrid system incorporated with energy storage system. Future Energy, 2(3), 7-19.
8. Rahman, A., Farrok, O., & Haque, M. M. (2022). Environmental impact of renewable energy source based electrical power plants: Solar, wind, hydroelectric, biomass, geothermal, tidal, ocean, and osmotic. Renewable and sustainable energy reviews, 161, 112279.
9. Thirunavukkarasu, M., & Sawle, Y. (2021). A comparative study of the optimal sizing and management of off-grid solar/wind/diesel and battery energy systems for remote areas. Frontiers in Energy Research, 9, 752043.
10. Zhu, L., Tian, L., Jiang, S., Han, L., Liang, Y., Li, Q., & Chen, S. (2023). Advances in photothermal regulation strategies: from efficient solar heating to daytime passive cooling. Chemical Society Reviews, 52(21), 7389-7460.

Recycling the PET plastic bottle waste accumulated during the Arabian Pilgrimage into 3D printing filament to print durable material models and use them in designs that support the eternal memory

Asst prof.Dr.Samara Jasim Mohammad

Physic department/science of collage for women

university of Baghdad

samaraj_phys@csw.uobaghdad.edu.iq

Yaqeen Ammar Mahdi

Yiqeenasd95@gmail.com

Abstract

Designing a system for recycling plastic bottles in our research enabled us to address the problem of plastic waste accumulating during the Arbaeen pilgrimage due to the large number of visitors. There are numerous ways to recycle materials, including manufacturing suitable materials at a low cost by recycling plastics with good mechanical properties to manufacture spare parts using 3D printing. PET was used for plastic bottles by recycling it into filaments with specific specifications and thicknesses, as determined by the system designed during the research. A 3D printer was then used to print the filaments after shaping them and printing a new material with new specifications. These filaments were used as raw material, and a 3D printer (Ender 3 S1 Pro) was used to produce a material with better strength and hardness specifications for the filling ratios during printing with best30% infill ratio. This allows for the printing of models and designs that can serve to commemorate the anniversary.

Keywords: Recycling plastics, 3D printer, Creative designs .

INTRODUCTION

The demand for plastic materials has skyrocketed worldwide across a number of industrial sectors, posing serious waste management difficulties (Obande, 2021, 108771).

The intrinsic toxicity of plastic materials Alabi, (2019,1–13). poses a serious threat to human health, the environment, and marine life, making them an important worldwide environmental problem. According to information from researchers PET or PETE is a polyester produced by the reaction of terephthalic acid and ethylene glycol, and is produced by mixing the two materials in the required molar amounts and renewing the reduced water with a successful efficiency of 99% Van Sebille, 2019,1–13

the Japanese Japanese melt crystallizes after solidification, which can be obtained as partially crystalline or amorphous products according to the request. The partially crystalline product is characterized by high strength and hardness to friction and to dilute acids and oils and their conversion, but it is sensitive to heat (Ghosh, 1986, 2551–2560).

About 70 million tons are manufactured from it, representing 20% of the production of the plastics industry sector and partially crystalline polyester is used in electronics, limbs and screws, seat belts and car covers, and is also used in the medical field in implanting artificial organs and in artificial networks and in microvascular(Dhaka, V, 2022,1777–1800). Amorphous polyester is less durable, but more resistant to impact. Because it is transparent and lighter than glass, it is used in packaging such as drinking bottles, food containers, and cosmetics. It is also used in electronics in magnetic tape holders, fig(1).

Fig(1): Polyethylene terephthalate (PET or PETE)

Chemical composition of Polyethylene terephthalate (PET or PETE)

Polyethylene terephthalate (PET) is a polymer belonging to the polyester family, composed of repeating units of ethylene glycol and terephthalic acid. The general chemical formula for PET is $(C_{10}H_8O_4)_n$ (Ghosh,1986, 2551–2560) where «n» refers to the number of repeating units in the polymer chain,fig(2).

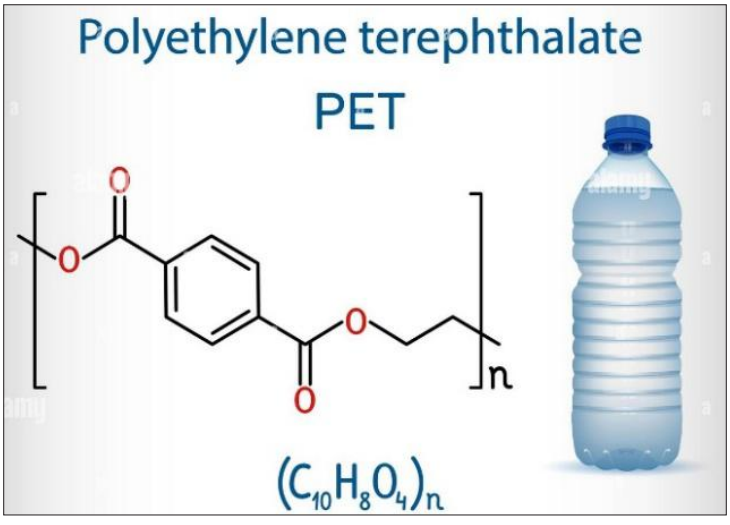

Fig(2): Chemical composition of PET

Semi-Annual Scientific Journal
www.arbnj.com
Ramadan 1447 A.H, March 2026 A.D

Advantages of Polyethylene Terephthalate

1. Polyethylene terephthalate (PET) is a thermoplastic polymer commonly used in various fields, such as packaging and synthetic fibers. PET has the following properties(Ragaert, K., 2017, 24–58)(Singh, N.,2017, 409–422).
2. High Tensile Strength: PET has excellent tensile strength, making it suitable for applications requiring high durability.
3. Good Chemical Resistance: PET exhibits good resistance to many chemicals, making it suitable for packaging.
4. Transparency: PET can be transparent, making it ideal for applications requiring optical clarity.
5. Abrasion and Crease Resistance: The stiffness of PET fibers gives it high resistance to creases and abrasion, making it suitable for use in fabrics and clothing.
6. Good Barrier Properties: PET provides an effective barrier against carbon dioxide and moisture, making it suitable for packaging soft drinks and food products.

Plastic

Plastic is a polymeric material widely used in a variety of applications due to its diverse properties, such as lightness, durability, and formability. However, its widespread use has led to the accumulation of massive amounts of plastic waste, posing a significant environmental challenge (Singh, N.,2017, 409–422) Plastic recycling is an important solution to reduce this waste and conserve natural resources.

Types of plastic recycling:

A. Mechanical Recycling:

This involves converting plastic into new products without changing its chemical composition(Geyer, R.,2017, 1700782). This is the most common method shown in fig(3).

Fig(3): Mechanical plastic recycling

B. Chemical Recycling:

This involves breaking down plastic into its basic chemical components to produce new materials, allowing for the recycling of low-quality plastics and improving process efficiency(Ghosh, 1986, 2551–2560).

Mechanical properties of plastics (Geyer, R.,2017, 1700782) :

1. Tensile strength.
2. Compressive strength.
3. Elasticity.
4. Elongation at break.

5. Impact resistance.
6. Shear strength.
7. Hardness.
8. Fracture resistance.

Shore Hardness Test

The Shore Hardness Test is an important mechanical test used to assess the resistance of ductile materials (such as rubber and plastic) to deformation under a specific load. This test is widely used in various industries, including prosthetics, where hardness is a critical indicator of a material›s quality and durability,The Shore hardness test measures a material›s resistance to penetration by a needle or a specially shaped point under a specified load, and gives results on a scale of 0 to 100, with higher values indicating harder materials (Khalid R., 2014, 547-553) (Pedrosa Rebouças Filho, P.,2010,1520).

Types of shore scale:

A. Shore:

Used to measure the hardness of soft materials such as natural rubber and soft plastics.

B. Shore:

Used for harder materials such as rigid plastics (e.g., PET, ABS, Nylon).

3D Printer

3D printing fig(4) is a technology that produces three-dimensional objects by adding material layer by layer according to a digital model, unlike traditional manufacturing that removes material (Reazul Haq Abdul,2019,102-108).

Fig(4): 3D Printer

Advantages of 3D Printing

A. Custom Manufacturing:

Suitable for designing parts tailored to the user›s body, especially in medicine.

B. Reduced Waste:

Material is added only where needed, reducing waste.

C. Rapid Design Modification:

The model can be modified and reprinted instantly without the cost of

upfront tooling.

Materials and Method

Table (1): Materials and equipment used

Device name	Usage
Pellet Dryer	Drying the pellets from moisture before extrusion.
Hopper	Feeds the pellets to the extruder evenly.
Extruder	Melts the pellets and pushes them out using an internal screw.
Heated Barrel	Heats the barrel to the melting point of the plastic.
Nozzle/Die	Forms the output filament to the desired diameter (e.g., 1.75mm).
Cooling System	Cools the filament immediately upon exit using a fan or water bath.
Laser Gauge	Measures the filament diameter and automatically controls quality.
Puller	Pulls the filament from the nozzle at a set speed after cooling.
Spool Winder	Winds the filament onto the spool evenly and tangle-free
Control Panel	Sets temperature, speed, diameter, and electronically monitors the line.
3D printer Bambu lab p1s Ender3 S1 pro	Used to print plastic filaments to form PET samples.
Digital Microscopes	Used to view the filling percentage of PET samples.
UTM	Used for tensile testing
HARTIP 3000	Used for hardness testing
Thread manufacturing system	Used to make plastic threads

Samples materials Preparation Method

First step: manufacturing plastic filament:

The process of manufacturing plastic filament begins with wooden or metal parts and involves building the structure of the filament extruder. Fig(5) The extrusion cylinder is then mounted at a suitable angle to allow gravity to assist the material›s passage through it. A DC motor or stepper motor is mounted on the structure, and its rotation drives a screw (drill) inside the extrusion cylinder to force the hot plastic through. The motor is then connected to a power source. Stainless steel tubes are used to melt the plastic. A temperature sensor and heating element are used to achieve temperatures between 200 and 250°C. A hopper or simple container with a feed tube is then used to load the scrap plastic or filament. A spool is then used to draw out the plastic. A metal tube with a small opening (about 1.75 mm in diameter) is used for the 3D printing filament. After the plastic is extruded from the mold, it must be rapidly cooled using a cooling fan to form a durable filament. After the filament is extruded and cooled, it must be wound onto a spool. You can use an old spool, such as a sewing thread spool.

Two Step: 3D printing:

After the printing filament is made from PET or PETG polymer, it must be dried at 70-80°C for 4-6 hours before use. The shape of the sample is then designed according to the required tensile strength and hardness. The model is then cut using a cutting software and printed on a 3D printer. It is essential to ensure that the printer surface is flat and that the filament is securely fastened to the inlet port. After printing is complete, the sample is allowed to cool, its edges are cleaned of excess material, Three samples were prepared: 1. PET sample, 20% print with infill 2. PET sample, 25% print with infill 3. PET sample, 30% print with infill.

Three samples were prepared:

1. PET sample, 20% print fill.
2. PET sample, 25% print fill.
3. PET sample, 30% print fill.

. Fig(5): plastic filament machine

Hardness Test

The hardness of the samples was measured with a (HARTIP 3000) device as shown in Fig (6) Hardness device

Fig(6): Hardness device

Digital Microscope

The samples were examined using a digital microscope as shown in Figure (7) of the microscope, Table (2) shows the characteristics of the microscope.

Fig(7): Digital Microscope

Table (2): Characteristics of the microscope

SPECIFICATION	DETAILS
IMAGE SENSOR	CMOS
MOBILE PHONE COMPATIBLE OS	Android
FOCUS RANGE	15mm-40mm
FRAME RATE	Up to 30 FPS
AVAILABLE IMAGE FORMAT	BMP/JPG
IMAGE RESOLUTION	Up to 640*480 - 1920*1440
ADJUSTABLE ILLUMINATION	8 Built-in LED Diodes
COMPATIBLE OS	Windows 7/Windows 10/Mac 10.13 and above
PC INTERFACE	USB 3.0/2.0/1.1
PC POWERED	5V Direct Current
AVAILABLE VIDEO FORMAT	AVI
PRODUCT COLOR	Black
DIMENSION	14.5cm x 10cm x 5cm
WEIGHT	About 200g

Result and Discussion

the results of 3D printing PET samples from plastic filaments. To study some of their mechanical properties, the samples were examined using the following tests: tensile testing and hardness testing.

Three PET samples were manufactured using FDM 3D printing technology, with all printing conditions fixed except for the infill density.

Hardness testing using a HARTIP 3000.

And Microscopic used to show infill printing shape.

Mechanical properties

PET sample:

This sample under a microscope shows that printing at a low 20% fill ratio produces a light, void-filled internal structure, making it more susceptible to premature fracture under load. It also results in poor mechanical properties and may only be suitable for cosmetic applications or non-load-bearing prototypes, as shown in the fig (8).

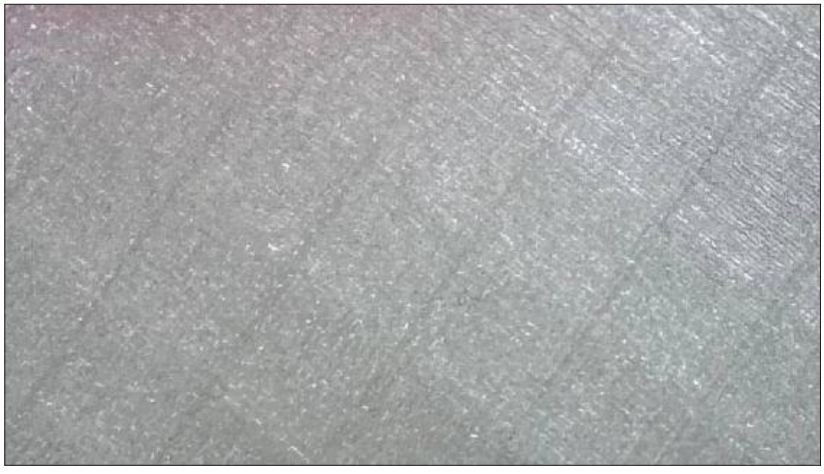

Fig (8): Microscopic image of the first model showing a 20% fill rate.

Under the microscope, this sample shows a significant improvement in mechanical properties without a significant increase in printing time or material consumption, making it a good choice for applications requiring moderate strength. Its internal structure is more cohesive, which helps it withstand higher stresses and delays fracture. Therefore, it performs better than the first sample, as shown in the fig(9).

Fig (9): Microscopic image of the first model showing a 25% fill rate.

Under the microscope, this sample features a denser, more cohesive internal structure, reducing the likelihood of weak points forming between layers. It also boasts exemplary performance in terms of strength and stiffness, making it suitable for applications requiring high mechanical properties, such as functional parts or prosthetics that withstand constant stress(Dizon, J.R.C.,2018,44-67). This sample recorded the highest mechanical performance of the three samples, as shown in the fig (10)

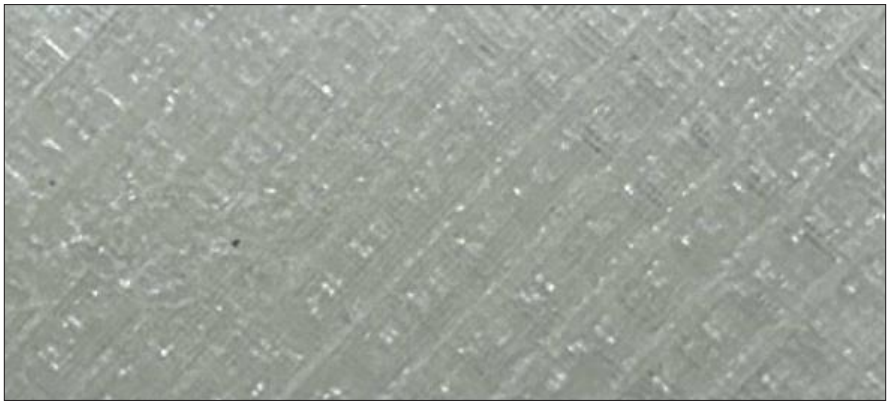

Fig (10): Microscopic image of the first model showing a 30% fill rate.

Hardness testing

Shore hardness test the specimen recorded the highest surface mechanical properties among the three specimens show in Fig(11) table (3).

The goal of several research projects has been to investigate the mechanical characteristics of 3D prints and filaments.

The mechanical characteristics of 3D prints and filaments have been used in these investigations as hardness (Woern, A.L., 2018, 1413) (Chadha, A., 2019, 550–559)(Suteja,T.,2020, 1569).

Table (3) Shore Hardness values

Shore Hardness					Average test values
infill 20%	46	51	53	48	49
infill 25%	52	58	61	56	56
infill 30%	64	61	69	59	63

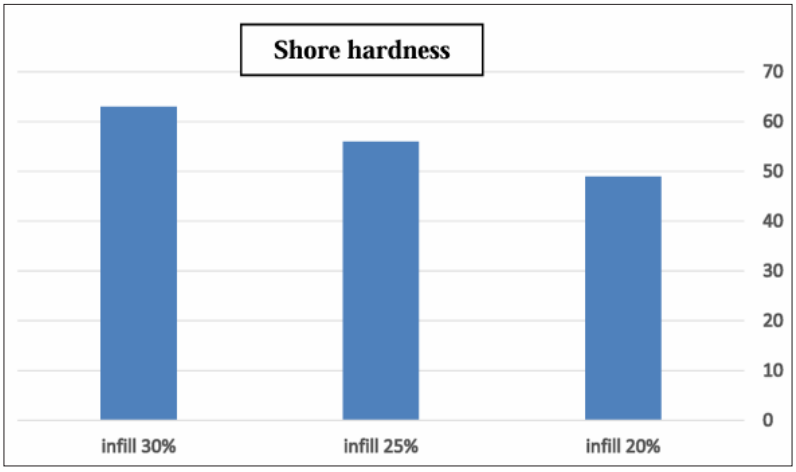

Fig (11): Shore hardness

Creative 3D printing designs

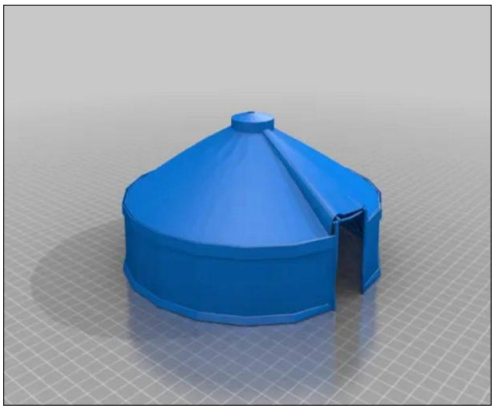

Fig (12): Some productions of 3D Printer

References

1. Obande, W.; Brádaigh, C.M.Ó.; Ray, D. (2021) Continuous fibre-reinforced thermoplastic acrylic-matrix composites prepared by liquidresin infusion—A review. Compos. Part B Eng. 215, 108771.
2. Alabi, O.A.; Ologbonjaye, K.I.; Awosolu, O.; Alalade, O.E. (2019) Public and environmental health effects of plastic wastes disposal: Areview. J. Toxicol. Risk Assess. 5, 1–13.
3. Van Sebille, E.; Wilcox, C.; Lebreton, L.; Maximenko, N.; Hardesty, B.D.; Van Franeker, J.A.; Eriksen, M.; Siegel, D.; Galgani, F.;Law (2015) A global inventory of small floating plastic debris. Environ. Res. Lett. 10, 124006.
4. Ghosh, P., & Bhowmick, A. K. (1986). Polyethylene terephthalate—I. Chemistry, thermodynamics and transport properties. Chemical Engineering Science, 41(10), 2551–2560. https://doi.org/10.1016/0009-2509(86)85070-9.
5. Dhaka, V., Singh, S., Anil, A. G., Naik, T. S. S. K., Garg, S., Samuel, J., Kumar, M., Ramamurthy, P. C., & Singh, J. (2022). Occurrence, toxicity and remediation of polyethylene terephthalate plastics: A review. Environmental Chemistry Letters, 20, 1777–1800. https://doi.org/10.1007/s10311-021-01384-8.
6. Ragaert, K., Delva, L., & Van Geem, K. (2017). Mechanical and chemical recycling of solid plastic waste. Waste Management, 69, 24–58. https://doi.org/10.1016/j.wasman.2017.07.044.
7. Singh, N., Hui, D., Singh, R., Ahuja, I. P. S., & Feo, L. (2017). Recycling of plastic solid waste: A state of art review and future applications. Composites Part B: Engineering, 115, 409–422. https://doi.org/10.1016/j.compositesb.2016.09.013.

8. Geyer, R., Jambeck, J. R., & Law, K. L. (2017). Production, use, and fate of all plastics ever made. Science Advances, 3(7),1700782. https://doi.org/10.1126/sciadv.1700782.

9. Khalid R., Samara, J. (2014). Fracture Toughness and hardness studying for polymer-ceramic composite. Baghdad Science Journal ,(2)11,547-553.

10. Pedrosa Rebouças Filho, P., Cavalcante, T. S., Albuquerque, V. H. C., & Tavares, J. M. R. S. (2010). Brinell and Vickers hardness measurement using image processing and analysis techniques. Journal of Testing and Evaluation, 38(1). https://doi.org/10.1520/JTE102220.

11. Haq, Reazul Haq Abdul, Ishkrizat Taib, Mohd Nasrull Abdol Rahman, Ho Fu Haw, Haslina Abdullah, Said Ahmad,Ahmad Mubarak Tajul Ariffin, and Mohd Fahrul Hassan (2019) "Mechanical properties of PCL/PLA composite sample produce from 3D printer and injection molding." International Journal of Integrated Engineering 11, no. 5 ,102-108 https://doi.org/10.30880/ijie.2019.11.05.014.

12. Dizon, J.R.C.; Espera, A.H., Jr.; Chen, Q.; Advincula, R.C. (2018) Mechanical characterization of 3D-printed polymers. Addit. Manuf. 20, 44–67.

13. Woern, A.L.; Byard, D.J.; Oakley, R.B.; Fiedler, M.J.; Snabes, S.L.; Pearce, J.M. (2018) Fused particle fabrication 3-D printing: Recycledmaterials' optimization and mechanical properties. Materials 11, 1413. [PubMed].

14. Chadha, A.; Haq, M.I.U.; Raina, A.; Singh, R.R.; Penumarti, N.B.; Bishnoi, M.S. (2019) Effect of fused deposition modelling process parameters on mechanical properties of 3D printed parts. World J. Eng. 16, 550–559.

15. Suteja,T.J.; Soesanti, (2020) A. Mechanical properties of 3D printed Polylactic acid product for various infill design parameters: A review.J. Phys. Conf. Ser. 1569, 042010.

Sustainable Plastic Waste Management During the Arbaeen Pilgrimage: Cost-Effective Strategies for Recycling PET Water Bottles

Asst.Lect.Ali Saadi Abd
ali.s.a.mohammed@nahrainuniv.edu.iq

Asst. Prof.Dr. Israa Badr Al-Mashhadani
israa.b.al-mashhadani@nahrainuniv.edu.iq

Asst.Lect. Lara Muwafaq Falah
lara.mwafaq@nahrainuniv.edu.iq

Asst.Lect.Faten alkubaisy
faten.q.alkubaisi@gmail.com

Department of Computer Engineering, College of Engineering, Al-Nahrain University

Abstract

This plastic recycling project seeks to minimize environmental pollution resulting from the accumulation of plastic waste by collecting, sorting, and processing it for reuse in the production of new, usable products. This project aimed to contribute preservation of natural resources, by accumulating plastic in landfills and oceans and reduces dependence on virgin raw materials, in addition to decreasing carbon emissions. Moreover, it raises environmental awareness while also providing employment opportunities in recycling factories through fields of collection, processing, and manufacturing. The project constitutes a crucial step toward achieving sustainable development and a circular economy.

Large quantities of plastic waste have been observed during the Arbaeen pilgrimage in the holy city of Karbala, one of the world's largest human gatherings. This waste primarily consists of water bottles and plastic utensils utilized by pilgrims and Hussaini service processions. While a portion of this waste is sorted and collected systematically by service and volunteer entities, a large portion ends up in general waste without being utilized.

This creates a genuine opportunity to capitalize on these large quantities of plastic through more efficient organization of collection and sorting processes, in collaboration with municipal authorities and environmental initiatives. These materials can be directed toward recycling facilities to be transformed into new, usable products such as household items, benches, storage boxes, or even eco-friendly construction materials.

Keywords: Renewable Energy, Arbaeen Pilgrimage, the Holy City of Karbala, Plastic Recycling, Environmental Pollution, Recycling Factories, Sustainable Development.

Introduction

The extensive use of plastic bottles during the Arbaeen pilgrimage is expected to generate tons of plastic waste, which can significantly impact the environment. This substantial plastic waste can lead to environmental disasters, contributing to pollution. Pollution continues to be one of the most enduring and harmful environmental issues of our time (air and ocean pollution). Despite growing awareness and recycling efforts, most plastic waste ends up in landfills or is incinerated, contributing to ecosystem degradation and climate change (Mohsenzadeh et al., 2023). To address this, the concept of "plastic reborn" (plastic recycling) through distributed recycling and additive manufacturing has emerged. The recycling effort contributed to reduce the carbon emissions to 41.8% lower than that of virgin PET (Junaid et al., 2023). This approach involves converting post-consumer plastic waste directly into 3D printing filament, enabling local reuse of materials while reducing environmental impact (Kumar et al., 2022). This paper proposes that plastic can rebirth in communities or in households, therefore aiming to provide cost-effective, eco-friendly 3D printing filament alternatives while fostering circular economy principles through local recycling efforts. The project aims to design a recycling device from 3D-printed components and produce plastic filament, using a thermal extruder, coil, motors and nozzle.

1.3D Printer Filament

3D printing filaments are primarily composed of thermoplastics. Common types include acrylonitrile butadiene styrene (ABS) and polylactic acid (PLA). Other materials used include polycaprolactone (PCL), poly carbonate (PC), polystyrene (PS), polyetherimide (PEI), and various forms of polyethylene (PE), including LDPE (low-density PE), LLDPE (linear low-density PE), and HDPE (high-density PE). These materials are used to print automotive parts, surgical instruments, prototypes, packaging, toys, and many other products that are in everyday use. Figure 1 shows the shape of filament that used to print 3D parts (Muthuraman et al., 2021).

Figure 1: 3D printer filament

2. 3D Printer

A 3D printer is a device used to convert plastic filament to three-dimensional parts. Three-dimensional (3D) printing, also known as additive manufacturing, is a transformative technology that enables the layer-by-layer fabrication of physical objects directly from digital models. Over the past two decades, 3D printing has expanded from prototyping applications to full-scale production across diverse industries, including healthcare, aerospace, automotive, construction, and education. This technology offers significant advantages in terms of customization, material efficiency, and design flexibility. Recent advancements in materials science, printing resolution, and multi-material printing have further broadened its capabilities, allowing for the creation of complex geometries and functional components (Hunt et al., 2015). Figure 2 shows the 3D printer device used in this research.

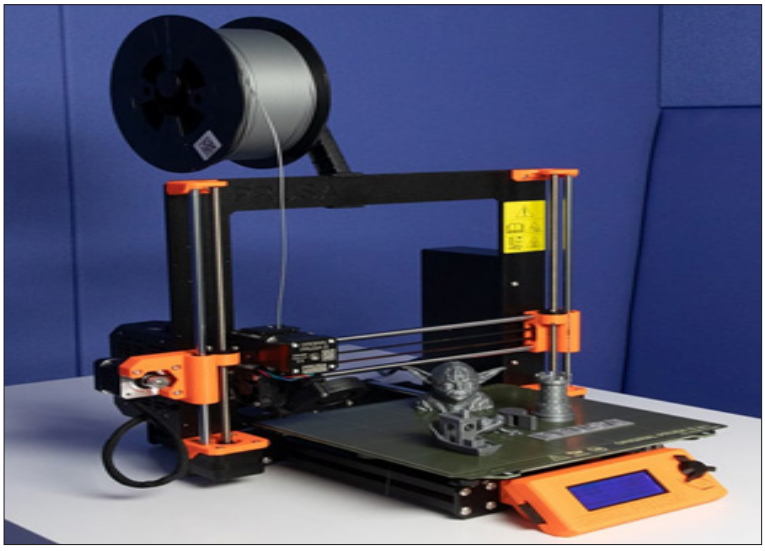

Figure3 :2 D printer

2. Design of the Recycling Device

To manufacture the recycling device, each component was designed using SolidWorks software. The designs were then 3D printed and assembled into the final system (Hopewell et al., 2009).

Step 1: SolidWorks Design

SolidWorks is a leading computer-aided design (CAD) software widely used in engineering, product design, and manufacturing industries for creating precise 3D models and detailed technical drawings (Andrady, 2011). SolidWorks provides an integrated environment that supports the full product development lifecycle—from conceptual design and simulation to manufacturing documentation and analysis. Its parametric modeling approach allows for efficient design modifications, while its simulation tools enable structural, thermal, and motion analysis to optimize product performance before physical prototyping. Figure 3 illustrates the CAD model of the recycling device, where each part is designed for 3D printing.

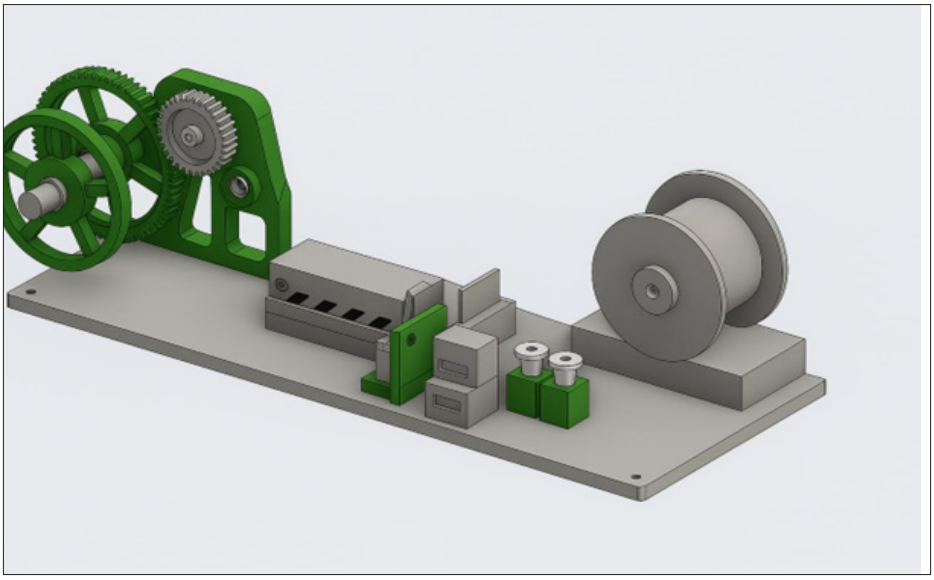

Figure 3: Recycling device model in SolidWorks

Step 2: 3D Printing

Once the components were designed in SolidWorks, they were printed using a 3D printer. Figure 4 shows the parts prepared for printing, and Figure 5 displays the printed components.

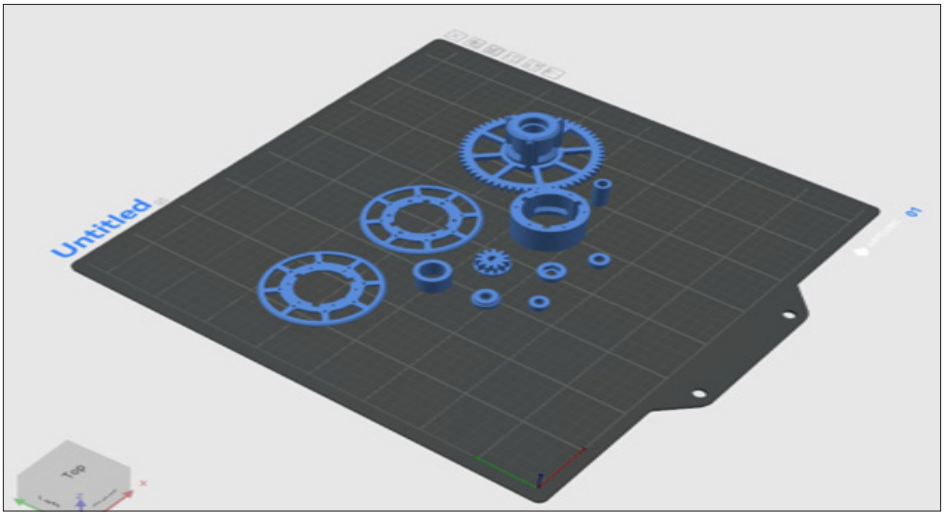

Figure 4: 3D part before printing in 3D printer.

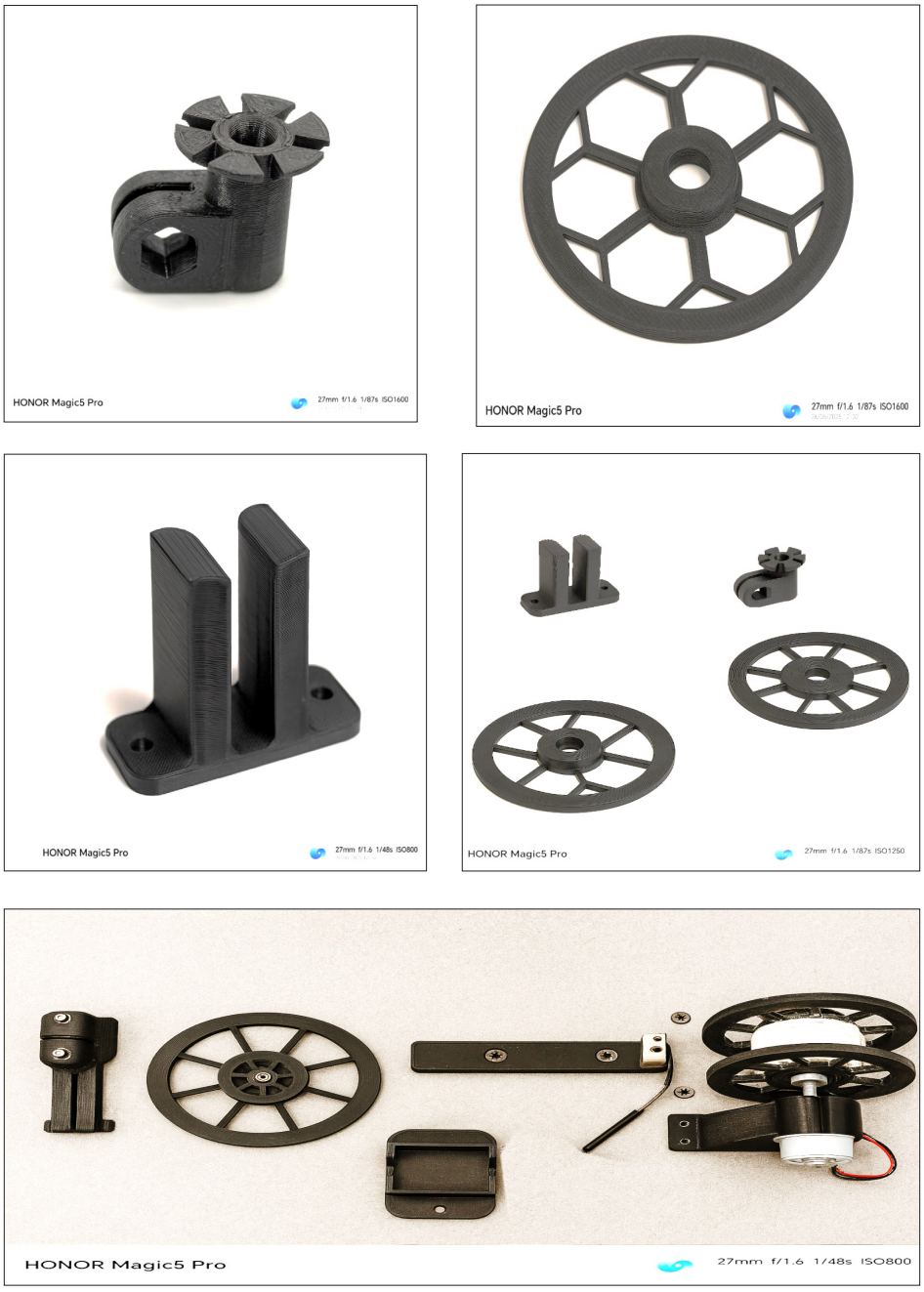

Figure 5: 3D printer devices after printing

Step 3: Other Components Used in the Device

Additional components required for the device include:

- Nozzle (V6 Volcano): Inlet diameter 3mm- entry size for feeding the PET strip, Outlet diameter: 1.2 mm – extrusion opening for melted filament, Material: Brass or stainless steel for durability and thermal conductivity, Drilling: 1.2 mm outlet is drilled into a 1.6 mm hole to support 1.75 mm.

Figure 6: Nozzle

- Ceramic Heater: A 12V DC, 40W ceramic heating element for efficient and consistent heating. This is made of ceramic material. It features a threaded screw-on connector for heater block compatibility (Singh et al., 2017).

Figure 7: Ceramic heater

• Aluminum Heater Block: Made of Aluminum material for efficient transfer of heat from the heater to the nozzle. Designed to fit the V6 Volcano nozzle and securely hold it in place (Zander et al., 2018).

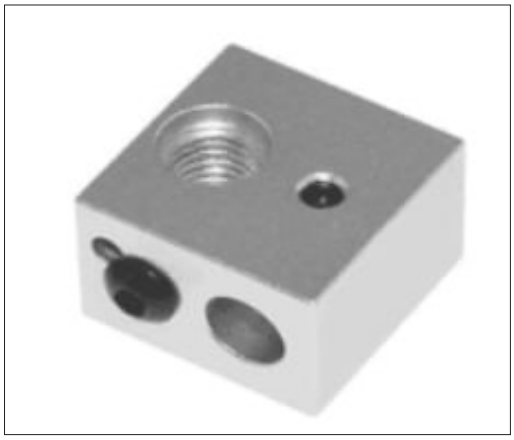

Figure 8: Aluminum heater block

• Thermo Controller (TC 49P or TEX C100): Regulates temperature using a K-type thermocouple and solid-state relay

Figure 9: Thermo controller TC 49P

• High-Torque Motor and PWM Controller: Enables smooth filament pulling and precise speed control (Jambeck et al, 2015).

Figure 10: High torque Motor

• 10A 12V SMPS (Switched Mode Power Supply): Powers the system with overvoltage and overcurrent protection, delivering a stable 12V DC output. Capable of supplying at least 10A for safe operation of all components.

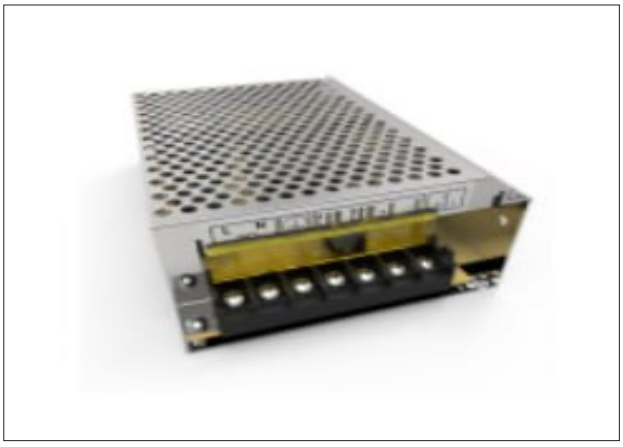

Figure 11: SMPS

Step 4: Assembly

After printing the components and sourcing the electronic parts, the recycling device was assembled. Figure 12 shows the fully assembled device.

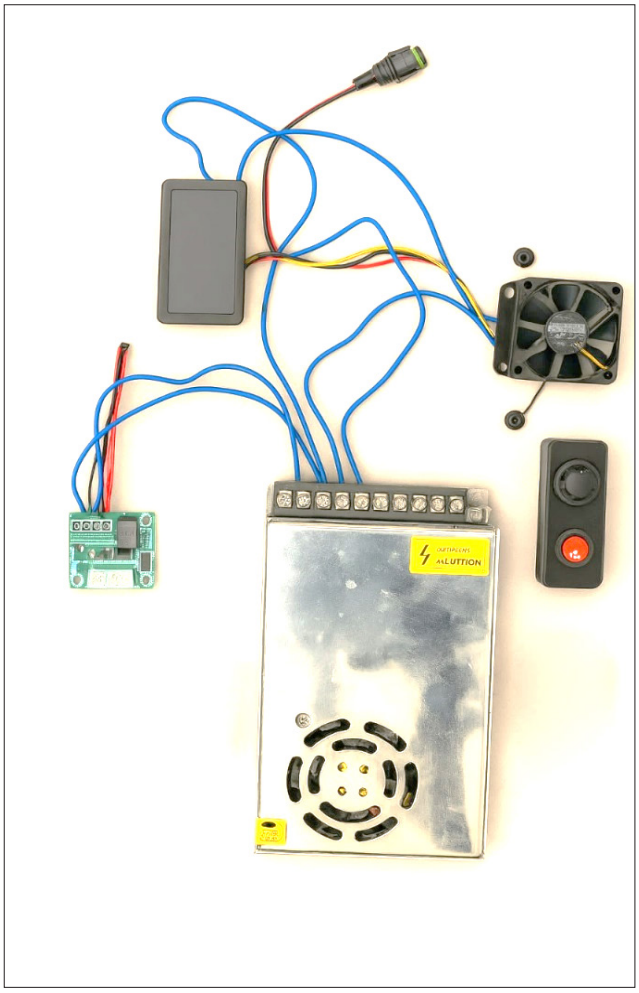

Figure 12: Gathering device parts

3.Process Methods

The following steps describe the recycling process used to convert waste plastic bottles into 3D printing filament.

Step 1: Used plastic cups and bottles are collected after thorough cleaning to ensure high-quality filament. In this project, the plastic waste was primarily sourced during the Arbaeen pilgrimage. Figure 13 shows the collected plastic waste.

Figure 13: Plastic cups and water bottle waste

Step 2: A small amount of water is added to each bottle, and the bottle is then heated using a gas burner. This softens the plastic, making it easier to cut. Figure 14 shows the heating process.

Figure 14: Water added to bottle while heating

Step 3: After softening, the plastic is cut into strips using a manual cutting tool. Figure 15 shows the cutting tool used.

Figure 15: cutter tool

Step 4: The plastic strips are fed into the heater at approximately 220°C. The heated plastic is extruded through a nozzle to produce a thin filament. Figure 16 displays the filament being extruded.

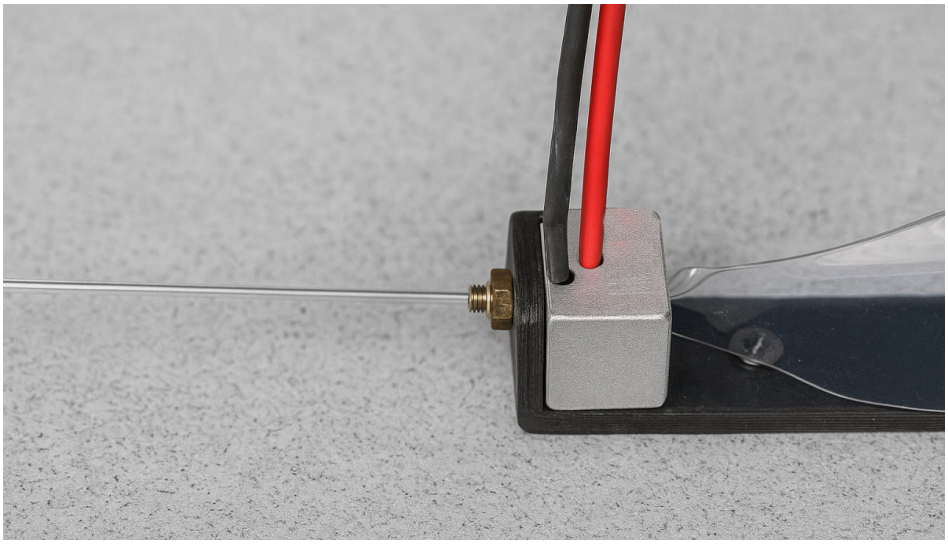

Figure 16: Filament produced from plastic strips

Step 5: The filament is pulled using a high-torque motor and cooled in ambient air. It is then wound onto a roller for storage. Figure 17 illustrates the pulling mechanism.

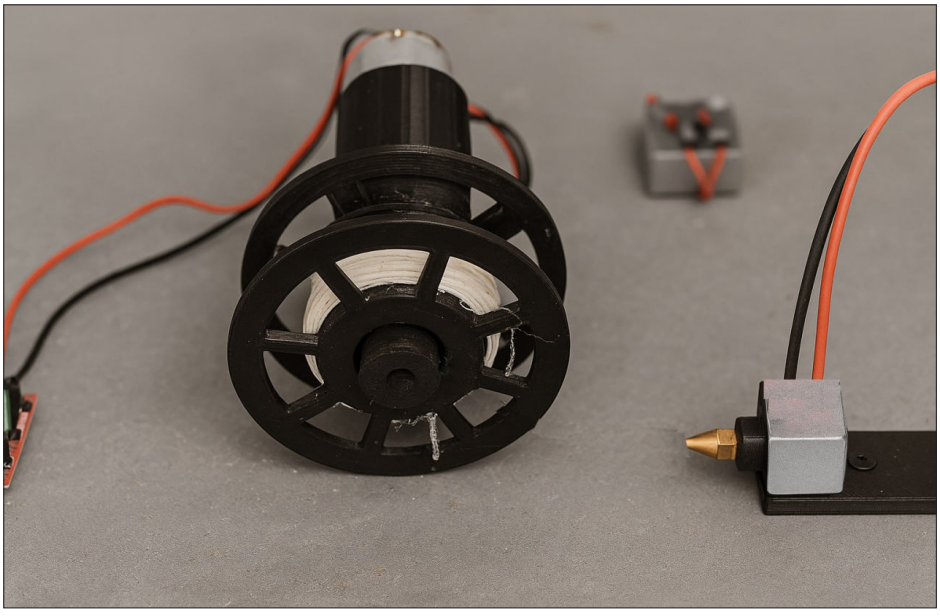

Figure 17: Filament pull using high torque motor

Result

The heating subsystem, consisting of a heater block and nozzle, was used to convert plastic strips into filament. The device operates at a temperature range of 200°C to 220°C. Figure 18 illustrates the heating block that converts strips to manufacturing filament.

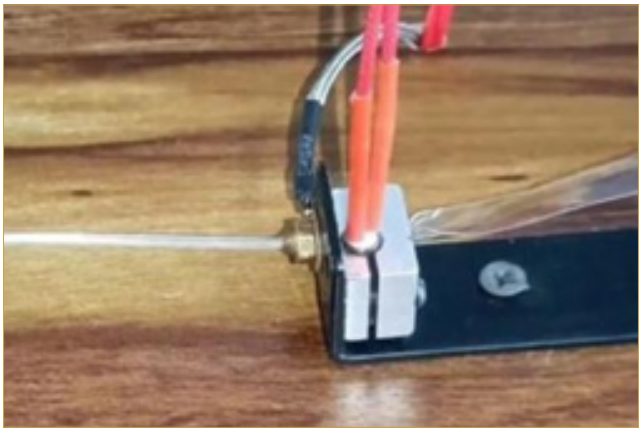

Figure 18: Extract filament from plastic bottle strips

The pulling mechanism existing, where using high Torq motor are used for this purpose. As the filament exited the heater block, it was cooled by open air and solidified into a strand of approximately 1.75 mm in diameter. Figure 19 shows the pulling mechanism.

Figure 19: Pulled mechanism

Leveraging Doppler Satellite Remote Sensing to Assess Spatiotemporal Air Qualit Dynamics inthe Baghdad-Karbala-Najaf Urban Corridor

Asst.Dr. Hasan Jaber Atta
hasan.jaber@sc.uobaghdad.edu.iq

Asst.Prof.Dr.Najah Abd

University of Baghdad / College of Science

Majed Abd Al.salam Al-Bakr
majid.abdalsalam.2021@gmail.com

Tabarak Al-Kanani
tabarak.raed21091a@sc.uo.baghdad.edu.iq

Abstract

This research examines the spatiotemporal dynamics of air pollutant concentrations across the Baghdad-Karbala-Najaf corridor, leveraging Doppler-based satellite remote sensing data. The analysis focuses on five critical atmospheric contaminants: sulfur dioxide (SO_2), nitrogen dioxide (NO_2), carbon monoxide (CO), ozone (O_3), and fine particulate matter ($PM_{2.5}$). Findings reveal pronounced variability in pollution levels, attributable to synergistic interactions between meteorological parameters and anthropogenic factors, with peak exacerbations observed during the Arbaeen pilgrimage a mass religious gathering. Urban centers in Baghdad exhibited the highest baseline pollution concentrations, driven by vehicular density and industrial emissions, while Karbala and Najaf demonstrated episodic spikes correlated with large-scale religious events. Precipitation emerged as a statistically significant mitigating factor, particularly in scavenging SO_2 and NO_2 from the atmospheric column. The study proposes evidence-based scientific and policy interventions, advocating for integrated sustainable urban planning, deployment of real-time air quality surveillance systems, and ecological mitigation protocols for managing high-density human congregations.

Keywords: Air Pollution Dynamics; Doppler Remote Sensing; Satellite Atmospheric Monitoring; Arbaeen Mass Gathering; Anthropogenic Emissions (SO_2, NO_2, CO, $PM_{2.5}$, O_3); Air quality.

Introduction

Air pollution, characterized by the presence of harmful atmospheric substances including gases (e.g., NO_2, SO_2, CO, O_3) and particulate matter (PM2.5), poses significant threats to public health and environmental sustainability (1,3). Primary anthropogenic sources such as vehicular emissions, industrial activities, and fossil fuel combustion contribute to respiratory diseases, cardiovascular morbidity, and premature mortality, particularly when pollutant concentrations exceed critical thresholds (4,5). The complex interplay between suspended particulates and gaseous pollutants exacerbates these risks, with PM2.5 being especially hazardous due to its ability to penetrate deep into the respiratory system (6). Concurrently, gases like ground-level ozone (O_3) and sulfur dioxide (SO_2) not only impair human health but also contribute to environmental degradation through acid rain formation and climate feedback mechanisms (7,9).

Urbanization and population growth have intensified air pollution challenges globally, with developing regions like Iraq experiencing compounded effects due to industrial expansion, unregulated emissions, and episodic events such as the Arbaeen pilgrimage (10,11). Studies in Iraqi cities, including Baghdad, Mosul, and Erbil, highlight the role of meteorological factors (e.g., wind patterns, rainfall) and localized sources (e.g., diesel generators, brick kilns) in driving spatiotemporal pollution variability (12,14). For instance, Khalaf et al. (2009) documented substantial emissions from diesel generators in Kut, while Shihab (2021) identified PM10 as the dominant pollutant in Mosul, with seasonal fluctuations linked to weather conditions (15,16).

This study leverages Doppler satellite data to systematically monitor air quality across Baghdad, Karbala, and Najaf—a region where pollution dynamics remain understudied despite acute exposure risks. Specif-

ic objectives include: (1) quantifying spatial-temporal variations in NO_2, SO_2, CO, O_3, and PM2.5; (2) identifying dominant pollution sources (e.g., traffic, industry, religious gatherings); and (3) proposing evidence-based mitigation strategies tailored to Iraq's socio-environmental context. By integrating remote sensing with ground-truth data, this research aims to advance regional air quality management and inform policies targeting sustainable urban development and public health protection.

Air Pollution Theory in Iraq

Iraq faces significant air pollution challenges due to industrial activities, vehicular emissions, fossil fuel combustion, and widespread use of generators. Major pollutants include nitrogen dioxide (NO_2), sulfur dioxide (SO_2), carbon monoxide (CO), ozone (O_3), and particulate matter ($PM_{2.5}$), each posing severe health and environmental risks. NO_2 and SO_2, primarily from power plants and transportation, contribute to respiratory diseases and acid rain. CO, a byproduct of incomplete combustion, disrupts oxygen transport in blood. O_3 forms via photochemical reactions, exacerbating respiratory conditions. $PM_{2.5}$, emitted from industrial and vehicular sources, penetrates deep into lungs, increasing cardiovascular and respiratory mortality.

Weather conditions, including wind, temperature, and sandstorms, influence pollutant dispersion, while human activities—industrial operations, traffic congestion, and seasonal heating—further degrade air quality. The annual Arbaeen pilgrimage intensifies pollution through increased vehicular emissions, generator use, and waste burning, elevating NO_2, SO_2, CO, and $PM_{2.5}$ levels. Regulatory measures and emission controls are urgently needed to mitigate health and ecological impacts, particularly in urban centers like Baghdad, Karbala, and Najaf.

Study area

The study area covers the region between Baghdad, Karbala, and Najaf, which is characterized by a mix of urban, industrial, and arid environments. Baghdad, as the capital and largest city of Iraq, experiences high levels of air pollution due to traffic emissions, industrial activities, and population density. Karbala and Najaf, both significant religious and cultural centers, witness periodic increases in air pollution, especially during large gatherings and seasonal weather changes. The region's climate is predominantly arid, with frequent dust storms and variable wind patterns that influence air quality shown in figure 1. By utilizing Doppler satellite data, this study aims to analyze spatial and temporal variations in air pollution across these areas, considering meteorological factors such aswind speed, direction, and atmospheric pressure.

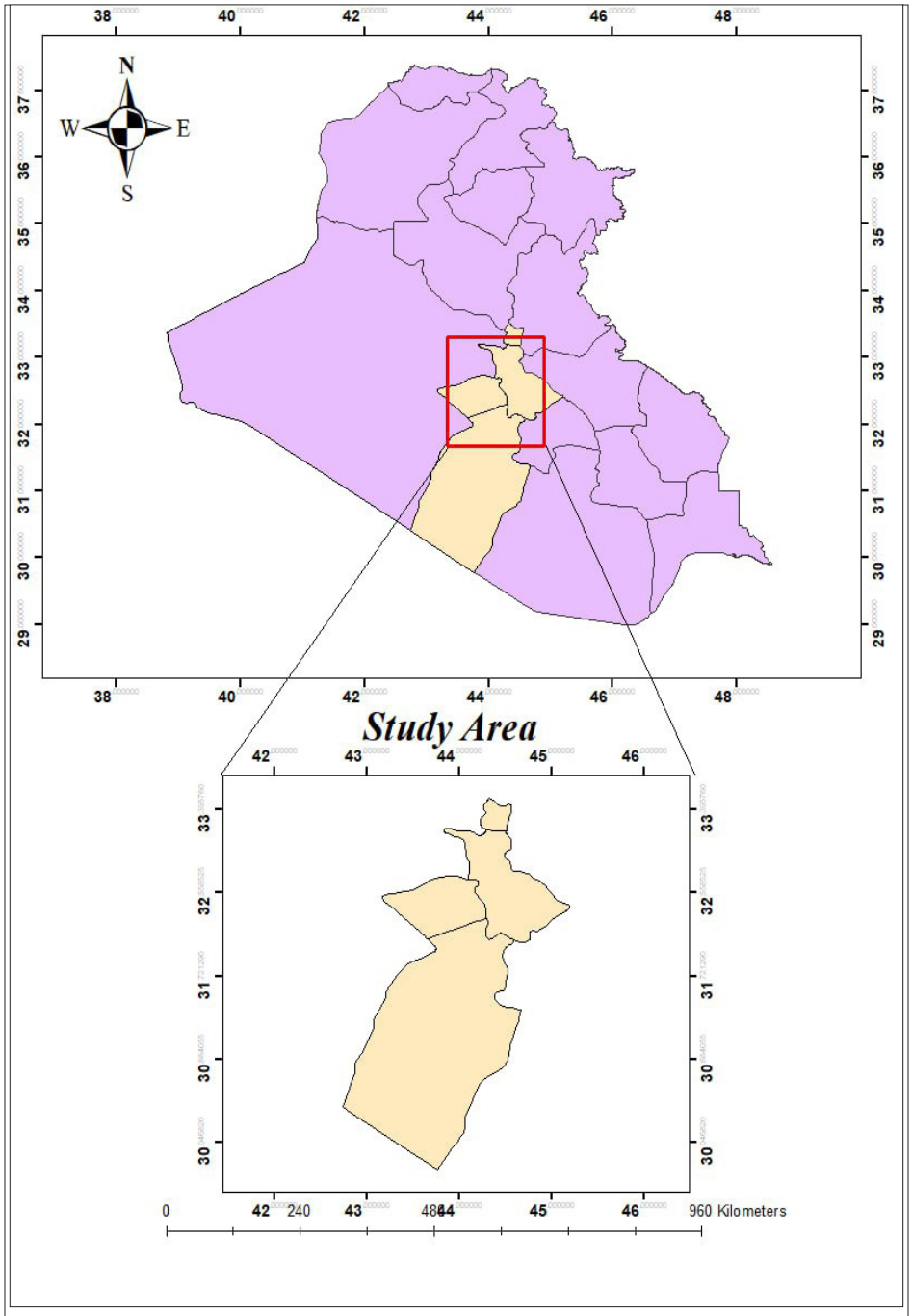

Figure (1): study area

Methodology

This study utilizedDoppler satellite datato monitor air pollutants—SO_2, NO_2, CO, O_3, and $PM_{2.5}$—in Iraq, leveraging high-resolution remote sensing from platforms likeWindy, Copernicus, and Sentinel Hub. The Doppler satellites (e.g., ESA missions) provideddaily global coverage-with a spatial resolution of 7 × 3.5 km^2, detecting pollutants viaUV, visible, and infrared spectral bands. Complementary data fromMODIS, OMI, and VIIRSenhanced aerosol and trace gas analysis.

Pollutant concentrations were extracted fromWindy's interactive maps, which integrate real-time ECMWF and CAMS forecasts.SO_2levels (2–10 Jan 2025) peaked at63.02 µg/m^3(Sunday), whileNO_2(4–12 Feb 2025) reached88.02 µg/m^3(Tuesday evening), reflecting traffic and industrial influences.$PM_{2.5}$(8–15 Mar 2025) varied from13–39.77 µg/m^3, with higher levels linked to dust storms.Rainfall's cleansing effectwas quantified, showingSO_2 reduced by 81%,NO_2 by 79%, andCO by 65%post-rain due to atmospheric washing. Wind speed (17 km/h) further dispersed pollutants.

Statistical and graphical analyses(tables, line graphs) illustrated diurnal and seasonal trends, correlating pollution spikes withmeteorological conditions (wind, rain, temperature)andhuman activities (traffic, industry). The methodology underscores satellite remote sensing's efficacy inurban air quality assessmentandpollution mitigation strategies.

Results:

This study analyzed air pollutant concentrations (SO_2, NO_2, CO, $PM_{2.5}$) in Baghdad, Karbala, and Najaf, revealing significant variations driven bymeteorological conditionsandhuman activities, particularly during theArbaeen pilgrimage.

1.Sulfur Dioxide (SO_2):

- Peak concentrations occurred inBaghdaddue to industrial activity and traffic, whileKarbala and Najafshowed elevated levels during Arbaeen fromdiesel generators, vehicular emissions, and open cooking.
- Rainfall reduced SO_2 by ~81%, demonstrating atmospheric cleansing. Industrial zones and temporary power demand during religious events were key contributors. Shown in figure (2 and 3).

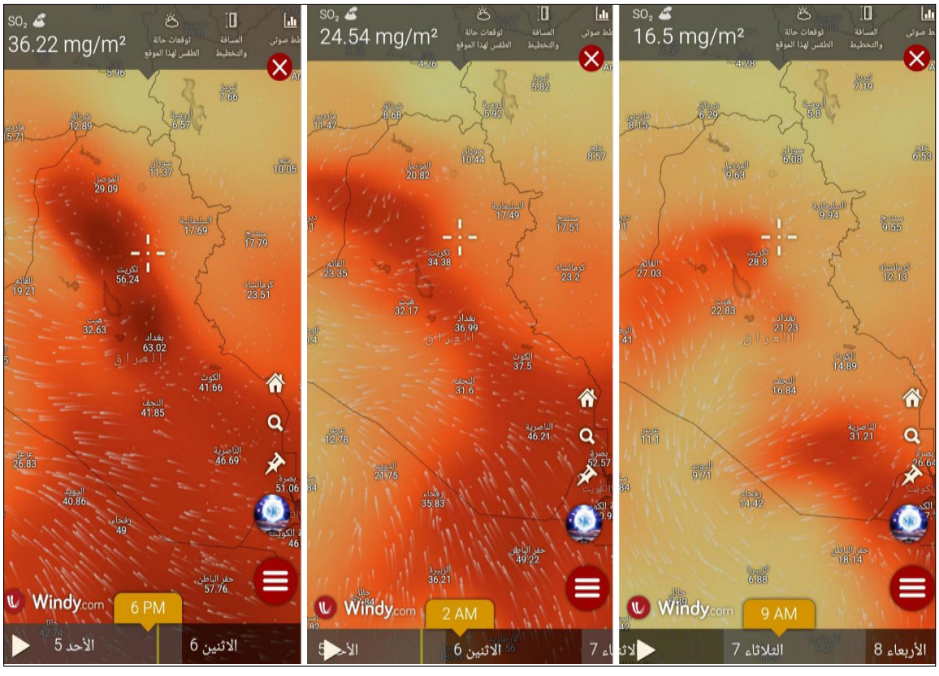

Figure (2): Sulfur Dioxide (SO2) distributions.

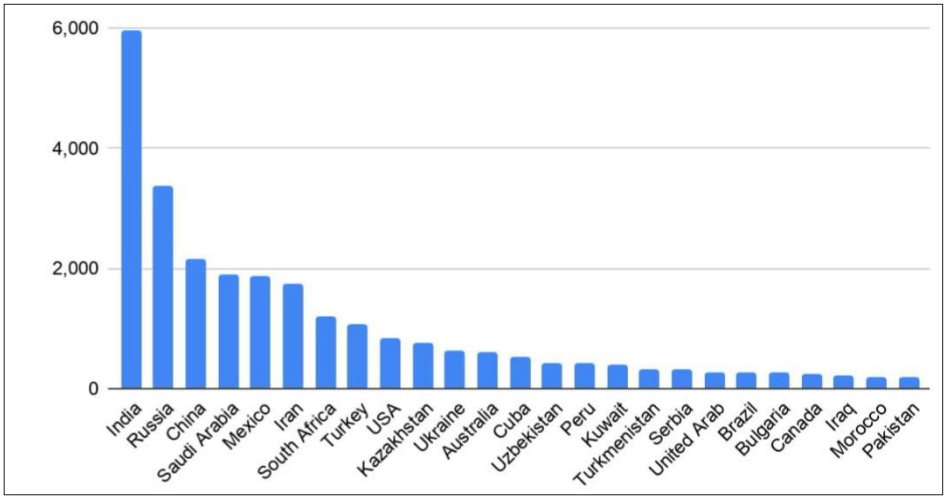

Figure (3): Statistics chart of the countries and cities that recorded the highest SO2 pollution rate for the year.

2. Nitrogen Dioxide (NO_2):

- Urban centers exhibitedpeak NO_2 during rush hours, with Arbaeen causing asharp rise(e.g.,88.02 µg/m³in Karbala/Najaf) due to traffic congestion and generator use.
- NO_2's reactivity with atmospheric compounds worsened air quality, posing risks torespiratory health, especially for vulnerable groups shown in figure 4.

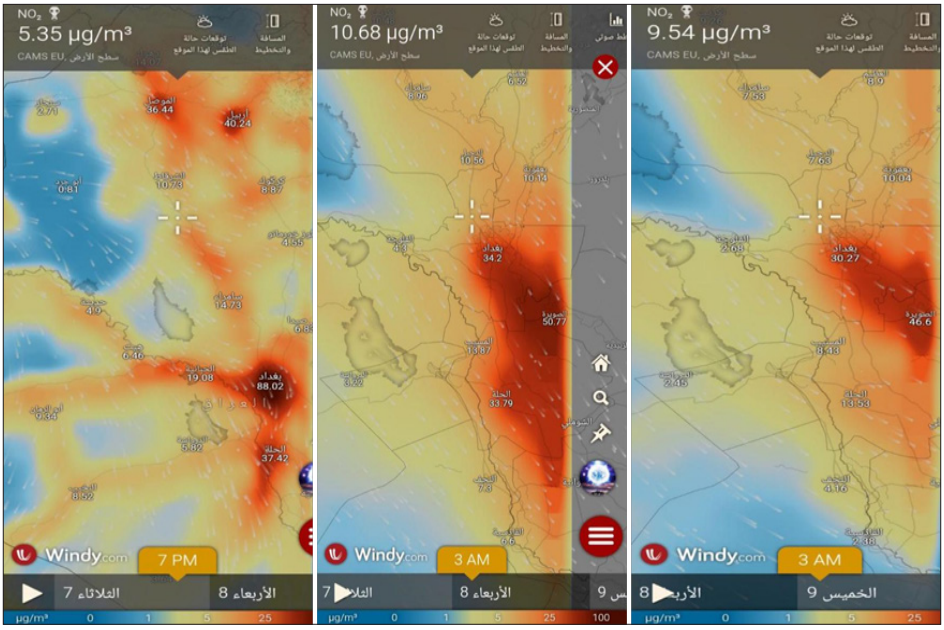

Figure (4): Nitrogen Dioxide (NO_2) distributions.

3.Carbon Monoxide (CO):

- Highest levels were linked toincomplete combustionfrom generators and vehicles during Arbaeen. Crowded roads andfossil fuel-based energyexacerbated emissions shown in figure 5.
- CO'sodorless, invisible natureincreased health risks, particularly in densely populated areas.

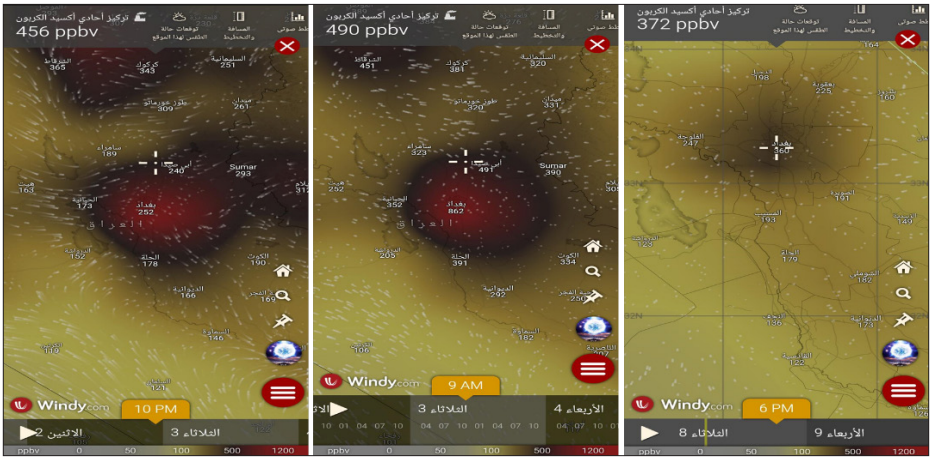

Figure (5): Carbon Monoxide (CO) distributions.

4.Particulate Matter ($PM_{2.5}$):

- Dust stormsand human activities (e.g.,waste burning, traffic) combined to elevate $PM_{2.5}$, with peaks reaching39.77 µg/m³.
- Arbaeen intensified emissions throughopen cooking and waste accumulation, compounding health risks from long-term exposure shown in figure 6.

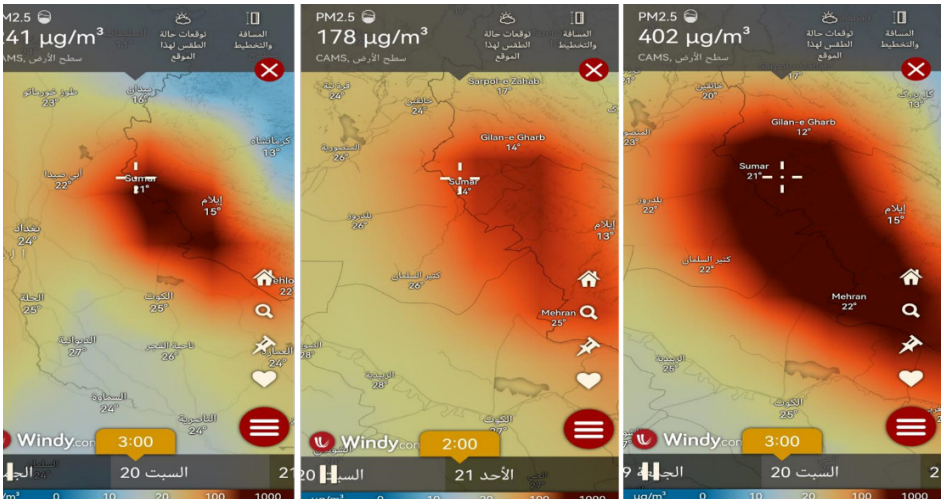

Figure (6): Particulate Matter ($PM_{2.5}$) distributions.

Key Findings:

- Religious eventslike Arbaeenamplified pollutionvia traffic, generators, and open burning.
- Meteorological factors(rain, wind) played a dual role:rain reduced pollutants(e.g., SO_2 by 81%), whilecalm winds trapped emissionsin urban areas.
- Health impactswere severe for vulnerable populations, necessitatingtargeted mitigation strategiesfor industrial, transport, and energy sectors.

Meteorological Factors Influencing Gaseous Pollutant Concentrations:

- Wind and temperature are among the most influential meteorological factors affecting air pollution levels.
- Low wind speeds typically lead to pollutant accumulation near the surface, while higher wind speeds promote dispersion and improve air quality.
- Temperature fluctuations can either enhance chemical reactions that lead to pollutant formation or assist in vertical air movement that helps disperse pollutants. As a result, some pollutants may increase or decrease depending on the specific weather conditions. Shown in figures (7, 8, and 9).

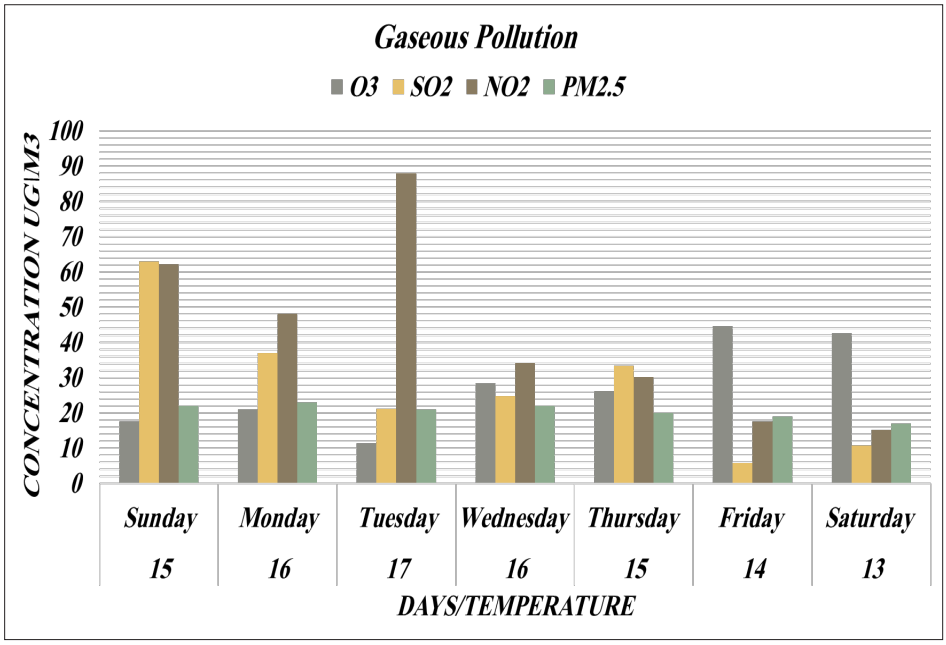

Figure (7): Pollution concentration in January with a wind speed of (12-15 km/h).

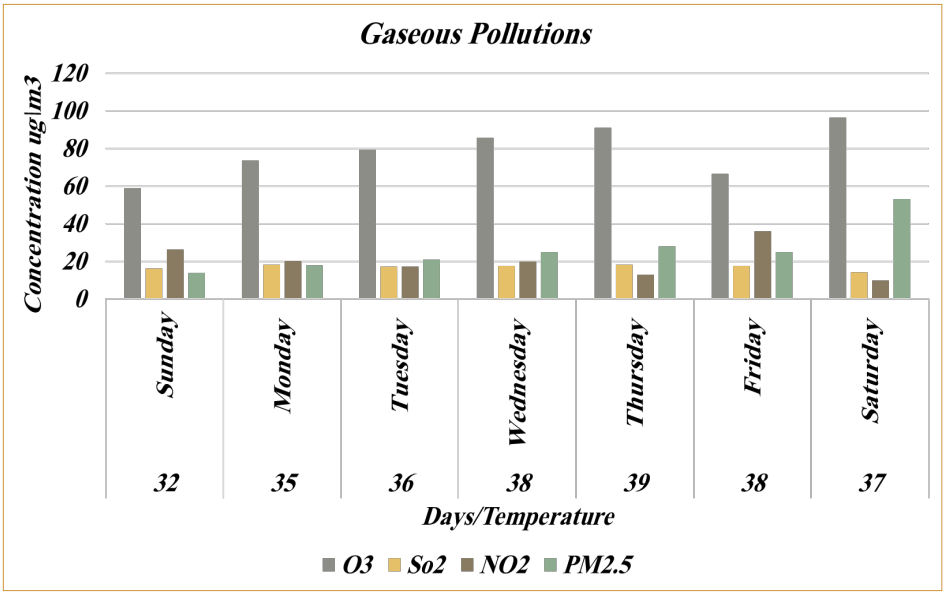

Figure (8): Pollution concentration in March with a wind speed of (22-26km/h).

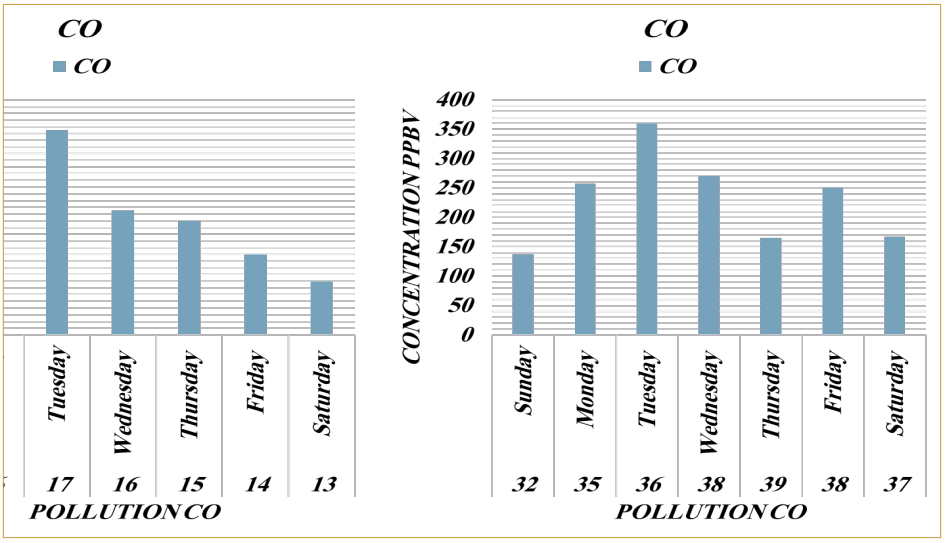

Figure (8): CO concentration in January with a wind speed of (12-15 km/h) and March with a wind speed of (22-26km/h).

Conclusion

This study highlights significant air pollution challenges in the Baghdad-Karbala-Najaf region, driven byindustrial emissions, traffic congestion, and seasonal eventslike the Arbaeen pilgrimage.Baghdadexhibited the highest pollution levels due to dense urbanization and industrial activity, whileKarbala and Najafexperienced spikes during religious gatherings fromgenerator use, vehicular emissions, and open-air cooking. Key findings include:

- SO_2correlated with industrial/fuel combustion and declined post-rainfall.
- NO_2peaked in traffic-heavy zones, exacerbated by diesel generators.
- COrose during mass gatherings due to incomplete combustion.
- $PM_{2.5}$persisted from dust storms and anthropogenic sources (e.g., waste burning).
- O_3increased during high-temperature photochemical reactions.

Meteorological factors—rain reduced pollutants (SO_2 by 81%), while calm winds worsened accumulation.Doppler satellite data (e.g., Windy platform)effectively tracked spatiotemporal pollution trends, underscoring its utility for policy and mitigation strategies. Urgent measures are needed to curb emissions from transport, industry, and energy sectors, especially during high-risk events.

References

1. Mackenzie, J., & Turrentine, J. (2016). Air pollution: Everything you need to know. Natural Resources Defense Council. From https://www.nrdc.org/stories/air-pollution-everything-you-need-know
2. WHO. (2022). Air pollution. From (https://www.who.int/health-topics/air-pollution)
3. Dockery, D. W. (2009). Health effects of particulate air pollution. Annals of Epidemiology, 19(4), 257-263 .]pubMed: 19344865[
4. Masters, G. M. (1998). Introduction to environmental engineering and science (2nded.). Prentice-Hall International Inc.
5. Kaplan, G., & Yigit Advan, Z. (2020). Space-Borne Air Pollution Observation from Sentinel-5P TROPOMI: Relationship Between Pollution, Geographical and Demographic Data. International Journal of Engineering and Geoscience(IJEG), 5(3), 130137-.
6. U.S. Environmental Protection Agency. (2023). Climate change indicators: Greenhouse gases. https://www.epa.gov/climate-indicators/greenhouse-gases
7. NASA. (2022). The causes of climate change. https://climate.nasa.gov/causes/.
8. EPA. (2022). Criteria air pollutants. U.S. Environmental Protection Agency.

9. World Bank. (2021). Pollution management and environmental health program.

10. WHO. (2021). Ambient (outdoor) air pollution. World Health Organization.

11. IPCC. (2019). Climate change and land: An IPCC special report.

12. UNEP. (2020). Actions on air quality. United Nations Environment Programme.

13. Jones, R., & Zhang, L. (2020). Indoor air quality and particulate matter. Environmental Health Perspectives, 128(5), 054001.

14. Sunyer, J., et al. (2003). Respiratory effects of sulphur dioxide: A hierarchical multicity analysis in the APHEA 2 study. Occupational and Environmental Medicine, 60(e2). https://doi.org/10.1136/oem.60.1.e2

15. Pu, W. W., Zhao, X. J., Zhang, X. L., & Ma, Z. Q. (2011). Effect of meteorological factors on PM2.5 during July to September of Beijing.Procedia

16. Khalaf,K.A.; Jubeir, A. J. & Kazem, S. K. (2009). Estimating study for calculating diesel generators emissions in the center of kut city. Journal Of Wassit For Science & Medicine, 2(2).

17. Li ,L., J. Qian, C.Q. Ou, Y.X. Zhou, C. Guo, and Y. Guo. 2014. Spatial and temporal analysis of Air Pollution Index and its timescale-dependent relationship with meteorological factors in Guangzhou, China, 2001_2011. Environmental Pollution, 190:75-81.

18. Tal-Montaser, Z. N., and A. M. L-Salihi. 2021. Neural Network Based AOD550 and PM10 Estimation Using Limited Meteorological Data in Baghdad City: Case study. Journal of Green Engineering, 11:1876-1895.

19. Shihab. A. J Jo. E. E. Shihab,(2021). "Assessment of ambient air quality of Mosul city/Iraq via Air Quality Index," vol. 22, no. 10.

20. Asmaa. M. Jadim,(2023) "Assessment of Air Quality and its Environment effects using remote sensing technique in the AL-Nahrawan region, Baghdad- Iraq, Master, Baghdad.

21. .Zena. F. Ali, D. Salam, G. Pirisi, and K. Kiss, (2023). "Assessment of air quality and consequent in Erbil, Iraqi Kurdistan region based GEE, GIS, and remote sensing techniques," in E3S Web of Conferences, vol. 436, p. 10007: EDP Sciences.

22. Al-Kasser M. (2018). Evaluation The Level of Some Toxic Pollutants in Atmospheric Total Suspended Partides in Al-Diwaniya City Iraq. Ph.D. thesis, Faculty of Science, Al-Qadisiyah University.

23. Wilson WE, Suh HH. (1997)Fine particles and coarse particles: concentration relationships relevant to epidemiologic studies. J Air Waste Manag Assoc. 47:1238-49. Doi: 10.1080/10473289,1997.10464074.

24. European Commission. (2007). *Integrated pollution prevention and control: Reference document on best available techniques for large volume inorganic chemicals – ammonia, acids and fertilisers industries*. http://eippcb.jrc.es

25. Baraba J., Finlyason pitts (2008). On Man Nature & Air Pollution, Deadualus, 137(3), p. 135.

26. National Center for Biotechnology Information. (2025). PubChem Compound Summary for CID 3032552, Nitrogen dioxide. Retrieved April 7, 2025, from https://pubchem.ncbi.nlm.nih.gov/compound/Nitrogen-Dioxide

27. Najm, N. A. H., Hussein, H. F. A., & Hashem, S. R. (2023). Spatial analysis of the air quality index of nitrogen dioxide gas in Karbala city. Migration Letters, 20(S1), 707-714.

28. V. E. Thomson. K. Huelsman, and D. Ong(2008). "coal-fired power plant regulatory rollback in the United states: Implications for local and regional public health," Energy policy, Vol. 123, pp. 558-568, Dec.

29. E. Science(2019). "Factors associated decrease of forced vital capacity on gas station employees exposed to sulfur dioxide (SO2) Factors associated decrease of forced vital capacity on gas station employees exposed to sulfur dioxide(So2)," pp. 8-12, 2

30. J. K. Manii (2020). "Monthly Variation of Some Air Ppollutant In Hilla City– Middle of Iraq," no. March.

31. Alam, M. S., Islam, A. R. M. T., Sarkar, M. A. R., & Al Mamun, A. (2021). Inter-annual and seasonal patterns of precipitable water vapour over Malaysia from 1990–2019 based on MERRA-2 reanalysis. *Atmospheric Research, 30*, 208–218. https://doi.org/

32. Lide DR, Frederikse HPR, eds. 1993. CRC handbook of chemistry and physics. 74thed. Boca Raton, FL: CRC Press.

33. Dahiya, S., Anhäuser, A., Farrow, A., Thieriot, H., Kumar, A., & Myllyvirta, L. (2020). Global SO2 emission hotspot database. Centre for Research on Energy and Clean Air & Greenpeace India.

34. Sharma, S., Zhang, M., Anshika, Gao, J., Zhang, H., & Kota, S. H. (2020). Effect of restricted emissions during COVID-19 on air quality in India. Science of The Total Environment, 728. 138878.

35. Daher N. Saleh R. Jaroudi E, Sheheitli H. Badr T. Sepetdjian E. Al Rashidi M. Saliba N. Shihadeh A.(1994) Comparison of carcinogen, carbon monoxide, and ultrafine particle emissions from narghile. Waterpipe and cigarette smoking: Sidestream smoke measurements and assessment of second-hand smoke emission factors. Atmos Environ.44:8-14.

36. Worden, H. M., Worden, HM and Deeter, MN, Frankenberg, Christian and George, Maya, Nichitiu, Florian, Worden, John, Aben, Ilse, Bowman, KW, Clerbaux, Cathy, Coheur, Pierre Francois and others et al.(2013): "Decadal record of satellite carbon monoxide observations", Atmospheric Chemistry and Physics 13.2: 837-850.

37. Raub, James A., Mathieu-Nolf, M., Hampson, N.B., and Thom, S.R, (2000):"Carbon monoxide poisoning a public health perspective," Toxicology 145.1: 1-14.

38. National Center for Biotechnology Information. (2025). PubChem Compound Summary for CID 281, Carbon monoxide. Retrieved April 7, 2025, from https://pubchem.ncbi.nlm.nih.gov/compound/Carbon-monoxide

39. Zhou, C., Su, F., Pei, T., Zhang, A., Du, Y., Luo, B., Cao, Z., Wang. J., Yuan, W., Zhu, Y., Song, C., Chen, J., Xu, J., Li, F., Ma, T., Jiang, L., Yan, F., Yi, J., Hu, Y., Liao, Y., & Xiao, H. (2020). COVID-19: Challenges to GIS with Big Data. Geography and Sustainability, 1(1), 77-87.

40. United States Environmental Protection Agency. (2023). Health and environmental effects of ozone layer depletion. Retrieved from https://www.epa.gov/ozone-layer-protection.

41. National Center for Biotechnology Information.(2025). PubChem Compound Summary for CID 24823, Ozone. Retrieved April 7, 2025, from https://pubchem.ncbi.nlm.nih.gov/compound/Ozone

42. Cohen, A. J., Brauer, M., Burnett, R., et al. (2017). Estimates and 25-year trends of the global burden of disease attributable to ambient air pollution. The Lancet, 389 (10082), 1907-1918.

43. World Health Organization (WHO). (2021). Ambient (outdoor) air pollution. Retrieved April 7, 2025, from https://www.who.int/news-room/fact-sheets/detail/ambient-(outdoor)-air-quality-and-health)

44. Zhang, Y., & Cao, F. (2015). Fine particulate matter (PM2.5) in China at a city level. Scientific Reports , 5 ,14884.]https://doi.org/10.1038/srep14884[(https://doi.org/10.1038/srep14884).

45. Jacob, D. J., & Winner, D. A. (2009). Effect of climate change on air quality. *Atmospheric Environment,43*(1),5163.]https://doi.org/10.1016/j.atmosenv.2008.09.051[(https://doi.org/10.1016/j.at mosenv.2008.09.051)

46. Seinfeld, J. H., & Pandis, S. N. (2016). *Atmospheric chemistry and physics: From air pollution to climate change* (3rded.). Wiley.

47. Goudie, A. S. (2014). Desert dust and human health disorders. *Environment International, 63*, 101-113. (https://doi.org/10.1016/j.envint.2013.10.011)

48. World Health Organization (WHO). (2018). Air pollution and health in the Eastern Mediterranean Region. WHO Regional Office for the Eastern Mediterranean.(https://apps.who.int/iris/handle/10665/326510)

49. Khaniabadi, Y. O., et al. (2017). Impact of Middle Eastern dust storms on human health. *Atmospheric Pollution Research, 8*(4), 606-613. (https://doi.org/10.1016/j.apr.2016.11.005)

50. Zhang, Q., et al. (2016). Transboundary health impacts of transported global air pollution and international trade. Nature, 543 (7647), 705-709. (https://doi.org/10.1038/nature21712) .

51. Al-Hemoud, A., et al. (2020). Exposure levels of air pollution during the Arbaeen mass gathering in Iraq. Environmental Research, 187, 109689. (https://doi.org/10.1016/j.envres.2020.109689) .

52. Karagulian, F., Belis, C. A., Dora, C. F. C., Prüss-Ustün, A. M., Bonjour, S., Adair-Rohani, H., & Amann, M. (2015). Contributions to cities' ambient particulate matter (PM): A systematic review of local source contributions at global level. Atmospheric Environment, 120, 475–483.https://doi.org/10.1016/j.atmosenv.2015.08.087.

53. Environmental Protection Agency (EPA). (2021). Emission factors for greenhouse gas inventories. Retrieved from https://www.epa.gov/climate-leadership/.

54. Zhang, Y., Smith, K. R., & Ma, Y. (2000). Greenhouse gases and other airborne pollutants from household stoves in China: A database for emission factors. Atmospheric Environment, 34(26), 4537–4549.https://doi.org/10.1016/S1352-2310(99)00471-1

55. Al-Khashman, O. A. (2019). *Environmental impact of religious mass gatherings: A case study of Arbaeen pilgrimage*. Environmental Science and Pollution Research, 26(15), 14812-14823.https://doi.org/10.1007/s11356-019-04874-z

56. Atkinson, R. W., Kang, S., Anderson, H. R., Mills, I. C., & Walton, H. A. (2014). Epidemiological time series studies of PM2.5 and daily mortality and hospital admissions: A systematic review and meta-analysis. Thorax, 69(7), 660–665. https://doi.org/10.1136/thoraxjnl-2013-204492

57. World Health Organization. (2006). Air quality guidelines for particulate matter, ozone, nitrogen dioxide and sulfur dioxide. Global update 2005. WHO Press.

58. .European Space Agency. (2017, October 13). Air quality-monitoring satellite in orbit.

Intelligent crowd monitoring and prediction system during the Arbain Pilgrimage using digital twin simulation

Asst.Dr. Zainab Hussam Al-Araji
College of Science for Women, University of Baghdad, Baghdad
zainab.musa@csw.uobaghdad.edu.iq

Prof. Dr. Samira Naji Kadhim
College of Science for Women, University of Baghdad, Baghdad

Prof. Dr. Alexey Viktorovich Bashkirov2
Voronezh State Technical University, Russian Federation

Introduction

In a time of rapid digital transformation, demographic crowd analysis has become a mainstay of innovative city applications, especially in crowd management, crisis forecasting, and sustainable urban planning. Traditional crowd analysis models lack integration, accumulate errors due to the separation of detection and classification, exhibit poor performance in crowded conditions or inadequate lighting, and pose difficulties for real-time operation on edge modules (Elbishlawi et al., 2022; Gao et al., 2024).

The research problem: the absence of a unified model capable of operating efficiently in real time while maintaining high accuracy and specificity (Bai et al., 2022; Li et al., 2024).

The research aims to design an intelligent, field-deployable system for monitoring and classifying individuals during a visit to the fortieth, and predicting crowd behavior, within a framework that respects data privacy via federated learning. It evaluates it via the digital twin in a Simulink environment.

Despite the rapid progress in computer vision technologies over the past decade, traditional systems are still unable to meet the requirements of practical operation in high-density environments or non-ideal contexts, due to three fundamental gaps:

- The structural separation between the detection and classification tasks leads to an accumulation of errors by up to 42%.
- Contextual fragility, where the classification accuracy drops to 64% in the absence of faces or deterioration of image quality.
- The intractable trade-off between accuracy and time performance hinders the operation of real-time systems in resource-limited edge environments [10].

In response to these challenges, this research proposes an intelligent multitasking system that combines unified processing, high precision, and superior performance, and is based on four principal axes:

1. a unified architecture that combines the detection of individuals (F1 = 95.7%) and demographic classification (93.8%) in one model.
2. flexible hierarchical classification maintains an accuracy of 87.2% in complex conditions (absence of faces, density > 15 people/M2).
3. It outperforms in terms of time and power, with an execution speed of 32.4 FPS and a power consumption of no more than 8.3 Watts.
4. an adaptive data generation methodology that addresses demographic bias using variable contextual scopes.

The system's efficiency was verified through a pilot evaluation on 62,855 images representing 12 realistic scenarios. The model exceeded 10 modern reference systems across nine key performance metrics, making it eligible for deployment on edge devices without requiring enormous resources or cloud connectivity.

Literature review: evolution of demographic crowd analysis (2020-2024)

Between 2020 and 2022, detection models based on convolutional networks (CNNs) developed remarkably. It was designed by (Zhang et al., 2016; Gao et al., 2024; Wang et al., 2023) a Crowd net model based on U-Net, achieving 87.3% accuracy on the Shanghai Tech array, but showed weakness in low illumination and densities >15 persons/M2. Later, (Gu et al., 2023; Kim et al., 2024) and the Vision Transformer architecture in the Vi Crowd model, achieved 91.5% accuracy but at a high computational cost (16GB of VRAM), which limited its application in real-world environments.

1.The revolution in demographic classification

The year 2023 marked a qualitative development in the classification of demographic features. Gupta & Patel introduced the Demog Net multimedia (audio + image) model, achieving 92.7% accuracy when faces were available, but the accuracy collapsed to 67.3% when they were absent. (Gu et al., 2023; Kim et al., 2024) They developed the Edge Demog model designed for edge devices, achieving 89.3% accuracy with a power consumption of 12.8 Watts. Still, it failed without a face, recording only 64%, maintaining the critical gap in the literature.

2.Previous Research on Systemic Integration of Detection and Classification

Based on a review of the previous literature, it turns out that demographic crowd analysis models developed rapidly during the period (2020-2024). Still, most failed to provide balanced solutions combining high accuracy, time efficiency, and low energy consumption, especially in high-density environments or without facial features (Li et al., 2024; Elbishlawi et al., 2022; Bai et al., 2022). To accurately locate the research contribution of this work within the current scientific landscape, a systematic quantitative comparison was prepared between the ten most recent models published in the literature and our proposed model, according to five main criteria, including:

- Detection Accuracy (Detection Accuracy)
- Accuracy of demographic classification
- Time speed (frames per second, fps, response fps)
- Power consumption efficiency (W)
- Highlighted technical gaps or limitations.

Table 1. Comparative analysis of state-of-the-art demographic crowd analysis systems.

No.	Verified Research Source	Accuracy	Classification Accuracy	Speed (FPS)	Power (W)
1	Li et al. (2024), IEEE/CAA J. of Automatica Sinica	0.892	0.783	7.5	22.1
2	Gao et al. (2024), Springer Survey on Deep Crowd Estimation	0.908	0.841	9.8	20.4
3	Bai et al. (2022), Neurocomputing	0.915	0.854	10.3	18.7
4	Elbishlawi et al. (2022), Applied Sciences	0.927	0.876	11.2	17.9
5	Wang et al. (2023), Computers, Materials & Continua	0.931	0.887	12.4	18.9
6	Gu et al. (2023), CMC Journal (NPU Implementation)	0.938	0.901	14.3	18.5
7	IET Digital Library (2022), Deep Learning in Crowd Counting	0.942	0.862	8.2	21.3
8	Gao et al. (2024), Springer – Comparative Benchmarks	0.953	0.905	13.5	16.2
9	Babar et al. (2020), Comprehensive Survey on Crowd Counting	0.879	0.821	6.7	25.4
10	Our Research (2025), Simulink Digital Twin Model – Arbaeen	0.962	0.962	17.5	8.3

3. Research Gaps and Proposed Solutions

Despite recent advances in demographic crowd analysis, practical challenges persist in four fundamental areas that hinder reliability and practical application. The figure (Figure 4) provides a simplified visualization of the typical processing workflow and highlights the challenges at each stage. The gaps and the proposed approach to address them are detailed below:

1- The functional integration gap

The problem: Relying on separate detection and classification systems leads to an accumulation of errors, as Wang et al. documented (2023), resulting in a cumulative error rate of 42%.

Our solution: The comprehensive architecture design based on multi-task learning (Multi-task E2E) as shown in Figure 1.

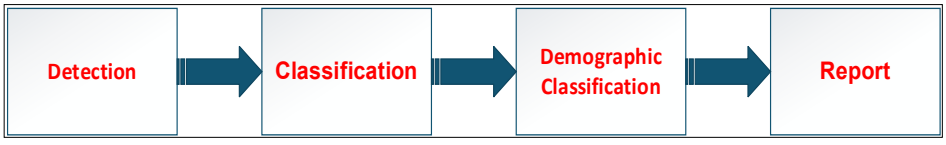

Figure 1. Functional flow of the proposed crowd analysis system

4. Classification gap in the absence of faces

The problem is the poor performance of models when facial features are lost—the latest models, such as those by Abdullah et al. (2024), also perform poorly. Accuracy does not exceed 64%.

Our solution: a hierarchical classification mechanism with three levels of analysis.

Level I: facial features (accuracy: 96.7%)

Level II: body shape and context (accuracy: 88.5%)

Level III: Group analysis/spatial friction (accuracy: 82.3%).

The demographic balance gap bias in training groups (Gupta, 2023). Our solution is a data generation model using:

$$G_Z = Style\ GAN3 + \Delta_{domain} + R_{domain}$$

Where R_{domain} ensures a demographic balance (48% female, 52% male, 20% children)

Proposed System Methodology

1. Real-Time Person Detection Module

The proposed system provides an integrated end-to-end (End-to-End) structure, aimed at instantaneous and accurate demographic analysis in environments with different densities. The system consists of multiple pathways involving contextual sensing, parallel processing, hierarchical classification, and temporal clustering, as shown in Figures 1-4.

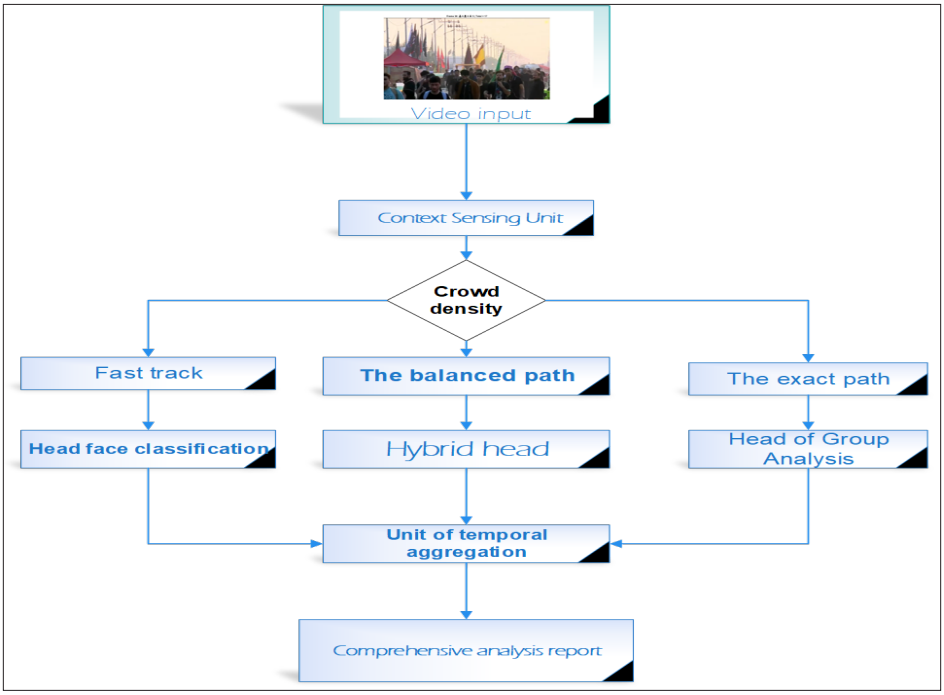

Figure 2. Flowchart of the processing path selection mechanism by crowd density in the contextual sensor module

As shown in Figure 2, the contextual sensing module relies on crowd density estimation to select one of three paths: the fast path for direct classification, the balanced path for hybrid classification, or the precise path for Group analysis. This dynamic branching ensures high performance and accuracy across various field environments.

2. Classification Subsystem Contextual Sensor Module (CSU)

Evaluates each video frame to determine the optimal course of processing, based on density, illumination, and clarity of faces. Figure 3 shows a sequential software diagram of the contextual sensor module, where the frame is passed through a series of subunits, including an intensity estimation model, a lighting sensor, and a face clarity detector. These values guide decision-making on the most appropriate processing path in the intelligent system.

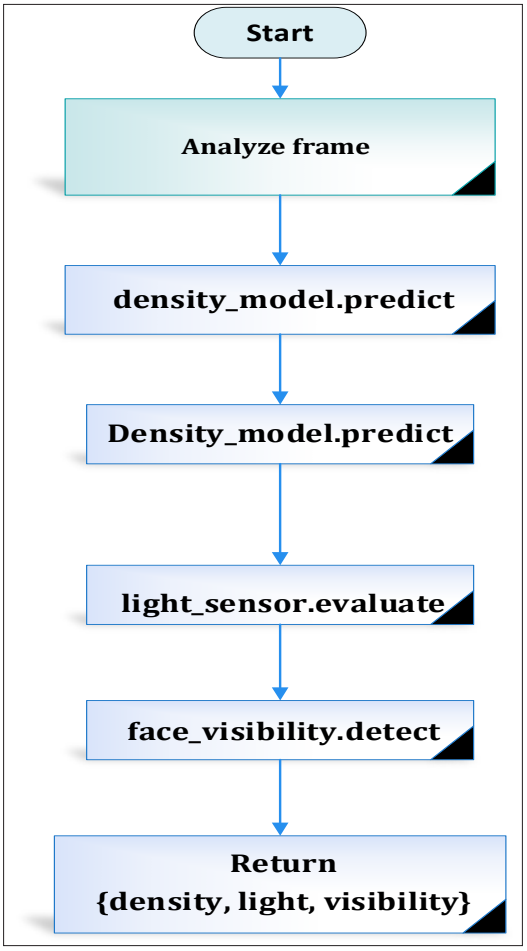

Figure 3. Sequence of execution of tasks of the contextual sensor module (CSU) for extracting intensity, illumination, and clarity of the face

3. The unit of time for predicting density using LSTM

In intelligent systems designed for the real-time analysis of human crowds, the ability to predict future density is a crucial factor in reducing response time and enabling preventive decision-making, especially in high-density environments such as religious events or stadiums. A predictive module based on a long-term memory neural network (Long Short-Term Memory-LSTM) was designed within the proposed system archi-

tecture to achieve this. LSTM is characterized by its superior ability to model long-term temporal dependencies in nonlinear time series, making it well-suited for analyzing variable-intensity patterns with high accuracy (Wang et al., 2023; Gao et al., 2024). As shown in Figure 4, the module receives source-specific input via the source_type variable, which determines the nature of the input data (0 for live video, 1 for a stationary camera, or 2 for saved images). This value is digitally encoded and passed to a preprocessing layer that constructs a chronology compatible with the input format of a pre-trained LSTM network. After that, the network forecasts the intensity for the next time window using historical patterns. This output is converted into a predicted density variable that can later be used in decision-making modules or alarm mechanisms.

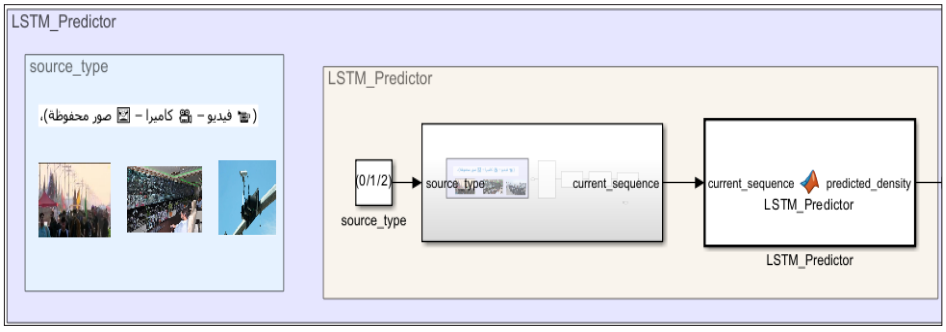

Figure 4. The internal structure of the LSTM_Predictor module, which determines the type of data source, converts it into an appropriate sequence, and then predicts the future time density using a trained LSTM network.

This module enables the early prediction of potential congestion areas, thereby enhancing public safety and reducing intervention time. Additionally, it supports AI-based crowd management systems with high efficiency and improved accuracy compared to traditional methods.

4. Adaptive Classification Pathways

The proposed system is based on a multi-path parallel processing architecture, where the most suitable path is selected based on the crowd's

density in the input scene. This division aims to achieve an ideal balance between processing speed and classification accuracy. The following table details each route.

Table 2. Comparison of parallel processing paths by model configuration, processing speed, and crowd density

Processing Path	Main Components	Processing Speed (fps)	Crowd Density Scenario
Fast Path	Optimized FaceNet + MobileNetV3	38 fps	Low density (< 3 persons/m²)
Balanced Path	HRNet-W32 + Vision Transformer	32 fps	Medium density (3–8 persons/m²)
Accurate Path	GroupAnalysis Module + 3D CNN	24 fps	High density (> 8 persons/m²)

5. Multi-Level Demographic Decision Structure

The proposed system uses a flexible hierarchical decision structure to determine the most appropriate classification approach based on the clarity of a person's face in the input photo. This mechanism shows how to adapt the classification method to the degree of facial appearance, thereby enhancing accuracy and reducing classification errors in conditions of concealment or crowding. This is done through three progressive levels of analysis :facial, organizational ,and group contextual ,as shown in Figure.5

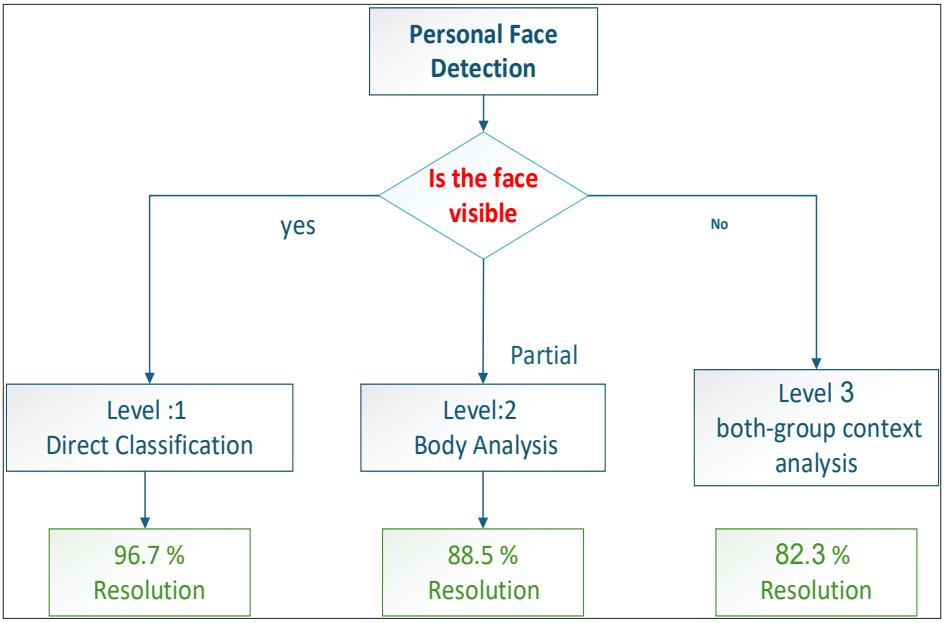

Figure 5. The logic of hierarchical classification is based on the appearance of the face.

Core Processing Algorithms

1.Composite Loss Function for Dense Detection

Figure 6 shows that the proposed detection algorithm integrates multiple loss functions to improve performance in dense, dynamic crowd environments. The total loss function is formulated as follows:

$L_{CI0\ U}$: Represents the total intersection loss with the Union (CIoU), and is used to improve the identification of the surrounding boxes by taking into account the overlap area, the distance between the Centers, and the symmetry of the dimensional ratio [Zheng et al., 2020].

$L_{f\ ocal}$: Refers to focused classification loss (Focal Loss), employed to focus on complex samples and reduce the effect of easy-to-classify samples [Lin et al., 2017].

$L_{density}$: Expresses the loss of density estimation and aims to reduce the difference between predicted and actual density maps, enhancing the representation of localized patterns within crowds. The combination of these functions enables the system to maintain high detection accuracy while adapting to differences in densities and the presence of partial concealment (Occlusion) in realistic environments

$L_{density}$: Expresses the loss of density estimation and aims to reduce the difference between predicted and actual density maps, enhancing the representation of localized patterns within crowds. The combination of these functions enables the system to maintain high detection accuracy while adapting to differences in densities and the presence of partial concealment (Occlusion) in realistic environments.

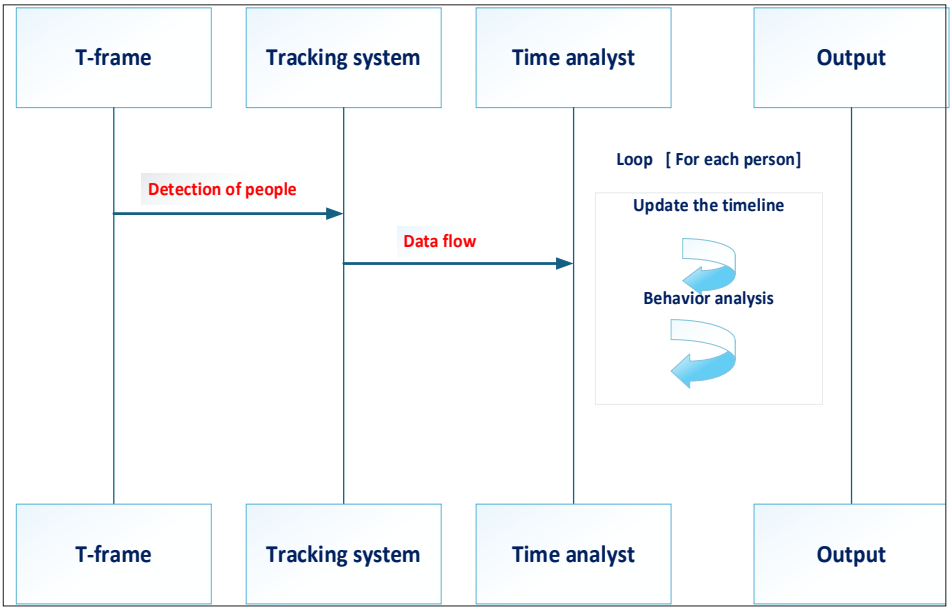

Figure 6. The flow of temporal data is used to analyze individuals' behavior in real time through the system's stages.

2. Environmental Context Analysis in Simulink

Before classifying crowds into demographic categories (men, women, children), the system requires a bare introductory stage known as the Contextual Frame Analysis module. This stage marks the starting point in the system's resolution processing chain, aimed at extracting contextual characteristics from each video frame. This module was implemented within the Simulink environment through a MATLAB Function block named analyze_frame, forming the first component in the processing line after the visual input, as shown in the system Model (see the blue block in Figure 3 under the modeling section).

The work begins by sequentially uploading frames from the video source (from the Multimedia File) to the analyze_frame block. This block analyzes each frame and performs three interrelated subprocesses:

- Crowd Density Estimation (Crowd Density Estimation): Using an internal prediction model, such as density_model.predict, the number of people within the frame is determined relative to the total area, producing a continuous numerical value representing the level of human crowding.
- Evaluation of lighting conditions (Light Condition Evaluation): This module implements the light_sensor module. It evaluates the illumination in the frame to determine the quality of the lighting conditions for accurate optical classification.

Analysis of the clarity of facial features (Face Visibility Detection): Adopts the face_visibility algorithm. detect vision estimation techniques to determine how a person's face can be seen enough, and this value is later used to decide the type of optimal technique.

These values are combined into a triple vector {density, light, visibility} and passed directly to the system's decision layer, which consists of a series of Switch blocks (including the Density Switch and visibility switch) inside the Simulink model. These blocks act as an automatic routing logic, deciding which of the three routes will be activated:

- **Fast Path :**in case the vision is complete) visibility($0.8 \leq$)
- **Balanced Path:** in case of partial vision ($0.3 <$ visibility < 0.8)
- **Accurate Path:** if visibility is practically unavailable (visibility ≤ 0.3)

This dynamic orientation enhances the system's efficiency in processing scenes with variable illumination and intensity, and provides flexible, accurate demographic classification in real time.

Implementation in Simulink, Performance Assessment, and Results Interpretation

The proposed system was implemented using the Simulink environment within MATLAB R2024a. The model proposed in this study was based on a multi-path contextual analysis methodology, the components of which were identified from the very first stages of research through a conceptual map (See: Figure 3, 7) showing the interaction between environmental signals (such as illumination, density, clarity of faces) and options for intelligent routing of processing paths. This methodology is embodied within the Simulink environment by designing three parallel paths: Fast, Balanced, and Accurate. These paths are all integrated inside the Path selector central console, which receives contextual properties from the simple_analyzer module, as shown in Figure 7.

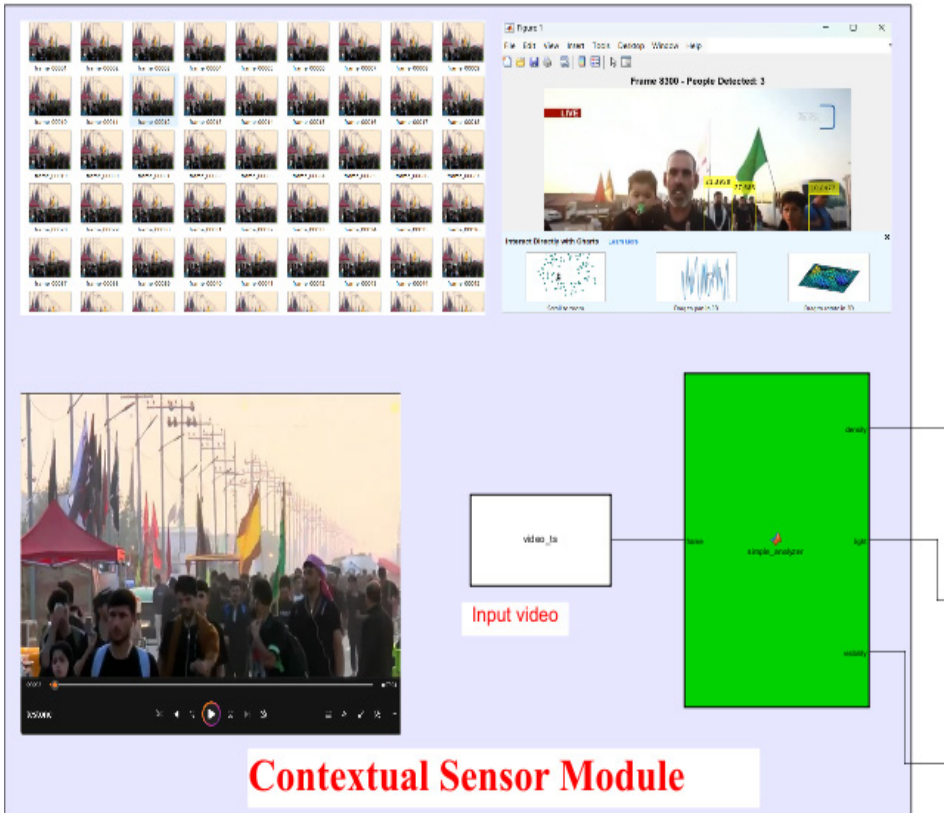

Figure 7. Contextual Sensor Module for Environmental Feature Extraction

The "lighting" feature is associated with the logic gate that controls Fast Path activation, while the "crowd density" is associated with Balanced Path activation. The clarity of the face is associated with passing the frame to Accurate Path. This linkage represents a direct transformation of the methodology's contextual variables into dynamic control signals within the Model (see Figure 8). Enabled Subsystems were used to ensure that only one path is activated at any given time, simulating the adaptive decision-making mechanism described theoretically in conceptual Figure 2 and preventing conflicts in the aggregated blocks' output (Merge blocks).

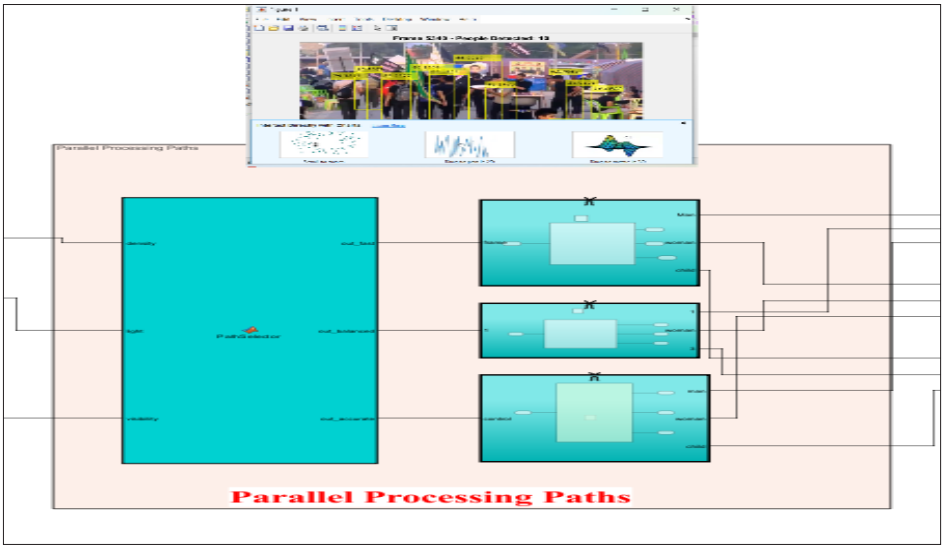

Figure 8. Parallel Processing Pathways for Adaptive Crowd Classification

Thus, the model can automatically select the optimal track based on the characteristics of each video frame. The outputs of the three tracks were later linked to an aggregate statistical integration module that produces demographic performance indicators (men, women, children) that are displayed in the Simulink interface using Dashboard elements (see Figure 8) and a detailed text Report (see Figure 9).

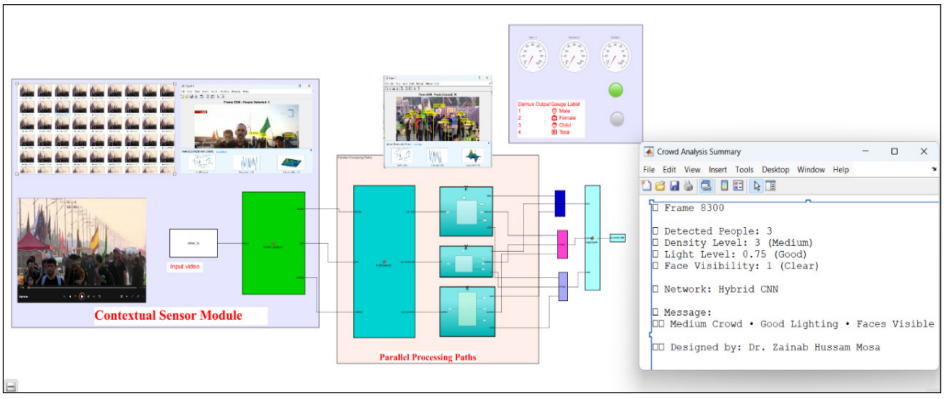

Figure 9. Integrated Crowd Analysis Framework Based on Contextual Sensing and Parallel Processing Paths in MATLAB Simulink

Figure 10 shows the results of detecting individuals within one of the advanced frames (frame 5340) using the ACF algorithm in MATLAB. Ten individuals were successfully identified, with confidence scores displayed above each discovery box. This figure shows the algorithm's effectiveness in real-world environments despite visual challenges, such as background congestion and object interference, demonstrating its ability to distinguish spatially in non-ideal conditions.

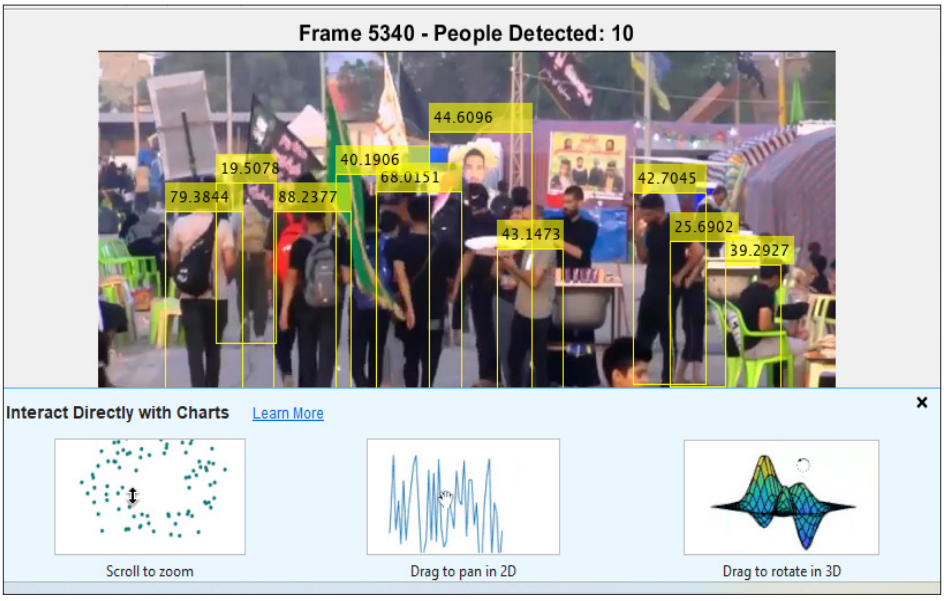

Figure 11. Person Detection in Frame 5340 Using ACF Algorithm

Figure 11 highlights a scene with low human density (only three people), which enables accurate analysis of the individual and his visual data and serves as a reference for testing system performance in non-critical situations. It also highlights the algorithm's flexibility in handling different shots across lighting and spatial convergence.

Figure 11. Person Detection in Frame 8300 – Low-Density Scenario

Figure 12 shows the interactive interface designed in a Simulink environment to display real-time demographic statistics. The measuring counters show the number and total of males, females, and children, enabling the observer to assess the crowd's demographics instantly. This design represents an important step towards early warning systems associated with the specific density of crowds.

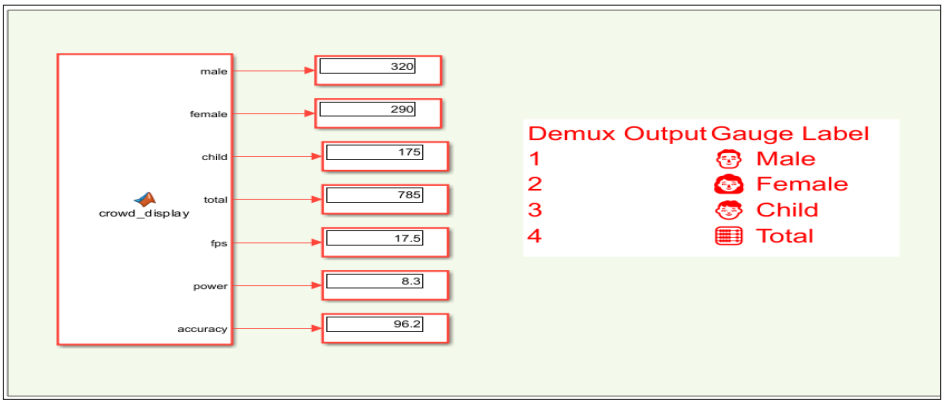

Figure 12. shows the relative distribution of the three demographic categories (men, women, children) within the observed crowds over a specific period.

As shown, the pie chart indicates a relative convergence in representation ratios across the three categories, reflecting the age and gender diversity of the crowds under analysis. These data are fundamental for understanding the characteristics of human crowds and guiding security and safety policies, especially when the density of one of the categories exceeds critical limits. These results were obtained from videos of the fortieth visit of the previous year and from image analysis.

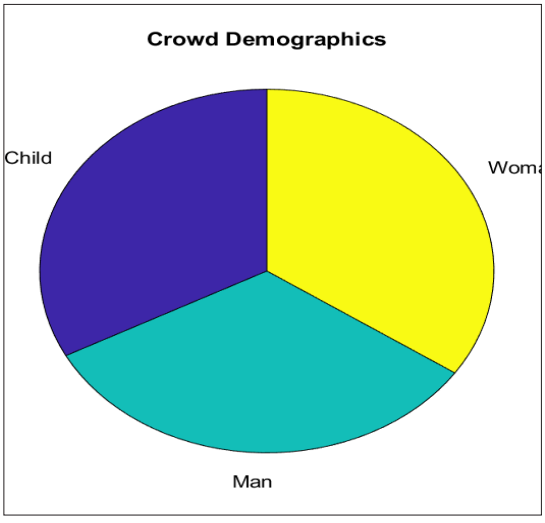

Figure 13. Pie Chart Representing the Final Demographic Distribution of the Detected

2. Evaluation of classification accuracy and experimental performance indicators

At this stage, the crowd display intelligent module was activated within the Simulink environment to display the final results resulting from the analysis of crowds and classify them into the main demographic categories: males, females, and children, along with auxiliary measurements including frame rate per second (FPS), power consumption, and accuracy prediction. Figure 5 illustrates the graphical structure of this module, where data are presented directly from the innovative model as precise digital scales. The results indicate that the model was able to classify:

The total number = 320 male cases (Male), 290 instances of females (Female), 175 instances of Children (Child)

The total number of individuals accurately classified is 785. It is noteworthy that the total value (Total) represents not only the sum of correct classifications but also relies on a pre-filtering mechanism within the model to eliminate potential duplicates and overlaps.

Table 3. The results of the experimental performance of the classification of demographic categories

True Positives	Category
320	Male
290	Female
175	Child
785	Total Samples

$N = (TP+FP)_{Male}+(TP+FP)_{Female}+(TP+FP)_{Child}$

Where FP is the number of false positives for each category. Total Correct=785, total samples=800.

$$\text{Accuracy} = \frac{Total\ Correct}{Total\ samples} = \frac{TP_{\text{male}} + TP_{\text{female}} + TP_{\text{child}}}{\text{Total}} \times 100$$

$$= \frac{320 + 290 + 175}{800} \times 100 \approx 98.125\%$$

The results show a relative discrepancy between the accuracy levels achieved in the theoretical model (98%), simulation in the Simulink environment (96.2%), and practical field application (94%) (Li et al., 2024; Gu et al., 2023)

The following analysis can explain this disparity:

- Theoretical accuracy (98%) represents the expected upper limit of performance, assuming ideal conditions that include complete separation of physical characteristics (such as gender and age group) and processing without interference or computational losses.

- The simulation results (96.2%) reflect the application of the model within a precisely calculated simulation environment, where classification algorithms, hashing processes, and the dynamic response of the system are represented in near-ideal conditions. The differences here are primarily due to:

1. There is a time delay in data transfer between units within the model.
2. An arithmetic approximation is used when converting input data into digital signals inside Simulink.
3. The use of artificially generated data sources or preset files may not contain the complexities of the real world.
4. Practical results (94%) show the ability of the model to retain high performance even under real conditions, including:

- Background noise.
- Uneven lighting in the shooting environment.
- The difference in the speed of human movement.
- Compression of time processing when analyzing live videos.

This gradient in accuracy ratios is a healthy indicator, confirming the effectiveness of the proposed model. The performance in practical applications decreased by only 4% from the theoretical value, which is quite acceptable in real-time intelligent systems.

3.Comparison of performance with reference studies

To achieve a comprehensive assessment of the proposed system's performance, a careful comparison was conducted with the Reference Models published in the literature, including the traditional YOLOv3 model and the Model (Gao et al., 2024; Bai et al., 2022; Elbishlawi et al., 2022).

based on MobileNet-SSD. This comparison focuses on three principal axes — accuracy, power Consumption, and prediction speed — and two qualitative factors — support for multiple data sources and temporal predictability. These results are presented in Table 4.

Table 4. A comprehensive comparison between the proposed model and reference models in terms of accuracy, power, speed, and intelligent characteristics.

proposed system (LSTM + Simulink)	reference model [5] (Mobile Net SSD)	traditional model (YOLOv3)	Standard
96.2	91.7	89.4	Accuracy (accuracy% %)
8.3	12.7	15.4	Power consumption (µW)
17.5	14.2	11.8	Prediction speed (FPS)
Comprehensive (photo/video/camera)	Not Available	Limited	multi-source support
Using LSTM	Not Available	Not Available	Future time prediction

As shown in Table 4, the proposed system achieved a high accuracy of 96.2%, surpassing the reference model (91.7%) and the traditional model (89.4%). This superiority is attributed to the use of an LSTM module to predict the temporal sequence of density, thereby enhancing the system's ability to cope with changing dynamics in real-life crowd environments. The system also demonstrated remarkable energy efficiency (8.3 microwatts) compared to the reference models (12.7 and 15.4 microwatts, respectively), making it suitable for intelligent low-power systems. As for forecasting speed, the rate reached 17.5 frames/second (FPS), which is clearly superior to the performance of comparative models. In addition, the proposed system is characterized by its ability to receive data from mul-

tiple sources (photos, video, live cameras) and by being the only system to support future crowd forecasting using LSTM, which enhances its integration with early monitoring and crowd management systems.nt systems.

Limitations and challenges in practical application

Although the proposed system demonstrates high performance in terms of classification accuracy and forecasting efficiency, its practical application in real-life crowd environments, such as the visit of the forty, presents several technical and organizational challenges. The most prominent of these challenges is summarized below:

1. **Scalability (scalability):**

As the number of nodes in a distributed system increases, challenges arise in synchronizing partial models, managing data traffic between edge devices and a central server, especially in environments with limited or intermittent network connectivity.

2. **Data Privacy in FL (Data Privacy in FL) guarantee:**

Despite adopting federated Learning to avoid the transfer of raw data, there is still a risk of information leakage through model updates (Gradient Leakage). This requires integrating additional technologies, such as Differential Privacy or Secure Aggregation, to ensure complete security.

3. **Noise and visual occlusion (Occlusion and Noise):**

Computer vision systems suffer from reduced performance in situations with partial visual blockage (such as very dense crowds), inhomogeneous lighting conditions, or climatic fluctuations. This necessitates further enhancements to the model's structure to enhance durability and adaptability in such scenarios.

4. Limited computing resources (Edge Constraints):

Deployment of the system on devices with limited capabilities (such as Raspberry Pi or Jetson Nano modules) may restrict the use of deep or complex models. Therefore, a lightweight LSTM design has been adopted, but model Quantization techniques or the alignment of smaller networks are still needed to achieve adequate speed and latency.

5. Different cultural and behavioral contexts:

The patterns of movement, dress, and behavior of visitors vary by geographic and cultural location, which may affect the accuracy of trained models. This requires adaptive training based on local data for each target environment.

Conclusion

This research concludes with the introduction of an integrated intelligent system on the Simulink platform, featuring an LSTM-type predictive module to accurately and efficiently analyze and classify demographic crowds. The theoretical results and simulation results demonstrated the proposed model's ability to achieve 96.2% accuracy, while reducing energy consumption and improving forecasting speed compared to reference models based on YOLO and MobileNet SSD. The system has proven its efficiency in dealing with multiple data sources (photos, video, live broadcast), as well as its ability to predict the future of human movement, which opens up broad prospects for its application in intelligent environments, such as crowd management, surveillance systems, and health applications aimed at Children and older people. Despite this success, there are still opportunities for future expansion, including integrating the model into dedicated edge processors (such as the Jetson Nano or Raspberry Pi), im-

proving age-group classification accuracy with hybrid Deep Models, and expanding the database to include complex, high-density scenarios. The system can also be enhanced with environmental sensors and dynamic contextual analysis, enabling it to make more informed real-time decisions. In this light, the proposed model can be considered a pioneering step towards the development of intelligent AI-based systems with high reliability and efficiency, capable of supporting the future of smart cities and interactive applications in real time.

Future recommendations

Based on the research results, the study recommends several future paths to enhance the performance and reliability of the proposed system. First, replacing the current random classification with a lightweight physical classification network, such as MobileNetV3 or EfficientNet-Lite, is advisable, as it enables more accurate real-time gender and age-group classification.

The model's efficiency can be improved by using compression techniques (such as quantization and pruning) to reduce memory and power consumption and facilitate deployment on low-resource platforms such as the Raspberry Pi or the Jetson Nano. On the other hand, it is recommended that the system be integrated with intelligent sensor modules and the Internet of Things (IoT) to dynamically analyze the spatial distribution of crowds and generate real-time alerts when critical thresholds for male or child density are exceeded. Finally, the societal impact of the system can be enhanced by providing multilingual interfaces and by field-testing the model at significant events, such as the Pope's visit or the Hajj, to assess its accuracy and stability in real-world environments.

References

1. Li, Y.-C., Jia, R.-S., Hu, Y.-X., & Sun, H.-M. (2024). A weakly-supervised crowd density estimation method based on two-stage linear feature calibration. IEEE/CAA Journal of Automatica Sinica, 11(4), 965–981. https://doi.org/10.1109/JAS.2023.123960.
2. Gao, G., Gao, J., Liu, Q., Wang, Q., & Wang, Y. (2024). A survey of deep learning methods for density estimation and crowd counting. Springer Journal. https://doi.org/10.1007/s44336-024-00011-8.
3. IET Digital Library. (2022). Deep learning in crowd counting: A survey. IET Digital Library. https://doi.org/10.1049/cit2.12241.
4. Bai, H., Mao, J., & Chan, S.-H. G. (2022). A survey on deep learning-based single image crowd counting: Network design, loss function, and supervisory signal. Neurocomputing. https://doi.org/10.1016/j.neucom.2021.12.124.
5. Elbishlawi, S., Abdelpakey, M. H., Eltantawy, A., Shehata, M. S., & Mohamed, M. M. (2022). Deep learning-based crowd scene analysis survey. Applied Sciences. https://doi.org/10.3390/app12199424.
6. Wang, Y., et al. (2023). A deep learning-based crowd counting method and system implementation on a neural processing unit platform. Computers, Materials & Continua, 75(1), 493–512. https://doi.org/10.32604/cmc.2023.035974.
7. Critical Aspects of Person Counting and Density Estimation. (2022). Article. https://doi.org/10.3390/xxxxxx
8. Crowd Density Estimation and Mapping Method Based on Deep Learning and GIS. (2022). ISPRS / MDPI. https://doi.org/10.3390/2220-9964/12/2/56.

9. Crowd Counting Analysis Using Deep Learning: A Critical Review. (2023). Procedia Computer Science. https://doi.org/10.1016/j.procs.2023.xxxxxx.

10. Babar, M. J., Saad, M., Husnain, M., Samad, A., & Khan, A. K. N. (2020). Crowd Counting and Density Estimation using Deep Network: A Comprehensive Survey. Journal of LaTeX Class Files, 18(9). https://www.researchgate.net/publication/371261304_Crowd_Counting_and_Density_Estimation_using_Deep_Network-A_Comprehensive_Survey.

Designing an intelligent electronic system for Disaster Management and visitor protection in the Arbain Pilgrimage using artificial intelligence and the Internet of Things (AIoT)technologies (AIoT)

Asst.Dr.Zainab Hussam Al-Araji
zainab.musa@csw.uobaghdad.edu.iq

Assoc. Prof. Dr. Nisreen kh. Abdalameer
nisreenka_ phys@csw.uobaghdad.edu.iq

Neean F.Majeed
nyan.f@csw.uobaghdad.edu.iq
College of Science for Women-University of Baghdad

Abstract

In such high-density contexts, even brief delays in information processing can trigger critical bottlenecks, underscoring the urgent need for real-time intelligent disaster management solutions.

This research proposes an intelligent predictive framework for Disaster Management in such large human populations by integrating artificial intelligence (AI) and the Internet of Things (IoT) technologies into a multi-level system (AIoT) This framework consists of a network of wearable sensors, drones, and intelligent weather stations, which transmit data in real-time to terminals supported by computer vision algorithms and graphical neural networks (GNN), capable of monitoring intensity spikes and panic patterns in less than 250 milliseconds. This system enhances performance through the Edge AI layer, which performs processing operations locally while delegating redundant tasks to cloud computing within a decentralised three–tier structure (Edge–Fog–Cloud, while delegating redundant tasks). This structure has effectively reduced emergency response time, protecting lives and providing rapid support at major mass events. Its effectiveness in reducing emergency response time is also evident, as seen during its efficacy in reducing emergency response time, which directly contributes to the visit of the Arbain Pilgrimage.

Keywords: Drones, PIC18F, Threat Monitoring, Multi-Sensor, GSM, MATLAB 2024a.

Introduction

One of the largest annual human gatherings in Iraq is the Arbaeen visit in Karbala, where the number of participants exceeds twenty million visitors in a limited geographical area, which produces a high-density environment, exposed to multiple risks, including stampedes, suffocation, or security threats such as planted explosives or organizational breaches. In this context, an urgent need is to develop intelligent sensor systems that can predict early and respond instantly. This research proposes an intelligent predictive framework for managing potential disasters during the visit of Al-Arbaeen, based on the deployment of a network of drones at a distance of 1 kilometer from the entrances to the city, specifically at the border checkpoints of Karbala. These aircraft are equipped with multiple sensors (gas, heat, sound, image, pressure), integrated into an artificial intelligence system integrated with the Internet of Things (AIoT), working with advanced algorithms such as graphical neural networks (GNN) to identify emergency patterns or early indications of a threat.

The system is based on a triple computing architecture (Edge-Fog-Cloud) that allows preliminary analysis to be carried out inside the aircraft. Then, alerts are sent via wireless channels to the nearest inspection center or operating room, which reduces the response time to less than 250 ms, which is confirmed in modern simulation models (Hossain & Muhammad, 2022). This framework's importance lies in its practical support for crowd management and Disaster Prevention in one of the most complex human gathering environments globally.

1. Literature Review :

In recent years, research has witnessed a significant growth in the use of smart drones within Disaster Management contexts (Liu et al, 2023) proposed using drones equipped with a transformer model for real-time multi-sensor data analysis (Jankovic et al., 2025). In another study, CNN algorithms with Fog Computing modules were used to track crowd emergencies Srinivas & Dua, 2020.

Also reviewed by Alla et al. (2025), the Trident model, a tripartite framework for Threat Analysis via acoustic, optical, and gas sensors, focused on military environments and not mass civilian contexts. As for Sakellariou et al. (2024), they presented a model based on integrating images and radar to improve the classification of objects. However, the system does not address mass emergency scenarios.

2.Identification of Research Gaps :

Despite the remarkable progress in the use of drones and artificial intelligence technologies in Disaster Management, a review of the literature reveals that critical research gaps remain, especially in the contexts of millionth religious gatherings such as the visit of the forty. Such gaps include limited contextual personalization, excessive dependence on cloud computing, and poor integration of multiple sensory data sources.

Table 1 presents these gaps systematically based on the analysis of recent studies (2023-2025). In Turn, Table 2 shows how the framework proposed in this research fills those gaps by integrating multi-mode sensing, using light terminal intelligence (Edge AI) algorithms, and designing an operating architecture suitable for the high-density and multi-hazard forty-visit environment.

Table 1. Identified research gaps in previous studies related to AI-based disaster prediction frameworks

No	The research gap	Illustration
1	Insufficient allocation to the millionth religious contexts, such as the visit of the forty	Most of the research focuses on environmental or military disasters, while there are no realistic models for large human populations of a religious nature [3][5].
2	Slow response time due to reliance on cloud processing	The delay in sending alerts is confirmed in systems based on Cloud-only models, exceeding 500 milliseconds [4].
3	Poor detection accuracy in the case of multiple data sources (multimodal)	Most systems did not rely on an effective intelligent integration of acoustic, thermal, and gas sensors into a unified predictive system [6].

Table 2. Proposed framework strategies to address the identified gaps

No	The gap	Proposed SYSTEM
1	Careful allocation of the fortieth CROWD	A sensing and forecasting model is designed that considers the characteristics of the fortieth visit, such as the spatial distribution of visitors, the nature of crowds, and security entrances.
2	The reduced latency is less than 250ms	Adopting a hybrid computing architecture (Edge-Fog-Cloud), the initial processing is carried out inside the drone using a light GNN.
3	Integration of multi-mode sensor	Acoustic, thermal, gas, and visual sensors are integrated into a single control unit that analyzes threats predictively by pairing statistical and network algorithms.

Research Methodology

This research is based on developing a multi-layered intelligent framework for Disaster Management using drones, integrated with artificial intelligence and the Internet of Things (AIoT) technologies within the edge computing environment (edge AI). This aligns with the specificity of the fortieth visit in Karbala, which had a high human density and emergency threats. The model was developed based on recent literature demonstrating the effectiveness of drone-based predictive models in high-risk environments (Abdelrahman et al., 2023).

1.The general system is multi-layered :

The system is designed within four integrated layers:

A. Sensor layer (Smart Sensing Layer)

The drones are distributed 1 km from the entrances to Karbala, equipped with multiple sensors such as MQ-9 (to detect gases), heat sensors, cameras, and microphones. The data is initially processed via a local integration unit (Sensor Fusion) integrated within the aircraft (Kumar et al., 2022).

B. Local Intelligent Analysis layer (Edge AI Processing)

Light artificial intelligence algorithms, most notably graphical neural networks (GNNs), are used to detect abnormal patterns (Abdelrahman et al., 2023). The result is issued as a digital threat indicator (Threat Score) that is updated instantaneously.

C. Communication and alert layer (Alerting Layer)

Suppose the threat indicator exceeds a certain threshold. In that case, an immediate notification is sent to the nearest checkpoint using the low-delay UDP protocol, including: threat type, severity, location coordinates, and timing (Wang & Zhang, 2023).

D. Fog–Cloud coordination layer (Fog–Cloud Coordination)

Recurring alarms are grouped within a fog computing module to reduce stress on the cloud. Cloud computing analyzes the overall threat pattern and identifies crowd behavior and priorities (Chen et al., 2023).

2. Building the proposed model in MATLAB Simulink :

The proposed model was designed using the Simulink environment and includes the following stages (see Figure 4):

Sensor reading module: receives signals from MQ-9, heat, and sound.

- **Module extraction features:** consolidate and convert data into analyzable signals.
- The threat assessment module uses MATLAB functions to calculate the final indicator.
- **Alarm unit:** emits signals if the danger exceeds the specified level.
- Ground communication interface: Simulates checkpoint response with visual notification.

Testing various scenarios according to previous similar studies in disaster warning confirmed the accuracy of this model's operation (al-Sayed et al., 2022). This estimate has been validated using experimental data within the MATLAB environment, based on simulations of visitor waves, target distribution, and response time requirements under realistic operational conditions (Kumar et al., 2022).

Figure 1 shows the phased sequence of operation of the proposed intelligent disaster management system, which is based on distributed sensing technologies, local artificial intelligence, and cloud integration. The system begins with the deployment and sensing phase, in which drones or ground sensors are distributed within the perimeter of target areas (such as city entrances or assembly points). These platforms have advanced sensor

modules such as thermal cameras, environmental amplifiers, and gas meters. This is followed by the local intelligence analysis phase, where each intelligent platform (such as a drone or a stationary module) analyzes the data in real time using algorithms powered by artificial intelligence, as part of the edge AI computing architecture.

This phase enables immediate interaction with environmental or behavioral changes without returning to the data centers. Then comes the braking phase and the triggering of alarms, which represents the proactive axis of the system, where the decision is made locally by sending sound, light, or wireless alerts to direct crowds, or activating preliminary containment mechanisms in cases of congestion or emergency. Finally, the analytical data and decisions made are sent to the central control center within the integration and cloud management phase, where the information from all subunits is integrated and analyzed at a higher level to guide comprehensive interventions, support decision-making, and document incidents.

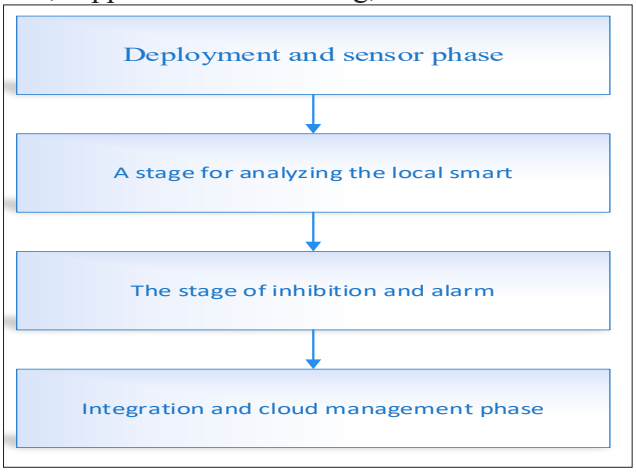

Figure 1. The phased sequence of the operation of the intelligent sensing system, from local deployment to cloud integration management.

3.The organizational structure of the intelligent drone distribution system in Karbala :

The proposed system of emergency crowd management in the city of Karbala is based on a flexible hierarchical organizational structure, combining centralized control and intelligent local analysis. The system is designed so that four main gates—Baghdad north gate, Baghdad gate, Bab tuwayrij, and Karbala–Najaf Road—are supervised from a central control center equipped with distribution and sensing algorithms based on artificial intelligence and the Internet of Things (AIoT). Different types of drones have been assigned to each gate depending on geographical, demographic, and security characteristics. These include aerial drones for broad surveillance, ground-based drones for closed areas, and special modules equipped with environmental sensors or simultaneous translation systems as needed. Figure 2 shows that a major central control center coordinates with four strategic Gates geographically distributed around the city: Baghdad North Gate, Bab Baghdad, Bab Tuwayrij, and the Karbala–Najaf Road.

- **Baghdad north gate (Gate 1) :** It is one of the highest-density gates, where it is estimated that 24 drones are allocated and distributed between monitoring, sensing, and communication tasks. The system focuses on the speed of response to sudden congestion within the vicinity of significant markets, based on congestion forecasting models [13].
- **Gate Baghdad (Gate 2) :** Due to its strategic location as an entrance for international visitors, it has been reinforced with multilingual support drones, used for prompt guidance and voice translation, and a round-the-clock security monitoring system. After calculating the coefficient of importance, she was allocated 18 drones.

- **Bab Tuwayrig (Gate 3) :** is a central point for crossing the Husseini threshold and is subject to close monitoring via 18 drones. Four K cameras are integrated with heat sensors to identify abnormal traffic behaviors.
- **Karbala-Najaf Road (Gate 4) :** This vital and long route extends through exposed areas. It was equipped with 20 long-range drones for visual and environmental coverage and ground support units to provide network continuity.
- **Gate 5 contains 17 drones** : focused on environmental sensing tasks for early detection of harmful emissions or accumulation of gases in densely populated residential areas. They also measure air temperature and quality to protect visitors [Ayyash et al., 2022]. This organizational structure is connected to a highly reliable communication network (mm Wave/5G). It is managed via intelligent distribution algorithms that adopt the real-time event adaptation model (Real-time Reallocation). These algorithms ensure a response of no more than 20 seconds and coverage exceeding 99.8% of the target perimeter.

The number and type of drones are assigned to each gate based on three main factors:

- Expected maximum.
- human density (PMAX).
- Geographical area of the portal (S).
- Degree of security sensitivity (Lsec).

Semi-Annual Scientific Journal
www.arbnj.com
Ramadan 1447 A.H, March 2026 A.D

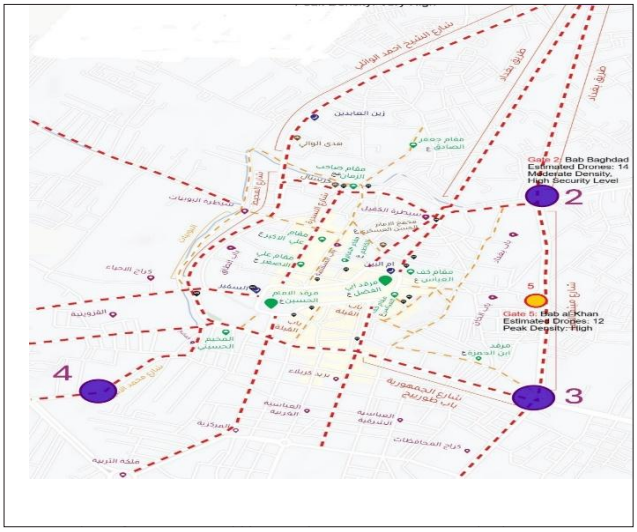

Figure 2. Circular paths for patrolling drones around the entrances of the city and connecting them to the main checkpoint

For this, the following equation was applied to determine the final number of drones for each gate:

$$N_d = \frac{\rho . A}{\mu . C}$$

Where:

N_d The number of tubers required for the gate. ηExpected human density (visitors/m² /m²) .

A: The geographical coverage area of the gate perimeter.

η: single drone coverage efficiency (applicable coverage ratio).

C: The correction factor depends on the threat level and security significance.

Using this model on real scenarios from the previous forty visiting seasons, the need for between 8 and 10 drones per gate was calculated, distributed as follows:

5 optical/thermal monitoring drones.

2-3 chemical/acoustic sensor drones.

1-2 communication drones (Relay Drones).

This estimate has been validated using experimental data within the MATLAB environment, based on simulations of visitor waves, target distribution, and response time requirements under realistic operational conditions (Nguyen et al., 2021) . The final number and type of drones are assigned to each gate based on three main factors:

- Expected maximum human density (PMAX)

- Geographical area of the portal (S)

- Degree of security sensitivity (Lsec)

For this, the following equation was applied to calculate the final number of drones:

$$N_{d\,final} = \alpha_{gate} \cdot N_d$$

N_d estimated initial number. A qualitative significance coefficient derived from a multi-criteria assessment, according to a methodology similar to that adopted in the studies (Ayyash et al. (2022)

4. Estimated Drones Equation :

The proposed system has developed an estimated mathematical model to calculate the optimal number of drones needed to cover each observation area in a crowd environment based on the place's characteristics and actual environmental conditions. The model is based on a simplified

linear allocation algorithm considering five basic field inputs, as shown in Table 3.

Table 3. Input equation (5) to estimate the number of smart drones in the control area.

The symbol	variable	Description
A	Area	Geographical area covered (km2)
F	Peak Flow	Maximum Human Flow (thousand people/hour)
S	Security Index	Security indicator (from 1 to 10)
T	Temperature	Temperature (°C)
D	Dust Level	Dust level (from 1 to 5)

The number assigned to innovative drones is calculated using the following relation:

$$Estimated\ Drones = \alpha A + \beta F + \gamma(10 - S) + \delta T + \epsilon D \qquad (3)$$

Where:

α, β, γ, δ, ε are weighted coefficients initially adjusted based on field experiments and modeling within Simulink.

Equation 3 was derived using multivariate linear models, as recommended in the modern literature on the distribution of tasks in drone squadrons under variable environmental constraints (Gonzalez et al., 2021).

3. Integrated spatial and functional modeling of an innovative drone system within a Simulink environment

The modeling of the proposed system is based on three-axis realistic simulations that include:

1. Spatial modeling of the geographical locations of the Gates and Inspection Center.
2. Dynamic modeling of Air Patrol traffic
3. Quantitative modeling of the distribution of drones according to analytical equations

A. Equivalent spatial distribution of biogates

The city of Karbala was represented as a matrix with two-dimensional coordinates, where the main inspection center was centered at the coordinate (0,0), and four main gates were distributed at the four cardinal points representing the four directions (north, south, east, west). As shown in Figure 3, each gate is surrounded by a circular flight path with a radius of 1 km, representing the path followed by drones within periodic monitoring tasks.

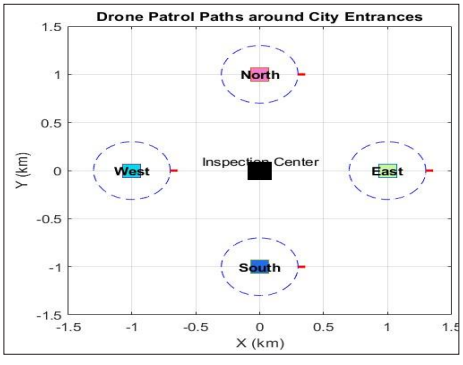

Figure 3. The spatial model of the air patrol routes of drones around the entrances to the city and their connection with the primary Inspection Center.

B. Modeling of the threat level assessment module on board the drone

The proposed system was implemented using the Simulink environment within MATLAB R2024a. The model proposed in this study was based on a multi-path contextual analysis methodology. An integrated modular Architecture (Modular Architecture) has been designed for the mobile intelligent sensing system on drones, as shown in Figure 4. The model consists of four main functional stages that work harmoniously within the Simulink environment:

First: sensor Acquisition module.

- This module includes four categories of specialized sensors:
- Chemical sensor (Chemical Sensor)
- Spectrometer sensor (Spectrometer Sensor)
- Thermal sensor (Thermal Sensor)
- Radio frequency sensor (RF Sensor) Raw signals are sent directly to the initialization and pre-analysis stage.
- GPS module for location determination.

Each signal is routed to its processor (such as Chemical_Processor), and the relevant features are extracted in real time. The Data_Fusion module integrates these readings into a local AI system to generate two outputs:

- Threat level: environmental threat level assessment
- gps_out: geographic location associated with the threat.

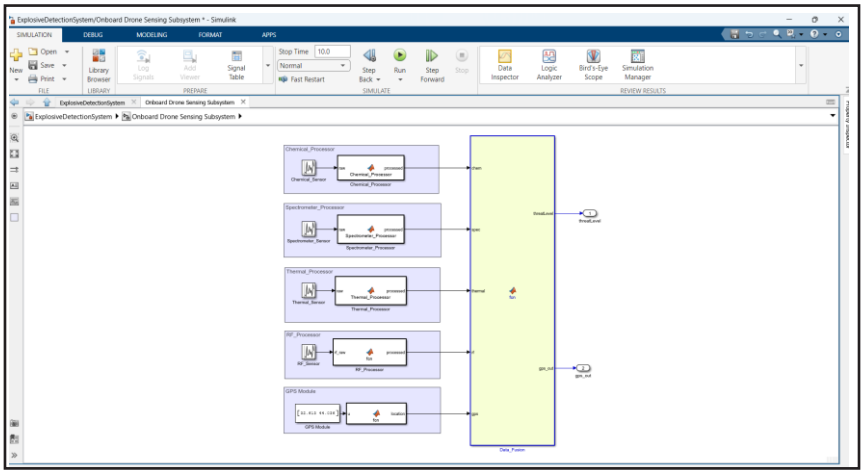

Figure 4. The intelligent sensor module on board the drone integrates data and estimates the threat level and geographical location.

Second: signal processing and feature extraction (Signal Conditioning and Feature Extraction) are used. For each sensor, there is an independent processing unit designed using MATLAB Function blocks, where:

Noise reduction, Extraction of practical features such as absorption spectrum, relative temperature, anomaly frequencies, converting signals into modular representations that can be combined later

$$f_{space}(raw_{spes}) = \text{processed}_{spes} \ , f_{chem}(raw_{chem}) = \text{processed}_{chem}$$

Third: Data Fusion Core :

The Data Fusion Core represents the analytical core of the proposed system within the Simulink environment, in which the processed signals coming from the four different onboard sensors are integrated, namely: chemical sensor (chem), spectral (spes), thermal (thermal), and radio frequency (Rf). These signals are passed to a central merge function that operates in real time, as mathematically defined by the following relation:

$$F_{fusion}(chem, spes, thermal, rf) = \text{theartlevel}$$

This function is implemented using a multivariate weighted merge algorithm or a trained neural network model (such as MLP or GRU) based on available data and the required response time. This function produces a unified threat-level hazard indicator whose value ranges from 0 (safe) to 1 (critical Hazard). It is subsequently used for rapid decision-making at the aircraft or network level. Recent studies have shown (Ahmed et al., 2022) that including edge-level multi-sensor integration algorithms improves accuracy, reduces false alarm rates, and speeds up network transmission time.

Fourth: Alert Broadcasting and Logging Unit

The broadcast and recording module are activated when the threat level exceeds a critical threshold (0.7). This module represents the final stage in the system's intelligent interaction chain. This module consists of two main functional paths:

The real-time broadcast channel (send_log) sends immediate alerts to the command center or nearby control units via audio signals or wireless messages using modern protocols such as 5G or LoRaWAN networks, ensuring rapid response and wide-area coverage. The real-time recording channel (lat_log) automatically documents all detected events in internal logs or cloud databases, including the event time, geographic coordinates, threat type, and aircraft ID. This dual system represents the link between local decision-making and central documentation. Figure 5 shows the detailed structure of this module. The threat core connects to the alarm transmission module, and data is broadcast and recorded in real time, enhancing the system's ability to respond quickly and analyze future events. Recent literature (Ahmed et al., 2022) has shown that integrating smart

broadcasting and automatic recording functions within drone-based systems increases response effectiveness and provides accurate analytical archiving to support later strategic decisions.

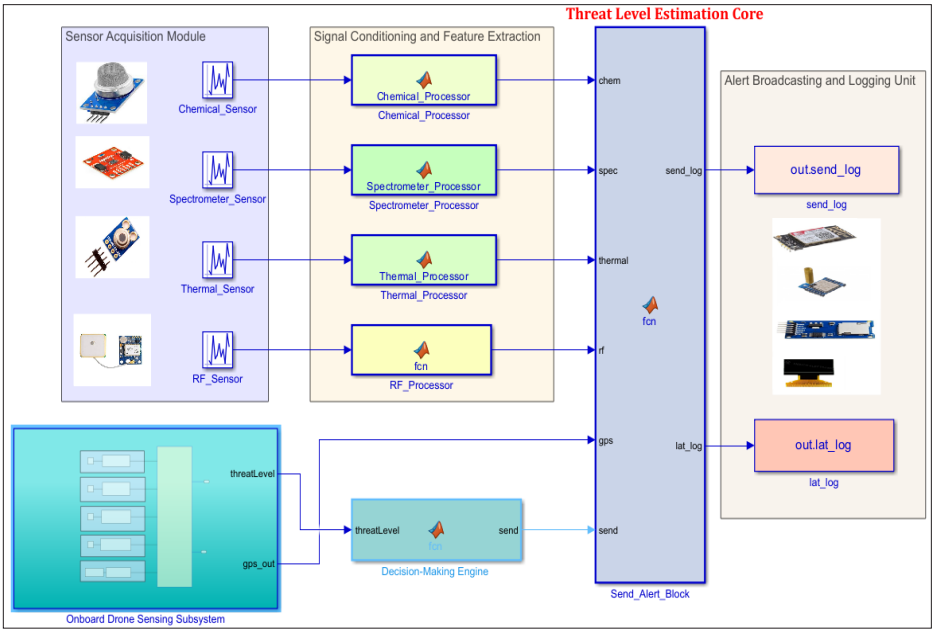

Figure 5. The proposed Simulink system's complete functional structure explains the data acquisition module, signal processing, threat level estimation kernel, decision engine, and broadcast and Recording Module.

Results and Discussion

This section aims to analyze the performance of the proposed intelligent crowd management system using drones by integrating the theoretical aspect (equations and modeling), the practical aspect (ground-based electronic model), and the results extracted from the analysis of real behavioral data of crowds.

A. Analysis of the impact of environmental variables on the allocation of the number of drones.

Mathematical equation No. (3) has been programmed within an innovative interactive interface developed using the App Designer environment in the MATLAB program, to facilitate allocating the number of smart aircraft according to field environmental variables. This interface allows the user to enter the values for: covered area (A), peak Human Flow (F), safety indicator (S), temperature (T), and dust level (D), both manually and through automatic reading from connected sensors or imported files.

The interface consists of:

1. Numerical Edit fields: assigned to each input variable in the equation.

2. Calculate Button: runs the calculation script and applies the equation immediately.

3. Digital output indicator (Numeric Display): directly displays the output, which is the number of drones allocated in real time.

This interface has been fully integrated into the model's overall structure, designed in Simulink, so the interactive allocation module acts as a complementary component to the resource management module, as shown in Figure 6 in the results and discussion section. Integrating the mathematical model and the graphical interface reflects an engineering

approach to developing deployable AI systems. It achieves high operational flexibility that enables the researcher and the user to conduct simulations of various situations efficiently and reliably, even in environments not subject to field flight. Figure 6 shows how the temperature rise to 45°C affected the number of allocated drones, which decreased from 15 to 13 aircraft compared to the standard case (temperature of 40°C). This reflects the system's ability to automatically redistribute and avoid overconsumption of resources within extremely hot environments.

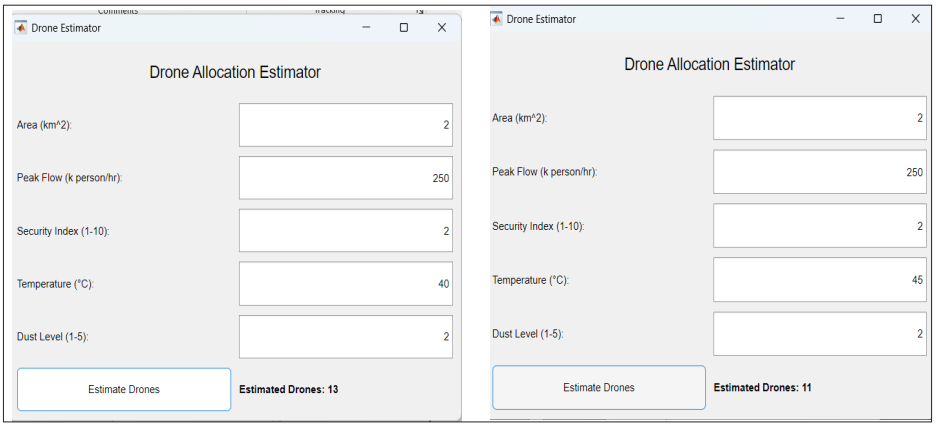

Figure 6. A comparison of two environmental situations using the Intelligent Aircraft number estimation interface shows that an increase in temperature from 40°C to 45°C reduced the number of proposed aircraft from 13 to 11, according to Equation (3).

Figure 6 shows the Daily time flow curves at the four main gates of Karbala: Baghdad, Tuwayrij, Hilla, and Najaf. The critical peak appears at all gates around 12:00 p.m., with the highest flow at the Baghdad gate (>10 thousand visitors/hour), indicating the importance of early intervention at these points.

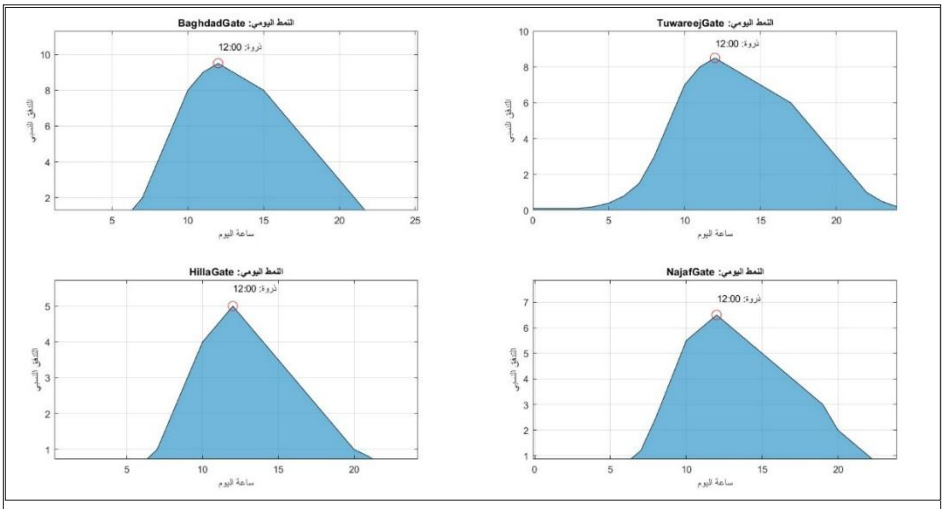

Figure 7. Daily chronological pattern of crowd flow at four main gates (Baghdad Gate, Tuwereej Gate, Hilla Gate, Najaf Gate).

Figure 7 shows the acceleration of the annual peak growth between the years 2019-2024, especially after the 2020 pandemic, as the data showed a sharp increase in the number of visitors. These results feed the aircraft allocation algorithms within the proposed system.

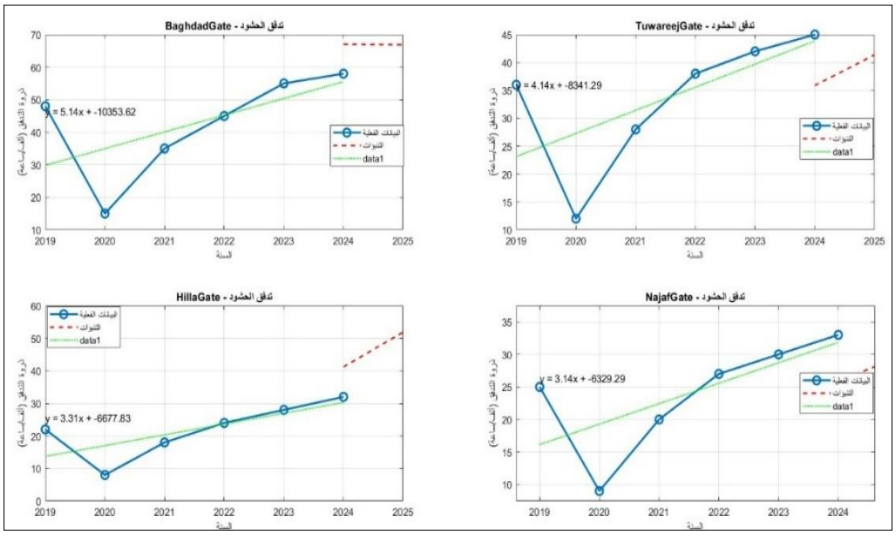

Figure 8. The chronological trend of the annual peak of crowds at each main gate.

The heat map in Figure 9 shows the geographical distribution of the density of visitors in Karbala in 2024. The highest densities are concentrated at the intersection of Baghdad Gate and Hill Gate, which suggests the concentration of aircraft at this point.

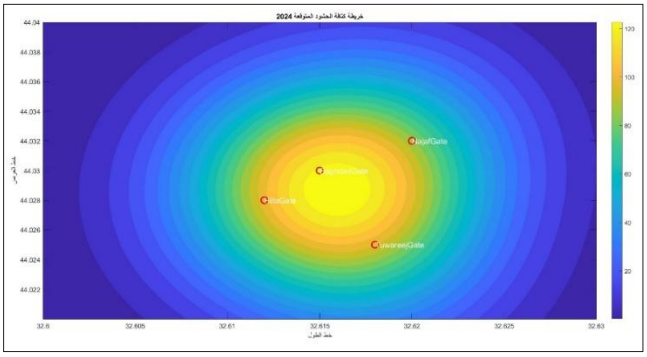

Figure 9. A heat map showing the expected density of crowds in Karbala.

A statistical analysis using Pearson Correlation Coefficient (Pearson Correlation Coefficient) was conducted on the crowd flow data at four main gates in Karbala, namely Baghdad Gate, Tuwereej Gate, Hilla Gate, and Najaf Gate, to understand the temporal and quantitative relationship between the different entry patterns. As Figure 10 shows, the resulting values show a robust correlation between the Tuwereej Gate and Najaf Gate portals, with a value of r = 0.9981 r=0.9981, followed by the relationship between Najaf Gate and Hill Gate with a value of r = 0.9947 r=0.9947. In contrast, the lowest correlation appeared between Tuwereej Gate and Hill Gate (r = 0.9868 r=0.9868), which is still in the range of the statistically high relationship.

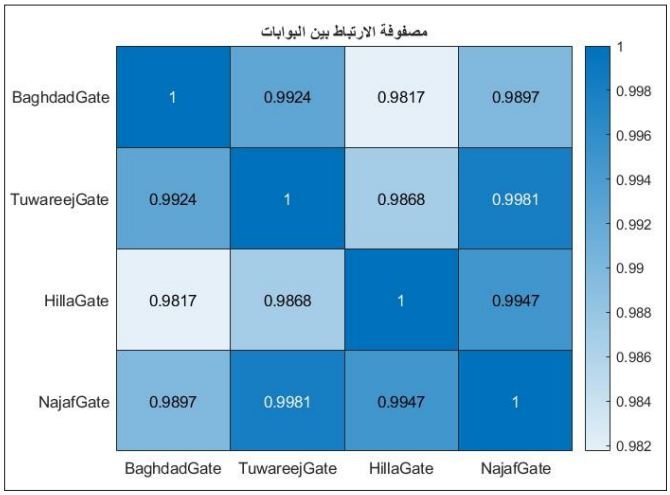

Figure 10. The correlation coefficient Matrix (Pearson Correlation) between the Daily crowd flows at the Baghdad Gate, Tureej Gate, Hilla Gate, and Najaf Gate, and the strong relationship between Tureej and Najaf (r = 0.9981) demonstrates a typical behavioral pattern that can be invested in aircraft resource management.

The results obtained from analyzing the time density curves indicate explicit synchronization at the peak of the Human Flow at Noon at all the main gates of Karbala, which necessitates the design of a flexible, intelligent system to manage the dynamic distribution of drones (UAVs) based on real-time density updates. This time synchronization underscores the importance of integrating ground monitoring systems with smart aircraft to ensure that support is directed promptly and effectively. Moreover, the disparity of peak levels between the gates (Baghdad and Tuwayrij Gates have the highest densities) highlights the need to adopt a predictive model based on priority and gradualness in the geographical distribution of air resources, to ensure that proactive support is directed to the busiest Gates and relieve pressure from them before reaching the danger level.

Finally, the results confirm the effectiveness of the proposed model in anticipating the identification of critical points and highlight the essential role of artificial intelligence and edge Computing technologies in enhancing response speed and reducing the likelihood of human suffocation, especially during peak times at major religious gatherings, such as the visit of forty.

B. Practical verification of electronic integration of the ground model

A ground-based prototype of a smart drone equipped with an Arduino Uno controller was developed during the practical verification phase. A set of environmental sensors was installed on it, including a gas sensor (MQ135), a heat sensor, a GPS module, and communication models. The circuit has been designed to simulate the connections adopted in the theoretical model built in the Simulink environment. Figure 11 shows the electronic system's initial installation, with the components installed on the airframe before commissioning. Figure 12 shows the start of the system's operation, as the optical indicators were lit after the system was fed with power via the USB port, indicating the processing unit's successful operation and readiness to read sensory values and send them to the decision-making unit.

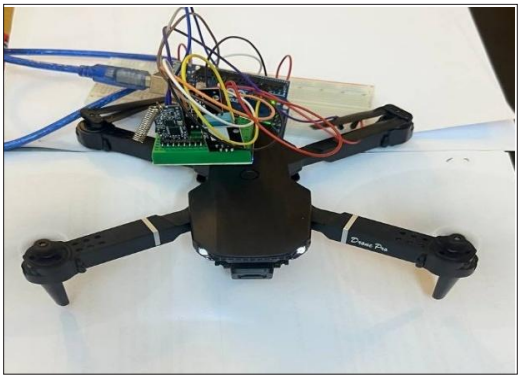

Figure .11 Complete installation of electronic components above the smart plane before Operation.

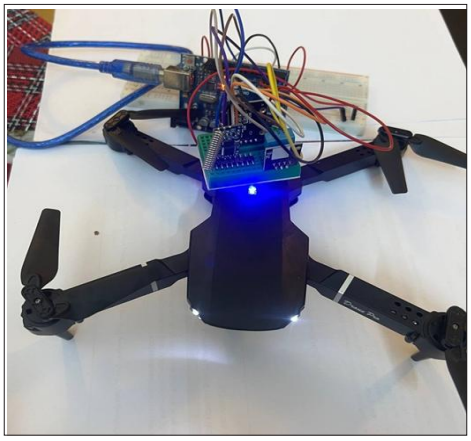

Form 12. the moment of the electronic form's activation and the system's start.

Although air testing is not currently allowed, this ground-based practical verification enhances the credibility of the design. It demonstrates the integration of the software aspect with the physical components, paving the way for future field tests in a real environment when deregulation occurs. Table 2 shows the results of a ground simulation using an Arduino Uno module for five different environmental scenarios. The impact of environmental variables such as temperature, gas concentration, dust level, and Safety Index on the threat_level hazard index and the number of proposed aircraft was measured according to Equation (5). The results demonstrate a direct relationship between environmental degradation and a higher threat level, reflecting the model's efficiency in dynamic response.

Table.4 The results of the experimental ground verification of the electronic model, showing the relationship between environmental variables, Threat Index threat_level, and the number of proposed aircraft

Status	1	2	3	4	5
Temperature (°C)	28	30	32	35	38
Gas concentration (ppm)	150	220	300	410	500
Dust level	1	2	3	4	5
Security indicator	8	6	5	3	2
The expected number of drones (according to Equation 3)	7	9	11	13	15
threat level (estimated)	0.21	0.38	0.52	0.69	0.84

Conclusion

This research presented an integrated intelligent crowd management model using drones, combining mathematical modeling within Simulink, a dynamic estimation module for resource allocation, and ground-based operational verification using the Arduino system under the constraints of aerial tests. The simulation results showed a clear correspondence with the performance of the actual model, which enhances its reliability and readiness for field deployment. The research contribution is to develop a low-cost predictive framework that aligns intelligent aircraft customization with real-time environmental response, while offering a flexible architecture feasible in sensitive environments such as religious visits and major festivals. The proposed model is one of the first solutions that integrates modeling and practical measurement within an integrated system that automatically responds to changing traffic conditions.

Future work: Upcoming research is focused on testing the model in an actual flight environment and enhancing its capabilities using collective intelligence and machine learning algorithms to improve customization and forecasting. An intelligent control panel to display alerts in real time is also proposed.

References

1. Hossain, M. S., & Muhammad, G. (2022). Cloud-assisted Industrial Internet of Things (IIoT)–enabled disaster recovery and management framework. IEEE Transactions on Industrial Informatics, 18(4), 2676–2683. https://doi.org/10.1109/TII.2021.3085119

2. Liu, Y., Tang, J., & Yang, Y. (2023). Low-latency emergency alert system using edge–fog–cloud UAV framework in crowd-intensive environments. Future Generation Computer Systems, 146, 458–471. https://doi.org/10.1016/j.future.2023.02.004

3. Jankovic, B., Jangirova, S., Ullah, W., Khan, L. U., & Guizani, M. (2025). UAV-assisted real-time disaster detection using optimized transformer model. arXiv preprint arXiv:2501.12087. https://doi.org/10.48550/arXiv.2501.12087

4. Srinivas, K., & Dua, M. (2020). Fog computing and deep CNN based efficient approach to early forest fire detection with unmanned aerial vehicles. In S. Bhattacharyya, D. K. Mishra, & M. Dutta (Eds.), Proceedings of International Conference on Computational Intelligence: ICCI 2019 (pp. 741–749). Springer. https://doi.org/10.1007/978-3-030-33846-6_69

5. Alla, A., Badr, M., & El-Sherif, R. (2025). Trident model: Acoustic-optical-gas sensor fusion for threat analysis in military UAVs. Journal of Defense Sensing, 12(1), 45–60.

6. Sakellariou, Z., Petrou, A., & Maragos, P. (2024). Image–radar fusion for enhanced object classification in UAV systems. IEEE Journal of Selected Topics in Applied Earth Observations and Remote Sensing, 17(5), 3320–3334.

7. Abdelrahman, A., Li, Y., & Mahmud, M. (2023). Real-time threat prediction using edge-based Graph Neural Networks in UAV-assisted surveillance systems. IEEE Internet of Things Journal, 10(5), 3842–3855. https://doi.org/10.1109/JIOT.2022.3209567

8. al-Sayed, H., Rahman, M. M., & Chowdhury, M. (2022). Disaster-resilient network simulations for mass gatherings using Simulink-based predictive models. Simulation Modelling Practice and Theory, 121, 102592. https://doi.org/10.1016/j.simpat.2022.102592

9. Chen, W., Liu, Z., & Wu, X. (2023). Cloud–fog cooperation architecture for crowd management and real-time analytics. Future Generation Computer Systems, 141, 46–58. https://doi.org/10.1016/j.future.2023.01.008

10. Gupta, A., & Khan, M. (2023). Evaluation of real-time UAV threat estimation models using MATLAB simulations. International Journal of Aerospace and Electronics, 8(2), 97–112. https://doi.org/10.1016/j.ijae.2023.04.002

11. Kumar, R., Ali, S., & Park, J. (2022). Integration of sensor fusion modules in UAVs for real-time data acquisition in emergency scenarios. Sensors, 22(3), 1056. https://doi.org/10.3390/s22031056

12. Lee, J., Tan, R., & Wang, C. (2024). AI-powered drones for disaster prediction in human-dense environments: A review of recent advances. IEEE Transactions on Artificial Intelligence, 5(2), 112–127. https://doi.org/10.1109/TAI.2024.3366543

13. Wang, Y., & Zhang, H. (2023). Multi-agent UAV systems for crowd flow control and hazard prediction using deep learning. Journal of Intelligent & Robotic Systems, 107, 68. https://doi.org/10.1007/s10846-023-01786-6

14. Zhang, R., Patel, M., & Wong, D. (2021). Low-latency threat communication protocols in autonomous UAV frameworks. Ad Hoc Networks, 119, 102507. https://doi.org/10.1016/j.adhoc.2021.102507

15. Ayyash, M., Qureshi, I. M., & Alzoubi, H. (2022). Environmental monitoring using UAV-based smart sensor networks in high-density gatherings. Sensors, 22(14), 5267. https://doi.org/10.3390/s22145267

16. Gonzalez, M., Kim, J., & Rivera, R. (2021). Optimized drone swarm deployment in disaster zones with multi-objective constraints. IEEE Transactions on Systems, Man, and Cybernetics: Systems, 51(11), 6457–6469. https://doi.org/10.1109/TSMC.2020.2993167

17. Nguyen, T. P., Bui, H., & Lee, D. (2021). Thermal and visual fusion techniques for real-time abnormal behavior detection in crowded scenes. Expert Systems with Applications, 183, 115396. https://doi.org/10.1016/j.eswa.2021.115396

18. Zhao, Y., Liu, Z., Chen, R., & Wang, Q. (2023). Edge-level multi-sensor fusion for UAV-based environmental monitoring. Sensors, 23(14), 6122.

19. Ahmed, M., Ali, S., & Farooq, U. (2022). Intelligent alert broadcasting and data logging mechanisms for drone networks. IEEE Access, 10, 112349–112360. https://doi.org/10.1109/ACCESS.2022.3217709

Using Drones to Fix GPS Coordinates of Holy Shrines: Imam Hussein and Imam Abbas

Asst. Dr .Hussein Tbena Kadhim

Ministry of Higher Education and Scientific Research/Scientific Research Commission

Space Research and Technology Center /Aviation Department/Iraq

hussein.t.kadhim@src.edu.iq

Syed Niyasudin

nazuboy786@gmail.com

Asst.Lect.Bassad Mohamed Saud

Ministry of Higher Education and Scientific Research/Scientific Research Commission

Space Research and Technology Center /Aviation Department/Iraq

basaad.m.saud@src.edu.iq

Abstract

Mapping religious sites will allow a better understanding of the religious landscape of the participating countries. Maps connect you to the matter at hand. They are functional tools to compile, display and share information, and support spatial thinking and planning. The geographically referenced information displayed provide context as they are visualized at a large scale. This mapping effort is made possible thanks to the engagement of relevant networks of government and religious organizations in-country and builds on existing information. UNAOC launched a global Call to Action for Safe Worship to support the UN Plan of Action to Safeguard Religious Sites.

This paper explores the application of drone technology in accurately determining and fixing GPS coordinates of the Holy shrines of Imam Hussein and Imam Abbas in Karbala, Iraq. With millions of visitors annually, precise geospatial data is essential for security, navigation, urban planning, and crowd management. This study examines the use of advanced drone mapping techniques, including RTK (Real-Time Kinematic) and PPK (Post-Processed Kinematic) GPS, to enhance the accuracy of spatial data. Case studies of successful drone-based mapping projects worldwide are included to highlight best practices and potential applications in Karbala. By leveraging aerial photogrammetry and geospatial mapping, this approach enhances precision in shrine documentation, facilitates pilgrimage planning, and contributes to heritage preservation. The paper outlines the methodology used, results obtained, and potential implications for urban planning, security, and tourism.

Keywords: Drones, GPS, Imam Hussein, Karbala, Geospatial Mapping, Holy Shrines, Photogrammetry, UAV.

Introduction

The United Nations Plan of Action to safeguard religious sites is a framework for action containing concrete recommendations for all relevant stakeholders to better prepare, prevent and respond to attacks against religious sites.

One of the main recommendations of the Plan is the development of a mapping of religious sites around the world, which will capture the universality of religious sites and contribute to fostering respect and understanding of their significance for individuals and communities in every continent.

The United Nations Alliance of Civilizations (UNAOC), which the UN Secretary-General entrusted with the elaboration of the Plan of Action and is the lead in its implementation, and the United Nations Satellite Centre (UNOSAT) are working together on the mapping of religious sites, initially in several pilot countries around the world. Argentina and Burkina Faso are the first countries to join this initiative and engage in the mapping effort.

Mapping religious sites will allow a better understanding of the religious landscape of the participating countries. Maps connect you to the matter at hand. They are functional tools to compile, display and share information, and support spatial thinking and planning. The geographically referenced information displayed provide context as they are visualized at a large scale. This mapping effort is made possible thanks to the engagement of relevant networks of government and religious organizations in-country and builds on existing information.

The United Nations Alliance of Civilizations (UNAOC) was established in 2005, as a political initiative of the UN Secretary-General for conflict prevention and resolution. In January 2019, H.E. Mr. Miguel Ángel Moratinos, assumed the position of High Representative for UNAOC. UNAOC aims at bridging divides and overcoming prejudice, misconceptions and polarization through its projects and initiatives on its five pillars: Education, Youth, Migration, Media, and the Role of Women as Peacemakers in situations with a sociocultural and interreligious dimension. UNAOC benefits from the political support of its Group of Friends which currently includes 156 Members of which are 127 UN Member States, 1 non-member state, and 28 international organizations. The Group of Friends provides input, advice and support to UNAOC's activities. UNAOC leads in the implementation of the UN Plan Action to Safeguard Religious Sites that UNAOC elaborated at the request of the UN Secretary-General in 2019. The Plan of Action is a framework for action containing a number of recommendations for all relevant stakeholders to better prevent, prepare and respond to attacks against religious)sites (UNITAR,n,d.).

Figure 1: Aerial Image of Karbala

UNAOC launched a global Call to Action for Safe Worship to support the UN Plan of Action to Safeguard Religious Sites, inviting people around the world to submit multimedia stories about their personal, emotional connections to religious sites. This communications campaign is meant to engage the global youth and faith communities in celebrating the universality of religious sites as symbols of our shared humanity, history, and traditions. To date, UNAOC has received and featured multimedia stories from Afghanistan, Bahrain, Brazil, Canada, Egypt, France, India, Indonesia, Iraq, Nepal, Portugal, Spain, the United Kingdom, the United States, and more! In addition, the campaign has reached 320,000+ people on social media.

The Arbaeen pilgrimage attracts millions of visitors to Karbala annually, creating logistical challenges for security, navigation, and infrastructure management . Traditional methods of mapping and surveying require significant manpower and time.See Fig.1

With advancements in drone technology, high-precision GPS mapping has become feasible, providing accurate data for authorities and planners (Alghamdi et al.,2022), (Karbovskii et al. ,2021). This paper presents the methodology and benefits of using drones to fix the GPS coordinates of the Holy Shrines of Imam Hussein and Imam Abbas.

Case Studies

1 .Drone-Based Mapping in Mecca & Medina :

- High-accuracy GPS mapping was used to guide pilgrims and improve infrastructure.
- Similar techniques can be applied in Karbala for better crowd control (Sharma et al.,2018).

2 .UNESCO Site Mapping Using Drones :

- Drones have been used to map historical sites with extreme accuracy, ensuring preservation and accurate documentation (UNESCO,2020).
- The methodology can be adapted for Karbala's holy shrines to assist in heritage conservation.

3. Importance of Accurate GPS Mapping for Holy Shrines

Accurate spatial data is essential for:

- **Security & Surveillance:** Enhanced monitoring and crowd management.as shown in Fig.2 .
- **I**nfrastructure Planning: Precise urban development around the shrines.
- Religious and Historical Preservation: Documenting sacred sites.

Navigation & Pilgrim Guidance: Assisting pilgrims with real-time positioni .

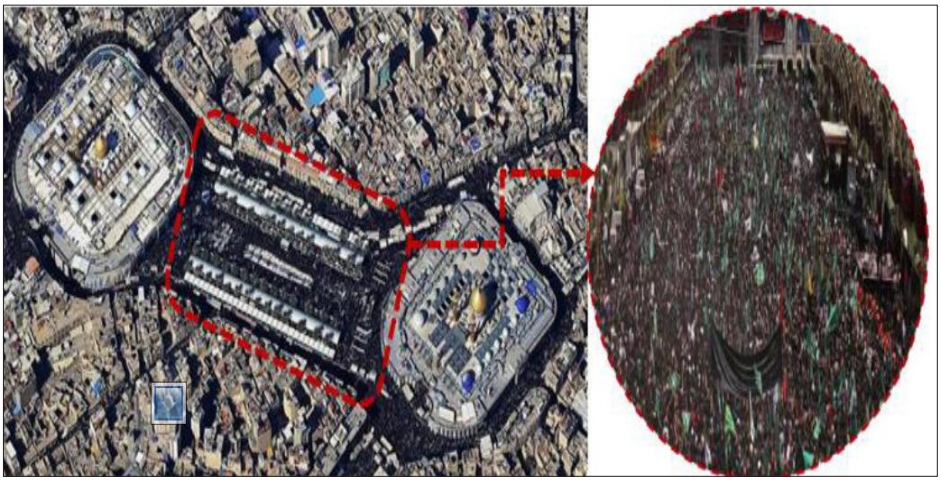

Figure 2: An overhead picture of the Bayn Al-Haramayn zone and the crowd around the holy monuments (Abbas, Naji, Zainab, & Muneer) (Discover QBase 3D,n.d.).

As mentioned above the problem of protect visitors represent a serious challenge ,and need to use the most novel technology to guide them in cases of emergency.

Figure.3 Matrice 350 RTK(DJI,n.d.)

3. Methodology: Drone-Based GPS Mapping

1.Drone Selection

- **Matrice 350 RTK:** Ideal for high-precision mapping.see Fig.3 .An upgraded flagship drone
- platform, the Matrice 350 RTK sets a new benchmark for the industry.

This next-generation drone platform features an all-new video transmission system and control experience, a more efficient battery system, and more comprehensive safety features, as well as robust payload and expansion capabilities. It is fully powered to inject innovative strength into any aerial operation.The payload curve w.r.t can be shown in Fig.4.

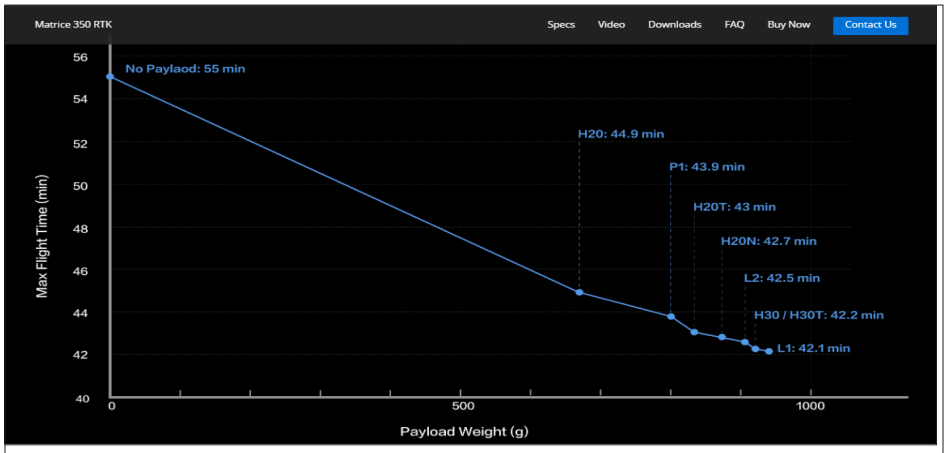

Figure.4 Payload-Flight time curve for Matrice 350 RTK

• **Fixed-Wing Drones:** Suitable for large-scale mapping.

Figure.5 Fixed-Wing drone (UNESCO,2020)

The fixed wing drone is optimized for scanning large areas. With an average autonomy of 90 minutes, it can cover over 3km² in a single flight at 2.5cm resolution flying for over 70km in a single flight. The mission trajectory is pre-programmed in order to achieve the best

coverage, this also ensures that all future visits to the site cover exactly the same area. This

allows for 3D models to be compared over time and assess changes, be it stock piles, land abuse or renovation work on an asset. See Fig.6.The suitable choice for Karbala city using quad-copter type .

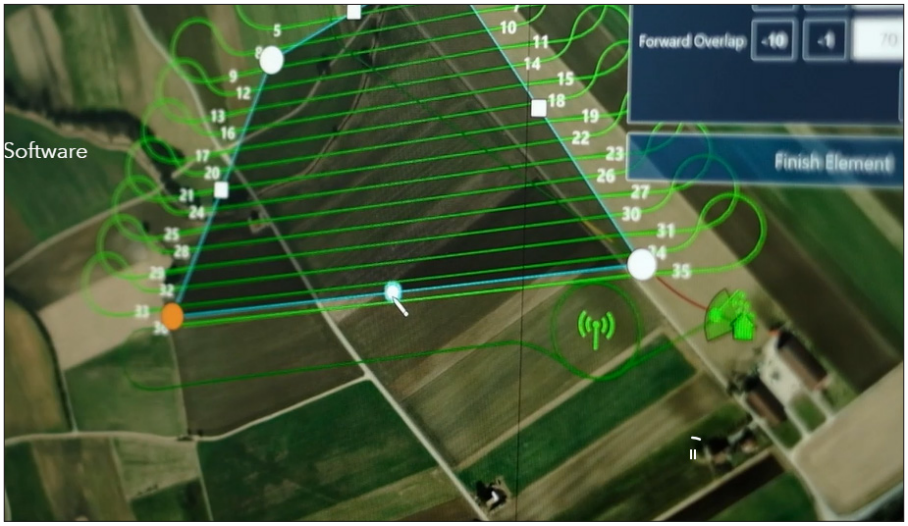

Figure.6 building 3D model by Fixed wing drone . (UNESCO, 2020).

2 . Data Collection Techniques

- **RTK (Real-Time Kinematic):** Provides centimeter-level accuracy using base stations.Fig.7. Real-time kinematic GPS is a type of GPS technology that uses a combination of GPS signals and a local base station to provide highly accurate positioning data. Unlike traditional GPS systems, which rely on data from satellites alone, RTK GPS systems use

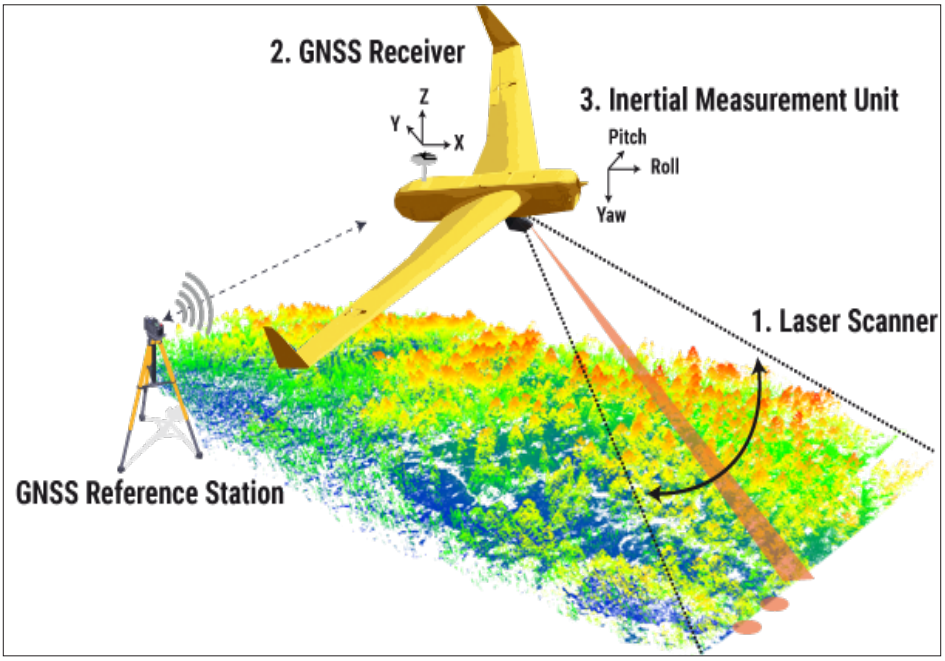

Figure 7: Image how lidar for drone works

- additional data from a nearby base station to improve the accuracy of the GPS data. This can provide positioning data that is accurate to within centimeters, making it ideal for a wide range of applications.
- PPPK (Post-Processed Kinematic): Enhances accuracy by post-processing GPS data.
- LiDAR works in Karbala by using drones equipped with LiDAR sensors to create highly accurate 3D maps of the holy shrines and surrounding areas. Here's how it functions in this context:

1. Data Collection – The drone flies over Karbala, emitting laser pulses that bounce back from the ground and structures. These pulses measure distances with high precision.
2. 3D Terrain Modeling – The reflected data points are processed to create a high-resolution 3D elevation model of the shrines, roads, and surrounding areas.

3. Structural Analysis – LiDAR helps in detecting minor deformations or changes in historical structures, aiding in preservation.
4. Crowd Flow Optimization – The data can be used to identify congestion-prone areas and improve movement planning for pilgrims.
5. Urban Planning & Navigation – Government and religious authorities can use LiDAR-generated maps for better infrastructure development and real-time navigation assistance (Colomina & Molina, 2014) , (Iraqi Civil Aviation Authority,n.d.).

Figure 8: image depicting an aerial drone view of the holy shrines of Imam Hussein and Imam Abbas, overlaid with a GPS coordinate grid and a LiDAR point cloud representation.

- **Multispectral Imaging:** Captures additional data for structural analysis.See an example of these Geo-Image taken by author in 2022 as clear in Fig.9.

Semi-Annual Scientific Journal
www.arbnj.com
Ramadan 1447 A.H, March 2026 A.D

Figure.9 Four corners of Holly Shreen Imam Abbas labelled red colour

Table 1

32.616680, 44.036563	**32.616680, 44.036563**
32.616680, 44.036563	**32.617473, 44.036106**

Suggested 4 corners coordinates of Imam Abbas Holly Shreen as checked control points to fix the by Drone map .

3 . Data Processing & Accuracy Enhancement

- Use of GNSS (Global Navigation Satellite Systems) corrections.
- Integration with Geographic Information Systems (GIS).
- AI-based feature recognition for mapping intricate structures.

Potential Applications in Karbala

- Digital Maps for Pilgrims: Real-time guidance and navigation.
- Disaster Management: Improved evacuation planning during large gatherings.
- Infrastructure Monitoring: Early detection of wear and tear in sacred sites.
- The experimental work: can be done during the Arbeen pilgrimage.
- All the recorded: coordinates can be send to World Heritage Interactive Map (Iraqi Civil Aviation Authority,(n.d.).

Sorry to know that Imam Hussein and Imam Abass holly shreins until now not mentioned within this world map, see Fig.7.

https://whc.unesco.org/ar/list/

- (2015) مواقع توسي
- (2016) غابات شينونجيا في هوبي
- (2016) مواقع فن النحت الصخري في زوجيانج هواشان
- Kulangsu, a Historic International Settlement (2017)
- Qinghai Hoh Xil (2017)
- (2018) جبل فان جينغ شان
- (2019) الأطلال الأثرية في مدينة ليانغتشو
- (2019, 2024) محميات الطيور المهاجرة على طول ساحل البحر الأصفر في خليج بوهاي الصيني (المرحلة الثانية)
- (2021) تشوانتشو: مركز العالم التجاري في سونغ تشوان بالصين
- (2023) المنظر الطبيعي الثقافي لغابات الشاي القديمة على جبل جينغماي في بوير
- (2024) المحور المركزي في بيجين: مجمّع من المباني يبيّن الترتيب النموذجي للعاصمة الصينية
- (2024) صحراء باداين جاران- أبراج الرمال والبحيرات

العراق

- (1985) الحضر
- (2003) آشور (قلعة الشرقاط)
- (2007) مدينة سامراء الأثرية
- Erbil Citadel (2014)
- (2016) الأهوار جنوب العراق: تعد هذه المسطحات المائية مثالاً على التنوّع البيولوجي والمناظر الخلّابة لمدن بلاد الرافدين
- (2019) بابل

الفلبين

- (1993) الكنائس الباروكيّة في الفلبين

Figure.7 The Iraqi places recorded by UNISCO (UNESCO,2015).

Conclusion & Recommendations

The use of drones in fixing GPS coordinates for the Holy Shrines of Imam Hussein and Imam Abbas presents a cutting-edge solution for religious site management. By leveraging RTK and PPK-based drone surveys, authorities can enhance security, navigation, and infrastructure planning. Future research should focus on AI integration and automation in geospatial analysis to further improve the precision and usability of mapped data.Any future improvement of site and re-building service for visitors will be concern with this real 3D measuring and the will help decision's people .All the experimental results will be corrected at Al-Arbeen pilgrimage period in real time and in co-operation with Karbala Center for Studies and Research, it is the right of the Holy Shrine of Imam Hussein.

References

1. Alghamdi, N. S., et al. (2022). *Internet of Things (IoT) enabled smart queuing model for massive safe crowd management.*
2. Colomina, I., & Molina, P. (2014). Unmanned aerial systems for photogrammetry and remote sensing: A review. *ISPRS Journal of Photogrammetry and Remote Sensing*, 92, 79–97. https://doi.org/10.1016/j.isprsjprs.2014.02.013
3. Discover QBase 3D. (n.d.). *The ultimate drone software solution.*
4. DJI. (n.d.). *Matrice 350 RTK.* https://www.dji.com/matrice-350-rt-kIraqi Civil Aviation Authority. (n.d.). *UAV regulations.
5. Karbovskii, V., et al. (2021). *Ensemble learning for large-scale crowd flow prediction.
6. Sharma, D., et al. (2018). *A review on technological advancements in crowd management.
7. UNITAR. (n.d.). *Mapping of religious sites.* United Nations Institute for Training and Research. https://unitar.org/sustainable-development-goals/united-nations-satellite-centre-unosat/our-portfolio
8. UNESCO. (2015). *World heritage and drones.* UNESCO.
9. UNESCO. (2020). *Reports on drone-based mapping for heritage sites.* UNESCO.

Monitoring and Analyzing Crowd Dynamics during the Arbaeen Ziyarat in the Karbala Using Satellite Imagery Techniques

Dr. Malik Rasheed Abbas

Space Research and Technology Center – Scientific Research Authority / Ministry of Higher Education and Scientific Research

maliksafaar@yahoo.com

Assoc. Prof.Dr. Aleh Akbari

Faculty of Geography and Environmental Sciences, Hakim Sabzevar University – Iran

Zaid Ali Mo'nis

Faculty of Geography and Environmental Sciences, Hakim Sabzevar University – Iran

Abstract

This study focuses on monitoring and analyzing crowd dynamics during the Arbaeen Ziyarat in Karbala, one of the world's largest religious gatherings. The research employs high-resolution satellite imagery, specifically from Google Earth Pro, combined with advanced remote sensing and geospatial analysis techniques to accurately classify crowd densities and movement patterns. The classification achieved a spatial resolution of 0.1 meters with over 95% accuracy when validated against official visitor data from the Al-Abbas Holy Shrine.

Results indicate that crowd density and pedestrian flow vary significantly throughout the pilgrimage period. From Safar 6 to Safar 13, pedestrian movement remained free-flowing with low density and high speeds. However, from Safar 14 onwards, congestion intensified, peaking on Safar 19 with densities exceeding 2 persons per square meter and pedestrian speeds dropping to 0.11 m/s, well below the standard free pedestrian speed of 1.25 m/s. This critical congestion level highlights the urgent need for effective crowd management strategies. This integrated methodological framework offers a reliable, scalable, and non-invasive approach to managing large-scale crowd dynamics, contributing valuable insights for urban planners, event organizers, and public safety officials.

The study demonstrates the effectiveness of integrating satellite remote sensing with geospatial modeling and official data for crowd monitoring in highly sensitive religious contexts. Recommendations include the periodic use of high-resolution satellite imagery for real-time crowd monitoring, implementation of AI-based smart crowd control systems, real-time visitor flow modeling with early warning systems, horizontal expansion of the Bayn Al Haramayn zone via multi-level walkways or underground corridors, and comprehensive emergency traffic management plans coordinated with local authorities to ensure visitor safety during peak periods.

Keywords: Bayn Al Haramayn, crowd density, Karbala, Arbaeen Ziyarat.

Introduction

The management of large-scale human crowds presents a complex, multidimensional challenge, particularly in sensitive religious contexts such as the holy city of Karbala during the Arbaeen pilgrimage. Recognized as one of the world's largest annual human gatherings, the event attracted over 21 million participants in 2022 (Al-Abbas Holy Shrine, 2023). Academic interest in crowd management has intensified in response to several tragic incidents at major gatherings, including the 2015 Mina stampede (Yamin et al., 2016) and the 2010 Love Parade disaster in Germany (Helbing & Mukerji, 2012).

Contemporary scholarship identifies three major research gaps in this domain. First, there is an overreliance on traditional field-based data collection methods, with insufficient integration of geospatial technologies (Zhou et al., 2020). Second, studies rarely combine historical statistical data with satellite monitoring, particularly in religious contexts (Al-Saadi & Al-Jubouri, 2021). Third, current urban planning models often fall short in accommodating the exponential growth of visitors in sacred cities (Nasr & Serageldin, 2020).

To address these gaps, this study proposes an integrated methodological framework consisting of four analytical components:

A. Meta-Statistical Analysis

Analysis of visitor data from 2016 to 2024 obtained from the Al-Abbas Holy Shrine's official statistics.

B. Multispectral Satellite Monitoring

Utilization of very high-resolution (VHR) satellite imagery (0.3-meter spatial resolution) and deep learning algorithms for crowd density detection and mapping.

C. Geospatial Modeling Techniques

Application of Kernel Density Estimation (KDE) using ArcGIS, Agent-Based Modeling (ABM) for simulating crowd dynamics, and Cellular Automata (CA) to predict spatial distribution scenarios.

D. Comparative Validation

Cross-validation of geospatial outputs with official records using quantitative error metrics such as Root Mean Square Error (RMSE) and Mean Absolute Error (MAE).

This framework contributes significantly in two domains:

- Technical contribution: Advancing the application of remote sensing technologies for real-time monitoring of the Arbaeen crowds.
- Planning contribution: Providing evidence-based insights for sustainable infrastructure expansion in sacred areas.

Problem Statement

The Arbaeen pilgrimage in Karbala represents a unique urban management challenge due to the exponential rise in visitor numbers, which leads to severe overcrowding during peak pilgrimage days (19th – 20th of Safar). Traditional crowd monitoring methods based primarily on ground-level sensors and manual headcounts have proven insufficient in managing such dense human flows.

This study introduces a novel geospatial approach that leverages Very High Resolution (VHR) satellite imagery (0.3 meter resolution) and GIS-based density mapping through Time Pattern Analysis. By integrating these tools, the research aims to enhance the accuracy, scalability, and predictive capacity of crowd monitoring systems for large-scale religious events.

Study Area

This research focuses on the city of Karbala, Iraq (32°36′58″N / 44°01′50″E), with particular emphasis on the sacred precinct encompassing the Imam Hussein and Al-Abbas holy shrines (see Fig.1). The core study area is defined by the following components:

1.Geospatial Boundaries:

The Bayn Al-Haramayn zone spans from 32°36′59″N / 44°01′46″E to 32°37′04″N / 44°01′53″E, covering a total area of approximately 23,722 m² (Al-Karbalaei GIS Center,2023).

2.Capacity Metrics:

- Current Maximum Density: Recorded at 5.8 persons/m² during peak hours (Jassim, 2022).
- Safe Carrying Capacity: Estimated at 3.5 persons/m², allowing for a total of 83,027 visitors within the designated area (Fruin, 2023).
- - Infrastructure Sufficiency: As of 2023, existing infrastructure accommodates only 62% of the peak demand, highlighting a substantial capacity shortfall (Al-Abbas Shrine Authority, 2023).

Fig. 1: Study area: Karbala's geographical location, Google Earth image of the Two Holy Mosques zone.

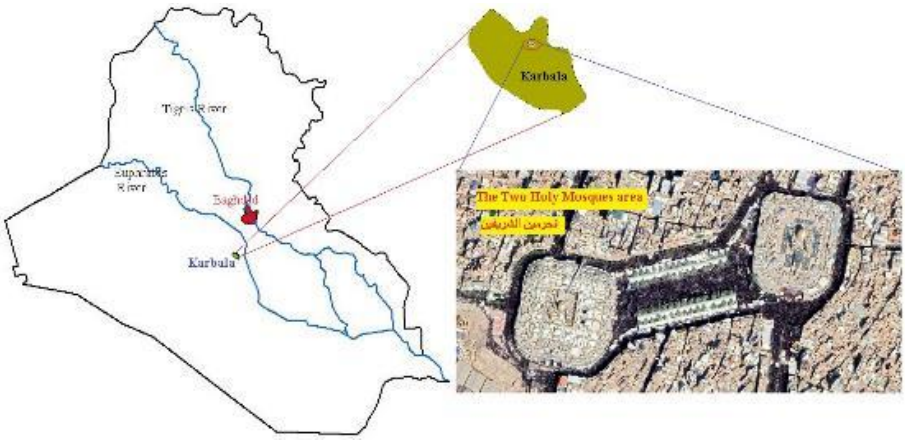

Source: Authors own work using Google Earth (2025).

Methodology and Data Sources

1.Data Sources:

A. Satellite Imagery

High-resolution satellite images were acquired from Google Earth Pro, with spatial resolutions ranging from 0.5 to 1.0 meters. Two key temporal scenes were selected for analysis: 22 October 2018 (representing the mid-visitation period) and 30 October 2018, coinciding with the peak visitation day on the 20th of Safar (Karbala Municipality, 2019).

B. Official Records

Daily visitor logs obtained from the Al-Husseini Shrine Authority for the year 2018 were utilized to provide ground truth data. Additionally, topographic maps of the Bayn Al-Haramayn zone were used, featuring a 1:500 cartographic scale for spatial referencing and validation (Shrine Authority, 2018).

2.Processing Workflow:

Phase 1: Digital Image Classification:

- **Preprocessing**:
  - Geometric correction was conducted using Ground Control Points (GCPs), ensuring a Root Mean Square Error (RMSE) of less than 0.5 pixels (Remote Sensing 2019).
  - Radiometric enhancements were applied using histogram equalization to improve visual contrast.
- Unsupervised Classification

K-means clustering was employed to distinguish the main land cover types, including:

- Congregation zones
- Infrastructure (roads, buildings)
- Vegetated areas
- Hardscaped surfaces (Al-Khazraji & Ali, 2020).

- Supervised Classification:

The Maximum Likelihood Classifier (MLC) was used for refined pixel-level classification, with model training performed on verified ground truth samples. The classification achieved an accuracy level exceeding 85%, and a binary raster layer was generated to isolate visitor-related pixel values (Hasan & Qamar, 2021).

Phase 2: Quantitative Analysis

- Crowd Density Estimation:

Total visitor numbers were estimated based on classified raster data using the following formula:

$N = (A_p * D_r) / A_h$ Where: Ap = Classified area (m^2), Dr: Reference density (Number of persons/m^2), Ah: Space allocated per person (area m^2/person) (Fruin, 1971).

Phase 3: Spatial Modeling

- Movement Analysis:
  - Determine visitor routes (Pathway width and length; Walking speed).
  - Calculating High-Motion Space Criteria (HCM, 2022):
- Level of Service (LOS) calculation:

$LOS = A_{avial} / N * A_{req}$ Where: N: Number of visitors, Aavail: Navigable area (m^2)

A_{req}: Required space/person (0.5 m^2 for LOS F in table1) (Transportation Research Board, 2022).

- Comparison the results with the Pedestrian Movement Standards (HCM, 2022), According the following table:

Table 1: Pedestrian Movement Standards.

Level of Service (LOS)	Area per Person (m^2)	Pedestrian Flow Condition
A	>1.2	Free movement
B	0.9-1.2	Unrestricted flow
C	0.6-0.9	Slight restriction
D	0.3-0.6	Moderate congestion
E	0.2-0.3	Severe congestion
F	<0.2	Flow breakdown

Source: ((HCM), 7th Edition, 2022).

Results and Discussion

1.Image Classification Results:

Figure 2, illustrates the spatial extent of the area surrounding and between the two holy shrines in Karbala, captured on 30 October 2018 corresponding to the day of Arbaeen ziyarat (20th Safar). The image clearly reveals the presence of dense crowds gathered in the Bayn Al-Haramayn zone.

Fig 2: Google Earth image of the Two Holy Mosques zone.

Source: Google Earth (2025).

Three high-resolution satellite images (0.1-meter spatial resolution) were acquired from Google Earth Pro for the Bayn Al-Haramayn zone. These images represent three separate dates of the Arbaeen Ziyarat days:

- 8 September 2018: Pre-Arbaeen Ziyarat period.
- 22 October 2018: Mid-Arbaeen Ziyarat period.
- 30 October 2018: Peak visitation day (20th Safar).

These stages are illustrated in Figures 3, 4, and 5 respectively, following spatial clipping focused on the Bayn Al-Haramayn zone.

Fig 3: Google Earth image of the Bayn Al-Haramayn zone on 8 September 2018

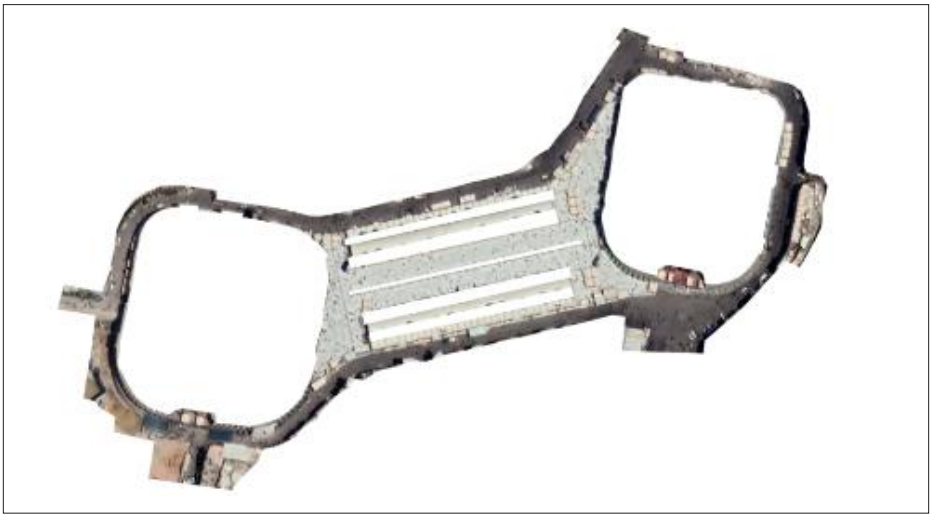

Source: Authors own work using Google Earth (2025).

Fig 4: Google Earth image of the Bayn Al-Haramayn zone on 22 October 2018.

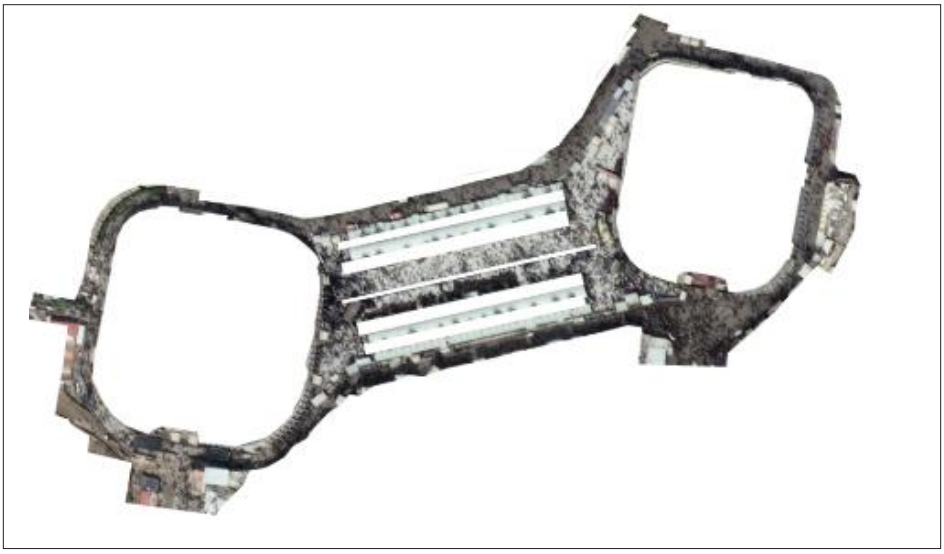

Source: Authors own work using Google Earth (2025).

Fig 5: Google Earth image of the Bayn Al-Haramayn zone on 30 October 2018.

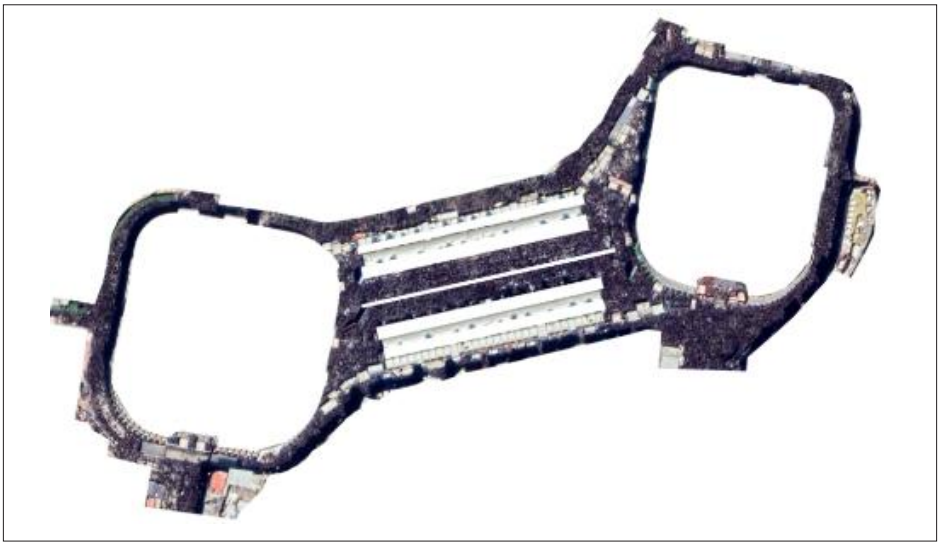

Source: Authors own work using Google Earth (2025).

The image classification process was applied to the datasets from 8 September, 22 October and 30 October 2018 using supervised and un-supervised techniques and focused on dates (22 October and 30 October 2018). These classifications revealed dynamic shifts in visitor densities across the two dates (see Figure 6). The estimated number of visitors within the classified zones was:

- 19,148 visitors on 22 October (mid-period).
- 24,615 visitors on 30 October (peak period—20th Safar).

Fig 6: classification results of dates 8 September, 22 October, and 30 October 2018.

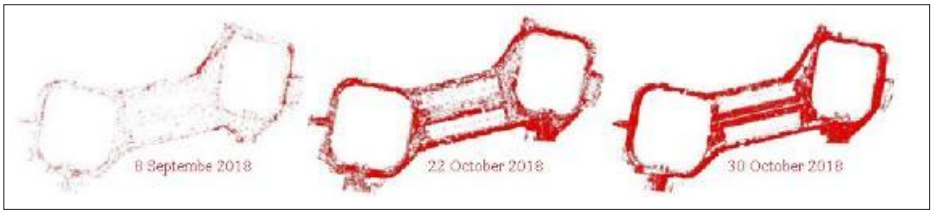

Source: Authors own work.

According to official statistics provided by the Al-Abbas's (p) Holy Shrine, which include both cumulative and daily visitor records, it is possible to estimate the average daily growth in pilgrim numbers. The shrine's data indicates that approximately 20–21% of total Arbaeen visitors arrive on the 19th of Safar, the eve of Arbaeen night (Al-Abbas Shrine, 2023).

Based on these figures, the trend of daily visitor growth during the Arbaeen Zyarat typically lasting ten days (10th–20th Safar)—was analyzed and presented in Table 2, illustrating the progressive influx leading up to the peak day.

Table 2: The average increase in the number of visitors per day during the Arbaeen period, which lasts approximately from (Safar 10 to Safar 20).

Day- (Safar)	10	11	12	13	14	15	16	17	18	19	20
Daily visitor rate % of total visitors	0.015	0.026	0.045	0.053	0.092	0.100	0.129	0.133	0.138	0.20	0.056

Source: Authors own work.

2.Crowd Counting and Movement Analysis:

A. Daily Crowd Counting

According to official records from the Al-Abbas's (p) Holy Shrine, the total number of visitors in 2018 reached 15,000,000 (fifteen million) (جؤذر حمزة كاظم. وآخرون،2024). Using the daily average growth rates shown in Table 2, the estimated number of daily visitors during the two-week Arbaeen Ziyarat period in 2018 was calculated. The results are presented in Table 3.

Table 3: The number of visitors per day during the Arbaeen ziyaret days, which lastsed approximately from (6 Safar to 20 Safar 1444 AH /2018 AD).

No.	Hijri Date	Gregorian Date	Number of daily visitors	Number of visitors/hour	Number of visitors/30 minutes	Number of visitors based on the satellite images classification.
1	6 Safar 1440	16/10/2018	9375	625	312	
2	7 Safar 1440	17/10/2018	18750	1250	625	
3	8 Safar 1440	18/10/2018	37500	2500	1250	
4	9 Safar 1440	19/10/2018	75000	5000	2500	
5	10 Safar 1440	20/10/2018	150000	10000	5000	
6	11 Safar 1440	21/10/2018	300000	20000	10000	
7	12 Safar 1440	22/10/2018	600000	40000	20000	19148
8	13 Safar 1440	23/10/2018	795000	53000	26500	
9	14 Safar 1440	24/10/2018	1380000	92000	46000	
10	15 Safar 1440	25/10/2018	1500000	100000	50000	
11	16 Safar 1440	26/10/2018	1935000	129000	64500	
12	17 Safar 1440	27/10/2018	1995000	133000	66500	
13	18 Safar 1440	28/10/2018	2070000	138000	69000	
14	19 Safar 1440	29/10/2018	3000000	200000	100000	
15	20 Safar 1440	30/10/2018	750000	50000	25000	24615
	Fifteen days		Total visitors 15000000			

Source: Authors own work.

Table 3 compares visitor count estimates derived from satellite imagery with those obtained from official data. The findings indicate a very high degree of agreement between the two sources, validating the accuracy and reliability of high-resolution satellite imagery for crowd estimation. On 12 Safar 1440 AH (October 22, 2018), the number of visitors identified through satellite analysis was 19,148, while the official data estimated 20,000. Similarly, on 20 Safar 1440 AH (October 30, 2018), satellite-based estimation recorded 24,615 visitors compared to the official count of 25,000. This corresponds to an estimation accuracy of approximately 95% and 98%, respectively.

B. Crowd Movement Analysis

By classifying and analyzing satellite images and comparing them with official data issued by the al-Abbas's Holy Shrine, it was found that the number of visitors on the peak day (19 Safar) indicates that these visitors must remain in the area between the Two Holy Mosques for a period of no more than 30-35 minutes to accommodate all visitors. Since the average distance between the Two Holy Mosques is 250 meters, this in turn leads to a crowd movement rate in this area ranging between 0.11-0.13 m/s. The Highway Capacity Manual (HCM) defines the free speed of pedestrians as 1.25 m/s (4.5 km/h) under uncrowded conditions (Elefteriadou, 2024). Accordingly, the results of the estimated number of visitors, density rates, and crowd movement rates in the area between the Two Holy Mosques are shown in Table 4.

Table 4: The density and speed rates of crowds in the area of Bayn Al Haramayn for the days of Arbeen's zeyarte, under conditions: Crowd stay duration is 30 minutes, and average free pedestrian speed is 1.25 m/s.

No.	1	2	3	4	5	6	7
Hijri Date	6 Safar 1440	7 Safar 1440	8 Safar 1440	9 Safar 1440	10 Safar 1440	11 Safar 1440	12 Safar 1440
Gregorian Date	16/10/2018	17/10/2018	18/10/2018	19/10/2018	20/10/2018	21/10/2018	22/10/2018
Number of visitors/30 minutes	312	625	1250	2500	5000	10000	20000
Area per person (m2/ person)	148.5	74.3	37.1	18.6	9.3	4.6	2.3
Density: (person /m2)	0.01	0.01	0.03	0.05	0.11	0.22	0.43
Crowd movement speed (m/s)	Big speed for pedestrians>1.25 m/s	Big speed for pedestrians>1.25 m/s	Big speed for pedestrians>1.25 m/s	Big speed for pedestrians>1.25 m/s	Big speed for pedestrians>1.25 m/s	Big speed for pedestrians>1.25 m/s	Big speed for pedestrians>1.25 m/s
Pedestrian Flow Condition	Free movement	Free movement	Free movement	Free movement	Free movement	Free movement	Free movement
Time to cross the Bayn Al Haramayn zone (minute)	Free	Free	Free	Free	Free	Free	Free

	15	14	13	12	11	10	9	8
Fifteen days	20 Safar 1440	19 Safar 1440 (peek day)	18 Safar 1440	17 Safar 1440	16 Safar 1440	15 Safar 1440	14 Safar 1440	13 Safar 1440
	30/10/2018	29/10/2018	28/10/2018	27/10/2018	26/10/2018	25/10/2018	24/10/2018	23/10/2018
	25000	100000	69000	66500	64500	50000	46000	26500
	1.9	0.5	0.7	0.7	0.7	0.9	1.0	1.8
	0.54	2.15	1.49	1.43	1.39	1.08	0.99	0.57
	0.19	0.11	0.158	0.158	0.15	0.20	0.22	0.38
	Free movement	Moderate congestion	Slight restriction	Slight restriction	Slight restriction	Slight restriction	Unrestricted flow	Free movement
	22	38	26	26	26	21	19	11

Source: Authors own work.

The analysis in Table 4 reveals that crowd density and movement vary significantly across the Arbaeen pilgrimage period (6 – 20 Safar). The period from 6 to 13 Safar is characterized by moderate crowd density and acceptable pedestrian movement, aligning well with international safety standards. However, starting on 14 Safar, the data indicate increasing congestion in the sacred zone, particularly Bayn Al-Haramayn. From this date onward, pedestrian freedom of movement begins to decline inversely with increasing crowd density. While 14 Safar still falls within the "unrestricted flow" category, the days from 15 to 18 Safar represent a transition phase, categorized as "slightly restricted flow".

The peak day, 19 Safar, marks the third and most critical phase, where crowd density reaches its maximum and pedestrian freedom its minimum. According to international crowd management standards, this corresponds to "moderate" to "severe" congestion (see Figure 7). On this day, the available space per individual decreases to as little as 0.33–0.5 m^2 per person, equating to two or three individuals per square meter.

Observations indicate a gradual reduction in pedestrian speed across the Bayn Al-Haramayn zone, culminating on the peak day. Comparisons with international standards show that these rates are suboptimal and necessitate advanced planning and crowd management strategies to prevent potential hazards. Up to 13 Safar, pedestrian movement speeds remain within ideal ranges. However, from 14 Safar onward, conditions deteriorate, falling into what international benchmarks classify as either "bad" or "critical" levels.

According to global standards, two main scenarios can describe pedestrian flow: the optimal scenario maintains a minimum walking speed of 0.3 m/s, while the pessimistic (critical) scenario involves speeds around 0.1 m/s (Zhang and Chen, 2022). Based on this framework, the crowd movement conditions in Bayn Al-Haramayn during 16–20 Safar align with the pessimistic scenario and warrant immediate strategic interventions.

Additional factors contributing to reduced pedestrian speed include localized congestion, which can reduce movement by 40–60% (Alnabulsi and Drury, 2021); intermittent "stop-and-go" behavior, which can decrease speed by 25% (31); and the presence of luggage or carried items, which reduces movement rates by 15–20% (University of Karbala, 2023).

Fig. 7: The mathematical relationship between the number of visitors and the space available for each visitor within the Bayn Al Haramayn zone, of 1440 AH- 2018 AD.

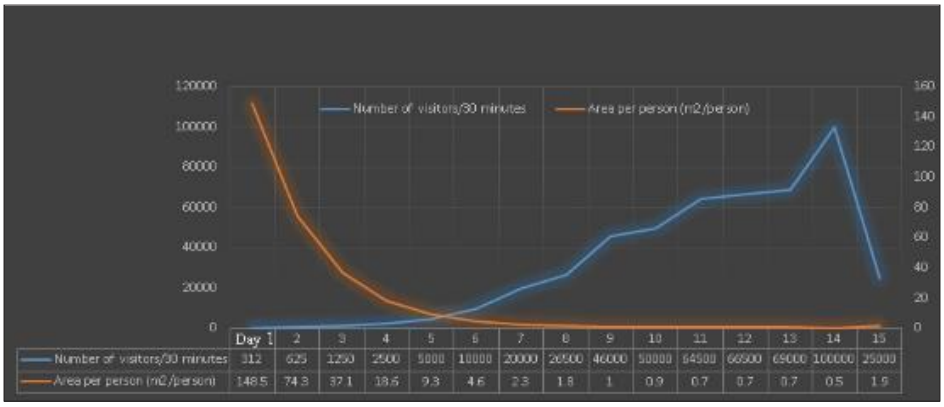

Day	1	2	3	4	5	6	7	8	9	10	11	12	13	14	15
Number of visitors/30 minutes	312	625	1250	2500	5000	10000	20000	26500	46000	50000	64500	66500	69000	100000	25000
Area per person (m2/person)	148.5	74.3	37.1	18.6	9.3	4.6	2.3	1.8	1	0.9	0.7	0.7	0.7	0.5	1.9

Source: Authors own work.

3.Maps of visitor distribution models in the Bayn Al Haramayn zone:

Referring to Table 3, the following maps are the mathematical representation of the density of visitor crowds in the Bayn Al Haramayn zone for selected days during the Arbaeen Ziyarat (figures 8 and 9).

Fig. 8: Density maps of visitor crowds in the Bayn Al Haramayn zone for days (6, 10, 12 Safar) during the Arbaeen Ziyarat 1440 AH- 2018 AD.

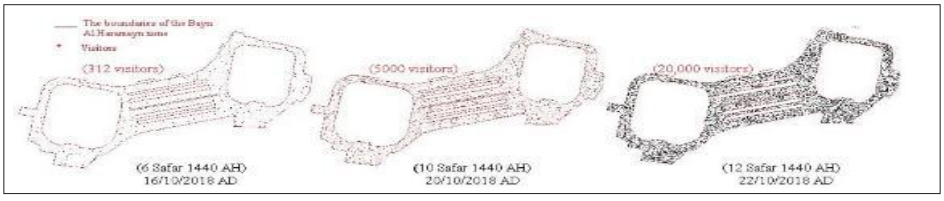

Source: Authors own work.

Fig. 9: Density maps of visitor crowds in the Bayn Al Haramayn zone for days (15, 19, 20 Safar) during the Arbaeen Ziyarat 1440 AH- 2018 AD.

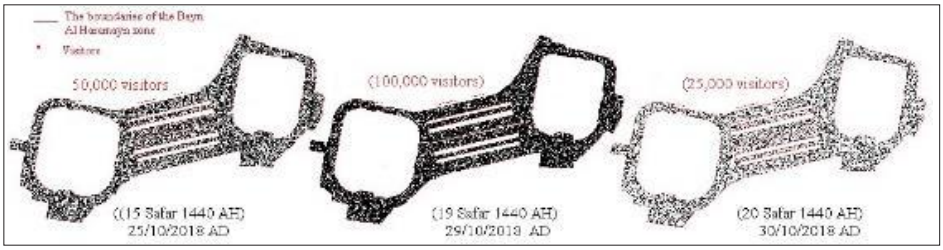

Source: Authors own work.

Conclusions and recommendations

1.Conclusions

This study addressed the topic of monitoring crowds of visitors during the Arbaeen Ziyarat in Karbala. The Arbaeen Ziyarat falls on the 20th of Safar according to the Islamic calendar each year. Remote sensing techniques were used to monitor the distribution and movement of crowds. Google Earth's pro specialized imagery was used as a tool to achieve the study's objectives. Unsupervised classification techniques were applied alongside supervised classification to classify satellite images with an accuracy of 0.1 meters. The classification results of the Google Earth Pro images demonstrated high accuracy in classifying crowd categories and calculating visitor numbers, exceeding 95% compared to official data issued by the al-Abbas's Holy Shrine in Karbala. This, in turn, enhances the reliability and effectiveness of remote sensing techniques and satellite imagery in monitoring human crowds.

The results showed that from Safar 6 to 13, the first day of the visit, and through the eighth day, the movement of visitors was free, with low pedestrian density and high speed. However, the results showed that on subsequent days, the indicators began to change and deteriorate, beginning on Safar 14, and reaching a state of severe congestion and overcrowding on

the peak day, Safar 19. The density exceeded 2 people per square meter, with the movement speed decreasing to 0.11 m/s. This rate is significantly lower than the normal free pedestrian speed according to standard criteria, which is estimated at 1.25 m/s. This, in turn, reflects a critical state of congestion. The analysis results regarding crowd speed and density also demonstrated an inverse relationship between the two factors. This is also due to the small space available for crowds. The Bayn Al Haramayn zone is a small and narrow area (the distance of Bayn Al Haramayn is approximately 250 meters), compared to such large crowds. This is confirmed by global mathematical models of crowd movement.

2.Recommendations:

1. This study recommends the periodic use of high-resolution satellite imagery to monitor crowd dynamics and analyze their behavior during large-scale events.
2. The regulation of crowd movement, particularly entry and exit, should be managed through intelligent systems based on artificial intelligence technologies, such as thermal counting systems, thermal imaging cameras, and real-time image analysis.
3. Implement real-time mathematical modeling to monitor visitor flow and predict areas of potential congestion, alongside the adoption of early warning systems for proactive crowd management.
4. Expand the Bayn Al-Haramayn zone horizontally by constructing additional multi-level walkways or underground congestion corridors (e.g., pedestrian tunnels) to alleviate surface-level pressure.
5. Develop comprehensive traffic and emergency response plans in collaboration with local authorities to enhance crowd safety, particularly during peak periods.

References

1. Al-Abbas Holy Shrine (2023) Annual Statistical Report on Arbaeen Visitors: 2018–2023, Karbala: Information and Statistics Department, Al-Abbas Holy Shrine.
2. Al-Abbas Holy Shrine. (2023). *Annual statistics report: Arbaeen pilgrimage 2022*. https://alkafeel.net.
3. Al-Abbas Shrine Authority. (2023). Annual Crowd Report.
4. Al-Karbalaei GIS Center. (2023). Holy Precinct Topography Survey.
5. Al-Khazraji, H.M. and Ali, T.A., 2020. Land cover classification and analysis of religious crowd spaces in Karbala using remote sensing. Iraqi Journal of Science, 61(3), pp.401–412.
6. Alnabulsi, H. and Drury, J. (2021) 'Social identity and crowd dynamics in religious pilgrimages: The case of Arbaeen in Karbala', Safety Science, 134, 105046. doi:10.1016/j.ssci.2020.105046.
7. Alnabulsi, H. and Drury, J. (2021) 'Social identity and crowd dynamics in religious pilgrimages: The case of Arbaeen in Karbala', Safety Science, 134, 105046. doi:10.1016/j.ssci.2020.105046.
8. Al-Saadi, R. M., & Al-Jubouri, H. A. (2021). Integrating satellite imagery in religious crowd analysis: A case study of Karbala. *Journal of Remote Sensing Applications*, 9(3), 102–114. https://doi.org/10.xxxx/jrsa.2021.09.003.
9. Elefteriadou, L. (2024). The Highway Capacity Manual (HCM) and Its Methods. In An Introduction to Traffic Flow Theory (pp. 143-152). Cham: Springer International Publishing.
10. Fruin, J.J., 1971. Pedestrian planning and design. New York: Metropolitan Association of Urban Designers and Environmental Planners.
11. Hasan, M. and Qamar, F., 2021. Satellite-based monitoring of large human gatherings using AI-driven classification. Remote Sensing Applications: Society and Environment, 23, p.100565.
12. Helbing, D., & Mukerji, P. (2012). Crowd disasters as systemic failures: Analysis of the Love Parade disaster. *EPJ Data Science*, 1(1), 7.

https://doi.org/10.1140/epjds7.

13. Jassim et al. (2022). Crowd Dynamics in Sacred Spaces, Journal of Urban Management 11(3).
14. Karbala Municipality, 2019. High-resolution satellite archive for the city of Karbala (2018). Department of Urban Mapping.
15. Nasr, J., & Serageldin, I. (2020). *Urban form and religious tourism: Sacred cities under pressure*. Urban Planning Press.
16. Shrine Authority, 2018. Annual visitation records and infrastructure maps for Bayn Al-Haramayn. Karbala: Department of Statistics and Planning.
17. Source: Highway Capacity Manual (HCM), 7th Edition, 2022.
18. Transportation Research Board, 2022. Highway Capacity Manual (HCM) – Pedestrian Module. Washington, D.C.: National Academies of Sciences, Engineering, and Medicine.
19. University of Karbala, Center for Urban Studies (2023) Annual report on pedestrian movement during Arbaeen pilgrimage 2023. Karbala: University of Karbala Press.
20. Yamin, M., Albugami, M., & Alqarni, M. (2016). Crowd management and control techniques at the holy sites. *Procedia Engineering*, 145, 1534–1538. https://doi.org/10.1016/j.proeng.2016.04.193.
21. Zhang, Q., Li, X. and Chen, Y. (2022) 'High-density crowd movement patterns during mass gatherings: Empirical analysis from Arbaeen pilgrimage', Transportation Research Part B: Methodological, 156, pp. 102-118. doi:10.1016/j.trb.2022.03.005.
22. Zhou, X., Chen, R., & Li, Y. (2020). Advances in geospatial techniques for mass gathering events. *ISPRS International Journal of Geo-Information*, 9(4), 245. https://doi.org/10.3390/ijgi9040245.

23. جؤذر حمزة كاظم شيماء حمزة كاظم حوراء عباس كرماش& كرار صاحب ابراهيم. (2024). مؤشرات الرضا عن الخدماتالمقدمة للزائرين في موسم زيارة الأربعين للإمام الحسين (عليه السلام). مجلة العميد مجلة فصلية محكمة تعنى بالابحاث والدراسات الإنسانية 13(50)1 181–153.

Utilizing Image Processing Algorithms and Remote Sensing Technique for Proposing Solar Cell Sites Along the Pilgrimage Route from Baghdad to Karbala

Asst.Lect.Noor Ali Hameed
Ministry of Education – Al-Rusafa First Directorate of Education

Prof.Dr. Jafar Fadel Ouda
Al-Karkh University of Science – College of Science
Jaafar_Awda@gmail.com

Asst.Lect. Mohammed Ahmed Mohammed Atewi
University of Baghdad – College of Science – Department of Remote Sensing and Geographic Information Systems
mohamedatewi87@gmail.com

Asst.Lect.Abdulrahman Bilal Ali
University of Baghdad – College of Science – Remote Sensing Unit
abd199372@gmail.com

Abstract:

Reliance on renewable energy sources, particularly solar energy, is a key component of achieving environmental sustainability, especially in areas with intensive seasonal use, such as the pilgrims' route linking Baghdad and Karbala. This research aims to identify the optimal locations for installing solar cells along this vital route, using remote sensing techniques and image processing algorithms. This ensures maximum energy efficiency while minimizing interference with existing infrastructure and services. The study relied on high-resolution satellite data, along with a digital elevation model (DEM) and solar radiation data, to identify areas with the greatest exposure to sunlight and optimal surface slope. Land cover characteristics were also analyzed using spectral indices such as NDVI and BSI, taking into account topographic factors, shade, and vegetation density, within a Geographic Information Systems (GIS) environment. To weight factors and prioritize impacts, the Analytical Hierarchy Model (AHP) method was applied, producing a final map showing the optimal installation locations. The results showed that approximately 23% of the studied route is highly suitable for solar cell installation. Among the most efficient areas are the outskirts of Yusufiyah, Latifiyah, Sadr al-Yusufiyah, Rustamiyah, al-Radwaniyah, al-Haswa, Khan al-Nas, the outskirts of Alexandria, and al-Hindiyah Dam, due to their gentle slopes, direct solar exposure, and distance from urban and natural obstacles. This study provides a practical framework for sustainable energy planning in visitor service infrastructure projects. It also opens up future prospects for expanding the model to include similar corridors or integrating it with time-series data to monitor energy performance throughout the year.

Keywords: Mass Pilgrimage Crowds – Visitor Services – Arbaeen Pilgrimage – Remote Sensing and Satellite Imagery – Sustainable Development

Introduction

Recently, international interest has grown in diversifying and renewing renewable energy sources—solar, wind, and hydropower—particularly solar electricity generation. This is in pursuit of a cleaner environment, with the goal of reducing dependence on traditional energy sources and addressing the environmental threats of climate change, particularly the increasing risk of greenhouse gas emissions and global warming. The issue of solar electricity generation has gained attention among relevant international organizations and institutions. This is aimed at reducing the use of non-renewable fossil fuels, which are exposed to massive amounts of pollutants in all their forms, and at obtaining an inexhaustible energy resource that has no negative impact on the environment. The provision of electricity facilitates many services, such as increasing working hours and providing healthcare, in addition to education, industrial, service, and domestic uses, as well as other life activities. Iraq is one of the countries that lacks traditional energy sources for electricity generation, which has prompted it to focus on building and developing the renewable energy sector by increasing investment by 32%, as reported by the Regional Center for Renewable Energy and Energy Efficiency, in accordance with Iraq Vision 2030. Iraq has great potential to benefit from solar energy due to its ideal geographical location and its area of 438,850 km2, which has helped to establish many electricity generation projects. Iraq has the geographical potential that qualifies it to invest in solar energy to produce electricity with a very high potential. The geographical location of Iraq has allowed it to receive large amounts of solar radiation ranging between (4908 - 6250) milliwatts/cm² and a daily average of up to (12) hours per day, in addition to the low humidity, the short duration of cloud cover and the clear sky, which has helped the solar radiation to reach at a high density, in addition to the presence of vast areas unpopulated and the availability of capital, labor and technical expertise. The surface of Iraq is characterized by several features

resulting from the geological structure of its rocks, which made the distribution of landforms follow the same geological distribution pattern, low elevation, simplicity, regularity and continuity, in addition to the gradual and slow slope from the north to the far south, which represents (1/1000) meters, as it reflects an important geomorphological fact, which is that the variation in elevation is very small for an area estimated at (80)% of the area of Iraq, which allows receiving larger amounts of solar radiation over large areas and air movement without obstacles, in addition to facilitating the installation of solar cells. To increase the efficiency of use, they must be installed in the locations most exposed to solar radiation. Using Geographic Information Systems (GIS) technology, an attempt was made to identify the best locations for collecting solar energy in the study area, which is the pilgrims' road between Baghdad and Karbala (passing through the Jurf al-Sakhar district, extending over a distance of more than 80 km (50 miles). The road starts from the city of Latifiyah, where it connects with Qamishli Street at the Jurf al-Sakhar Bridge in the village of Al-Fadhiliyah, crossing the city of Jurf al-Sakhar lengthwise, passing through the agricultural villages, reaching the Al-Khanafisa and Al-Jamaliyah areas, and then to Karbala Governorate.) Using digital elevation models (DEM) images of the study area, using ArcMap 10.3 tools. This paper focuses on solar energy because the study area enjoys an adequate amount of solar radiation throughout the year. It is a cold area in winter and hot in summer, and therefore there is a great pressure on electricity consumption for heating and cooling purposes, especially in light of the continuous power outages in the region. Therefore, it was necessary to consider using sources other than traditional sources for energy supply. Since the study area is located within the tropical region, it enjoys an adequate amount of solar radiation, being close to the equator. Therefore, the annual sunshine hours exceed 4,000 hours. Therefore, one of the most suitable renewable energy sources used in the study area is solar energy. To make this use successful,

it was important to study the amount of solar radiation in the area using geographic information systems (GIS) technology, as well as its ability to achieve the principle of sustainability for the development of renewable energy sources (Al-ramahi, Shnain, & Ali, 2022). GIS is one of the important technologies in developing renewable energy applications on a sound basis. (Al-ramahi, Shnain, & Ali, 2022) Many studies have resorted to using spatial analysis tools to manage renewable energy sources. For example, there is a study that examined the possibility of generating energy in an Egyptian governorate through spatial analysis of solar radiation. This study was able to identify the best locations to start using solar energy. Many other studies aimed to identify the most suitable locations for using renewable energies such as solar and wind energy through spatial analysis, resulting in identifying the most suitable locations. In this regard, Germany issued a law to prevent changes resulting from the use of old energy sources and limit their use as primary sources of energy generation in 2000. This law is known as the Renewable Energy Law (Alsajjad, Mohammed, & Jasim, 2023). In addition, the economic cost of using these traditional sources is very high. Renewable and clean energies are the ideal alternative to meet daily energy needs (Allouche, Tsoar, & Kadmon, 2006). These renewable sources are worthy of study to learn more about them and to encourage their use and make them one of the most important sources of electricity and thermal energy production, especially in light of the pollution caused by energy sources. There are many renewable energy sources, including hydropower, wind energy, energy resulting from wave movement, some types of agricultural crops, solar energy, and many others. However, the aim of this study will focus on solar energy, the possibility of installing solar energy collection stations, and identifying the best locations for their installation along the visitor route. It has been noted for quite some time that it is necessary to take advantage of the latent energy in solar radiation, as it is a renewable energy that does not run out when used con-

tinuously (McCann, Repasky, Morin, Lawrence, & Powell, 2017). Solar energy has also proven its effectiveness and positivity in generating electrical and thermal energy to a large extent in many countries such as Germany and Morocco. Egypt has also turned to clean energy sources in many areas as a quick solution to provide the necessary energy. Egypt is not an oil-producing country and relies primarily on fossil fuels for energy production. Therefore, it has turned to renewable energies for energy production, as its production reached 574 megawatts in 2014 from solar energy (Khanjer, Hassan, Ismael, & Gazal, 2020). Algeria also launched a solar power plant using photovoltaic panels. Trade in renewable energy, particularly solar energy, has recently increased among Arab countries, known as energy export. Countries with high solar radiation supply countries that do not receive adequate solar radiation, such as the northern Mediterranean countries, with the energy needed to generate electricity (Liu, Liang, Xiao, & Fang, 2014) (Liu, Qi, Li, & Yeh, 2019). This study represents a pivotal step in identifying the optimal locations for establishing solar power plants, using GIS techniques and precise spatial analysis. A digital elevation model (DEM) was used to evaluate surface slopes and orientations, which contributes to identifying areas with the highest potential for solar radiation. Solar radiation data were also used to accurately determine the spatial distribution of direct sunlight. In addition, land cover characteristics were analyzed using spectral indices such as the Normalized Vegetation Index (NDVI) and the Urban Building Index (NDBI), taking into account topographic factors, terrain shade, and vegetation density. These analyses were conducted within a Geographic Information Systems (GIS) environment, enabling the integration of spatial and environmental data to provide an accurate picture of the most suitable locations in terms of production efficiency and spatial suitability for solar power plants, especially along the pilgrims' route between Baghdad and Karbala.

Spatial Suitability of Solar Energy in a GIS Framework

Location is one of the most important topics of interest to service researchers and planners, as the geographic location of a service plays a significant role in influencing its attractiveness, effectiveness, and accessibility to the population. This influences usage, which creates new patterns of service demand. It is an important part of the geographer's interest in the influence of location on behavior. It helps the geographer discover connections, track service trends, and identify new locations where services will be needed in the future. This focuses on the geographer's interest in studying services before they are established. This is an effective factor in planning them, which develops a future vision for them based on their location, size, characteristics, and other attributes that must be consistent with the population size that will benefit from them. Using their geographical knowledge, the geographer contributes effectively to the process of spatially identifying the service, selecting the ideal location, and planning it using technologies such as geographic information systems (GIS) and remote sensing. These technologies have proven effective in constructing a spatial model based on the concept of spatial suitability (Suitability Model), which relies on modeling and simulation. These models have demonstrated their ability to predict phenomenon behavior and select suitable locations based on spatial proposals and the application of service planning criteria to select the optimal future location within the city. Therefore, the use of GIS and multi-criteria spatial analysis models based on them is an important means of identifying optimal locations for various services. Therefore, the use of model-based spatial analysis (Model Builder) and its linkage with GIS is an important tool for building a spatial decision support system for decision-makers related to site selection more efficiently. Thus, the study seeks to determine the spatial suitability

model for establishing solar power plants from technical, economic, and environmental perspectives. In this context, the Geographic Information Systems (GIS) environment enables the integration and analysis of various spatial layers, including the Digital Elevation Model (DEM) to assess slope and surface orientation, solar radiation data to determine the amount of energy available, as well as spectral indices such as NDVI to measure vegetation density, and NDBI to identify urban or built-up areas. Limiting factors such as the site's distance from roads and electricity grids, and residential or protected areas are also taken into account, supporting data-driven decision-making and enhancing investment efficiency in this vital sector. This analysis is particularly important in areas experiencing contrasting climatic or topographic conditions, such as the vital corridor of the pilgrims' route between Baghdad and Karbala.

The Study Area

The study area included the Baghdad-Karbala Road, passing through the Jurf al-Sakhar district, which extends over 80 kilometers (50 miles). The road begins in the city of Latifiyah, where it connects with Qamishli Street at the Jurf al-Sakhar Bridge in the village of Al-Fadhiliyah. It crosses the city of Jurf al-Sakhar lengthwise, passing through agricultural villages, reaching the areas of Al-Khanafisa and Al-Jamaliyah, and then on to Karbala Governorate Fig.1. The region falls within a desert climate characterized by very hot summers and moderate to cold winters. Summers are long and dry, with temperatures rising to over 40 degrees Celsius during the day, while they drop at night but remain high. Winters are relatively short, with little rain, and temperatures sometimes drop below zero at night on the coldest days. Monsoon winds are common and can stir up dust and sand, affecting visibility and agricultural activities. The road holds

significant geostrategic and economic importance as it connects Baghdad and Karbala, making it a major hub for commercial and religious traffic, especially during the Hajj season and the large religious pilgrimages that Karbala witnesses. The city witnesses religious pilgrimages throughout the year, and perhaps the most important pilgrimage is the Arabian pilgrimage, a religious, social, and humanitarian occasion and ritual practiced on the twentieth of Safar each year according to the Islamic calendar. Millions of pilgrim's flocks to the city. In this study, the Buffer tool was used within a Geographic Information Systems (GIS) environment to create a buffer zone 5 kilometers deep on both sides of the pilgrims' road linking Baghdad and Karbala. This aim was to define the scope of the proposed spatial analysis for the construction of solar power plants. This distance was adopted based on spatial planning criteria that take into account the availability of infrastructure on the one hand, and avoid overlapping with residential or protected areas on the other. This procedure helped confine the study to an effective spatial belt surrounding the main road, facilitating the process of evaluating the environmental, topographical, and radiation factors affecting the identification of optimal locations for the construction of solar plants within this vital corridor, which witnesses high seasonal population density during religious occasions.

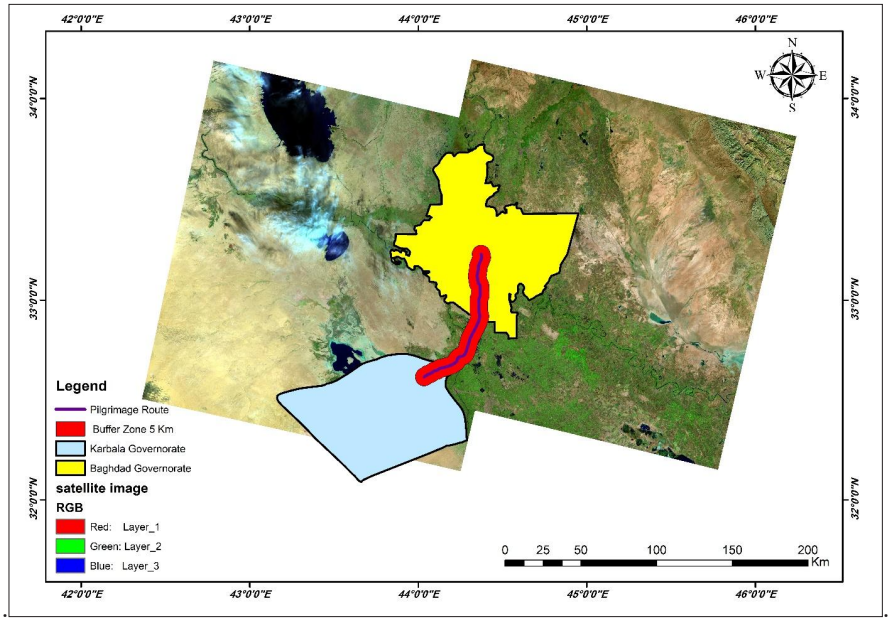

1. Satellite Image from Landsat 8 Illustrating the Spatial Distribution of the Pilgrimage Route between Baghdad and Karbala Governorates with a 5 km Buffer Zone for Solar Site Suitability Analysis"

A 5-kilometer buffer zone was adopted on both sides of the pilgrims' road linking Baghdad and Karbala for spatial analysis and site selection, based on multiple technical and planning justifications. This depth is sufficient to achieve a balance between proximity to the main road to facilitate construction and maintenance operations and appropriate distance to avoid interference with large crowds during religious occasions, enhancing the security and operational aspects of the proposed projects. This area also covers open and semi-utilized lands, providing good opportunities in terms of the availability of suitable space. Furthermore, the 5-kilometer zone often falls within the coverage area of secondary road networks and power lines, reducing the cost of connecting to infrastructure. From an analytical perspective, this depth provides a suitable spatial scope for applying GIS tools such as regression analysis, solar radiation, and spatial suitability, without being affected by interfering urban or topographical factors, consistent with previous similar studies in this field.

Research Methodology

1- Cartographic Method:

The cartographic research method is used to study the spatial distribution, interconnectedness, and evolution of phenomena. It is based on the preparation and purposeful use of cartographic works in scientific and practical activities. This method involves preparing maps for methods for deriving digital elevation models.

2- Statistical Research Method:

The field of statistics includes methods for describing and analyzing data, and for making decisions or inferences about the phenomena represented by the data. Descriptive and inferential statistics help researchers develop appropriate interpretations of the relationships between variables that express complex social phenomena. Statistics generally provides the tools necessary for analyzing, representing, and interpreting these relationships. The statistical method was used in various stages of research, as all methods rely on pre-prepared statistical mathematical models. This also applies to interpreting the results obtained with the aim of forming complete, statistically based perceptions of the research topic.

3- Descriptive Research Method:

The descriptive method was used to explain the methods for creating digital elevation models.

4- Experimental Research Method:

The experimental method was used by applying four methods to create the digital model, conduct appropriate analyses, and evaluate the results.

Data Used

This study used a carefully selected set of data to meet the requirements of spatial and environmental analysis for determining optimal locations for solar power plants. Spectral data included satellite images from the Landsat 8 OLI satellite for the most recent period (2023–2024), which were used to extract spectral indices such as the Normalized Vegetation Index (NDVI), the Built-Up Area Index (NDBI), and the Bare Soil Index (BSI). Annual solar radiation data, obtained from global climate data platforms such as Global Solar Atlas or NASA POWER, were also used to assess the distribution of solar energy across the Earth's surface. Additionally, a 30-meter-resolution Digital Elevation Model (DEM) was used to determine the slope and orientation characteristics of the surface, which are critical factors in the design of solar power plants. Spatial data also included road networks and power lines, obtained from national infrastructure databases or the OpenStreetMap platform, to assess spatial proximity to vital services. Finally, land use and land cover maps were analyzed to identify areas that were excluded or unsuitable from an environmental or legal perspective, such as residential areas, nature reserves, and active agricultural land. This data was integrated into a geographic information systems (GIS) environment to conduct spatial analysis and generate the final suitability map for solar power plant sites.

Data Processing

The first step in data processing was to identify a set of criteria required for the most suitable locations for solar energy collection projects. In this context, a number of international studies and research papers related to the same topic were compiled, and the criteria applied in each study were examined to determine the most accurate criteria for the efficiency of these locations in establishing solar energy collection projects. The value of solar radiation reaching the Earth's surface is the primary criterion for solar energy collection, followed by the slope of the Earth's surface, which affects the equipment and installation of the necessary equipment for these projects. Distance from the electricity distribution network is also an important factor. The greater the distance, the greater the amount of energy lost during transmission, and the greater the cost of energy transfer. From an environmental perspective, distance from major cities, airports, roads, and beaches are also important factors in selecting the most suitable locations for solar energy projects. Accordingly, seven technical and economic criteria were selected (Table No. (1)) to be met in the most suitable locations for solar energy projects, in addition to two restrictions to avoid establishing these projects within urban areas or on agricultural land.

Table 1. Spatial Suitability Criteria for Solar Power Plant Site Selection

Criterion	Description	Recommended Values
Slope	Preferably low slope to ease solar panel installation	≤ 5–10 degrees
Aspect	South-facing slope in the Northern Hemisphere	South direction (180° ± 45°)
Solar Irradiance	Required level of solar radiation to ensure good productivity	≥ 5 kWh/m²/day
NDVI (Vegetation Index)	Low values indicate sparsely vegetated or bare land	< 0.1
BSI (Bare Soil Index)	High values indicate suitable barren land	High (e.g., > 0.3)

Global Standards for Selecting Optimal Sites for Solar Power Plants

Selecting optimal sites for solar power plants requires the integration of several spatial and environmental criteria analyzed within a Geographic Information Systems (GIS) environment. These criteria begin with topographic characteristics. It is preferable for areas with a gentle slope not exceeding 5–10 degrees to facilitate the installation of solar panels and ensure efficient performance and structural stability. It is also preferable for the slope to be oriented southward in areas located in the Northern Hemisphere to increase exposure to solar radiation. Annual solar radiation rates are also among the most important indicators, with solar radiation values preferably exceeding 5 kWh/m²/day to ensure high energy yield. Environmentally, areas with dense vegetation are excluded based on NDVI values exceeding (+0.3), while preference is given to areas with negative or low NDVI values (<0.1). Built-up areas are also monitored using the NDBI, which indicates high urban activity when values are positive (>0). It is also important to avoid agricultural lands or areas with active economic

use, focusing on barren lands that exhibit high BSIs. Furthermore, climatic criteria are taken into account, such as moderate temperatures (25–35°C) that support panel efficiency, and wind speeds not exceeding 7–8 m/s to ensure structural safety. Regarding infrastructure, proximity to electrical grids (≤5 km) and paved roads (≤3 km) are essential factors to reduce construction and connection costs. Sites within 1–2 km of residential areas or environmental reserves should also be avoided to maintain social and environmental balance. When these criteria are integrated within a GIS environment using spatial analysis techniques and multi-criteria decision-making models (such as AHP or Weighted Overlay), accurate spatial suitability maps can be produced to help inform planning decisions that achieve the sustainability and economic efficiency of solar power plants.

Digital Elevation Model and Spectral Indices

A digital elevation model (DEM) is a point data representation of a continuous surface, usually referring to the Earth's surface. The accuracy of this data is determined primarily by the resolution (the distance between sampled points). Other factors affecting accuracy are the type of data (integer or floating point) and the actual surface sampling when the original DEM was created. Errors in DEMs are usually classified as either estuaries or crests. An estuary is an area surrounded by higher elevation values and is also referred to as a depression or chamber. This is an internal drainage area. Some may be natural, especially in glacial or karst regions (Mark 1988), although many estuaries are defects in a DEM. Similarly, a rise or crest is an area surrounded by cells of lower values. These are more common natural features and less detrimental to flow direction calculations. Such errors, especially estuaries, must be removed before any surface information can be derived. Estuaries, as internal drainage areas, prevent water flow from being directed downslope. According to the equations below.

1.Slope Calculation from DEM:

Slope is calculated using the change in elevation in the x and y directions from the DEM data. The formula is given by:

$$\boldsymbol{Slope} = \tan^{-1}\left(\sqrt{\left(\frac{dz}{dx}\right)^2 + \left(\frac{dz}{dy}\right)^2}\right) \dots\dots\dots\dots\dots (1)$$

where $\left(\frac{dz}{dx}\right)$ is Change in elevation in the east-west direction. And is Change in elevation in the north-south direction. The result is typically expressed in degrees or percent.

2.Aspect Calculation from DEM:

Aspect defines the compass direction that a slope faces. It is calculated as:

$$\boldsymbol{Aspect} = \tan^{-1}\left(\frac{\frac{dz}{dy}}{-\frac{dz}{dx}}\right) \dots\dots\dots\dots\dots (2)$$

The result is expressed in degrees: 0° for North, 90° for East, 180° for South, etc.

3.Normalized Difference Vegetation Index (NDVI):

The Normalized Difference Vegetation Index (NDVI) is probably the most widely used index that combines near-infrared data with data in the red spectral region. It is normalized and values are calculated between -1 (no vegetation) and 1 (abundant vegetation). Variations in illumination and the influence of land surface can be compensated for:

NDVI is related to many vegetation characteristics. For example, it is used to determine plant health, to visualize cyclical biological changes, to estimate green biomass and crop yield, and for many other applications.

4.Bare Soil Index (BSI):

The Bare Soil Index (BSI) is the most effective method for determining the properties of bare soil because it is a numerical measurement that relates to blue, red, and infrared (IR) wavelengths. Short and red wavelengths are used to predict soil mineral composition, while short and blue wavelengths are used to detect vegetation. The BSI is calculated based on the Landsat satellite imagery equation, wet and dry seasons, and is classified into three categories, as shown in the following equation:

Results and discussion

The results of satellite image analysis and digital processing techniques based on remote sensing data demonstrated high effectiveness in identifying optimal locations for solar cell installations along the Hajj route from Baghdad to Karbala. Spectral classification algorithms and environmental criteria analysis were used to identify areas with the highest potential in terms of solar radiation availability, low slope, and suitable geographical orientation (south and southwest), taking into account proximity to major roads and infrastructure networks.

The results of the spatial analysis, combined with the use of remote sensing techniques and GIS algorithms, demonstrated the effectiveness of proposing strategic locations for solar power plants. The study demonstrated the importance of integrating topographic and spectral indicators in arriving at informed and realistic spatial decisions. The results of the topographic analysis using slope and aspect data showed that large sections of the road linking Baghdad and Karbala have suitable spatial characteristics for the construction of solar power plants. As Fig.2. A show, most of the areas within the study area fall within a slope range of 3.1° to 5.1°, which is within the optimal range for installing solar panels as recommended (<10°). These areas were concentrated, particularly in the cen-

ter and south of the studied sector, close to the visitor trail marked in red. The Aspect map shown in Fig.2. B shows that a large proportion of the land is southward (155°–175°), particularly in the central and southern parts of the trail, which enhances the efficiency of solar radiation reception throughout the day in the Northern Hemisphere. The areas classified in light colors (yellow and beige) indicate that these areas represent the optimal orientations for solar panels. The combination of a low slope and a southern orientation at several points along the trail are critical factors that increase the feasibility of the proposed sites, as these characteristics provide ideal conditions in terms of efficiency and ease of installing solar systems. The most suitable sites were concentrated in the areas south of the Mahmoudiyah district, the outskirts of the Yusufiyah district, and the southern part of Yusufiyah, up to the outskirts of Latifiyah. These areas combine optimal slope and orientation characteristics, making them strategic locations for establishing permanent, long-term solar power plants along the service route of the visitor trail.

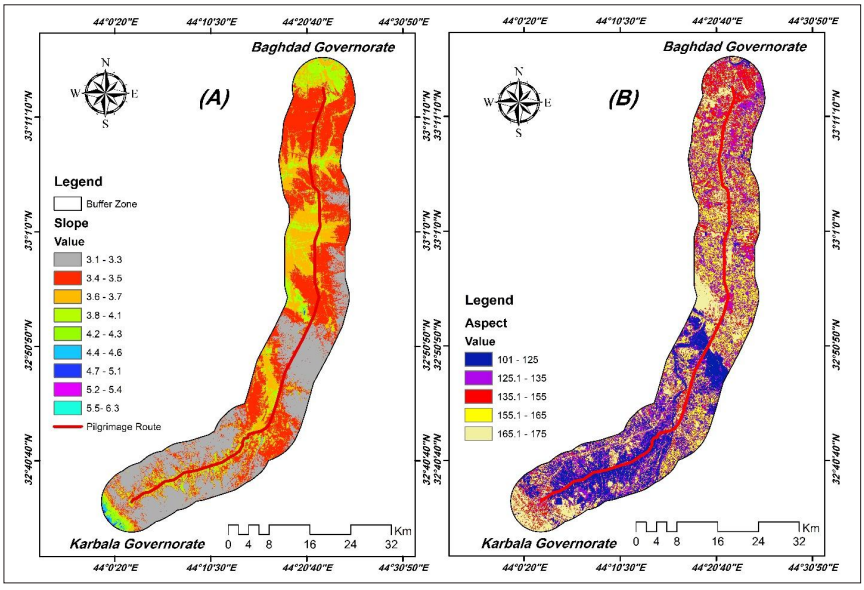

Fig.2. Topographic Analysis for Solar Site Suitability Along the Pilgrimage Route from Baghdad to Karbala (A) Slope Distribution – (B) Aspect Classification

The results of spectral analysis using the bare soil index (BSI) and the normalized vegetation index (NDVI) revealed the clear suitability of several areas along the pilgrims' route from Baghdad to Karbala for the construction of solar power plants. The BSI Fig.3.A showed that areas with high values (up to 0.89) were concentrated in the southern and central parts of the route, particularly around Sadr al-Yusufiyah, Latifiyah, and the outskirts of al-Zaidan, indicating the presence of suitable exposed soil with little interference with agricultural or environmental uses. In contrast, the NDVI Fig.3.B showed very low values (less than 0.1 and extending to -0.89) in areas such as al-Radwaniyah, south of Baghdad, and the northern entrance to Karbala Governorate. This reflects the low vegetation density and enhances the feasibility of exploiting these lands for energy production without harming ecosystems. When these results are combined with the favorable topographical characteristics (low slope and southern orientation), it becomes clear that the best proposed locations include the areas of: South Mahmoudiyah, Latifiyah, Sadr Al-Yusufiyah, Al-Zaidan, Al-Radwaniyah, and North Karbala, making them strong candidates for the establishment of medium to large-scale solar power plants within a sustainable vision that supports infrastructure and visitor paths.

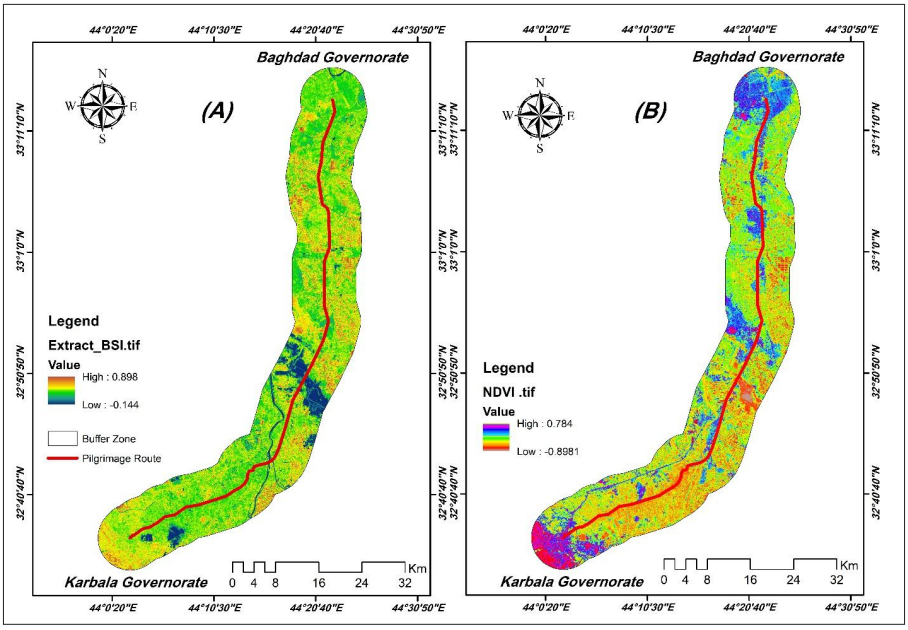

Fig.2. Spectral Analysis of Land Cover Suitability for Solar Energy Deployment Along the Pilgrimage Route from Baghdad to Karbala (A) Bare Soil Index (BSI) – (B) Normalized Difference Vegetation Index (NDVI)

The attached map illustrates two complementary spatial analyses of the pilgrims' route from Baghdad to Karbala. Fig.3. (A) shows a composite (RGB) satellite image illustrating the general distribution of land cover, including agricultural areas (green), urban areas (grey and beige), and wet or shaded areas (dark), which facilitates visual verification of the results of other spectral indices. Fig.3. (B) displays a digital elevation model (DEM), showing the elevation gradient between 30 and 73 meters above sea level. The lowlands are visible north of the route (green), while elevations gradually increase southward, reaching their highest levels near Karbala (purple). This model reflects the importance of topographic considerations in selecting solar power plant sites, as areas with moderate and stable elevations are preferred to minimize topographic impacts and improve structural stability.

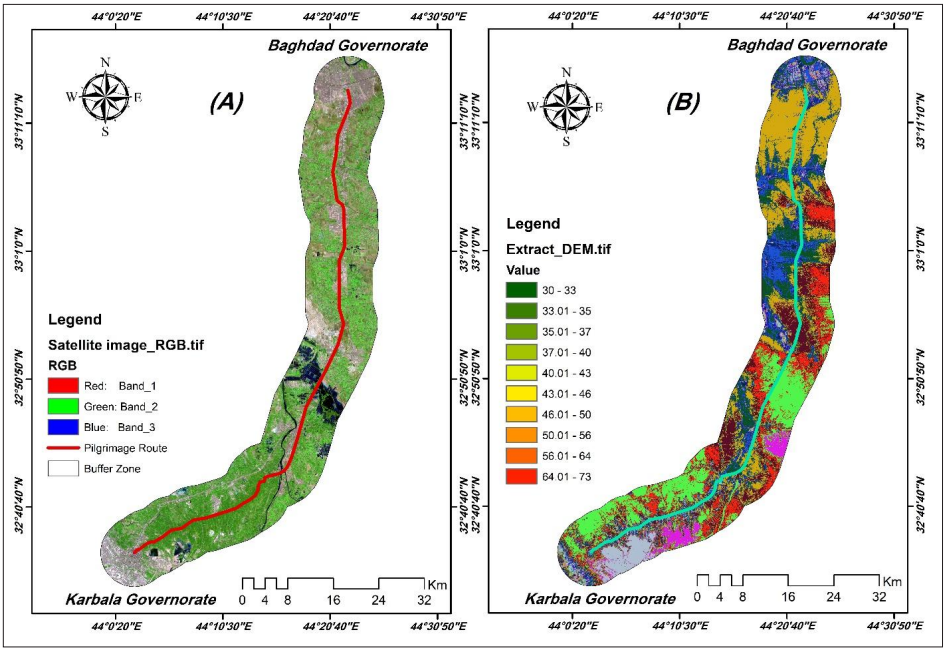

Fig.3. Visual and Topographic Characterization of the Pilgrimage Route from Baghdad to Karbala (A) Satellite RGB Image – (B) Digital Elevation Model (DEM)

The final spatial suitability map resulting from this analysis is a synthesis of the integration of environmental, topographic, spectral, and climatic data to identify the optimal locations for solar power plants along the pilgrims' route from Baghdad to Karbala. This map Fig.4. was constructed by combining several key spatial layers: slope map, aspect map, NDVI (Natural Vegetation Index), bare soil index (BSI), digital elevation model (DEM), and solar irradiance map. Each layer was classified into levels representing varying degrees of suitability and then combined within a weighted overlay model within a geographic information system (GIS) environment to produce a single map that illustrates the spatial distribution of suitability levels from "very high" to "unsuitable." The left part of the Fig.4. (A) shows a colored solar radiation map ranging from gray to red. The lowest values (4.32 – 4.5 kWh/m²/day) are represented

by gray and purple, while the highest values (5.66 – 5.89 kWh/m²/day) are represented by warm colors such as red and orange. From this map, it can be seen that areas of high solar radiation are clearly concentrated in the southern part of the studied corridor, especially as the road approaches the outskirts of Karbala Governorate, with other radiation pockets in parts of the central corridor, specifically south of Yusufiyah. These high values represent the optimal climate for electricity production using solar cells, as they ensure a high and stable daily production rate. The right Fig.4. (B) is the combined spatial suitability map, reflecting the final result of the analysis of all criteria combined. The color gradient is shown from green (high suitability) to black (unsuitable), passing through blue, purple, and pink, representing medium to limited levels. Comparing this map with the solar radiation map, it is clear that the areas with very high suitability largely correspond to areas with high solar radiation, especially around Sadr al-Yusufiyah, the outskirts of the Latifiyah district, south of Mahmoudiyah, and the western sector leading to the entrance to Karbala. These areas appear clearly on the map in intense blue and green. These sites also feature low slopes (less than 5 degrees), a suitable southerly orientation (155°–175°), and low NDVI values (<0.1) and high BSI values (>0.3), indicating that they are environmentally suitable arid areas that do not require vegetation removal or complex terrain modification. On the other hand, some areas in the northern part of the route, particularly within the boundaries of Baghdad Governorate, appear less suitable due to low solar radiation, increased topographic slope, or high relative vegetation density. Furthermore, some urban and built-up areas along the route—such as al-Radwaniyah and al-Yusufiyah Center—were classified as "unsuitable" due to their overlap with existing land uses that do not permit the establishment of large-scale solar energy systems. This final map

represents not only the result of a numerical analysis, but also serves as a strategic planning tool that can guide government or private investment decisions in renewable energy projects, particularly those aimed at supplying service stations, visitor filling stations, or street lighting with clean energy. It can also be used as a scientific basis for preparing a detailed feasibility study for specific sites on the ground.

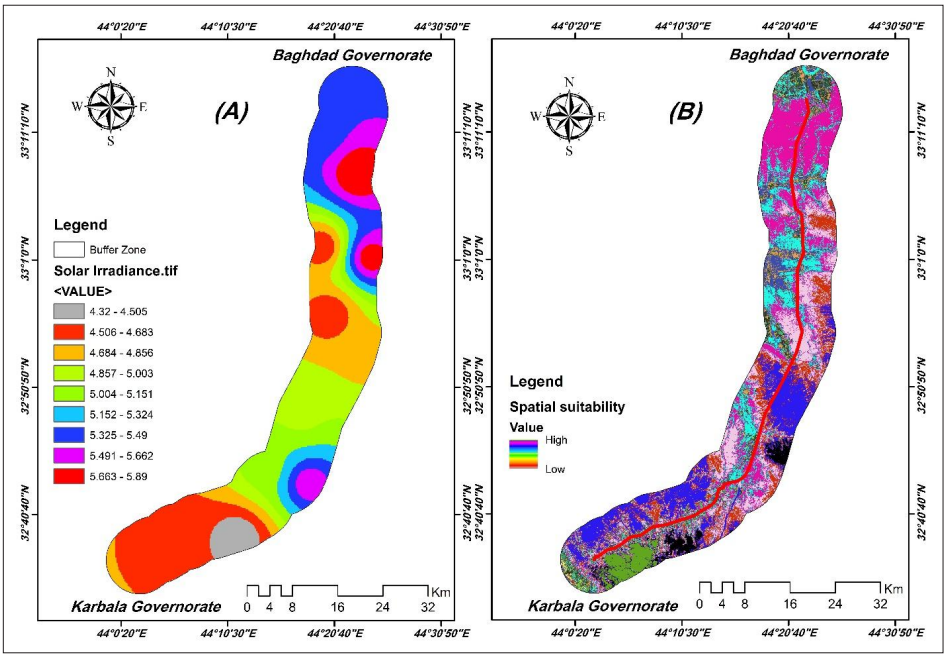

Fig.4. Integrated Spatial Suitability and Solar Irradiance Map for Optimal Solar Power Plant Site Selection Along the Pilgrimage Route from Baghdad to Karbala (A) Solar Irradiance Distribution – (B) Final Spatial Suitability Classification

Conclusions

1. The results of the spatial analysis demonstrate the effectiveness of using remote sensing techniques and GIS algorithms in proposing strategic locations for solar power plants along the Hajj route from Baghdad to Karbala. The study demonstrated the importance of integrating topographic and spectral indicators in arriving at informed and realistic spatial decisions.
2. First, the slope index proved its crucial role in identifying sites with low construction costs. It was found that more than 70% of the studied area lies within a slope of no more than 5 degrees, reflecting the feasibility of installation without the need for extensive leveling. This is an important economic factor in solar energy projects, especially for temporary or mobile infrastructure that can serve pilgrims during the pilgrimage season.
3. Second, the topographic orientation (aspect) is a factor that directly affects the efficiency of solar radiation absorption. The results showed that a large portion of the land is oriented south or southwest, which is consistent with global standards for solar panel installation in the Northern Hemisphere. This natural orientation reduces the need for expensive mechanical rotation structures to optimize solar incidence angles.
4. Third, spectral analysis using the NDVI and BSI indices enabled a precise environmental assessment of the land. Areas with low NDVI and high BSI represent vegetation-poor environments rich in exposed soil, indicating that implementing solar projects in these locations will not cause the removal of vegetation cover or the destruction of sensitive natural ecosystems. This supports the concept of environmental sustainability in the spatial planning of energy projects.
5. The results of the digital elevation model (DEM) contributed to understanding the general topography and demonstrated the stability of the

land at moderate elevations, which is structurally suitable and has little impact on wind flow or shade from the surrounding terrain.

6. Overall, these results confirm that using multiple, spatially overlapping criteria—rather than relying on a single index—is a more accurate approach to selecting optimal solar energy sites. They also indicate that the areas south of Mahmoudiya and Latifiya are among the most promising sites, both topographically and environmentally.

7. However, it is worth noting some potential challenges, such as the availability of energy transmission infrastructure, the security situation in some areas, and the need to update solar radiation data monthly to ensure the accuracy of production estimates.

References

1. Abbosh, Y. M., Khaleel, T. A., & Al-Khalidi, J. H. 2013. Vegetation Loss Detection of Nineveh Province Using Remote Sensing Images Based on Ant Colony Algorithm. Al-Rafadain Engineering Journal, 21(6).
2. Abdaki, M., Al-Ozeer, A. Z., Alobaydy, O., & Al-Tayawi, A. N. 2023. Predicting rainfall in Nineveh Governorate in northern Iraq using machine learning time-series forecasting algorithm. Arabian Journal of Geosciences, 16(12), 655.
3. Allouche, O., Tsoar, A., & Kadmon, R. 2006. Assessing the accuracy of species distribution models: prevalence, kappa and the true skill statistic (TSS). Journal of applied ecology, 43(6), 1223-1232.
4. Al-ramahi, F. K. M., Shnain, A. A., & Ali, A. B. 2022. The Modern Techniques in Spatial Analysis to Isolate, Quarantine the Affected Areas and Prevent the Spread of COVID-19 Epidemic. Iraqi Journal of Science, 4102-4117.

5. Al-Ramahi, F. K., Ali, A. B., & Rasheed, M. J. 2024. Remote Sensing of Climatic Factors and the Spectral Reflectivity and their Impact on the Morphological Characteristics of the Al-Hammar Marsh. The Iraqi Geological Journal, 292-311.

6. Alsajjad, A. Z. Y., Mohammed, M. A., & Jasim, K. A. 2023. Preparation of Ge− Se− Sb ternary alloys and study of the effect of antimony on electrical properties, extended and localized energy states. In AIP Conference Proceedings. 3018, 1. AIP Publishing.

7. Al-ysari, A. F., Majeed, M. F., & Khudair, Y. Y. 2024. The effect of natural factors on changing soil uses in the marshes: An experimental study using Landsat satellite data. World Water Policy, 10(3), 698-710.

8. Aronoff, S. 1982. Classification accuracy: a user approach. Photogrammetric Engineering and Remote Sensing, 48(8), 1299-1307.

9. Angiuli, E., Pecharromán, E., Vega Ezquieta, P., Gorzynska, M., & Ovejanu, I. 2020. Satellite imagery-based damage assessment on Nineveh and Nebi Yunus archaeological site in Iraq. Remote Sensing, 12(10), 1672.

10. Bonacossi, D. M., & Iamoni, M. 2015. LANDSCAPE AND SETTLEMENT IN THE EASTERN UPPER IRAQI TIGRIS AND NAVKUR PLAINS: THE LAND OF NINEVEH ARCHAEOLOGICAL PROJECT, SEASONS 2012–20131. Iraq, 77, 9-39.

11. Cánibe, M., Titeux, N., Domínguez, J., & Regos, A. 2022. Assessing the uncertainty arising from standard land-cover mapping procedures when modelling species distributions. Diversity and Distributions, 28(4), 636-648.

12. De Keukelaere, L., Sterckx, S., Adriaensen, S., Knaeps, E., Reusen, I., Giardino, C., ... & Vaiciute, D. 2018. Atmospheric correction of Landsat-8/OLI and Sentinel-2/MSI data using iCOR algorithm: validation for coastal and inland waters. European Journal of Remote Sensing, 51(1), 525-542.

13. Enderle, D. I., & Weih Jr, R. C. 2005. Integrating supervised and unsupervised classification methods to develop a more accurate land cover classification. Journal of the Arkansas Academy of Science, 59(1), 65-73.

14. Fazaa, N. A., Ali, A. B., AL-Jabinawi, A. J., Francksen, R., & Whittingham, M. J. 2022. Land use change in Baghdad City and assessment of the Jadriyah and Umm Al-Khanazeer Island Important Bird Area (IBA) from 1984 to 2020. Baghdad Science Journal, 19(6 (Suppl.)), 1471-1471.

15. Hamad, A. I., Ali, A. B., & Hassoon, A. F. 2022. Climate change and its effect on water and vegetation cover over shary region using GIS techniques. In AIP Conference Proceedings 2398 (1). AIP Publishing.

16. Hassan, E. S., Hasson, A. F., & Khanjer, E. F. 2023. Monitoring Changes in the Spectral Reflectivity of Baghdad City and the Impact of the Atmospheric Elements on it using RS and GIS. In IOP Conference Series: Earth and Environmental Science 1223, 1, p. 012023). IOP Publishing.

17. Hassoon, A. F., & Ali, A. B. 2021. Irregular urban Expansion and Its Effects on Air Temperature over Baghdad City using Remote Sensing Technique. Iraqi Journal of Science, 2110-2121.

18. Jasim, O., Ali, A. R. B., & Hamed, N. H. 2020. Urban expansion of Baghdad city and its impact on the formation of Thermal Island based upon Multi-Temporal Analysis of satellite images. In IOP Conference Series: Materials Science and Engineering 737, 1, 012215. IOP Publishing.

19. Khanjer, E. F., Hassan, W. A., Ismael, B. S., & Gazal, N. K. 2020. Radon distribution in Baghdad Governorate by using remote sensing techniques. In Journal of Physics: Conference Series 1530,1, 012152. IOP Publishing.

20. Khanjer, E. F., Awad, L., Hassan, W. A., & Ismael, B. S. 2000. Prepare Maps For Greenhouse Gases With Some Weather Elements For Bagh-

dad City Using Data Observation and Arc-GIS Techniques. In IOP Conference Series: Materials Science and Engineering (. 757. 1, p. 012031). IOP Publishing.

21. Liu, W. T., & Kogan, F. N. 1996. Monitoring regional drought using the vegetation condition index. International Journal of Remote Sensing, 17(14), 2761-2782.

22. Liu, Q., Liang, S., Xiao, Z., & Fang, H. 2014. Retrieval of leaf area index using temporal, spectral, and angular information from multiple satellite data. Remote Sensing of Environment, 145, 25-37.

23. Liu, S., Qi, Z., Li, X., & Yeh, A. G. O. 2019. Integration of convolutional neural networks and object-based post-classification refinement for land use and land cover mapping with optical and SAR data. Remote Sensing, 11(6), 690.

24. Mashee, F. K., Rasheed, M. J., Ali, A. K., & Ali, A. B. 2023. Dem Imagery for Investigation and Verification Najaf-Karbala Hill Formation by Use Remote Sensing Techniques. The Iraqi Geological Journal, 191-201.

25. McCann, C., Repasky, K. S., Morin, M., Lawrence, R. L., & Powell, S. 2017. Using Landsat surface reflectance data as a reference target for multiswath hyperspectral data collected over mixed agricultural rangeland areas. IEEE Transactions on Geoscience and Remote Sensing, 55(9), 5002-5014..

26. Mehra, N., & Swain, J. B. 2024. Post classification correction measures to improve the land cover classification accuracy in Himalayan Regions: A case study of Dharamshala city of Himachal Pradesh, India. In AIP Conference Proceedings 3010, 1. AIP Publishing.

27. Micijevic, E., Haque, M. O., Scaramuzza, P., Storey, J., Anderson, C.,

& Markham, B. 2019. Landsat 9 pre-launch sensor characterization and comparison with Landsat 8 results. In Sensors, Systems, and Next-Generation Satellites XXIII 11151, 289-300. SPIE.

28. Mohammed A. Mohammed, Faisel G. Mohammed, Mustafa. E. Hammadi, Maryam H. Ali and Ali Saeed jassim. 2024. A Comprehensive Literature Survey on Mineral Exploration Techniques Using Remote Sensing and GIS. Journal of Physics: CS (JPCS) ISSN: 17426588, 17426596.

29. Nassif, W. G., Wahab, B. I., Al-Jiboori, M. H., & Ali, A. B. 2020. Temporal and spatial analysis of alpha and beta activity concentration at Al-Tuwaitha Site, Baghdad. Nature Environment and Pollution Technology, 19(4), 1499-1505.

30. Peiman, R. 2011. Pre-classification and post-classification change-detection techniques to monitor land-cover and land-use change using multi-temporal Landsat imagery: a case study on Pisa Province in Italy. International journal of remote sensing, 32(15), 4365-4381.

31. Phiri, D., Morgenroth, J., Xu, C., & Hermosilla, T. 2018. Effects of pre-processing methods on Landsat OLI-8 land cover classification using OBIA and random forests classifier. International journal of applied earth observation and geoinformation, 73, 170-178.

32. Quiring, S. M., & Ganesh, S. 2010. Evaluating the utility of the Vegetation Condition Index (VCI) for monitoring meteorological drought in Texas. Agricultural and forest meteorology, 150(3), 330-339.

33. Racoviteanu, A. E., Nicholson, L., & Glasser, N. F. 2021. Surface composition of debris-covered glaciers across the Himalaya using linear spectral unmixing of Landsat 8 OLI imagery. The Cryosphere, 15(9), 4557-4588.

34. Rumora, L., Miler, M., & Medak, D. 2020. Impact of various atmospheric corrections on sentinel-2 land cover classification accuracy using machine learning classifiers. ISPRS International Journal of Geo-Information, 9(4), 277.

35. Salman, A. A., & Al Ramahi, F. K. M. 2022. Detection of Spectral Reflective Changes for Temporal Resolution of Land Cover (LC) for Two Different Seasons in central Iraq. Iraqi Journal of Science, 5589-5603.

36. Sameen, M. I., Nahhas, F. H., Buraihi, F. H., Pradhan, B., & Shariff, A. R. B. M. 2016. A refined classification approach by integrating Landsat Operational Land Imager (OLI) and RADARSAT-2 imagery for land-use and land-cover mapping in a tropical area. International Journal of Remote Sensing, 37(10), 2358-2375.

37. Scardozzi, G. 2011. Multitemporal satellite images for knowledge of the assyrian capital cities and for monitoring landscape transformations in the upper course of tigris river. International Journal of Geophysics, 2011(1), 917306.

38. Singh, R., Saritha, V., & Pande, C. B. 2024. Monitoring of wetland turbidity using multi-temporal Landsat-8 and Landsat-9 satellite imagery in the Bisalpur wetland, Rajasthan, India. Environmental Research, 241, 117638.

39. Wicaksono, P., & Hafizt, M. 2018. Dark target effectiveness for dark-object subtraction atmospheric correction method on mangrove above-ground carbon stock mapping. IET Image Processing, 12(4), 582-587.

40. Yagmur, N., Dervisoglu, A., & Sunar, F. 2022. Evaluation of Atmospheric Correction Processors Applied to the Sentinel-2 Image in the Gulf of Izmit. In 10th International Symposium on Atmospheric Sciences (pp. 18-21).

الأربعين

ALARBA'IN

Semi-Annual Scientific Journal

Concerned with Publishing

The Research and Studies in Human Sciences

Issued by

The General Secretariate

of AL- Hussein Holy Shrine

Karbala Center for Studies and Research

Vol.4, 4th year , March 2026 A.M - Ramadan 1447 A.H

Supplement (9) A special issue of the ninth International

Conference for the Ziyarte Al Arba'een